

This document was produced
by scanning the original publication.

Ce document est le produit d'une
numérisation par balayage
de la publication originale.



Natural Resources
Canada

Ressources naturelles
Canada



Littoral mudflat stability monitoring
the Humber estuary, S. Yorkshire, England
LISPUK - April, 1995

by

C. L. Amos(1), M. Brylinsky(2), S. Lee(3)
and D. O'Brien(3)

(1) Geological Survey of Canada

(2) ACER, Acadia University

(3) Department of Earth Sciences
University of Wales, Cardiff

G.S.C.'s Open File Report # 3214

Internal Cruise Report

15 July, 1996

beatland

APPENDIX 2

WATER CONTENT ANALYSES OF GRAVITY CORES

Water content procedure

Samples were taken from the core at 5 cm intervals. A petri dish was then weighed for the first sample and a plastic sampling device used to take the sample from the core. The sample was then weighed with the petri dish and put into an oven at approximately 40°C for 48 hours. This was repeated for each sample. After 48 hours, the sample and petri dish were weighed. The following equation was then used to obtain the water content of the sample:-

$$\frac{(Weight\ wet\ sample + dish) - (Weight\ dry\ sample + dish)}{(Weight\ dry\ sample + dish) - (Weight\ dish)} \times 100$$

SITE A				
Depth (m)	Weight dish	Weight (dish + wet sample)	Weight (dish + dry sample)	Water Content (%)
0	7.923	14.807	12.770	42.026
0.05	8.191	17.556	14.573	46.741
0.1	7.919	15.299	13.106	42.279
0.15	7.861	16.796	14.273	39.348
0.2	7.385	14.716	12.976	31.121
0.25	8.090	13.799	12.426	31.665
0.26	7.519	12.961	11.692	30.410

SITE B				
Depth (m)	Weight (dish)	Weight (dish+ wet sample)	Weight (dish + dry sample)	Water Content (%)
0	7.515	14.488	11.978	56.240
0.05	8.066	26.369	20.594	46.097
0.1	7.523	19.85	15.901	47.135
0.15	8.019	20.085	16.38	44.313
0.2	7.927	15.886	13.828	34.875
0.25	8.189	18.508	16.354	26.381
0.29	7.689	19.892	16.974	31.427

SITE B/C				
Depth (m)	Weight dish	Weight (dish + wet sample)	Weight (dish + dry sample)	Water Content (%)
0	7.911	16.788	14.071	44.107
0.05	8.188	19.286	15.488	52.027
0.1	7.697	17.031	13.669	56.296
0.15	8.016	18.931	14.983	56.667
0.2	7.935	18.53	14.645	57.899
0.25	7.516	17.554	14.024	54.241
0.3	8.085	17.721	14.478	50.727
0.35	8.069	22.735	18.339	42.804
0.4	7.375	16.981	14.251	39.703
0.45	7.752	19.798	15.917	47.532
0.5	7.499	19.772	15.286	57.609
0.55	7.856	17.069	14.137	46.680
0.6	8.015	17.754	13.548	76.017
0.65	7.706	15.652	13.543	36.132
0.7	8.074	13.929	12.688	26.896

SITE C				
Depth (m)	Weight (dish)	Weight (dish + wet sample)	Weight (dish + dry sample)	Water Content (%)
0	8.018	14.857	12.786	43.435
0.05	8.084	23.869	18.751	47.980
0.1	7.396	22.899	18.031	45.773
0.15	8.066	24.712	18.597	58.067
0.2	7.519	24.188	17.791	62.276
0.25	8.012	26.894	21.921	35.754
0.3	7.922	23.082	18.585	42.174
0.35	8.179	21.837	18.047	38.407
0.4	7.681	21.814	15.523	80.222
0.45	7.756	23.946	17.942	58.944
0.5	7.876	28.852	19.449	81.249
0.55	7.860	24.158	18.777	49.290
0.6	8.075	20.713	16.133	56.838
0.65	8.081	24.225	18.713	51.843
0.7	7.700	13.905	12.226	37.097

SITE C/D				
Depth (m)	Weight (dish)	Weight (dish + wet sample)	Weight (dish + dry sample)	Water Content (%)
0	7.520	16.312	13.789	40.246
0.05	7.925	23.574	18.195	52.376
0.1	7.910	20.978	16.961	44.382
0.15	7.909	23.521	18.446	48.164
0.2	8.073	18.880	14.761	61.588
0.25	7.698	18.501	14.872	50.585
0.3	7.516	20.087	16.460	40.552
0.35	8.081	20.760	15.174	78.754
0.4	7.380	16.013	12.304	75.325
0.45	7.858	20.697	15.128	76.602
0.5	7.507	16.245	13.859	37.563
0.55	7.755	18.090	15.435	34.570
0.58	7.757	12.061	10.700	46.245

APPENDIX 4

VANE SHEAR STRENGTH MEASUREMENTS OF GRAVITY CORES

SITE D				
Depth (m)	Weight (dish)	Weight (dish + wet sample)	Weight (dish + dry sample)	Water Content (%)
0	8.189	13.391	11.307	66.838
0.05	7.759	27.430	21.138	47.029
0.1	7.883	27.013	21.345	42.104
0.15	7.850	24.664	20.755	30.291
0.2	7.566	25.397	20.939	33.336
0.25	8.086	27.021	21.930	36.774
0.3	7.402	22.881	16.422	71.608
0.35	8.066	24.108	18.069	60.372
0.4	7.521	26.065	19.482	55.037
0.45	8.016	25.603	20.408	41.922
0.5	7.922	22.500	18.199	41.851
0.55	8.187	27.338	21.480	44.068
0.6	7.688	22.080	17.957	40.150
0.65	7.750	21.485	17.175	45.729
0.7	7.880	23.660	18.456	49.206
0.75	7.861	27.222	21.175	45.418
0.8	7.558	27.280	21.288	43.642
0.85	7.910	12.536	11.456	30.457

XRD sample preparation and procedure

The sample was washed in distilled water in order to allow any salts to be dissolved (Sykes, 1992). Without this, in XRD analysis, an untreated sample would show halite (NaCl) as the main mineral as it has a masking effect on the other minerals. The sample was then centrifuged at 3500 r.p.m for 20 minutes. This concentrates the sediment but leaves the salts in solution which can then be removed. The sediment was then resuspended in distilled water and placed in a sonic bath for 10 minutes. In order to obtain the clay particles, the sediment was sieved through a 63 μm sieve. Material finer than 63 μm was then centrifuged at 1000 r.p.m for 5 minutes. The remaining liquid was decanted and the sediment (the silt-size fraction) put aside. This liquid was then centrifuged at 1700 r.p.m for 15 minutes, the liquid decanted and the sediment (the clay-size fraction) pipetted onto a glass slide. This was then left to dry at room temperature. Once dry, the glass slide was placed in the a Phillips PW1729 x-ray generator and scanned from 5-35°2 θ .

Interpretation of results

Percentages of the individual clay minerals were calculated using the method described by Biscaye (1965).

Biscaye, P.E., 1965. Mineralogy and sedimentation of recent deep-sea clay in the Atlantic Ocean and adjacent seas and oceans. *Geol. Soc. American Bull.*, **76**, pp. 803-832.

Sykes, T.J.S., 1992. *Synthesis of volcanogenic sediment distributions in the Indian Ocean*. Unpub. M.Phil. thesis, University of Wales. 4-4 pp.

	Lat/Lon	% Illite	% Chlorite	% Kaolinite	% Calcite
SITE A	53°37.410'N	47.29	22.81	27.81	2.10
	00°04.283'E				
SITE B	53°38.193'N	57.05	11.97	29.26	1.72
	00°04.091'E				
SITE B/C	53°37.99'N	66.23	16.71	13.69	3.37
	00°03.88'E				
SITE C	53°37.754'N	49.43	15.93	32.34	2.30
	00°04.026'E				
SITE C/D	53°37.754'N	46.30	14.75	36.45	2.50
	00°04.026'E				
SITE D	53°37.412'N	42.89	17.24	38.40	1.48
	00°03.863'E				

Vane shear strength procedure

The vane shear strength of the sediments was carried out using an unmodified Wykeham Farrance Ltd. vane shear apparatus. The shear device consisted of a 4-bladed vane, with each blade 90° from the others. This was driven by a motor at a rotation rate of 89° per minute via pre calibrated springs of differing strengths. When the vane is inserted into the sediment, torque is applied to the vane axis until the sediment shears. When the sample is sheared, the stress pointer moves around the dial, the angle noted and used in the calculation for shear strength. Using Boyce (1977) the shear strength was calculated as follows:-

$$\text{Vane shear strength } (s_u) = \frac{2 \cdot t}{[\pi D^2 (H + \frac{D}{3})]} \times (\text{max. degree spring stress})$$

where:

t = spring torque factor (kNm per degree)

D = vane diameter (0.0127 m)

H = vane height (0.0127 m)

Boyce, R.E., 1977. Deep Sea Drilling Project procedures for shear strength measurement of clayey sediment using modified Wykeham Farrance laboratory vane apparatus. In: Barker, P., Dalziel, I.W.D. *et al.*. *Init. Repts. D.S.D.P. 36*. U.S. Government Printing Office: Washington. pp. 1059-1068.

Site A		
Depth (m)	Water content (%)	Su (kPa)
0	42.026	
0.05	46.741	6.442
0.1	42.279	13.301
0.15	39.348	10.183
0.2	31.121	12.469
0.25	31.665	17.873
0.26	30.410	

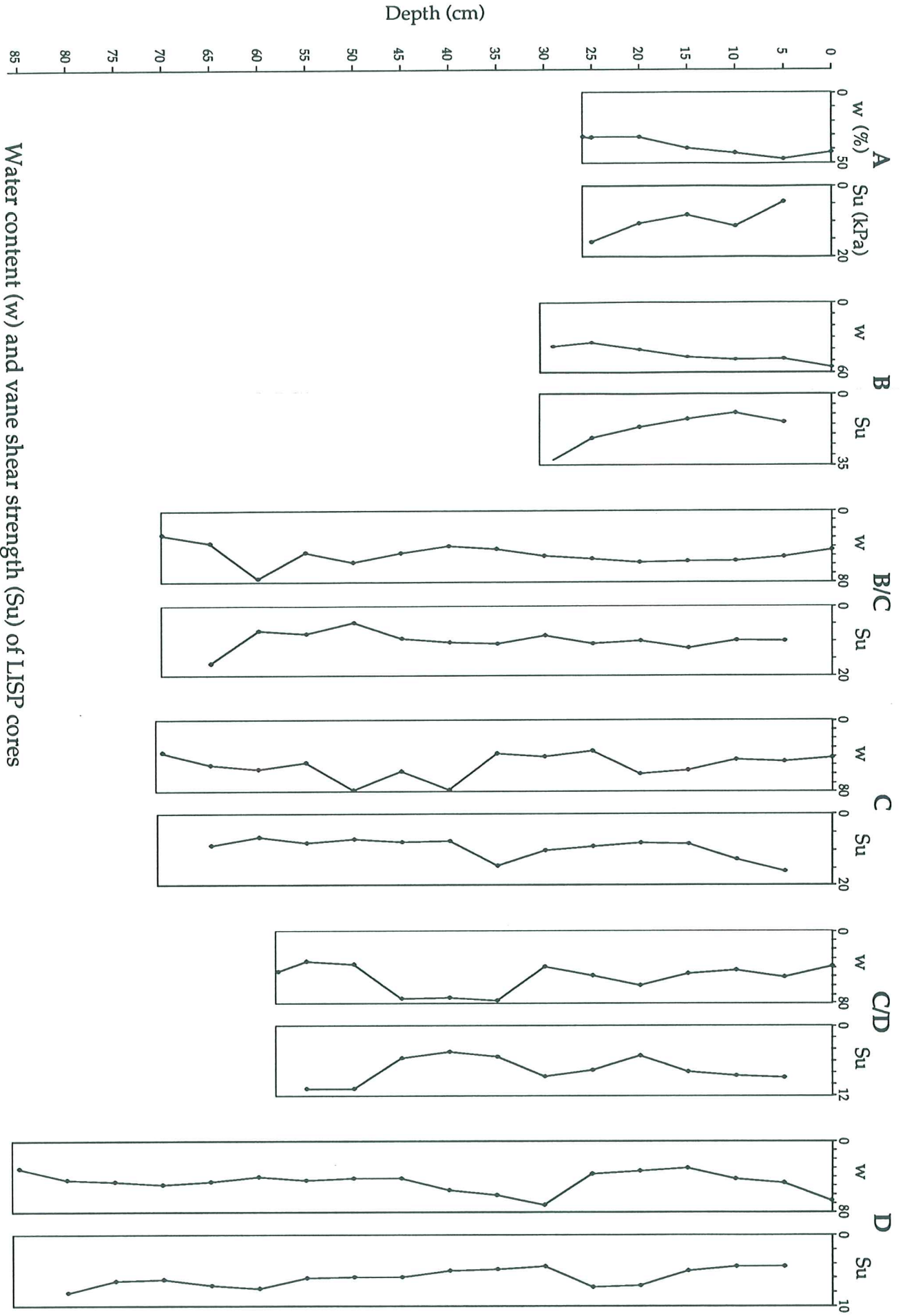
Site B		
Depth (m)	Water content (%)	Su (kPa)
0	56.240	
0.05	46.097	13.924
0.1	47.135	9.352
0.15	44.313	12.469
0.2	34.875	16.210
0.25	26.381	21.971
0.29	31.427	32.701

Site B/C		
Depth (m)	Water content (%)	Su (kPa)
0	44.107	
0.05	52.027	10.079
0.1	56.296	9.872
0.15	56.667	12.054
0.2	57.899	9.975
0.25	54.241	10.807
0.3	50.727	8.521
0.35	42.804	10.807
0.4	39.703	10.391
0.45	47.532	9.352
0.5	57.609	4.780
0.55	46.680	7.897
0.6	76.017	7.066
0.65	36.132	16.522
0.7	26.896	

Site C		
Depth (m)	Water content (%)	Su (kPa)
0	43.435	
0.05	47.980	16.095
0.1	45.773	12.774
0.15	58.067	8.431
0.2	62.276	8.175
0.25	35.754	9.197
0.3	42.174	10.219
0.35	38.407	14.562
0.4	80.222	7.664
0.45	58.944	7.920
0.5	81.249	7.153
0.55	49.290	8.209
0.6	56.838	6.546
0.65	51.843	8.936
0.7	37.097	

Site C/D		
Depth (cm)	Water content (%)	Su (kPa)
0	40.246	
0.05	52.376	8.936
0.1	44.382	8.625
0.15	48.164	7.897
0.2	61.588	5.196
0.25	50.585	7.689
0.3	40.552	8.729
0.35	78.754	5.299
0.4	75.325	4.468
0.45	76.602	5.611
0.5	37.563	10.807
0.55	34.570	10.807
0.58	46.245	

Site D		
Depth (m)	Water content (%)	Su (kPa)
0	66.838	
0.05	47.029	4.364
0.1	42.104	4.364
0.15	30.291	4.988
0.2	33.336	7.066
0.25	36.774	7.274
0.3	71.608	4.364
0.35	60.372	4.780
0.4	55.037	4.988
0.45	41.922	5.923
0.5	41.851	5.923
0.55	44.068	6.027
0.6	40.150	7.482
0.65	45.729	7.066
0.7	49.206	6.235
0.75	45.418	6.442
0.8	43.642	8.105
0.85	30.457	



Water content (w) and vane shear strength (Su) of LISP cores

APPENDIX 5

GRAIN SIZE ANALYSES OF SURFACE SEDIMENTS

Grain size procedure

A sample approximately 2 g in size was taken from the surface of the core. This was then immersed in Calgon (10%) and left for 24 hours. The sample was then wet sieved through a 90 micron sieve. Any sediment retained in the sieve was placed to dry in the oven. Once dry, this was weighed in order to calculate the percentage greater than 90 microns in diameter and thus the percentage finer than 90 microns. When this was known, the finer fraction was placed in an sonic bath for 2 minutes and then run through a Micromeritics Sedigraph™ to produce the grain size distribution for the finer fraction.

GRAIN SIZE

PAGE 1

SediGraph 5100 V2.02

SAMPLE DIRECTORY/NUMBER: SVLHUM /6
 SAMPLE ID: SITE A SURFACE
 SUBMITTER: UWCC EARTH SCIENCES
 OPERATOR: J.HERNIMAN
 SAMPLE TYPE: CLAY
 LIQUID TYPE: Water
 ANALYSIS TEMP: 31.5 deg C RUN TYPE: High Speed

UNIT NUMBER: 1
 START 16:14:11 10/20/95
 REPRT 16:18:45 10/20/95
 TOT RUN TIME 0:04:14
 SAM DENS: 2.7500 g/cc
 LIQ DENS: 0.9958 g/cc
 LIQ VISC: 0.7766 cp

STARTING DIAMETER: 90.00 μ m
 ENDING DIAMETER: 0.50 μ m

REYNOLDS NUMBER: 1.15
 FULL SCALE MASS %: 87

MASS DISTRIBUTION

MEDIAN DIAMETER: 27.40 μ m

MODAL DIAMETER: 43.00 μ m

DIAMETER (μ m)	CUMULATIVE MASS FINER (%)	MASS IN INTERVAL (%)
90.00	88.6	3.4
75.00	81.5	2.1
63.00	77.7	3.8
53.00	72.4	5.3
44.00	65.8	6.6
37.00	59.6	6.2
31.00	53.7	5.9
26.00	48.6	5.1
22.00	44.3	4.3
18.00	39.5	4.8
15.00	36.4	3.1
13.00	33.6	2.8
11.00	31.9	1.7
9.20	30.2	1.7
7.80	28.6	1.6
6.40	27.0	1.7
5.40	25.6	1.4
4.60	24.1	1.5
3.90	22.5	1.6
3.20	21.3	1.1
2.70	20.7	0.7
2.30	19.7	1.0
2.00	18.3	1.1
1.60	17.2	1.3
1.30	16.5	0.7
1.10	15.8	0.7
0.98	15.2	0.6
0.82	14.2	1.0
0.68	13.2	1.0

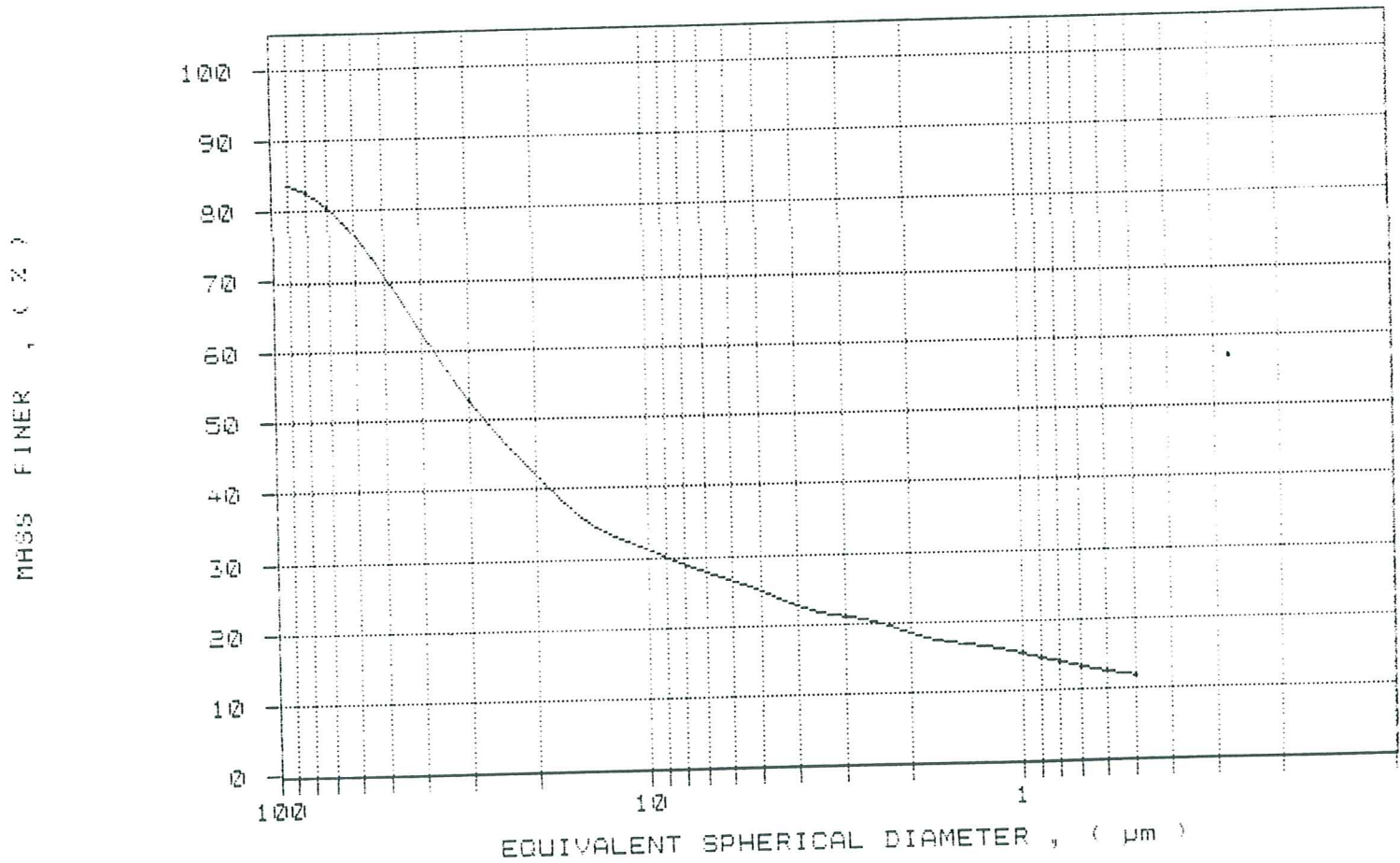
GRAIN SIZE

SediGraph 5100 V2.02

SAMPLE DIRECTORY/NUMBER: SVLHUM /6
SAMPLE ID: SITE A SURFACE
SUBMITTER: UWCC EARTH SCIENCES
OPERATOR: J.HERNIMAN
SAMPLE TYPE: CLAY
LIQUID TYPE: Water
ANALYSIS TEMP: 31.5 deg C RUN TYPE: High Speed

UNIT NUMBER: 1
START 16:14:11 10/20/95
REPRT 16:18:45 10/20/95
TOT RUN TIME @:04:14
SAM DENS: 2.7500 g/cc
LIQ DENS: 0.9953 g/cc
LIQ VISC: 0.7766 cp

CUMULATIVE MASS PERCENT FINER VS. DIAMETER



GRAIN SIZE

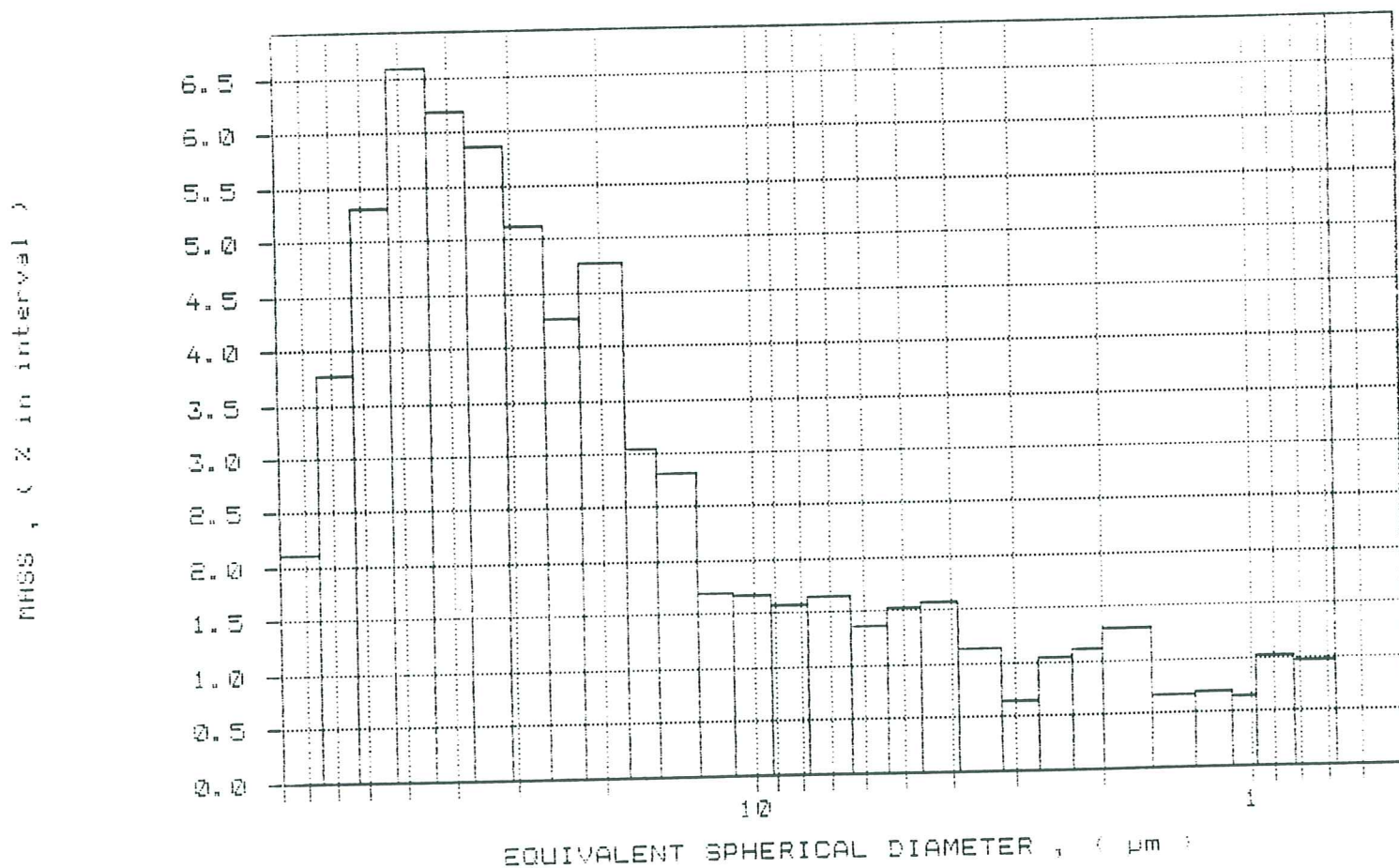
SediGraph 5100 V2.02

SAMPLE DIRECTORY/NUMBER: SVLHUM /6
 SAMPLE ID: SITE A SURFACE
 SUBMITTER: UWCC EARTH SCIENCES
 OPERATOR: J.HERNIMAN
 SAMPLE TYPE: CLAY
 LIQUID TYPE: Water
 ANALYSIS TEMP: 31.5 deg C

UNIT NUMBER: 1
 START 16:14:11 10/20/95
 REPR 16:18:45 10/20/95
 TOT RUN TIME @:04:14
 SAM DENS: 2.7500 g/cc
 LIQ DENS: 0.9953 g/cc
 LIQ VISC: 0.7766 cp

RUN TYPE: High Speed

MASS POPULATION VS. DIAMETER



GRAIN SIZE

SediGraph 5100 V2.02

SAMPLE DIRECTORY/NUMBER: SVLHUM /1
 SAMPLE ID: SITE B SURFACE
 SUBMITTER: UWCC EARTH SCIENCES
 OPERATOR: J.HERNIMAN
 SAMPLE TYPE: CLAY
 LIQUID TYPE: Water
 ANALYSIS TEMP: 34.7 deg C RUN TYPE: High Speed

UNIT NUMBER: 1
 START 11:54:10 09/19/95
 REPR 11:58:41 09/19/95
 TOT RUN TIME @:04:13
 SAM DENS: 2.7500 g/cc
 LIQ DENS: 0.9942 g/cc
 LIQ VISC: 0.7270 cp

STARTING DIAMETER: 90.00 μ m
 ENDING DIAMETER: 0.50 μ m

REYNOLDS NUMBER: 1.31
 FULL SCALE MASS %: 100

MASS DISTRIBUTION

MEDIAN DIAMETER: 6.72 μ m

MODAL DIAMETER: 35.31 μ m

DIAMETER (μ m)	CUMULATIVE MASS FINER (%)	MASS IN INTERVAL (%)
90.00	99.2	0.8
75.00	98.0	1.1
63.00	96.6	1.4
53.00	94.7	2.0
44.00	91.4	3.3
37.00	87.0	4.4
31.00	82.2	4.8
26.00	78.0	4.1
22.00	74.6	3.5
18.00	69.9	4.6
15.60	66.2	3.7
13.00	61.3	4.9
11.00	57.3	4.0
9.20	54.3	3.0
7.80	52.2	2.1
6.40	49.2	3.0
5.40	46.6	2.6
4.60	44.5	2.1
3.90	42.6	2.0
3.20	40.1	2.4
2.70	37.7	2.4
2.30	35.6	2.1
2.00	34.2	1.4
1.60	31.7	2.5
1.30	29.4	2.3
1.10	28.3	1.1
0.98	27.5	0.8
0.82	25.6	1.8
0.68	23.5	2.2

GRAIN SIZE

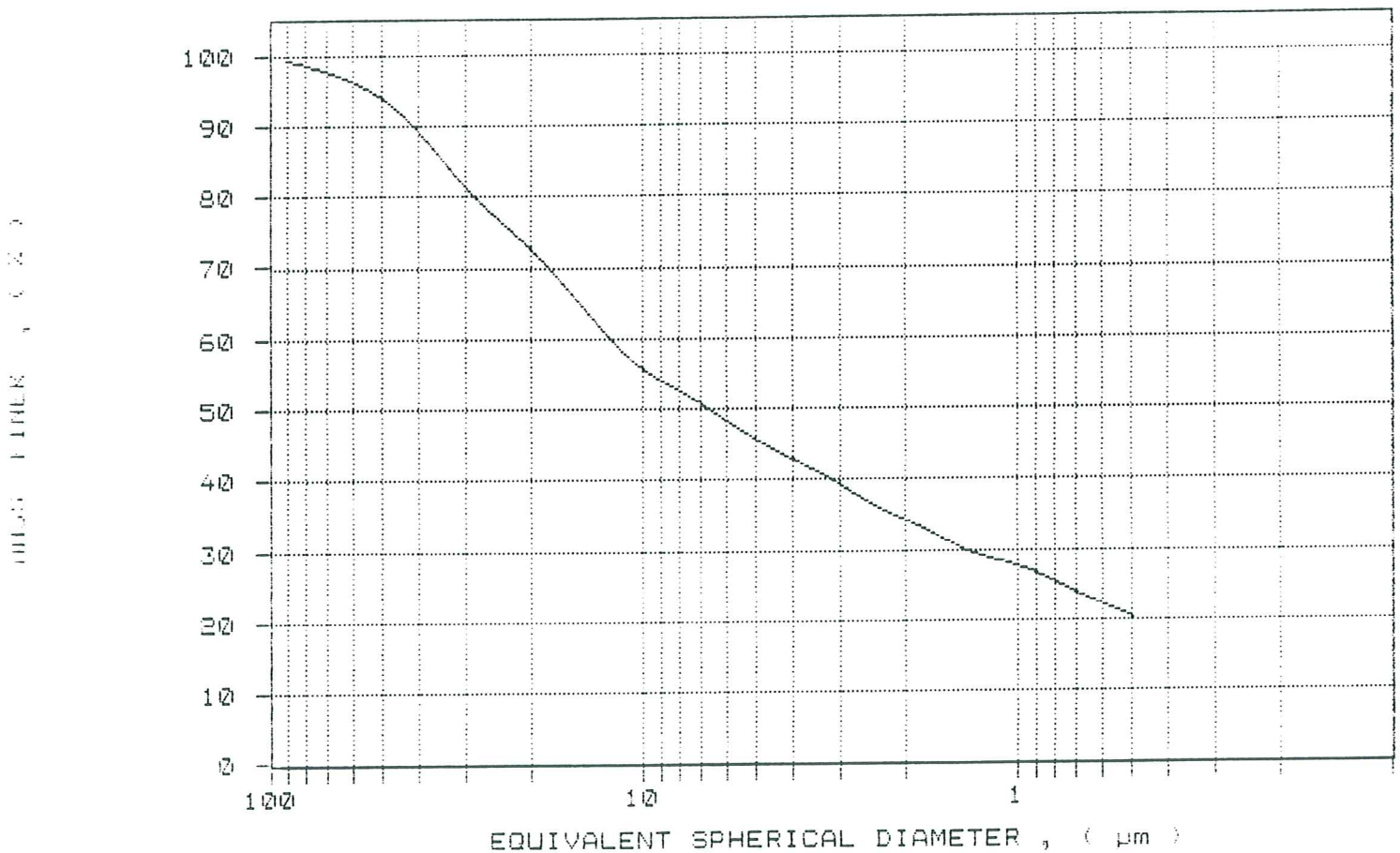
SediGraph 5100 V2.02

PAGE 2

SAMPLE DIRECTORY/NUMBER: SVLHUM /1
SAMPLE ID: SITE B SURFACE
SUBMITTER: UWCC EARTH SCIENCES
OPERATOR: J.HERNIMAN
SAMPLE TYPE: CLAY
LIQUID TYPE: Water
ANALYSIS TEMP: 34.7 deg C RUN TYPE: High Speed

UNIT NUMBER: 1
START 11:54:10 09/19/95
REPT 11:58:41 09/19/95
TOT RUN TIME 0:04:13
SAM DENS: 2.7500 g/cc
LIQ DENS: 0.9942 g/cc
LIQ VISC: 0.7270 cp

CUMULATIVE MASS PERCENT FINER VS. DIAMETER



GRAIN SIZE

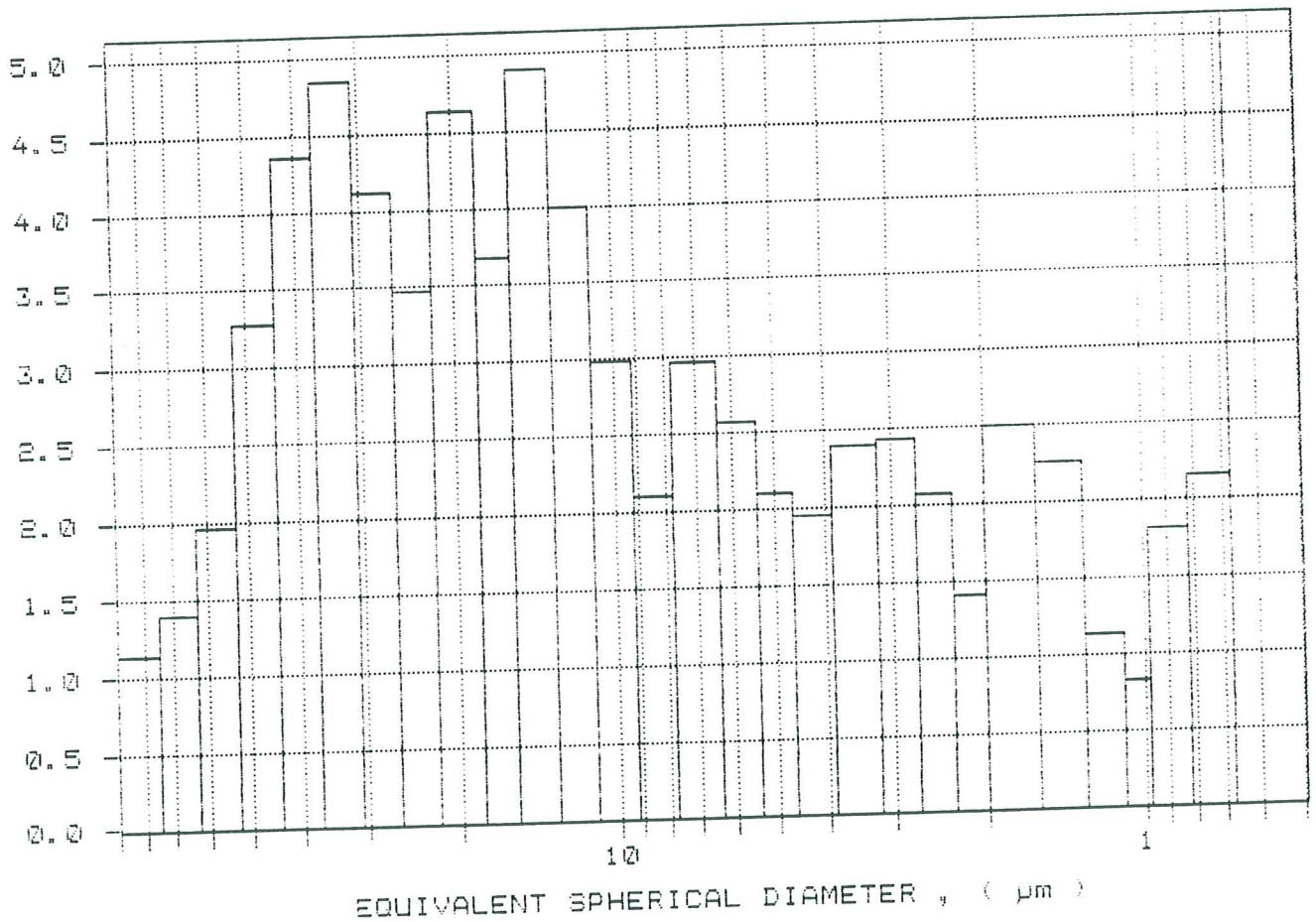
SediGraph 5100 V2.02

SAMPLE DIRECTORY/NUMBER: SVLHUM /1
 SAMPLE ID: SITE B SURFACE
 SUBMITTER: UWCC EARTH SCIENCES
 OPERATOR: J.HERNIMAN
 SAMPLE TYPE: CLAY
 LIQUID TYPE: Water
 ANALYSIS TEMP: 34.7 deg C

RUN TYPE: High Speed

UNIT NUMBER: 1
 START 11:54:10 09/19/95
 REPT 11:58:41 09/19/95
 TOT RUN TIME @:04:19
 SAM DENS: 2.7500 g/cc
 LIQ DENS: 0.9942 g/cc
 LIQ VISC: 0.7270 cp

MASS POPULATION VS. DIAMETER



SediGraph 5100 V2.02

SAMPLE DIRECTORY/NUMBER: SVLHUM /4
 SAMPLE ID: SITE B/C SURFACE
 SUBMITTER: UWCC EARTH SCIENCES
 OPERATOR: J.HERNIMAN
 SAMPLE TYPE: CLAY
 LIQUID TYPE: Water
 ANALYSIS TEMP: 31.4 deg C RUN TYPE: High Speed

UNIT NUMBER: 1
 START 15:38:26 10/20/95
 REPR 15:43:08 10/20/95
 TOT RUN TIME 0:04:26
 SAM DENS: 2.7500 g/cc
 LIQ DENS: 0.9958 g/cc
 LIQ VISC: 0.7777 cp

STARTING DIAMETER: 90.00 μ m
 ENDING DIAMETER: 0.50 μ m

REYNOLDS NUMBER: 1.15
 FULL SCALE MASS %: 99

MASS DISTRIBUTION

MEDIAN DIAMETER: 14.12 μ m

MODAL DIAMETER: 33.07 μ m

DIAMETER (μ m)	CUMULATIVE MASS FINER (%)	MASS IN INTERVAL (%)
90.00	95.0	4.0
75.00	94.1	0.9
63.00	92.5	1.6
53.00	89.9	2.6
44.00	85.3	4.4
37.00	80.2	5.4
31.00	74.0	6.1
26.00	66.1	6.9
22.00	58.0	6.1
18.00	57.2	5.6
15.60	53.0	4.2
13.00	47.5	5.5
11.00	43.3	4.3
9.20	40.1	3.2
7.80	37.3	2.6
6.40	35.0	2.6
5.40	32.4	2.6
4.60	29.9	2.5
3.90	27.8	2.1
3.20	25.9	1.9
2.70	24.0	1.9
2.30	21.7	2.3
2.00	19.7	1.9
1.60	17.6	2.2
1.30	15.5	2.0
1.10	13.6	1.8
0.98	12.7	1.1
0.82	11.6	1.4
0.68	9.9	1.4

GRAIN SIZE

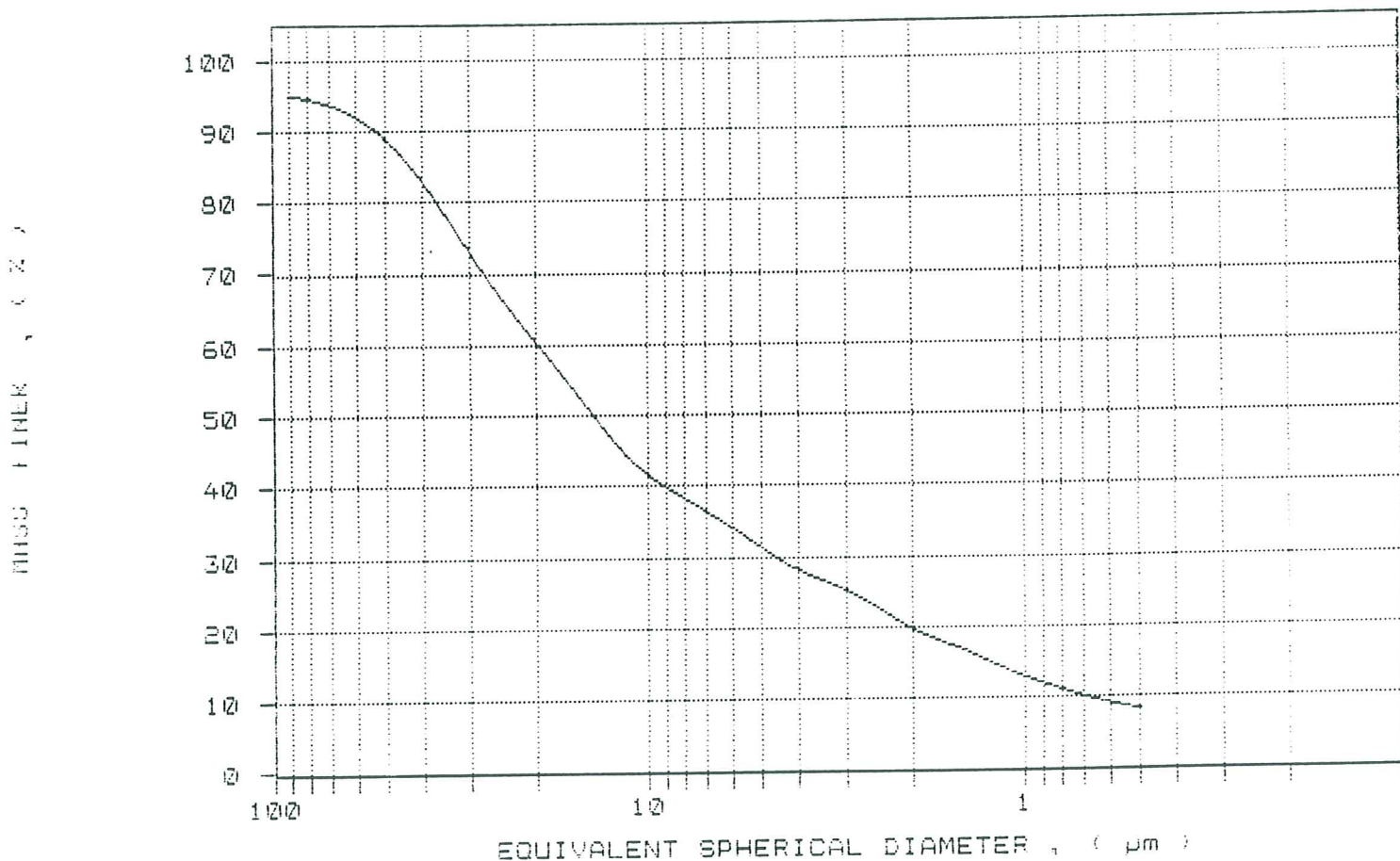
SediGraph 5100 V2.02

PAGE 2

SAMPLE DIRECTORY/NUMBER: SVLHUM /4
SAMPLE ID: SITE B/C SURFACE
SUBMITTER: UWCC EARTH SCIENCES
OPERATOR: J.HERNIMAN
SAMPLE TYPE: CLAY
LIQUID TYPE: Water
ANALYSIS TEMP: 31.4 deg C RUN TYPE: High Speed

UNIT NUMBER: 1
START 15:38:26 10/20/95
REFRT 15:43:08 10/20/95
TOT RUN TIME 0:04:26
SAM DENS: 2.7500 g/cc
LIQ DENS: 0.9956 g/cc
LIQ VISC: 0.7777 cp

CUMULATIVE MASS PERCENT FINER VS. DIAMETER



GRAIN SIZE

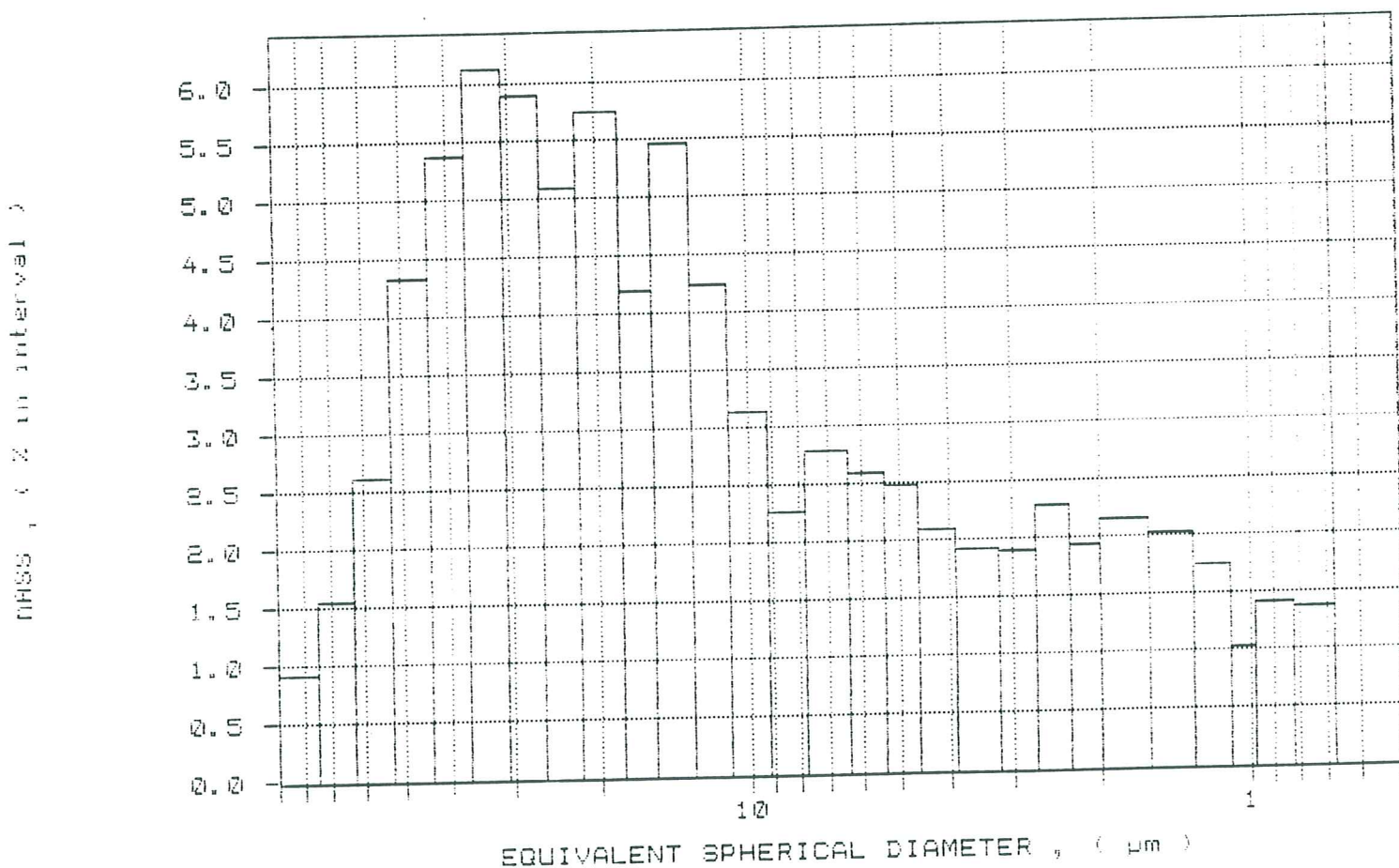
SediGraph 5100 V2.02

SAMPLE DIRECTORY/NUMBER: SVLHUM /4
 SAMPLE ID: SITE B/C SURFACE
 SUBMITTER: UWCC EARTH SCIENCES
 OPERATOR: J.HERNIMAN
 SAMPLE TYPE: CLAY
 LIQUID TYPE: Water
 ANALYSIS TEMP: 31.4 deg C

UNIT NUMBER: 1
 START 15:38:26 10/20/95
 REPT 15:48:08 10/20/95
 TOT RUN TIME 0:04:25
 SAM DENS: 2.7500 g/cc
 LIQ DENS: 0.9998 g/cc
 LIQ VISC: 0.7777 cp

RUN TYPE: High Speed

MASS POPULATION VS. DIAMETER



SediGraph 5100 V2.02

GRAIN SIZE

PAGE 1

SAMPLE DIRECTORY/NUMBER: SVLHUM /2
SAMPLE ID: SITE C SURFACE
SUBMITTER: UWCC EARTH SCIENCES
OPERATOR: J.HERNIMAN
SAMPLE TYPE: CLAY
LIQUID TYPE: Water
ANALYSIS TEMP: 34.7 deg C RUN TYPE: High Speed

UNIT NUMBER: 1
START 12:08:49 09/19/95
REPT 12:59:22 09/19/95
TOT RUN TIME 0:08:58
SAM DENS: 2.7500 g/cc
LIQ DENS: 0.9942 g/cc
LIQ VISC: 0.7268 cp

STARTING DIAMETER: 90.00 μ m
ENDING DIAMETER: 0.50 μ m

REYNOLDS NUMBER: 1.81
FULL SCALE MASS %: 91

MEDIAN DIAMETER: 28.05 μ m MASS DISTRIBUTION MODAL DIAMETER: 50.02 μ m

DIAMETER (μ m)	CUMULATIVE MASS FINER (%)	MASS IN INTERVAL (%)
90.00	87.8	3.2
75.00	85.6	2.1
63.00	80.8	4.9
53.00	73.6	7.2
44.00	65.2	8.3
37.00	58.3	7.0
31.00	52.5	5.7
26.00	48.4	4.1
22.00	45.8	2.7
18.00	43.5	2.3
15.00	41.8	1.7
13.00	39.4	2.4
11.00	37.6	1.7
9.20	36.2	1.4
7.30	34.9	1.3
6.40	33.2	1.7
5.40	31.4	1.8
4.60	30.0	1.4
3.90	29.2	0.8
3.20	28.0	1.1
2.70	26.5	1.5
2.30	24.9	1.6
2.00	23.6	1.3
1.60	21.7	1.9
1.30	19.7	2.0
1.10	18.3	1.4
0.98	17.5	0.8
0.82	16.1	1.4
0.68	14.8	1.2

GRAIN SIZE

SediGraph 5100 V2.02

PAGE 2

SAMPLE DIRECTORY/NUMBER: SVLHUM /2
SAMPLE ID: SITE C SURFACE
SUBMITTER: UWCC EARTH SCIENCES
OPERATOR: J.HERNIMAN
SAMPLE TYPE: CLAY
LIQUID TYPE: Water
ANALYSIS TEMP: 34.7 deg C RUN TYPE: High Speed

UNIT NUMBER: 1
START 12:08:49 09/19/95
REPT 12:59:22 09/19/95
TOT RUN TIME 0:05:58
SAM DENS: 2.7500 g/cc
LIQ DENS: 0.9942 g/cc
LIQ VISC: 0.7258 cp

CUMULATIVE MASS PERCENT FINER VS. DIAMETER



SediGraph 5100 V2.02

GRAIN SIZE

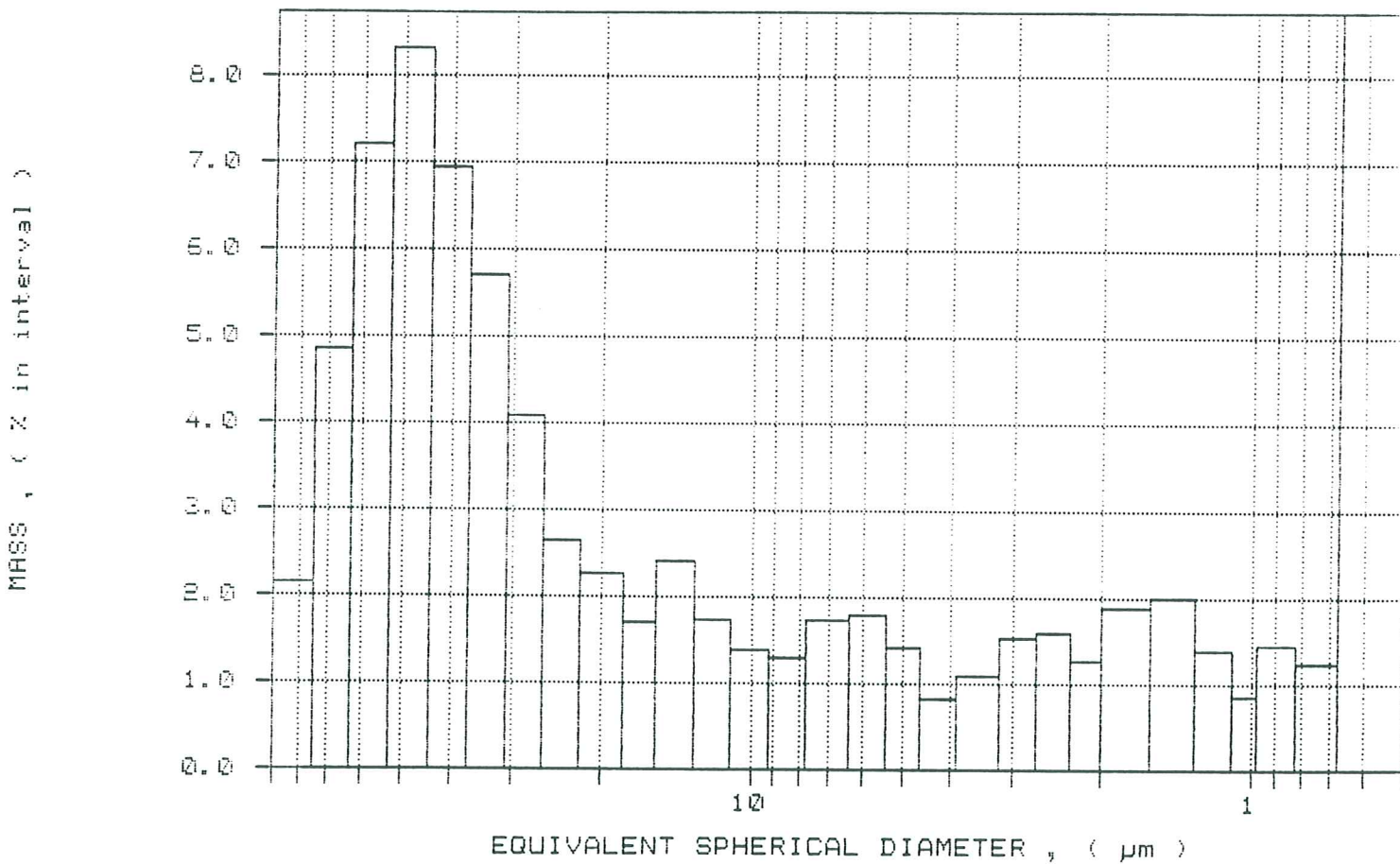
PAGE 1

SAMPLE DIRECTORY/NUMBER: SVLHUM 1/2
SAMPLE ID: SITE C SURFACE
SUBMITTER: UNCC EARTH SCIENCES
OPERATOR: J.HERNIMAN
SAMPLE TYPE: CLAY
LIQUID TYPE: Water
ANALYSIS TEMP: 34.7 deg C

RUN TYPE: High Speed

UNIT NUMBER: 1
START 12:08:49 09/19/77
REPT 12:59:22 09/19/77
TOT RUN TIME 0:08:17
SAM DENS: 2.7500 g/cc
LIQ DENS: 0.9942 g/cc
LIQ VISC: 0.7268 cP

MASS POPULATION VS. DIAMETER



GRAIN SIZE

SediGraph 5100 V2.02

SAMPLE DIRECTORY/NUMBER: SVLHUM /5
 SAMPLE ID: SITE C/D SURFACE
 SUBMITTER: UWCC EARTH SCIENCES
 OPERATOR: J.HERNIMAN
 SAMPLE TYPE: CLAY
 LIQUID TYPE: Water
 ANALYSIS TEMP: 31.4 deg C RUN TYPE: High Speed

UNIT NUMBER: 1
 START 16:00:18 10/20/95
 REPR 16:04:45 10/20/95
 TOT RUN TIME 0:04:09
 SAM DENS: 2.7500 g/cc
 LIQ DENS: 0.9958 g/cc
 LIQ VISC: 0.7769 cp

STARTING DIAMETER: 90.00 μ m
 ENDING DIAMETER: 0.50 μ m

REYNOLDS NUMBER: 1.15
 FULL SCALE MASS %: 98

MASS DISTRIBUTION

MEDIAN DIAMETER: 17.81 μ m

MODAL DIAMETER: 47.82 μ m

DIAMETER (μ m)	CUMULATIVE MASS FINER (%)	MASS IN INTERVAL (%)
90.00	99.4	-1.4
75.00	91.4	8.1
63.00	87.2	4.2
53.00	81.0	6.2
44.00	73.5	7.5
37.00	67.0	6.5
31.00	61.5	5.5
26.00	57.1	4.4
22.00	53.7	3.4
18.00	50.2	3.5
15.60	47.7	2.4
13.00	45.0	2.7
11.00	42.9	2.1
9.20	40.4	2.5
7.80	38.0	2.4
6.40	35.4	2.6
5.40	33.5	1.9
4.60	31.9	1.6
3.90	30.4	1.5
3.20	28.4	2.0
2.70	26.7	1.7
2.30	25.2	1.5
2.00	24.0	1.2
1.60	22.0	1.9
1.30	20.4	1.6
1.10	19.1	1.3
0.98	18.3	0.8
0.82	17.2	1.1
0.68	16.1	1.1

GRAIN SIZE

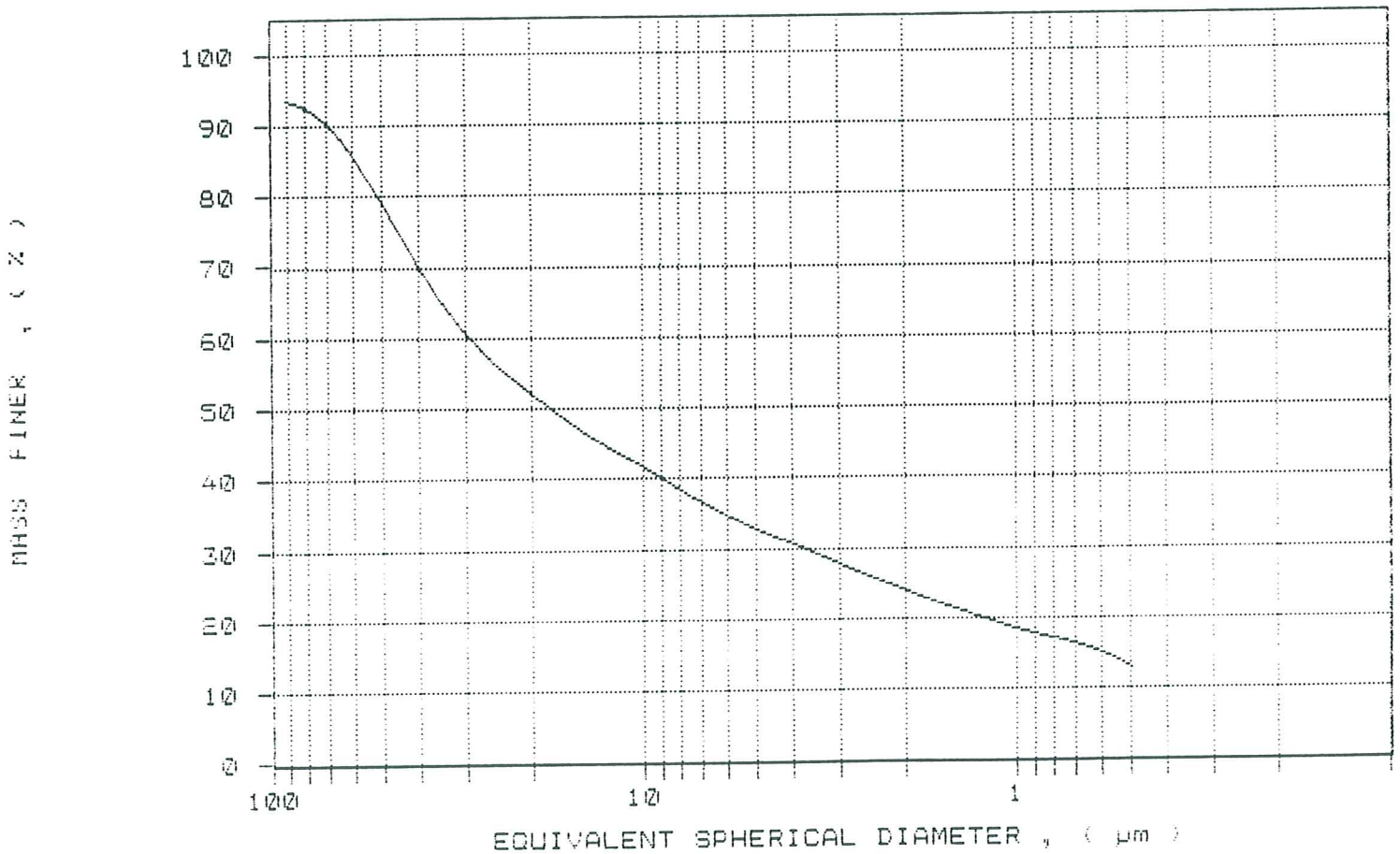
SediGraph 5100 V2.02

PAGE 2

SAMPLE DIRECTORY/NUMBER: SVLHUM /5
SAMPLE ID: SITE C/D SURFACE
SUBMITTER: UWCC EARTH SCIENCES
OPERATOR: J.HERNIMAN
SAMPLE TYPE: CLAY
LIQUID TYPE: Water
ANALYSIS TEMP: 31.4 deg C RUN TYPE: High Speed

UNIT NUMBER: 1
START 16:00:18 10/20/95
REPT 16:04:45 10/20/95
TOT RUN TIME 0:04:09
SAM DENS: 2.7500 g/cc
LIQ DENS: 0.9958 g/cc
LIQ VISC: 0.7769 cp

CUMULATIVE MASS PERCENT FINER VS. DIAMETER



GRAIN SIZE

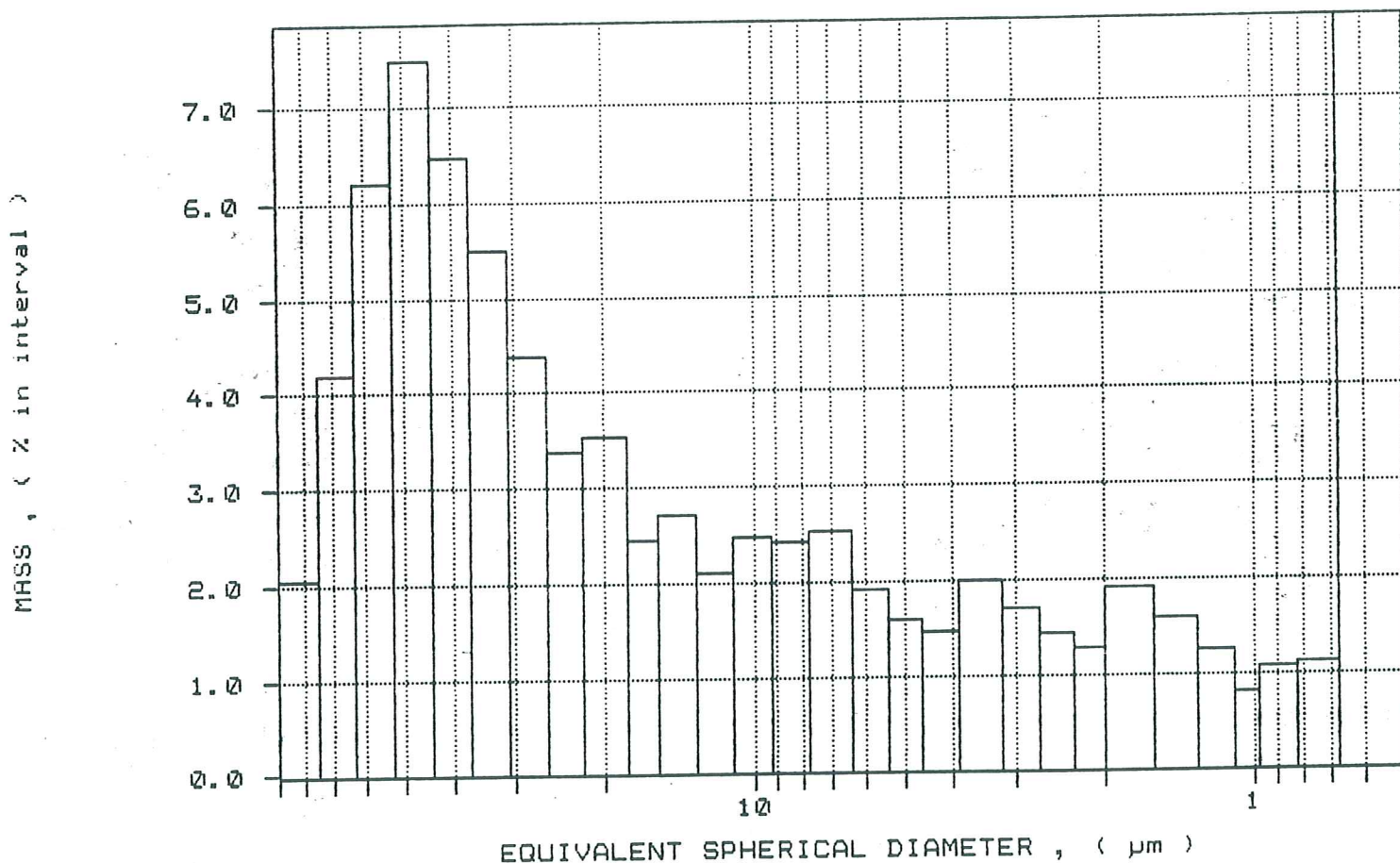
SediGraph 5100 V2.02

SAMPLE DIRECTORY/NUMBER: SVLHUM /5
 SAMPLE ID: SITE C/D SURFACE
 SUBMITTER: UWCC EARTH SCIENCES
 OPERATOR: J.HERNIMAN
 SAMPLE TYPE: CLAY
 LIQUID TYPE: Water
 ANALYSIS TEMP: 31.4 deg C

UNIT NUMBER: 1
 START 16:00:18 10/20/95
 REPT 16:04:45 10/20/95
 TOT RUN TIME 0:04:09
 SAM DENS: 2.7500 g/cc
 LIQ DENS: 0.9953 g/cc
 LIQ VISC: 0.7769 cp

RUN TYPE: High Speed

MASS POPULATION VS. DIAMETER



GRAIN SIZE

SediGraph 5100 V2.02

PAGE 1

SAMPLE DIRECTORY/NUMBER: SVLHUM /3
 SAMPLE ID: SITE D SURFACE
 SUBMITTER: UWCC EARTH SCIENCES
 OPERATOR: J.HERNIMAN
 SAMPLE TYPE: CLAY
 LIQUID TYPE: Water
 ANALYSIS TEMP: 34.7 deg C RUN TYPE: High Speed

UNIT NUMBER: 1
 START 13:12:17 09/19/95
 REPR 13:16:30 09/19/95
 TOT RUN TIME 0:03:56
 SAM DENS: 2.7500 g/cc
 LIQ DENS: 0.9942 g/cc
 LIQ VISC: 0.7268 cp

STARTING DIAMETER: 90.00 μ m
 ENDING DIAMETER: 0.50 μ m

REYNOLDS NUMBER: 1.31
 FULL SCALE MASS %: 93

MASS DISTRIBUTION

MEDIAN DIAMETER: 12.03 μ m MODAL DIAMETER: 35.29 μ m

DIAMETER (μ m)	CUMULATIVE MASS FINER (%)	MASS IN INTERVAL (%)
90.00	91.3	1.7
75.00	90.2	1.1
63.00	87.4	2.8
53.00	83.1	4.3
44.00	78.0	5.2
37.00	73.0	5.0
31.00	67.3	5.2
26.00	63.2	4.6
22.00	59.7	3.5
18.00	56.2	3.5
15.60	53.9	2.3
13.00	51.1	2.8
11.00	48.3	2.3
9.20	46.5	2.3
7.80	44.6	1.9
6.40	42.3	1.9
5.40	41.1	1.6
4.60	39.3	1.8
3.90	37.5	1.8
3.20	35.3	1.8
2.70	33.3	2.0
2.30	31.6	2.2
2.00	30.1	1.5
1.60	28.5	1.6
1.30	26.4	2.1
1.10	24.3	2.1
0.98	23.0	1.3
0.82	21.3	1.8
0.68	19.5	1.8

GRAIN SIZE

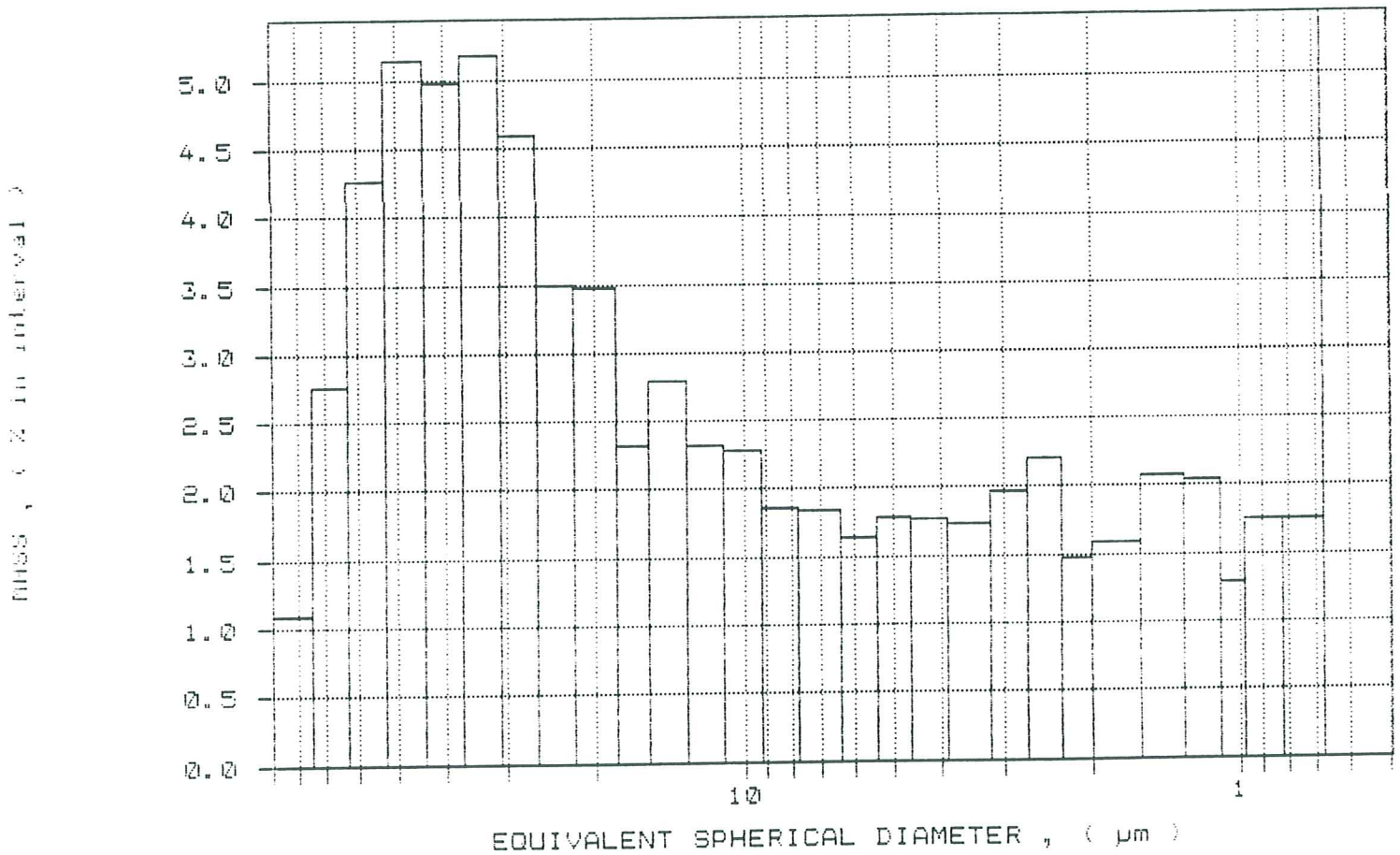
SediGraph 5100 V2.0E

PAGE 2

SAMPLE DIRECTORY/NUMBER: SVLHUM /3
 SAMPLE ID: SITE D SURFACE
 SUBMITTER: UWCC EARTH SCIENCES
 OPERATOR: J.HERNIMAN
 SAMPLE TYPE: CLAY
 LIQUID TYPE: Water
 ANALYSIS TEMP: 34.7 deg C

UNIT NUMBER: 1
 START 13:12:17 09/19/95
 REPT 13:16:30 09/19/95
 TOT RUN TIME @:08:56
 SAM DENS: 2.7500 g/cc
 LIQ DENS: 0.9942 g/cc
 LIQ VISC: 0.7268 cp

MASS POPULATION VS. DIAMETER



SediGraph 5100 V2.02

GRAIN SIZE

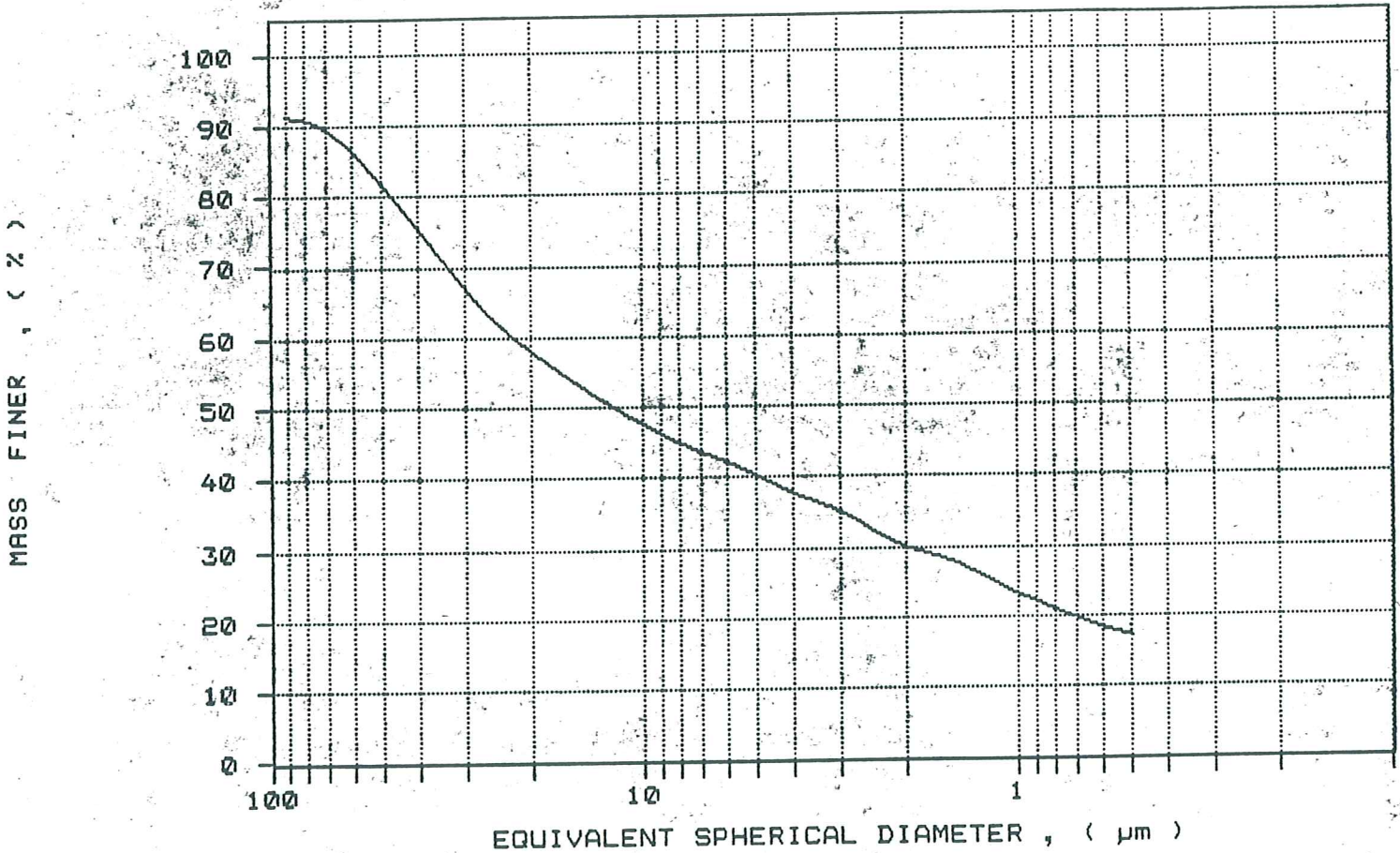
PAGE 1

SAMPLE DIRECTORY/NUMBER: SVLHUM /3
SAMPLE ID: SITE D SURFACE
SUBMITTER: UWCC EARTH SCIENCES
OPERATOR: J.HERNIMAN
SAMPLE TYPE: CLAY
LIQUID TYPE: Water
ANALYSIS TEMP: 34.7 deg C




UNIT NUMBER: 1
START 13:12:17 09/19/95
REPRT 13:22:59 09/19/95
TOT RUN TIME 0:03:56
SAM DENS: 2.7500 g/cc
LIQ DENS: 0.9942 g/cc
LIQ VISC: 0.7268 cp

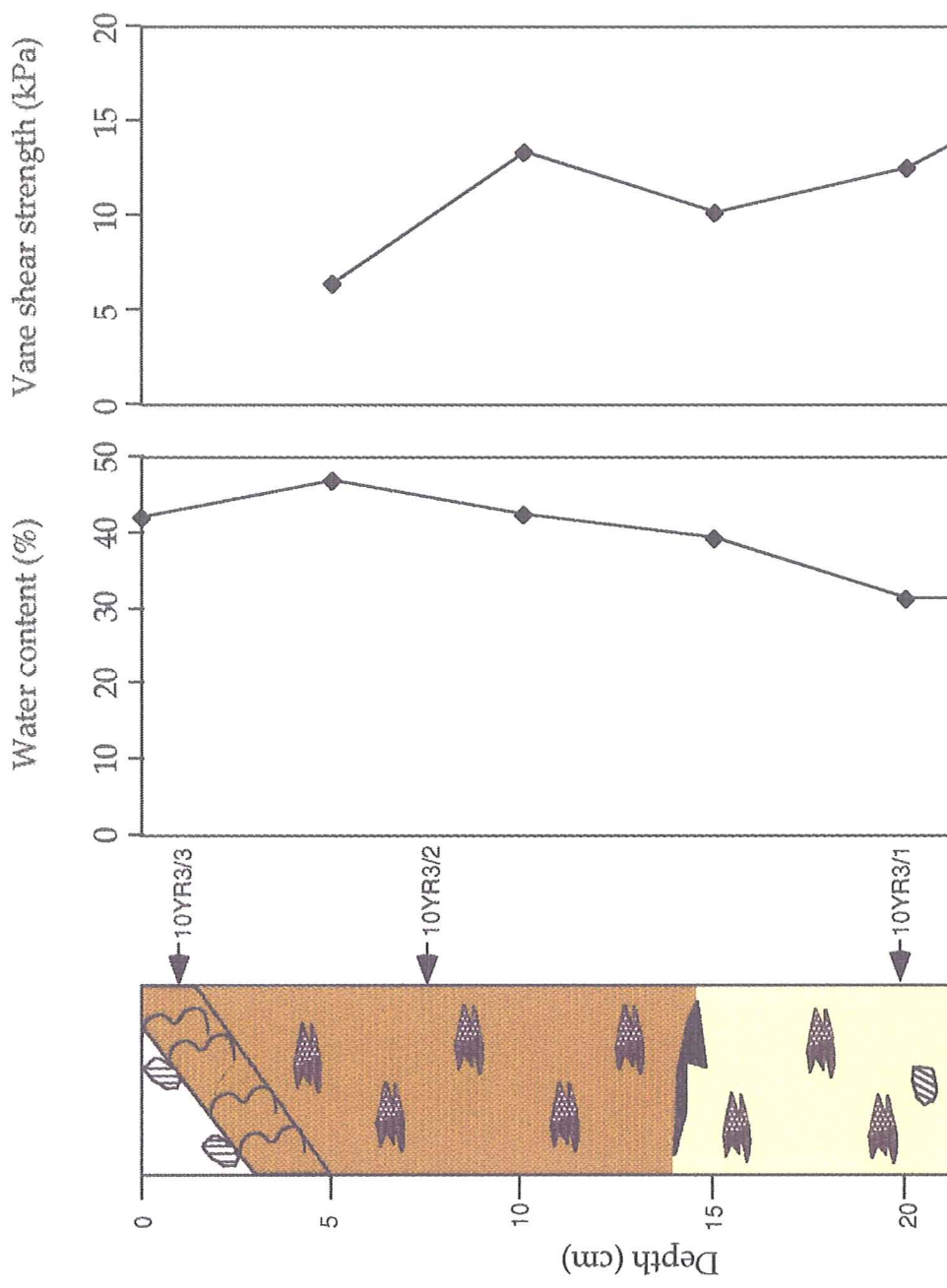
RUN TYPE: High Speed

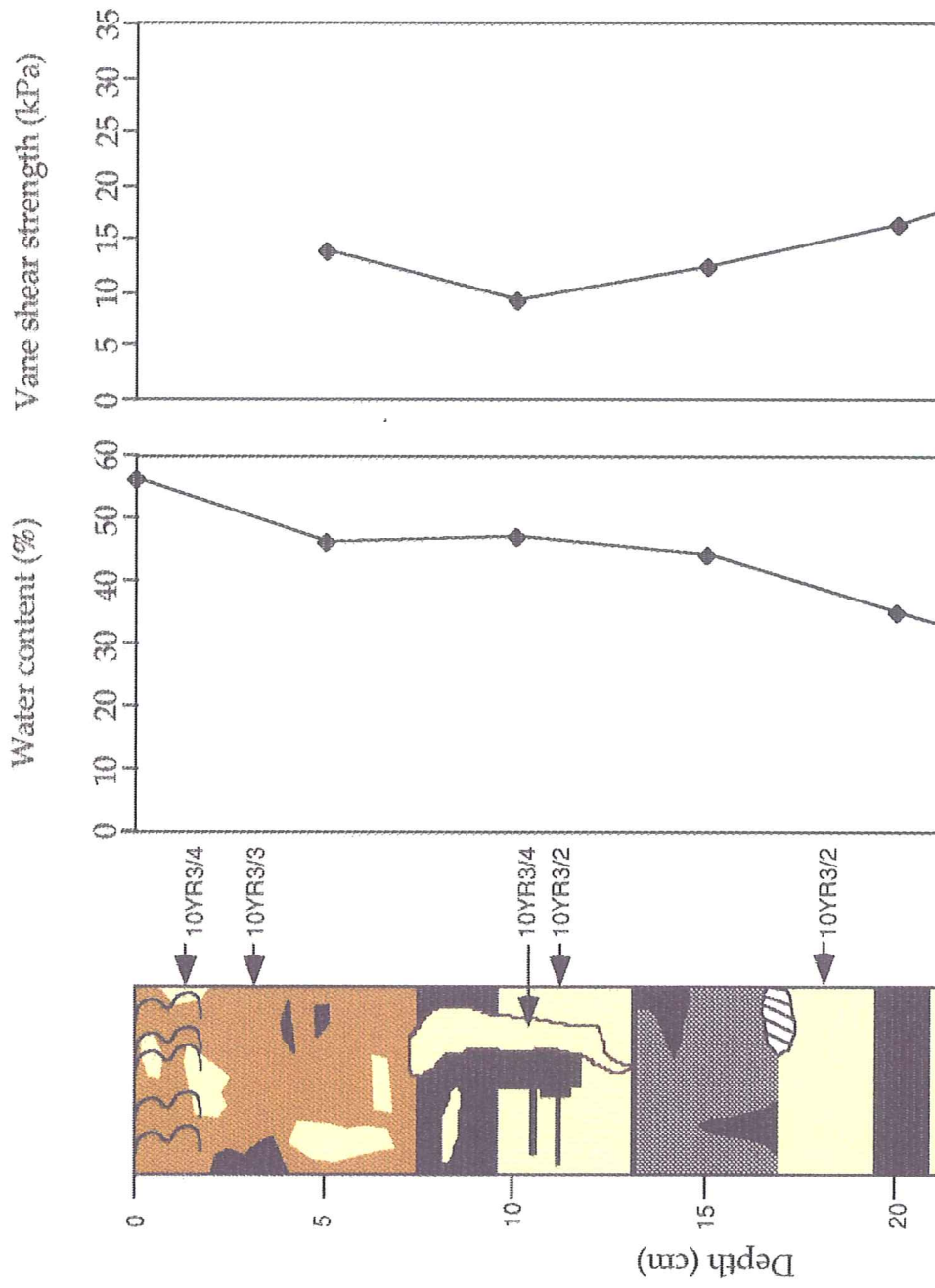
CUMULATIVE MASS PERCENT FINER VS. DIAMETER



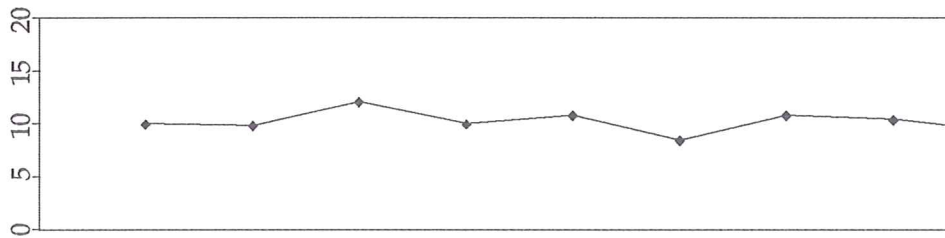
Key

	Coarse sand
	Sand
	Silty clay
	Clay
	Black organic-rich clay
	Grey organic-rich clay
	Interbedded sand, silty clay, clay and organic-rich clay

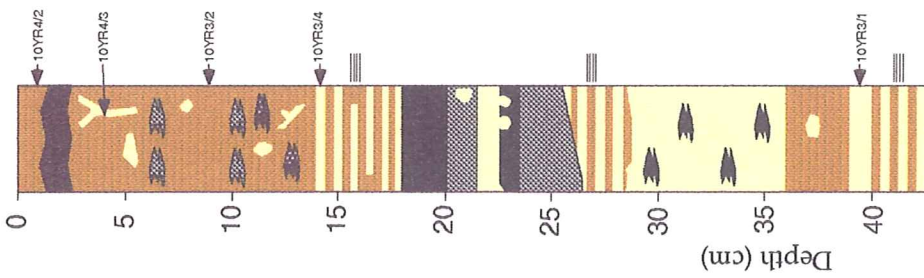
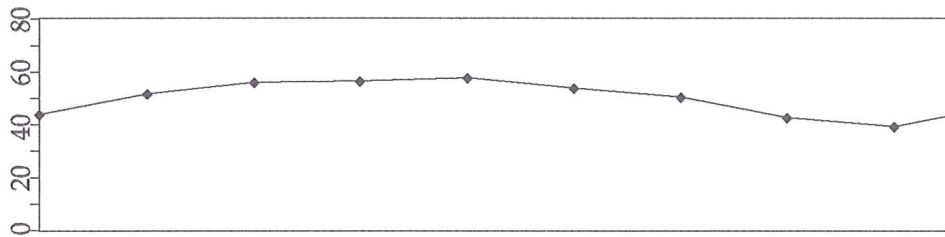




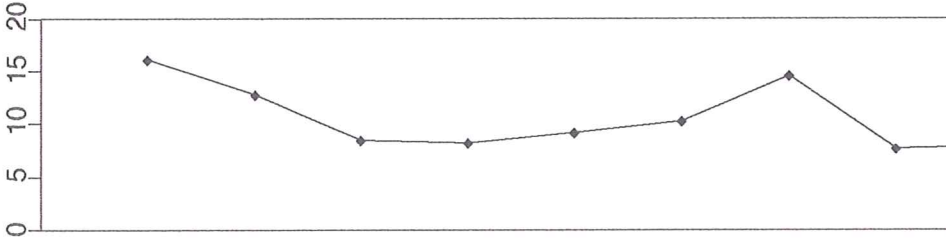
Vane shear strength (kPa)



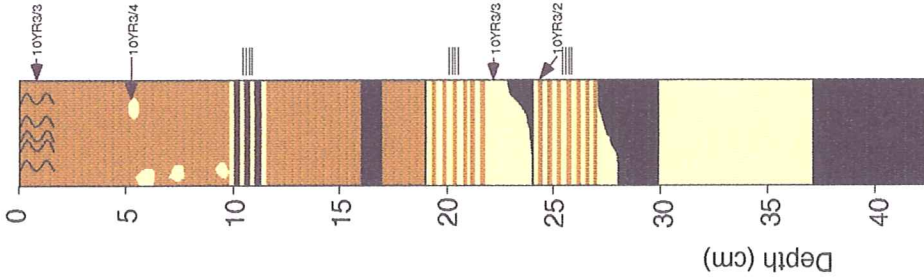
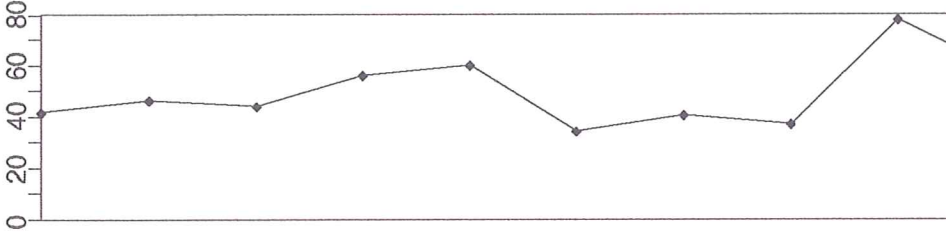
Water content (%)



Vane shear strength (kPa)

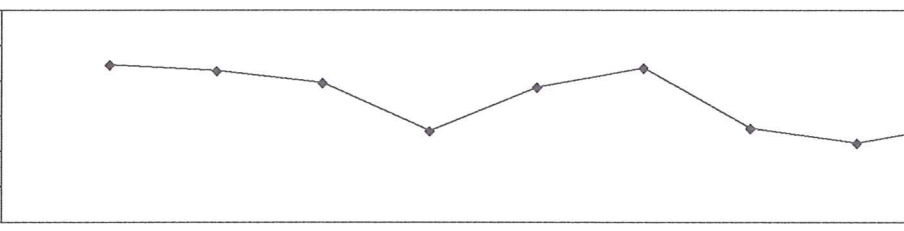


Water content (%)



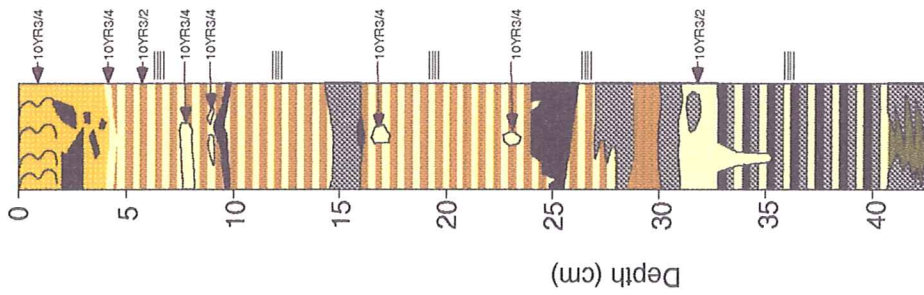
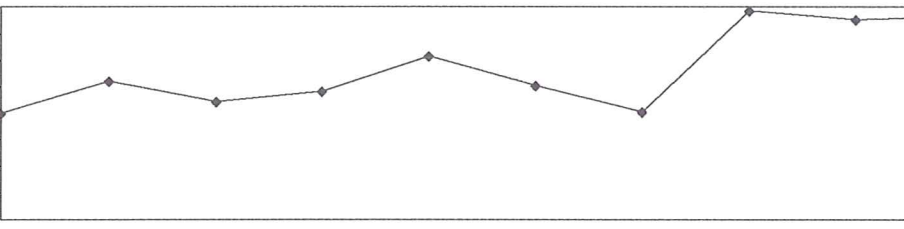
Vane shear strength (kPa)

0 2 4 6 8 10 12



Water content (%)

0 20 40 60 80

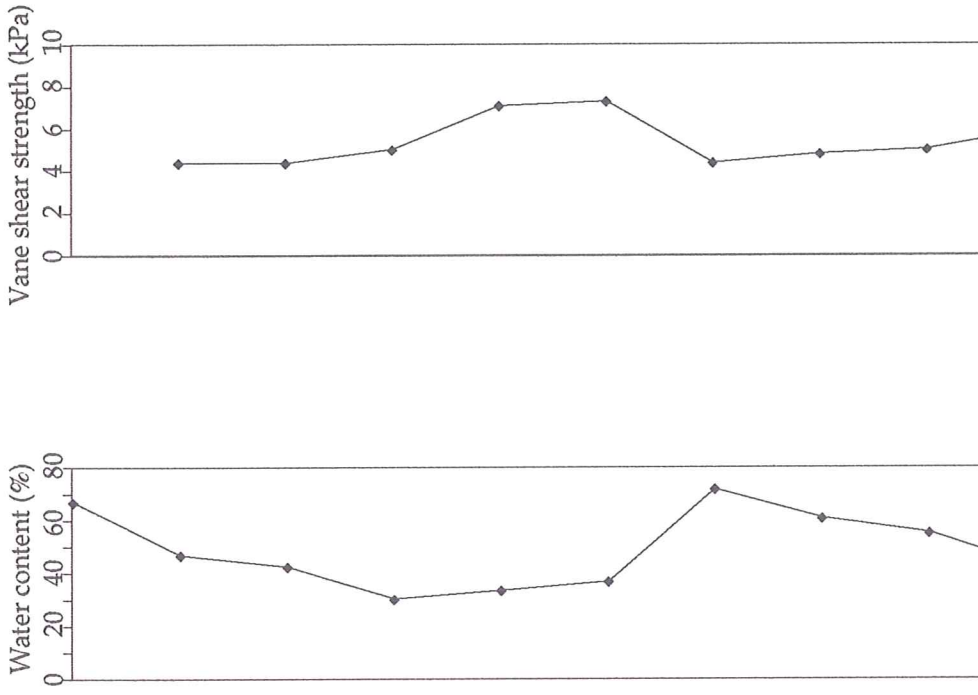
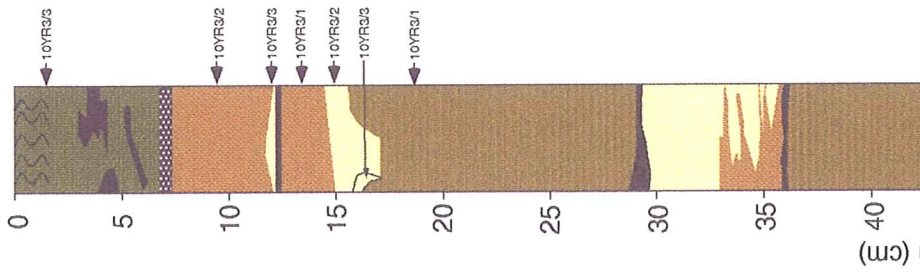


Vane shear strength (kPa)

0 2 4 6 8 10

Water content (%)

0 20 40 60 80



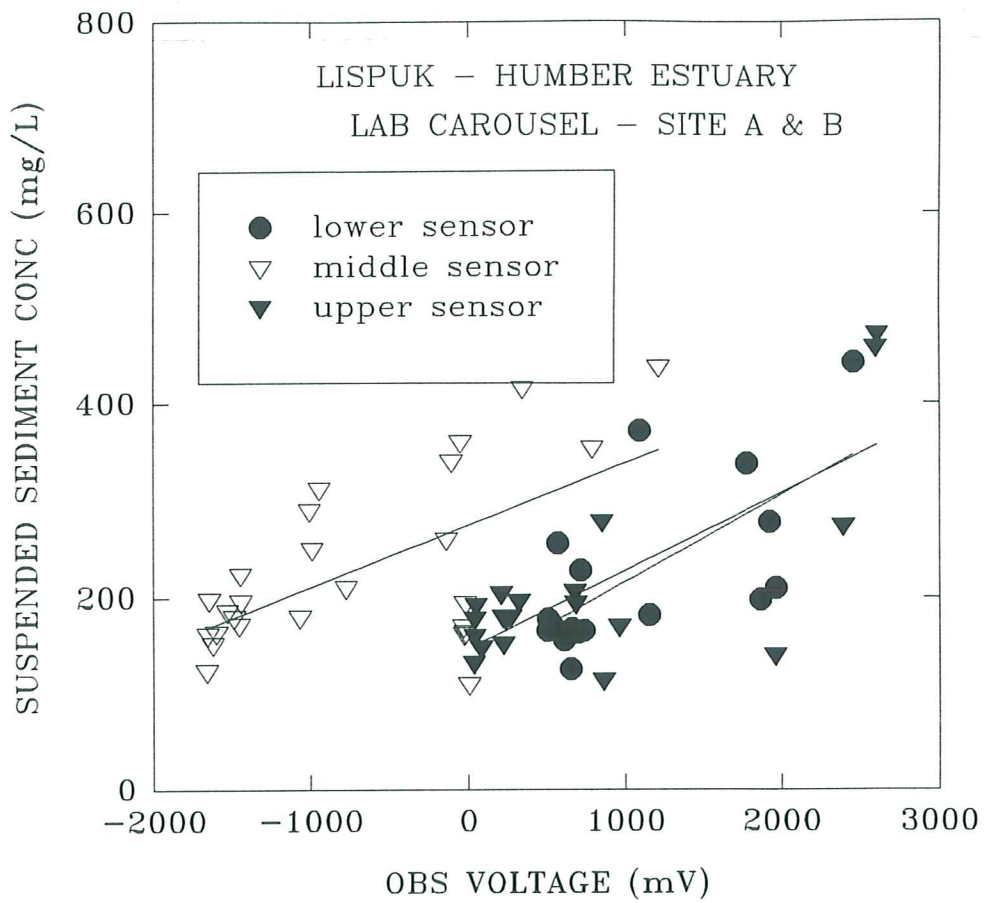


Figure 6.1.1.1. A calibration plot of OBS output voltage from Sea Carousel versus dry-weight suspended sediment concentration. The calibration is for site A and B samples combined.

SEA CAROUSEL – LISPUK13 (Humber estuary)

SITE A – 14 APRIL, 1995

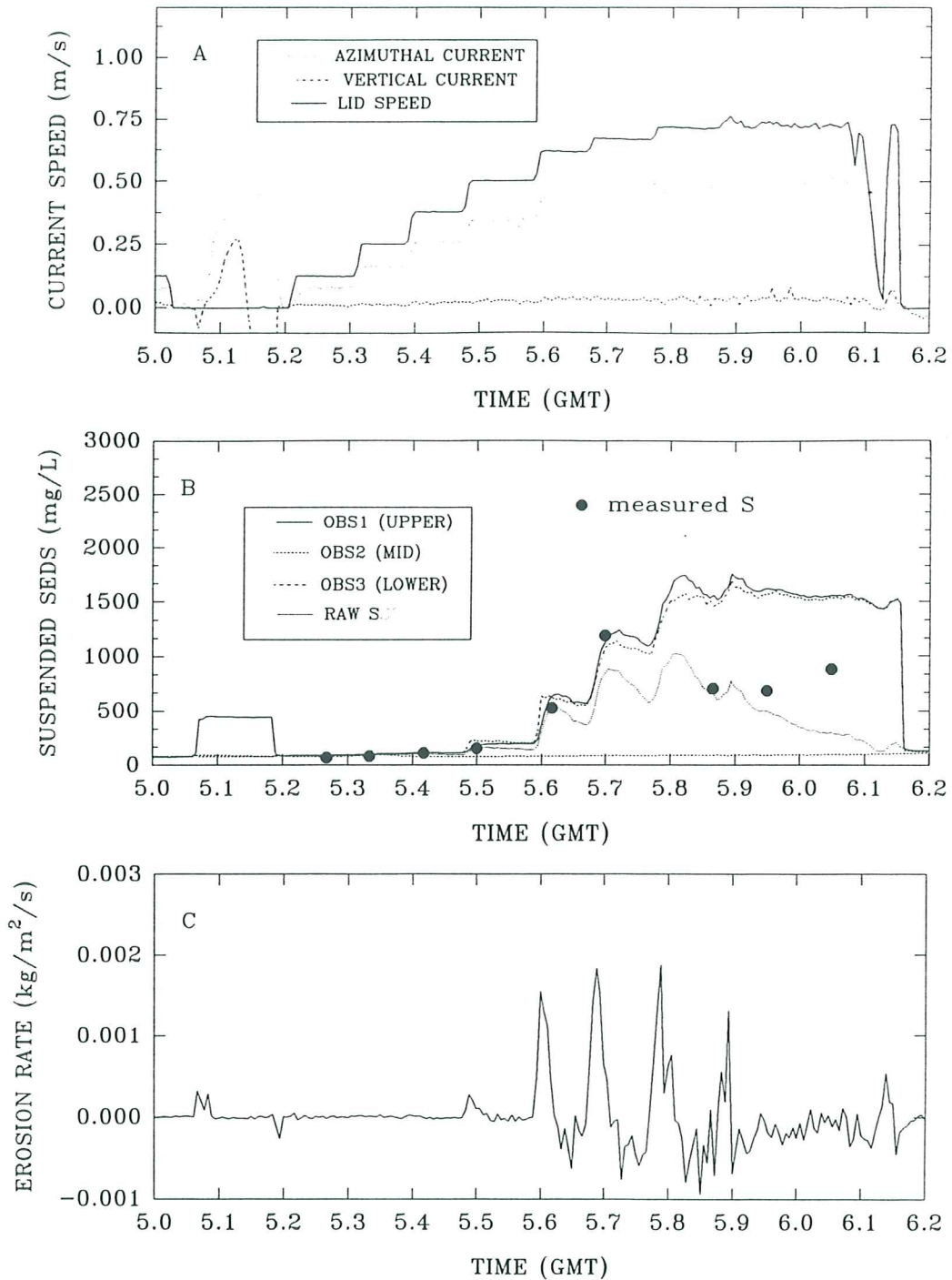


Figure 6.1.1.2. A time-series plot of results from Sea Carousel recorded at site A (LISPUK13) on 14 April, 1995. (A) lid speed and azimuthal and vertical currents at the reference height (0.18 m); (B) suspended sediment concentrations from the three OBS sensors (OBS1 and OBS3 are internal, OBS2 is external) and from pumped samples; and (C) erosion rate. Notice the prevalence of Type I erosion.

SEA CAROUSEL – LISPUK14 (Humber estuary)

SITE A – 14 APRIL, 1995

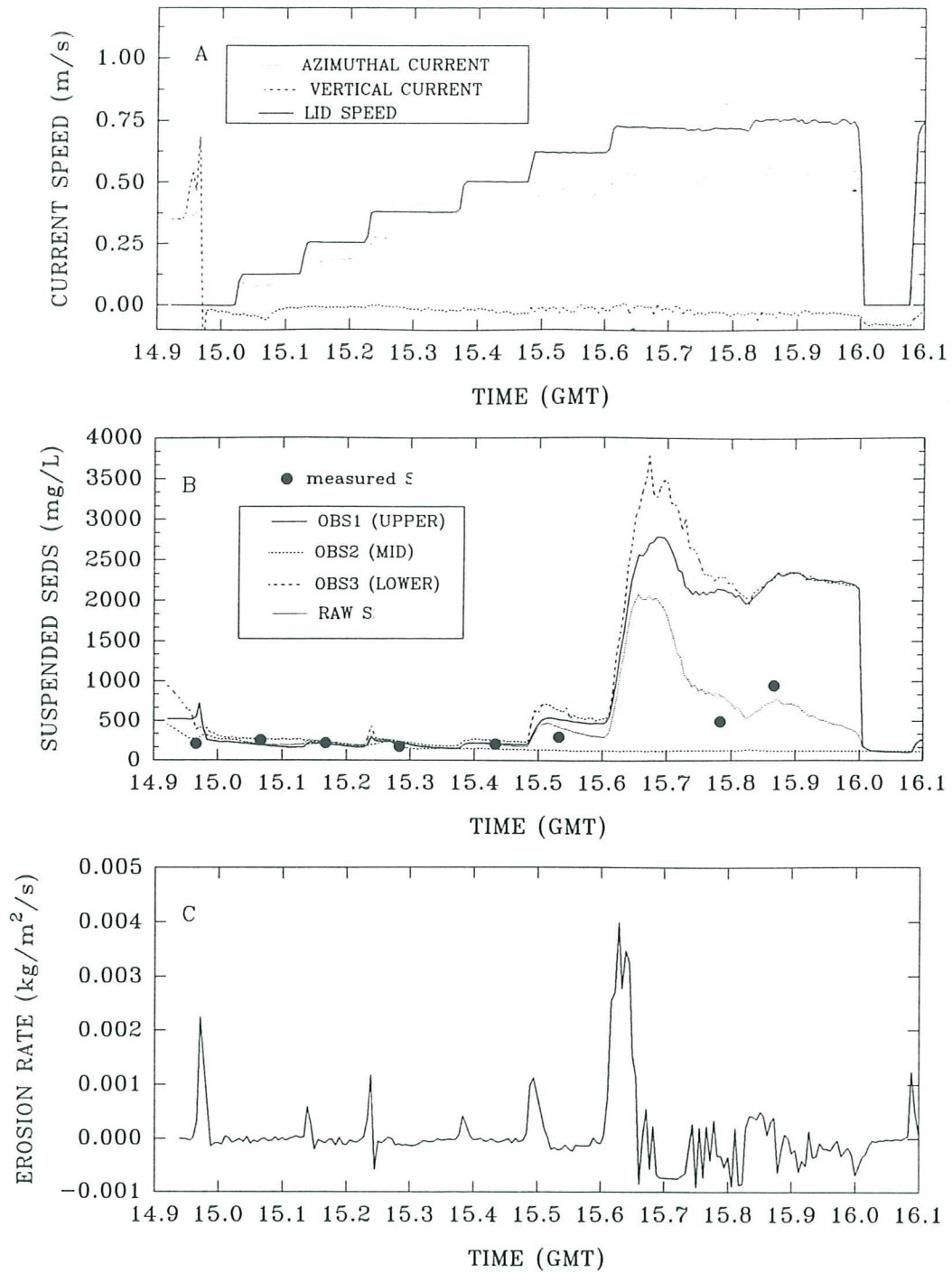


Figure 6.1.1.3. A time-series plot of results from Sea Carousel recorded at site A (LISPUK14) on 14 April, 1995. (A) lid speed and azimuthal and vertical currents at the reference height (0.18 m); and (B) suspended sediment concentrations from the three OBS sensors (OBS1 and OBS3 are internal, OBS2 is external) and from pumped samples; and (C) erosion rate.

SEA CAROUSEL – LISPUK15 (Humber estuary)

SITE A – 14 APRIL, 1995

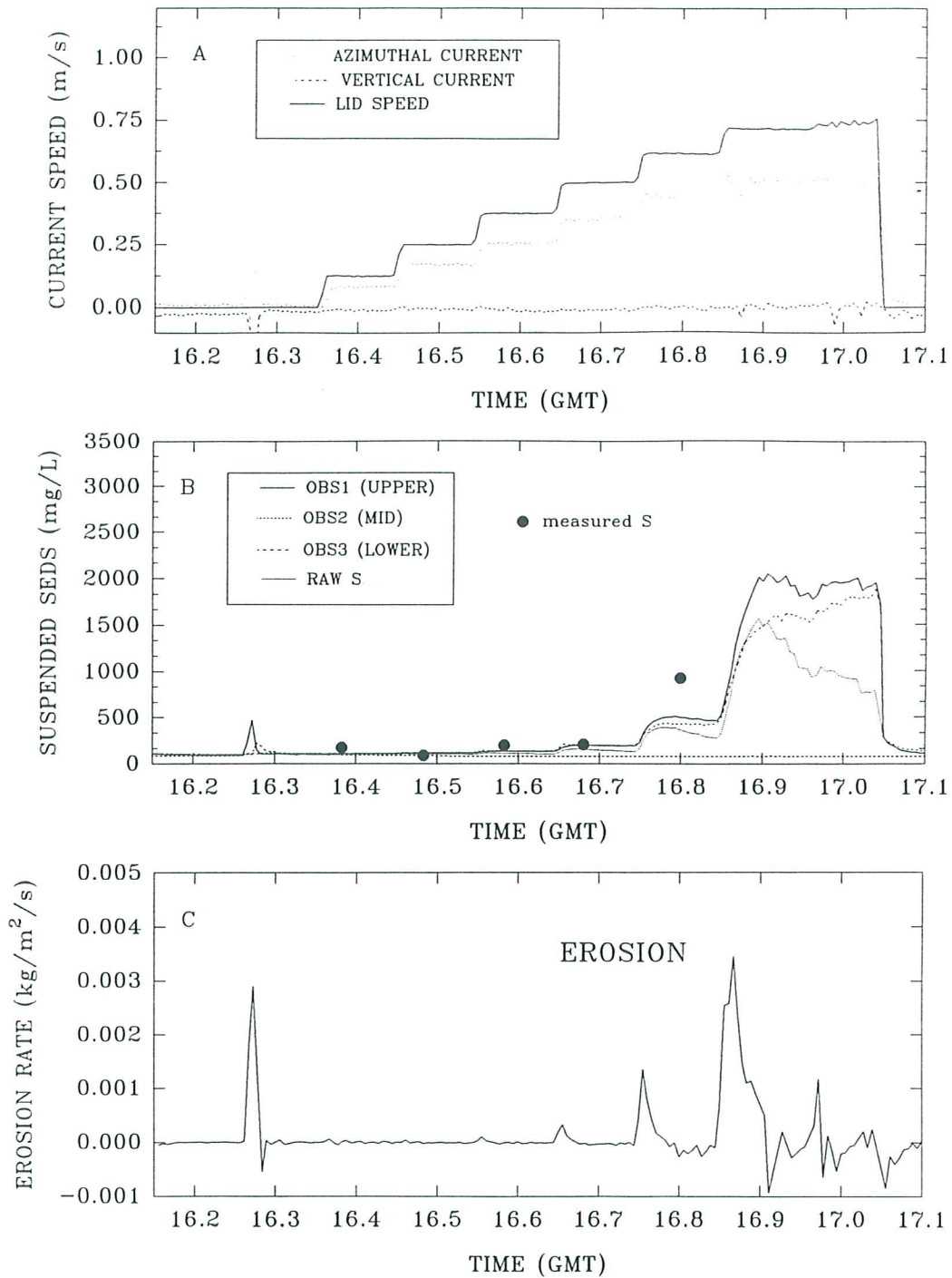


Figure 6.1.1.4. A time-series plot of results from Sea Carousel recorded at site A (LISPUK15) on 14 April, 1995. (A) lid speed and azimuthal and vertical currents at the reference height (0.18 m); and (B) suspended sediment concentrations from the three OBS sensors (OBS1 and OBS3 are internal, OBS2 is external) and from pumped samples; and (C) erosion rate.

STATION LISPUK13, SITE A - 14 APRIL, 1995

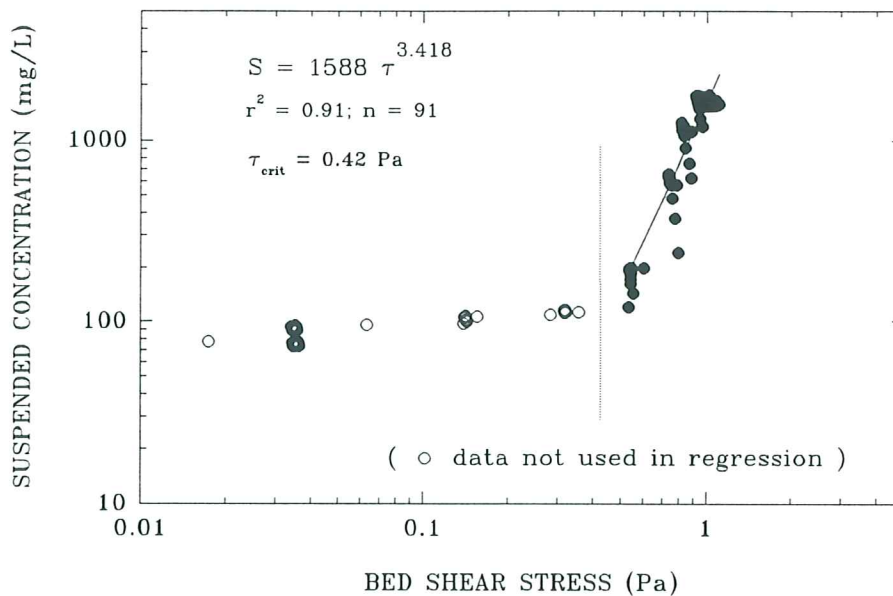
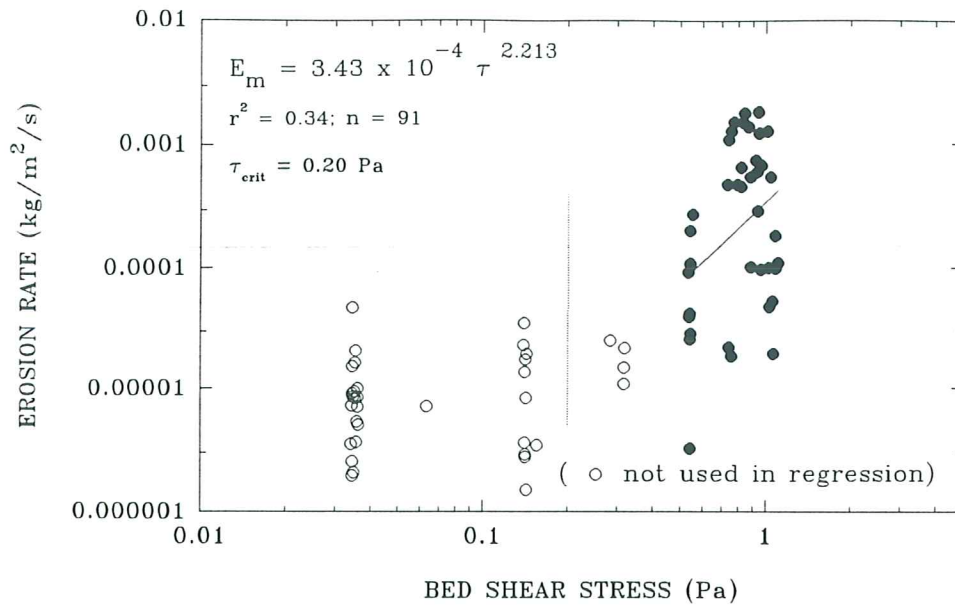


Figure 6.1.1.5. Estimates of the erosion threshold for deployment LISPUK13, site A. The upper panel shows erosion rate versus applied bed stress; the threshold ($\tau_c(0)$) is equated with the stress for a base erosion of $3 \times 10^{-5} \text{ kg}/\text{m}^2/\text{s}$ and yields a value of 0.20 Pa. The lower panel shows suspended sediment concentration versus applied bed shear stress; the threshold is equated with the stress at ambient concentration and yields a value of 0.42 Pa.

STATION LISPUK14, SITE A - 14 APRIL, 1995

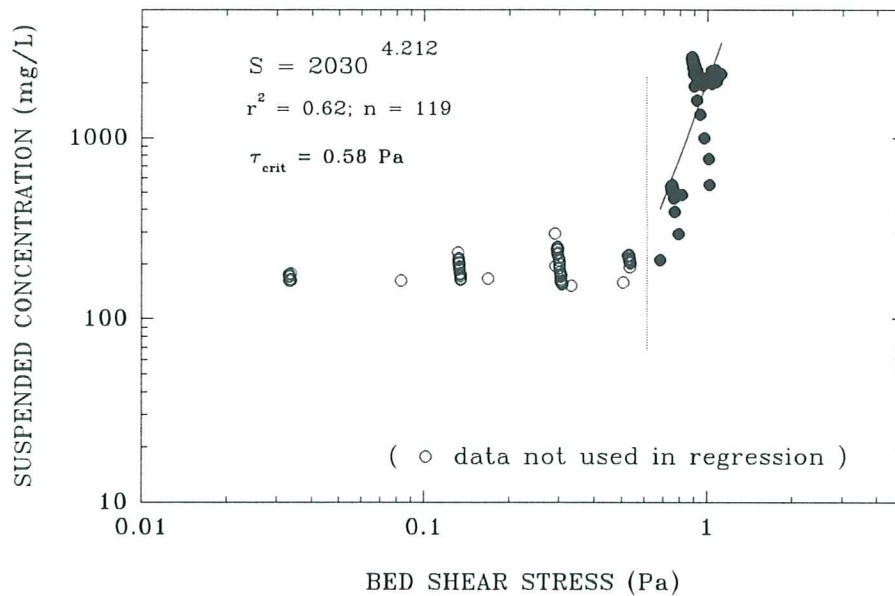
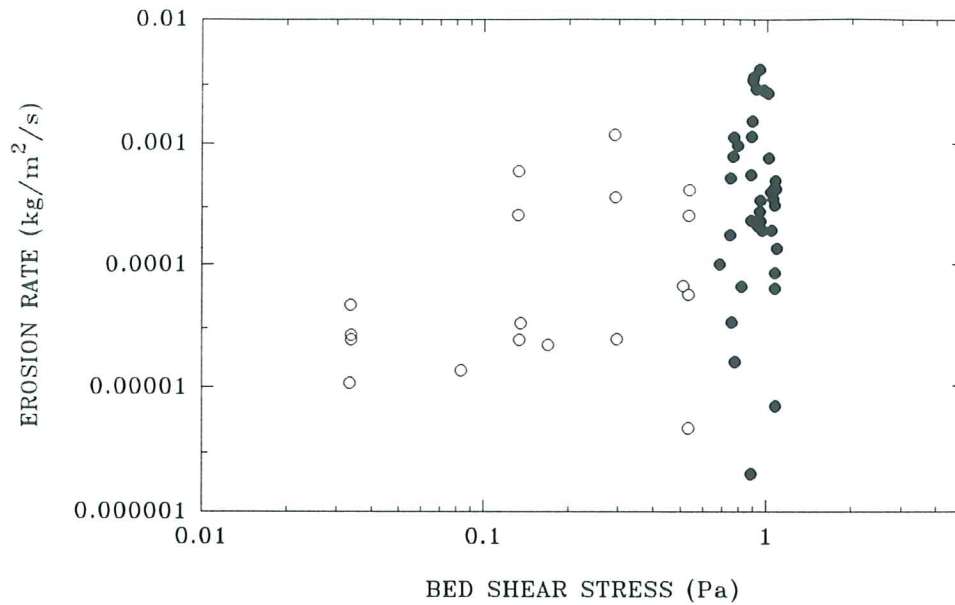


Figure 6.1.1.6. Estimates of the erosion threshold for deployment LISPUK14, site A. The upper panel shows erosion rate versus applied bed stress; it is not possible to derive the threshold from this plot. The lower panel shows that suspended sediment concentration increases as a power function of applied bed shear stress; the threshold is equated with the stress at ambient concentration and yields a value of 0.58 Pa.

STATION LISPUK15, SITE A - 14 APRIL, 1995

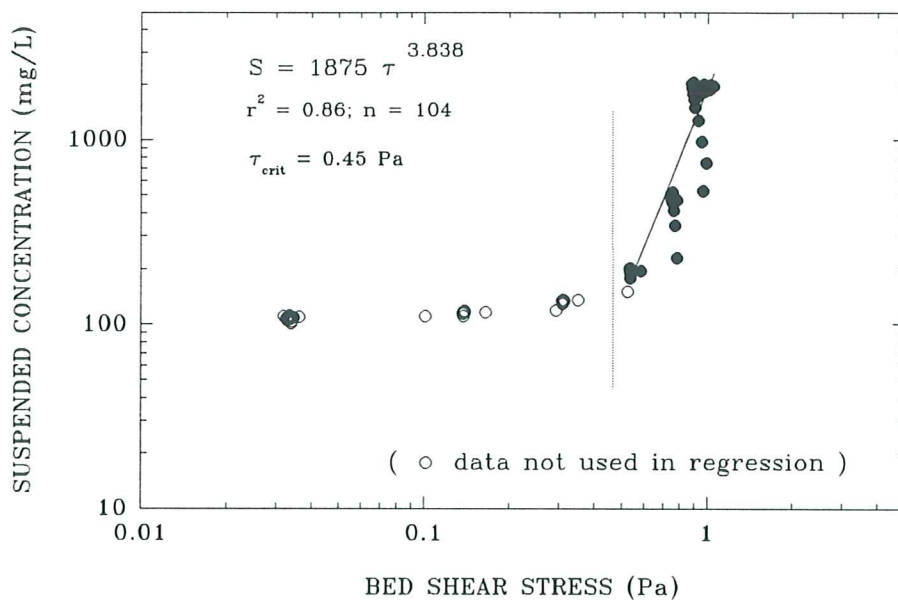
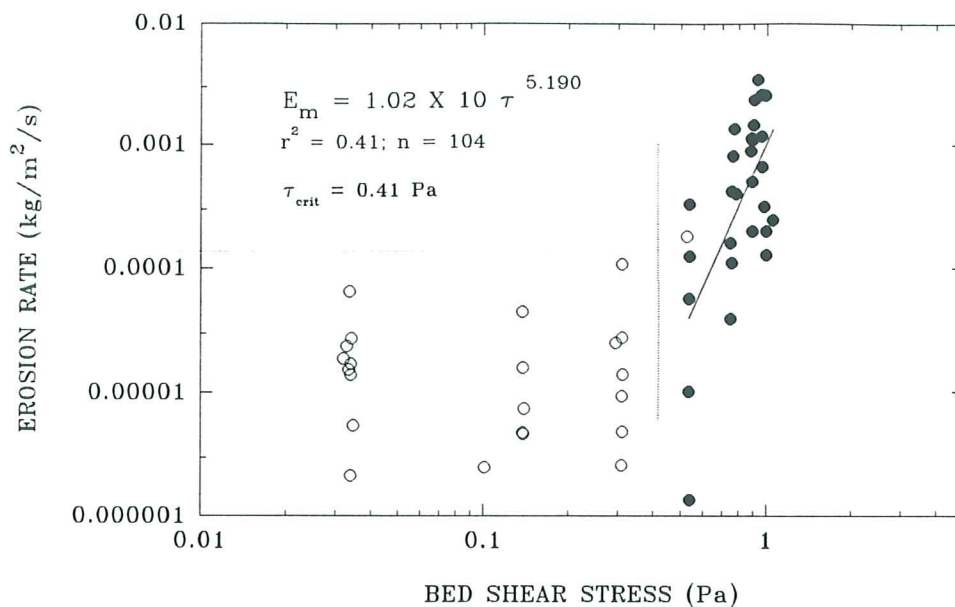


Figure 6.1.1.7. Estimates of the erosion threshold for deployment LISPUK15, site A. The upper panel shows that erosion rate is a power function of applied bed stress; the estimated erosion threshold is 0.41 Pa. The lower panel shows that suspended sediment concentration increases as a power function of applied bed shear stress; the threshold is equated with the stress at ambient concentration and yields a value of 0.45 Pa.

LAB CAROUSEL – LISPUK (Humber estuary)

SITE A (LABEXP2) – 7 APRIL, 1995

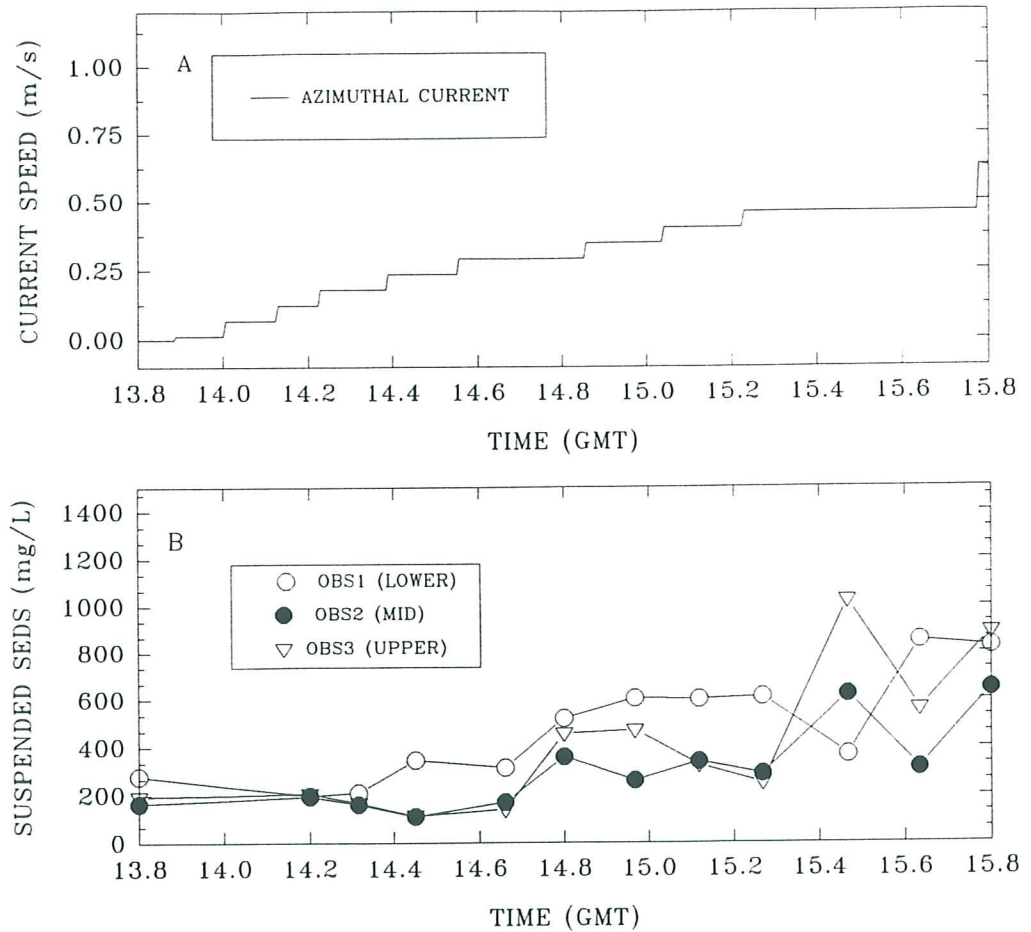


Figure 6.1.2.1. A time-series of Lab Carousel experiment (Labexp2) on a site A bulk sample. (A) the azimuthal reference current for a height of 0.18 m above the bed (based on lid rotation); and (B) measured dry-weight suspended sediment concentration from three sample ports at heights of 0.03, 0.10, and 0.20 m above the base.

LAB CAROUSEL – LISPUK (Humber estuary)

SITE A (LABEXP3) – 9 APRIL, 1995

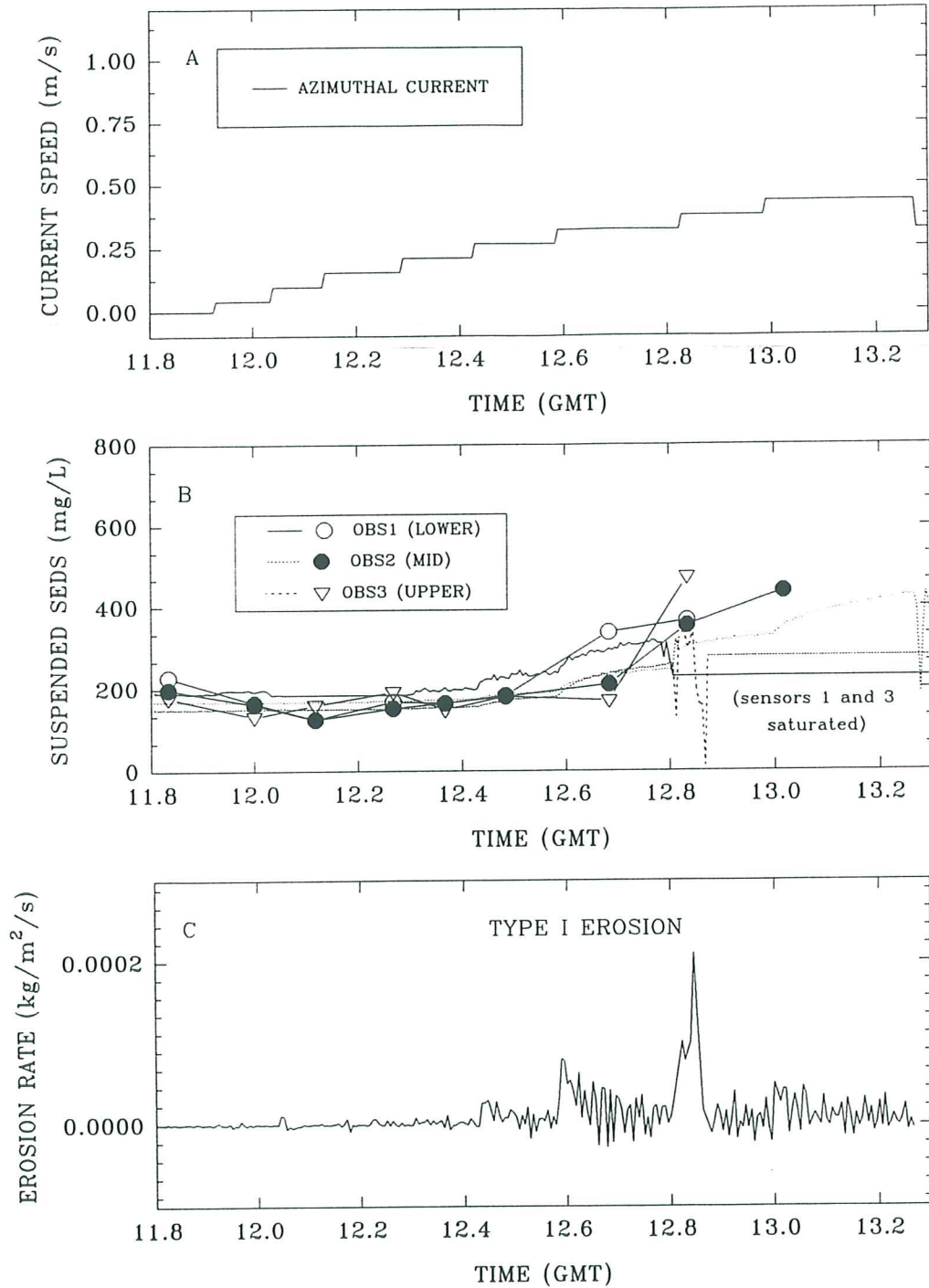


Figure 6.1.2.2. A time-series of Lab Carousel experiment (Labexp3) on a site A bulk sample. (A) the azimuthal reference current for a height of 0.18 m above the bed (based on lid rotation); (B) measured dry-weight suspended sediment concentration from three sample ports at heights of 0.03, 0.10, and 0.20 m above the base; and (C) erosion rate. Notice the prevalence of Type I erosion at early stages of erosion and sensor saturation during later stages.

LAB CAROUSEL – LISPUK (Humber estuary)

SITE A (LABEXP5) – 12 APRIL, 1995

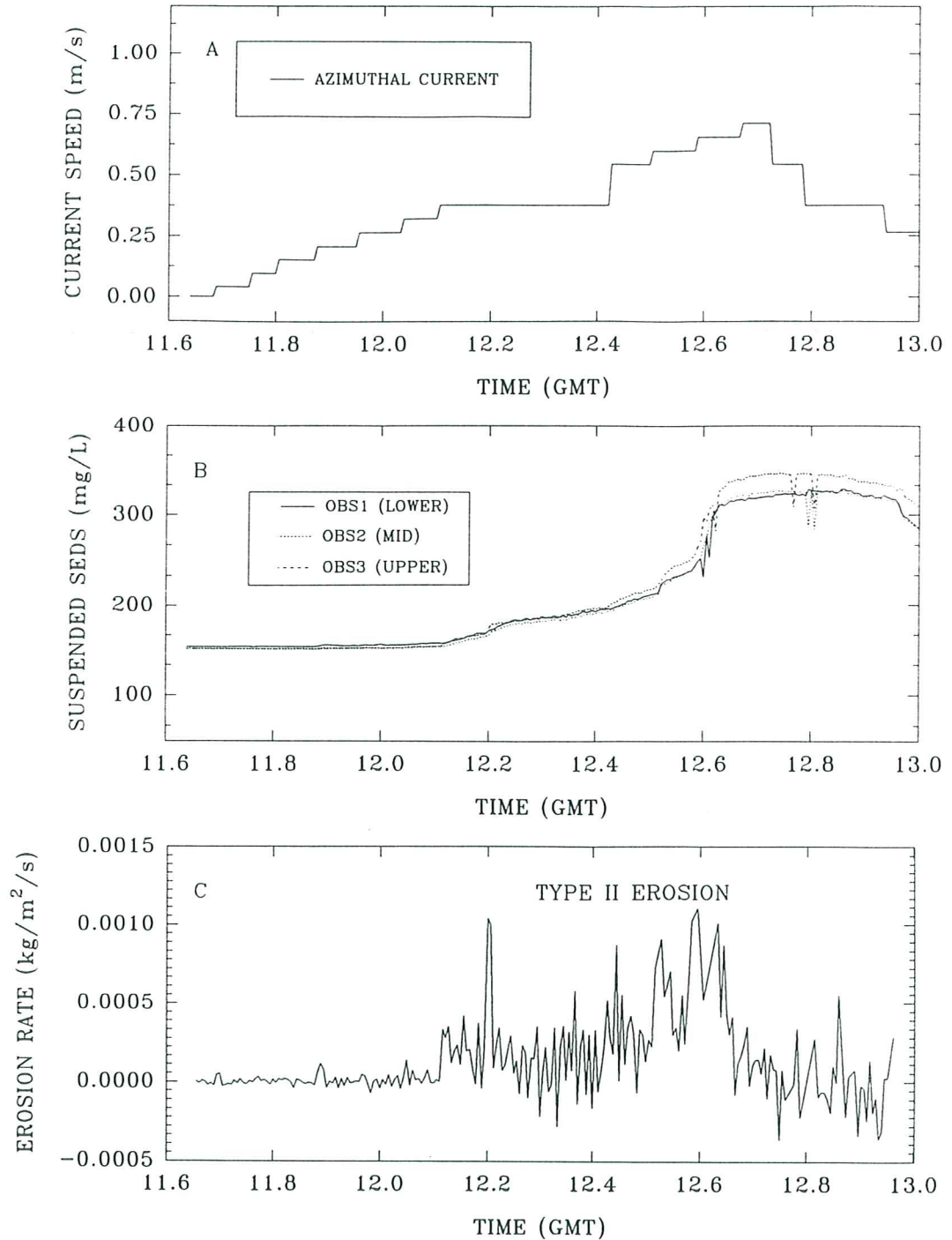


Figure 6.1.2.3. A time-series of Lab Carousel experiment (Labexp5) on a site A bulk sample. (A) the azimuthal reference current for a height of 0.18 m above the bed (based on lid rotation); (B) suspended sediment concentration from three OBS's at heights of 0.03, 0.10, and 0.20 m above the base; and (C) erosion rate. Notice the prevalence of Type II erosion.

LAB CAROUSEL – LISPUK (Humber estuary)

SITE A/B (LABEXP9) – 19 APRIL, 1995

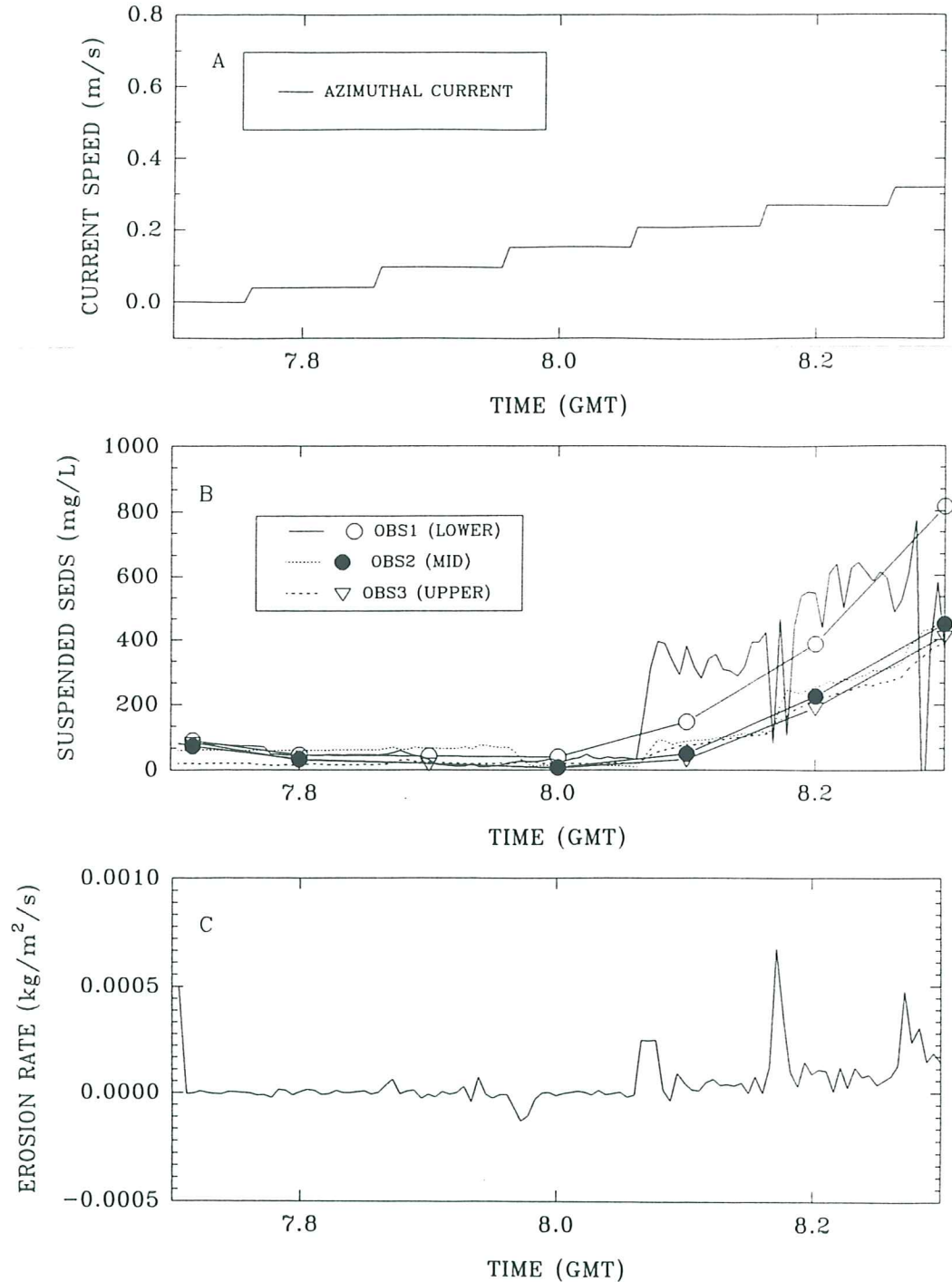


Figure 6.1.2.4. A time-series of Lab Carousel experiment (Labexp9) on a site A/B bulk sample. (A) the azimuthal reference current for a height of 0.18 m above the bed (based on lid rotation); (B) suspended sediment concentration from three OBS's and pumped samples at heights of 0.03, 0.10, and 0.20 m above the base; and (C) erosion rate.

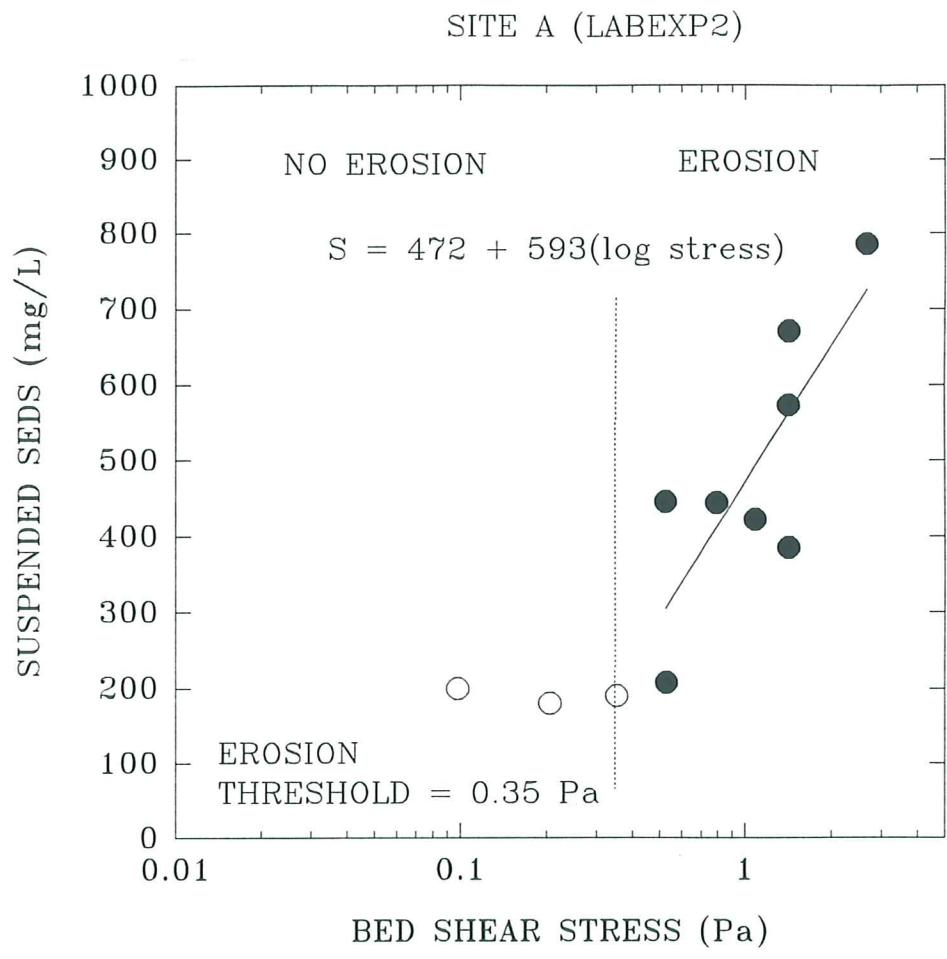


Figure 6.1.2.5. Suspended sediment concentration versus the log of applied bed shear stress for Labexp2, site A. The erosion threshold is evaluated at 0.35 Pa. Also shown is the functional relationship between sediment concentration (S) and bed shear stress.

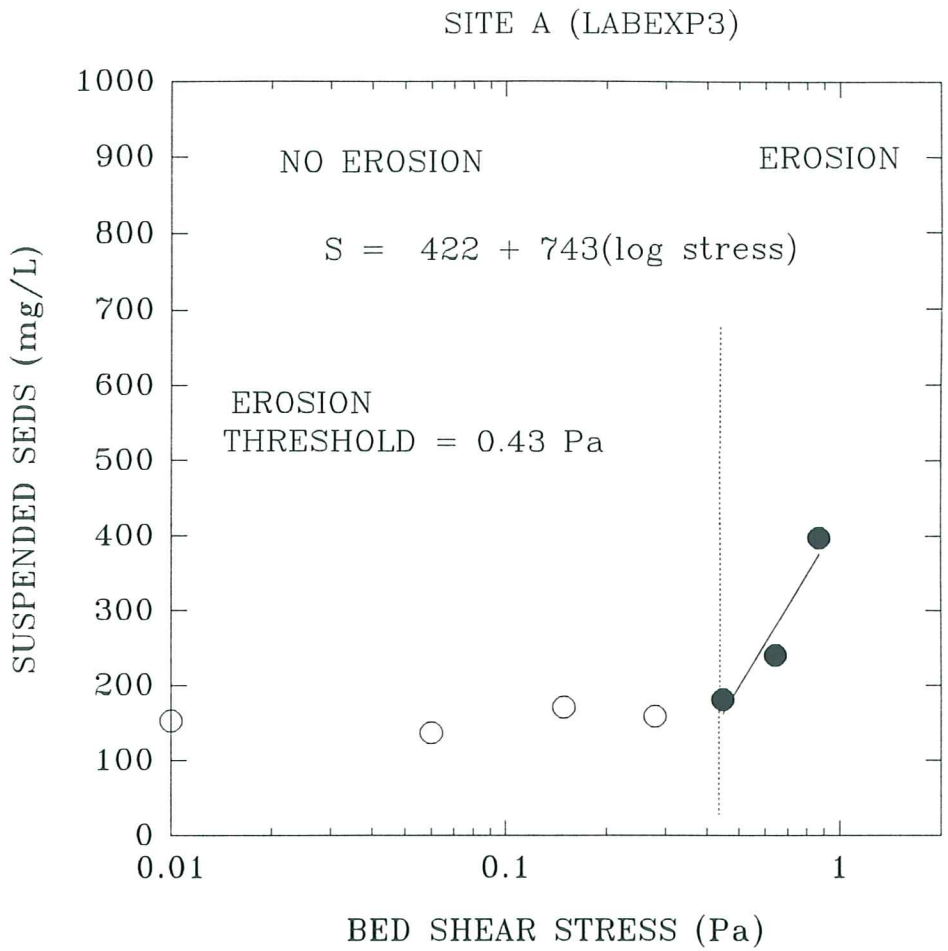


Figure 6.1.2.6. Suspended sediment concentration versus the log of applied bed shear stress for Labexp3, site A. The erosion threshold is evaluated at 0.43 Pa. Also shown is the functional relationship between S and τ_o (the applied bed shear stress).

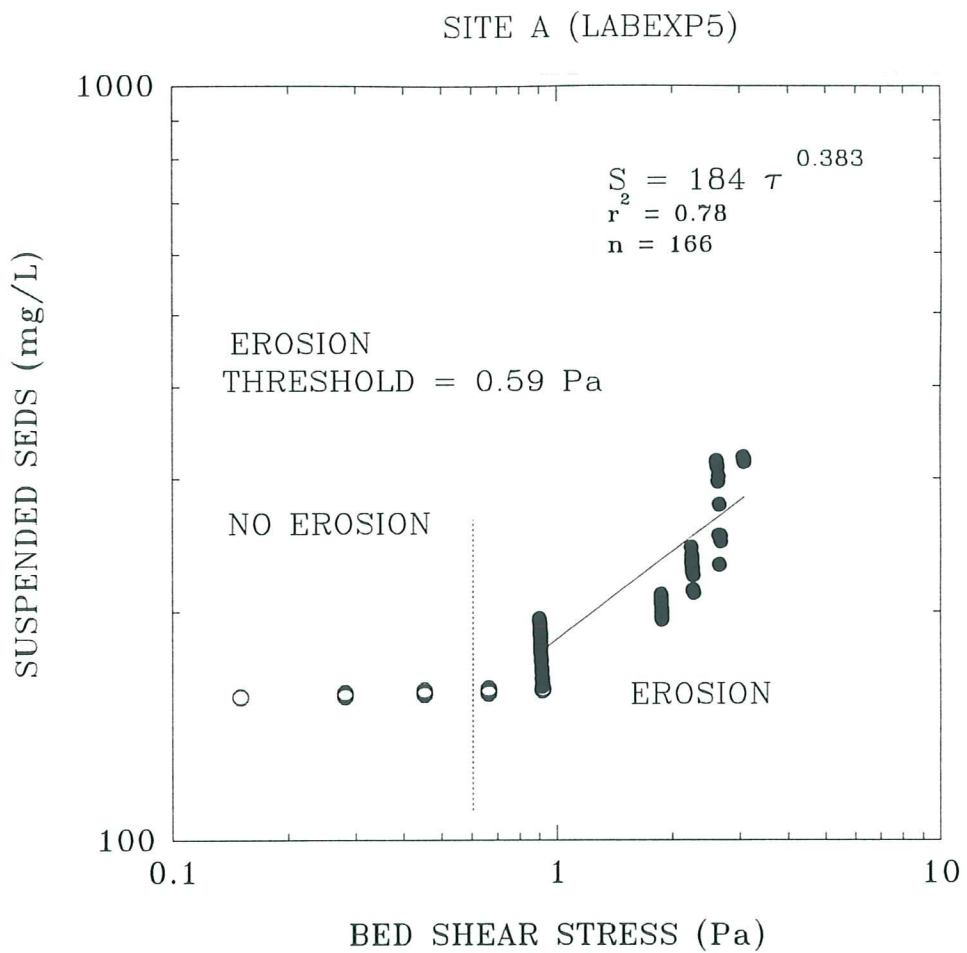


Figure 6.1.2.7. Log eroded mass (kg) versus the log of applied bed shear stress for Labexp5, site A. The erosion threshold is evaluated at 0.59 Pa.

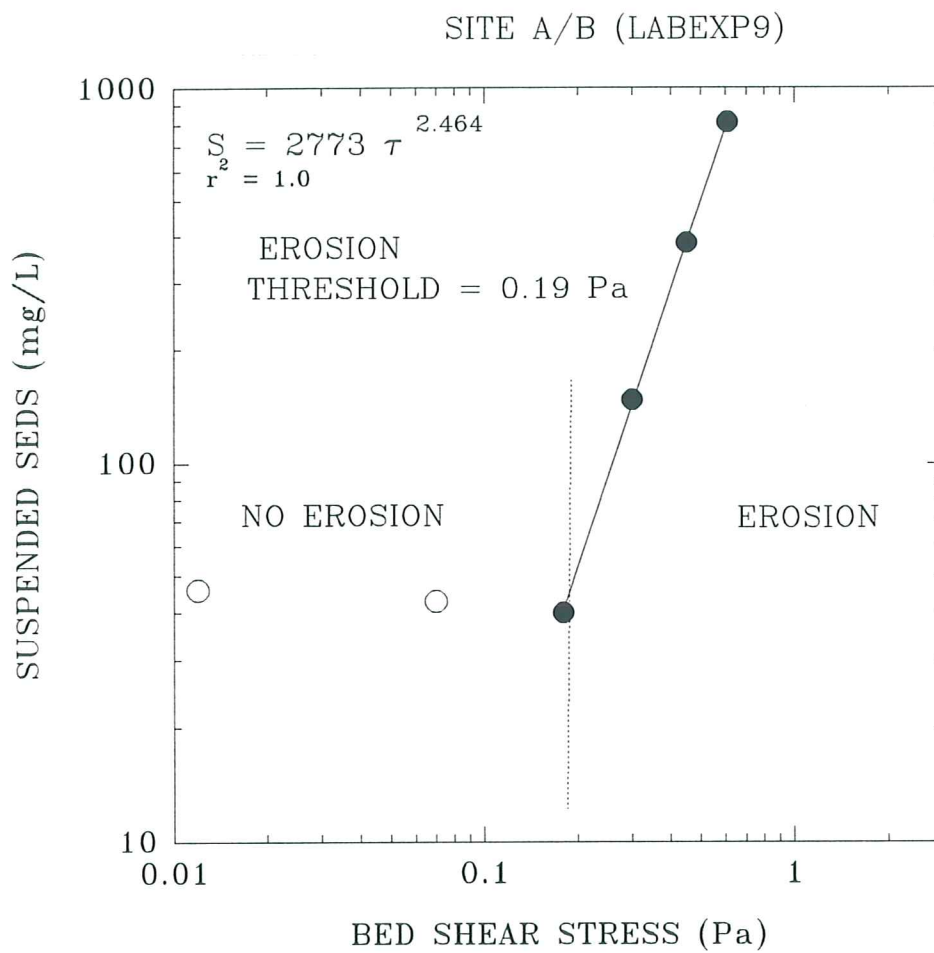


Figure 6.1.2.8. Log suspended sediment concentration versus the log of applied bed shear stress for Labexp9, site A/B. The erosion threshold is evaluated at 0.19 Pa. Also shown is the functional relationship between S and τ_o .

LISPUK LAB CAROUSEL SEDIMENT SETTLING

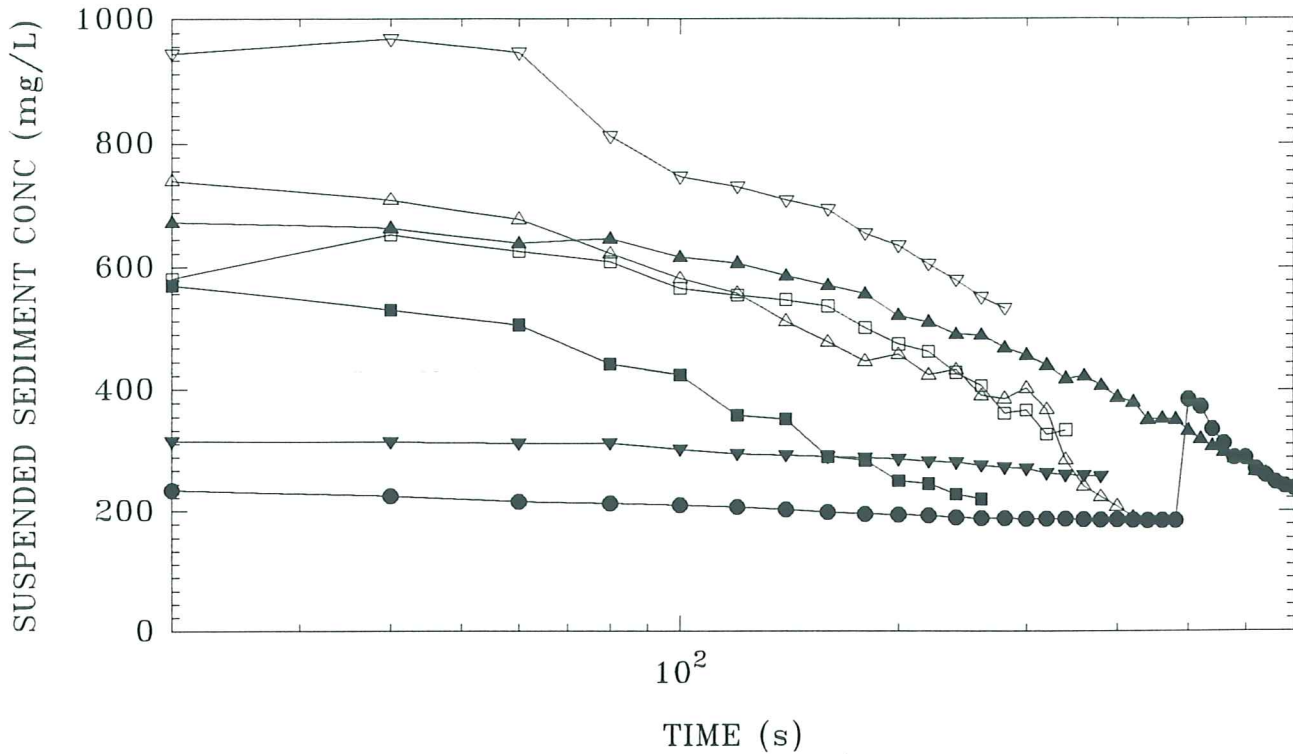
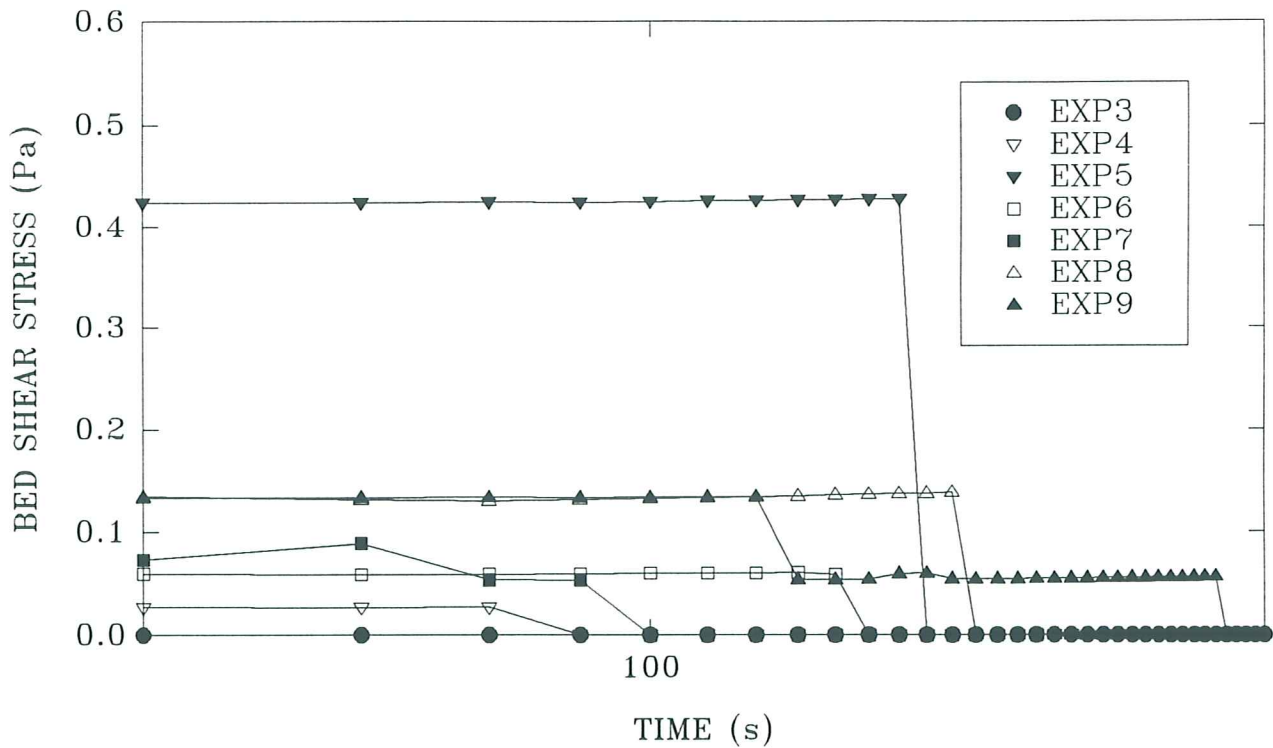


Figure 6.1.2.9. Time-series plots of suspended sediment concentration (A) and applied bed shear stress (B) during the settling phase of all Lab Carousel experiments carried out in this study. Mass settling rate (W_s) and depositional threshold (τ_d) have been determined from these data.



LISPUK - SITE A, Humber estuary

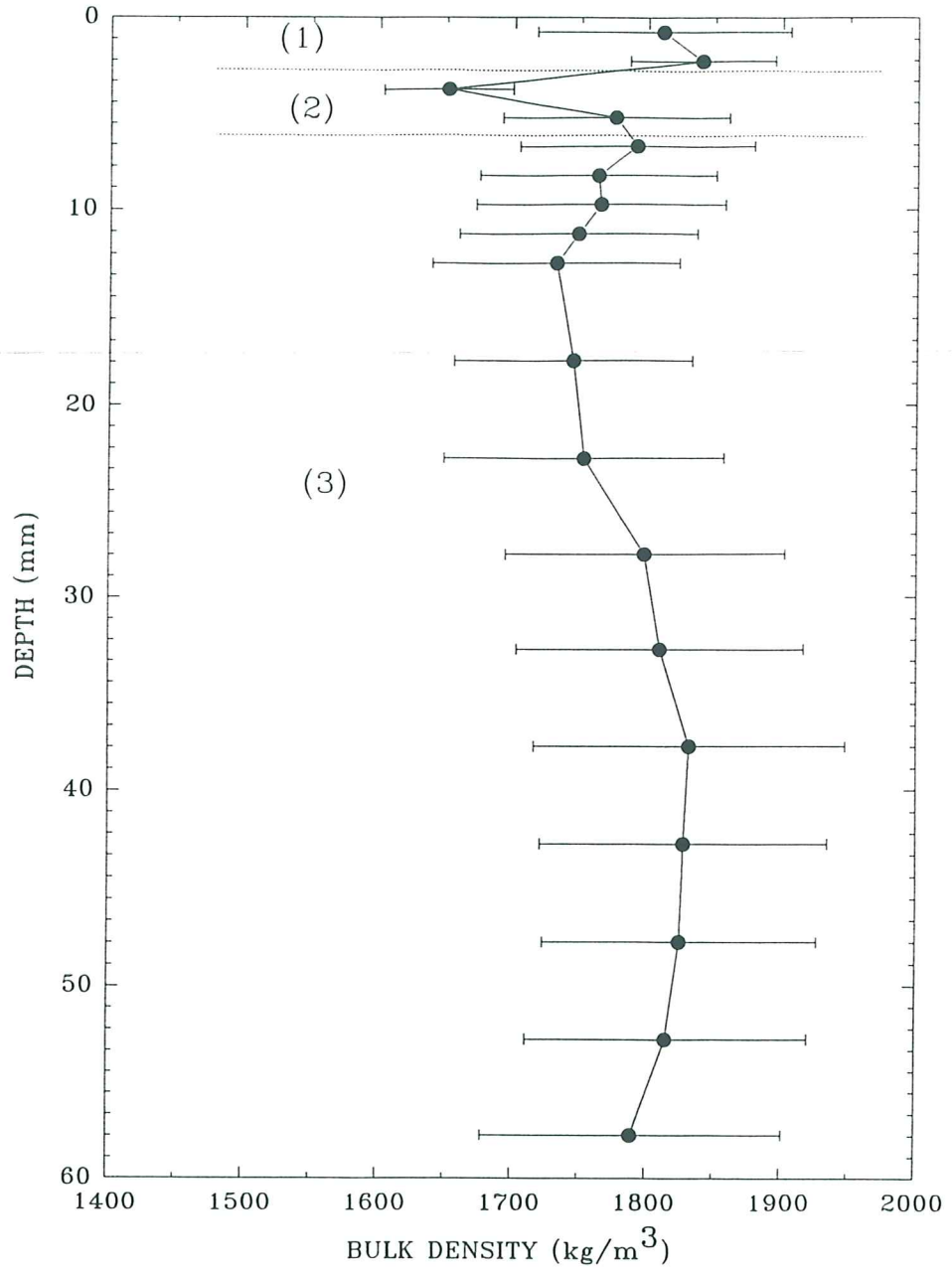


Figure 6.1.3.1. A log of the wet-weight bulk density derived from a Catscan analysis of a syringe core collected at site A. Three layers are evident: (1) a surface layer of relatively high density (2 mm thick); (2) a transitional layer of rapidly changing density (5 mm thick); and (3) the substrate.

SEA CAROUSEL – LISPUK17 (Humber estuary)

SITE B – 18 APRIL, 1995

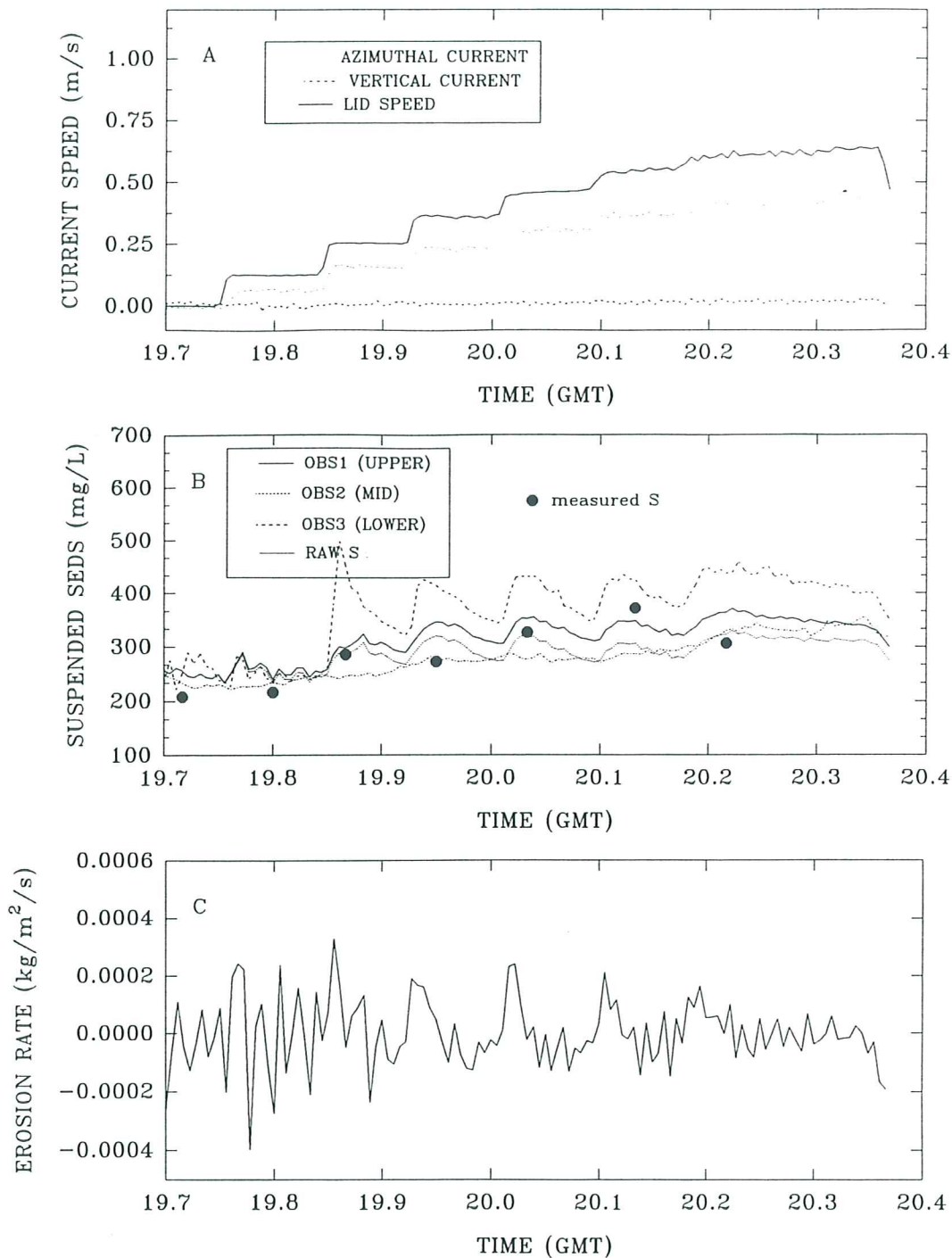


Figure 6.2.1.1. A time-series plot of results from Sea Carousel recorded at site B (LISPUK17) on 18 April, 1995. (A) lid speed and azimuthal and vertical currents at the reference height (0.18 m); (B) suspended sediment concentrations from the three OBS sensors (OBS1 and OBS3 are internal, OBS2 is external), and from pumped samples; and (C) erosion rate. Notice the prevalence of Type I erosion.

SEA CAROUSEL – LISPUK18 (Humber estuary)

SITE B – 18 APRIL, 1995

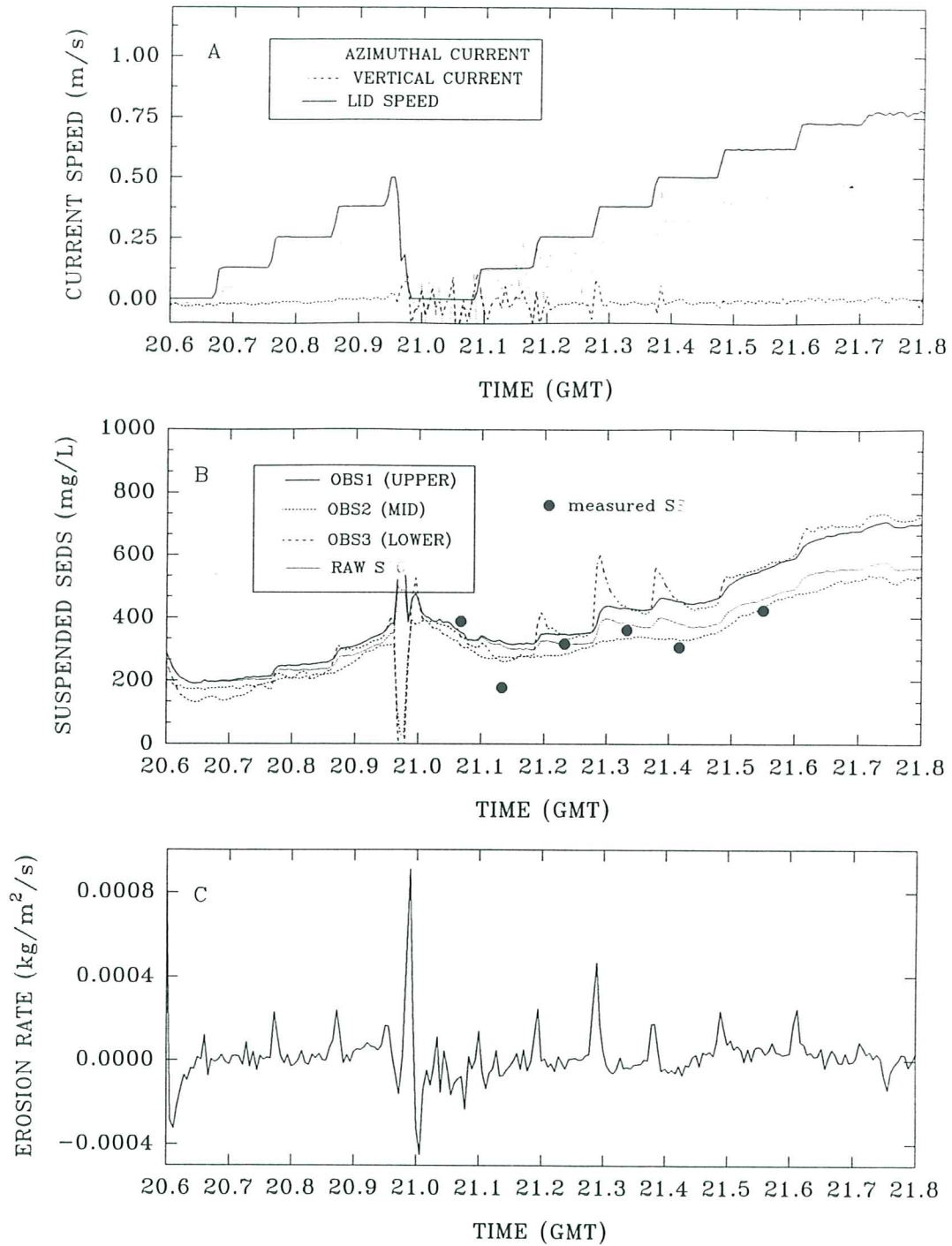


Figure 6.2.1.2. A time-series plot of results from Sea Carousel recorded at site B (LISPUK18) on 18 April, 1995. (A) lid speed and azimuthal and vertical currents at the reference height (0.18 m); (B) suspended sediment concentrations from the three OBS sensors (OBS1 and OBS3 are internal, OBS2 is external), and from pumped samples; and (C) erosion rate.

SEA CAROUSEL – LISPUK19 (Humber estuary)

SITE B – 18 APRIL, 1995

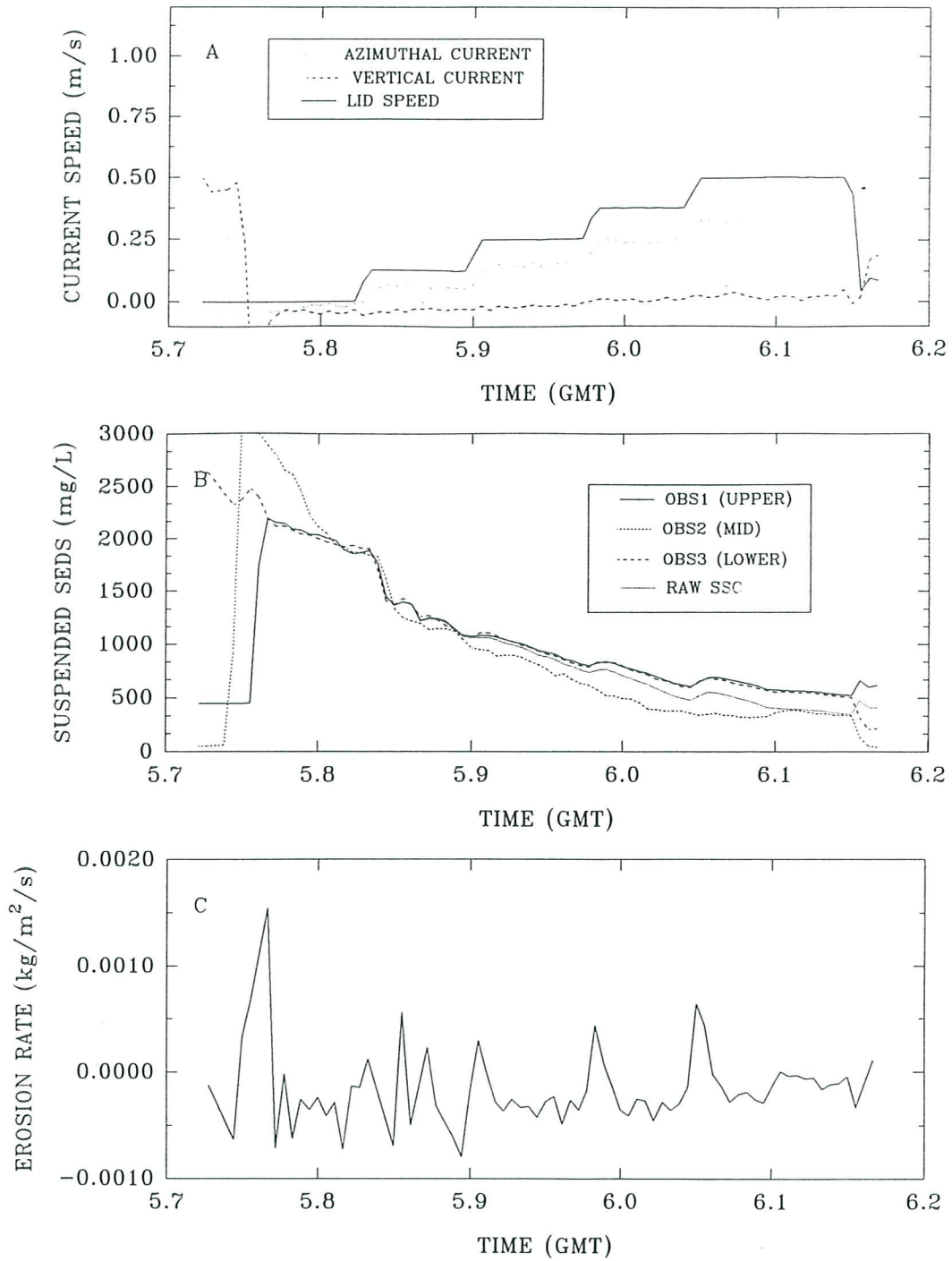


Figure 6.2.1.3. A time-series plot of results from Sea Carousel recorded at site B (LISPUK19) on 18 April, 1995. (A) lid speed and azimuthal and vertical currents at the reference height (0.18 m); (B) suspended sediment concentrations from the three OBS sensors (OBS1 and OBS3 are internal, OBS2 is external); and (C) erosion rate. Notice the dominant effect of the passage of the flood tide turbidity maximum on the sediment concentration signal inside the flume.

STATION LISPUK17, SITE B - 18 APRIL, 1995

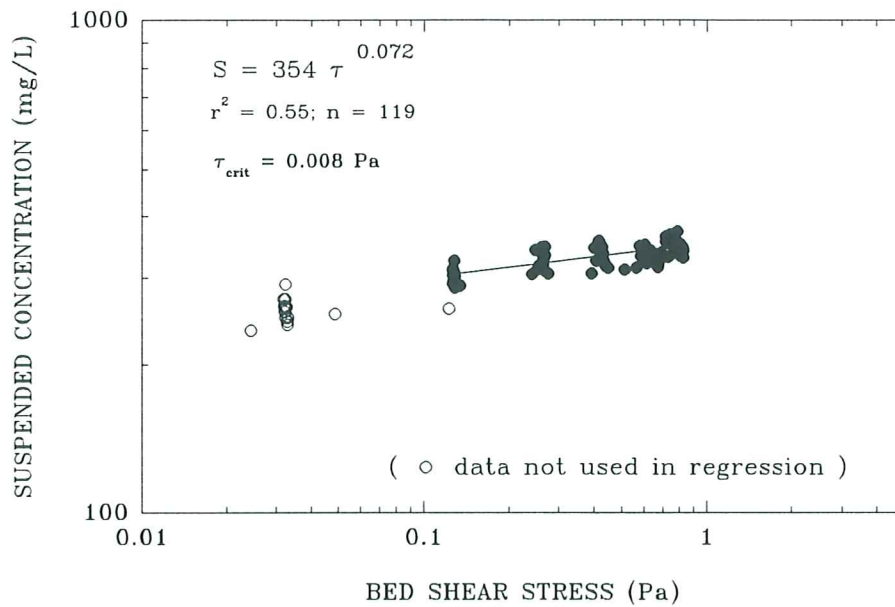
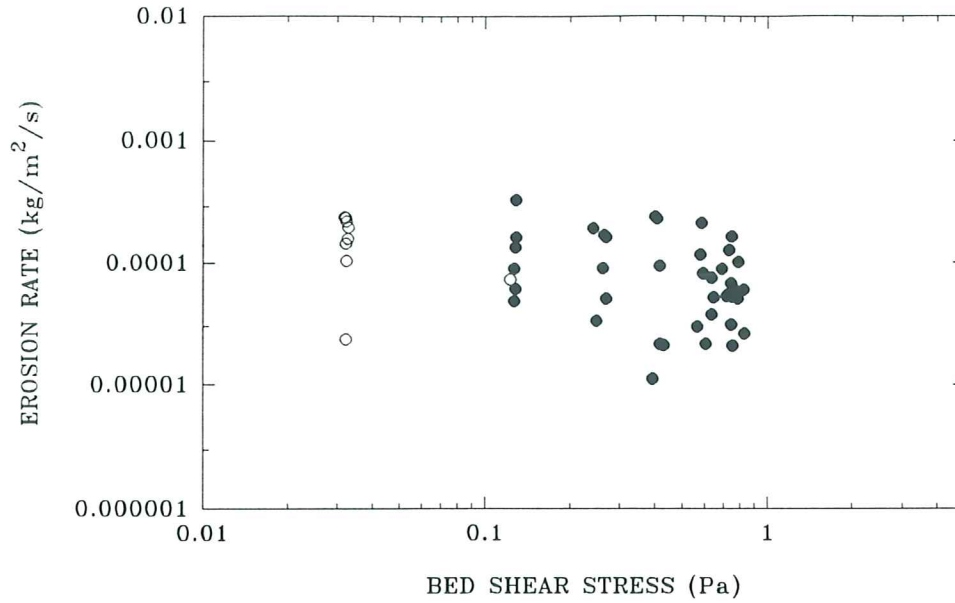


Figure 6.2.1.4. Estimates of the erosion threshold for deployment LISPUK17, site B. The upper panel shows that erosion rate is a power function of applied bed stress; it is not possible to derive erosion threshold from this plot. The lower panel shows that suspended sediment concentration increases as a power function of applied bed shear stress; the threshold is equated with the stress at ambient concentration and yields a value of 0.008 Pa.

STATION LISPUK18, SITE B - 18 APRIL, 1995

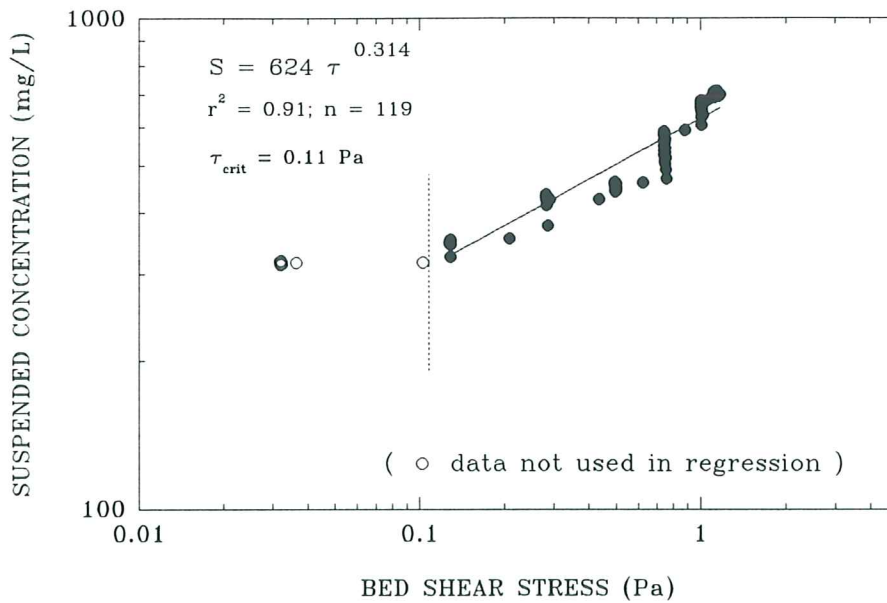
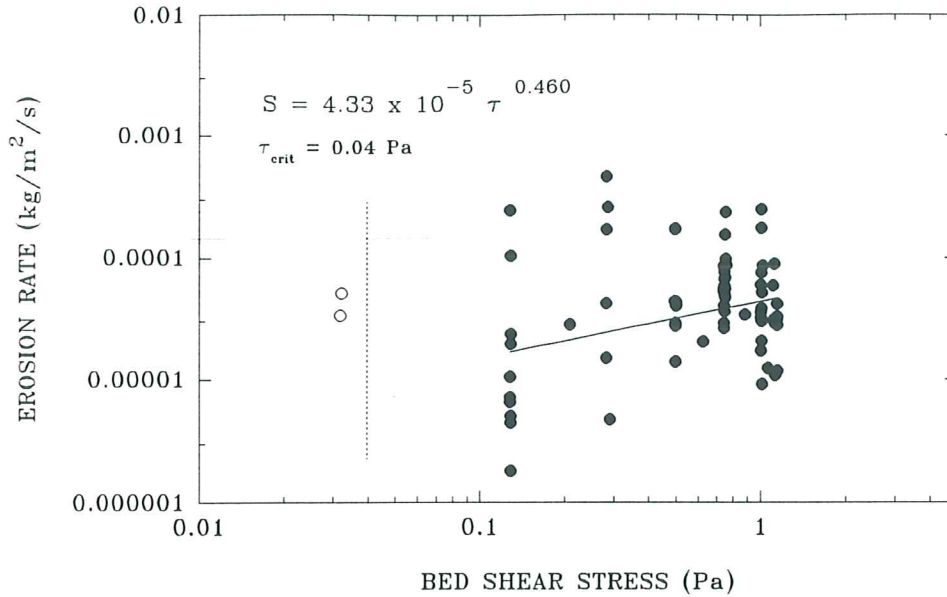


Figure 6.2.1.5. Estimates of the erosion threshold for deployment LISPUK18, site B. The upper panel shows that erosion rate is a power function of applied bed stress; the erosion threshold is evaluated as 0.04 Pa. The lower panel shows that suspended sediment concentration increases as a power function of applied bed shear stress; the threshold is equated with the stress at ambient concentration and yields a value of 0.11 Pa.

LAB CAROUSEL – LISPUK (Humber estuary)

SITE B (LABEXP4) – 11 APRIL, 1995

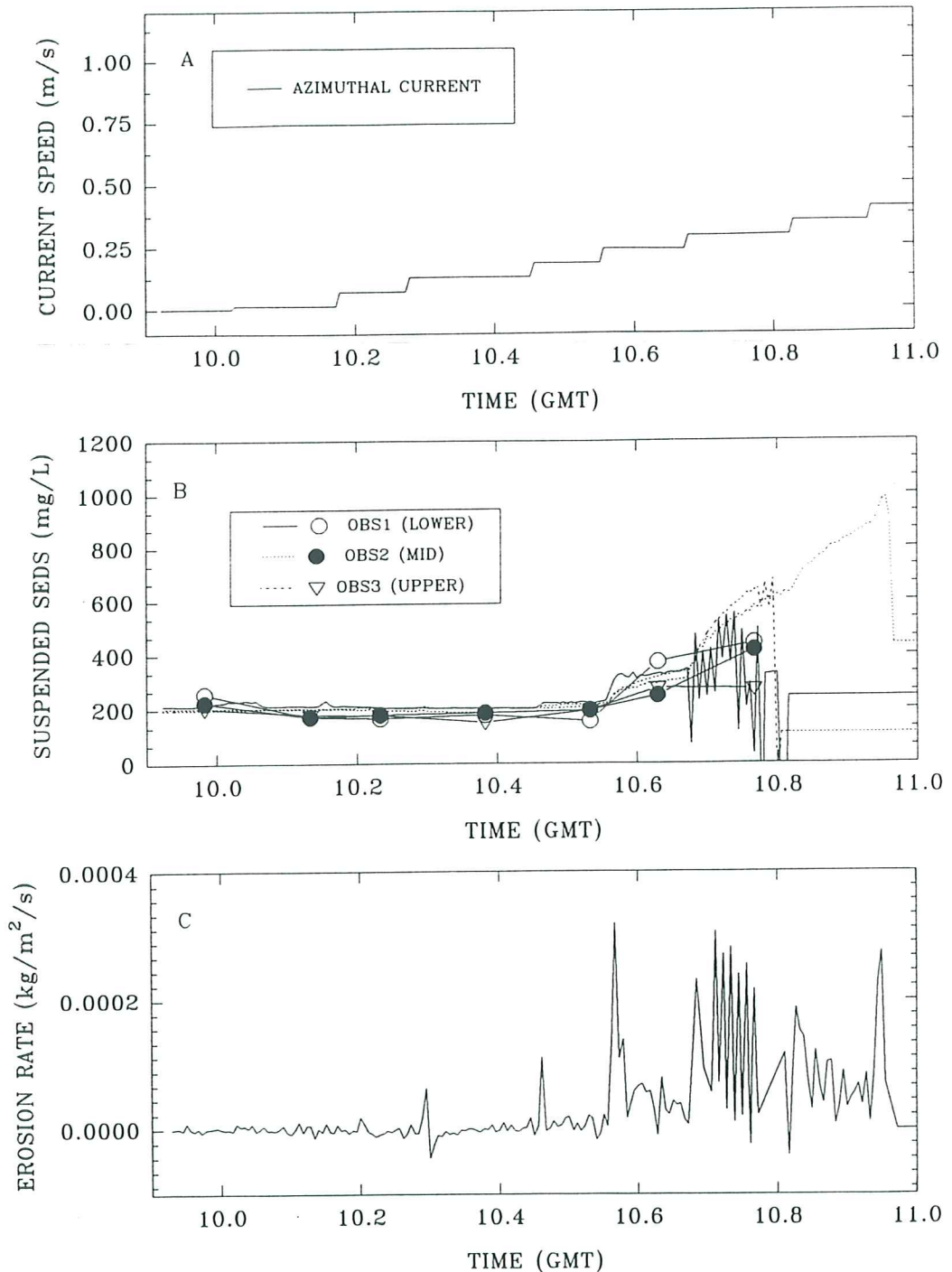


Figure 6.2.2.1. A time-series of Lab Carousel experiment (Labexp4) on a site B bulk sample. (A) the azimuthal reference current for a height of 0.18 m above the bed (based on lid rotation); (B) suspended sediment concentration from three OBS's and pumped samples at heights of 0.03, 0.10, and 0.20 m above the base; and (C) erosion rate. The intermittent effects of sensor saturation are clearly seen during the eroding phase.

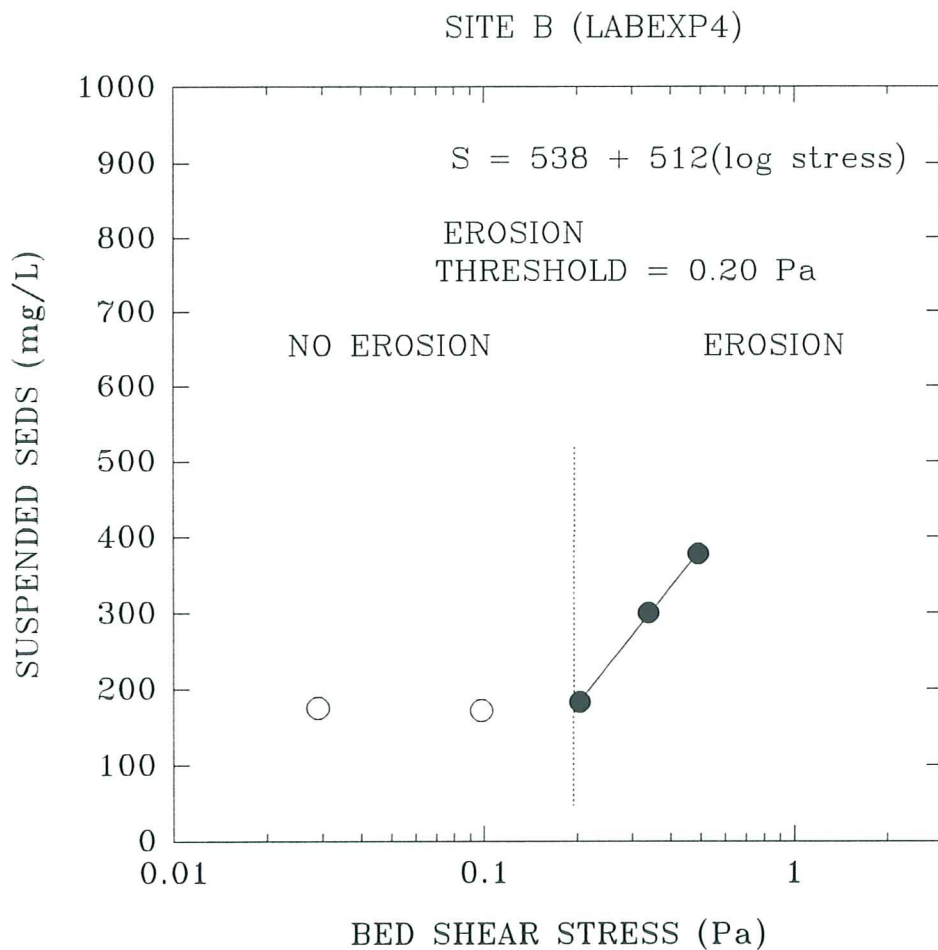


Figure 6.2.2.2. A plot of measured suspended sediment concentration (from pumped samples) versus applied bed shear stress in Sea Carousel. Notice the onset of erosion at 0.2 Pa which is based on the extrapolation of concentration to ambient levels.

LISPUK - SITE B, Humber estuary

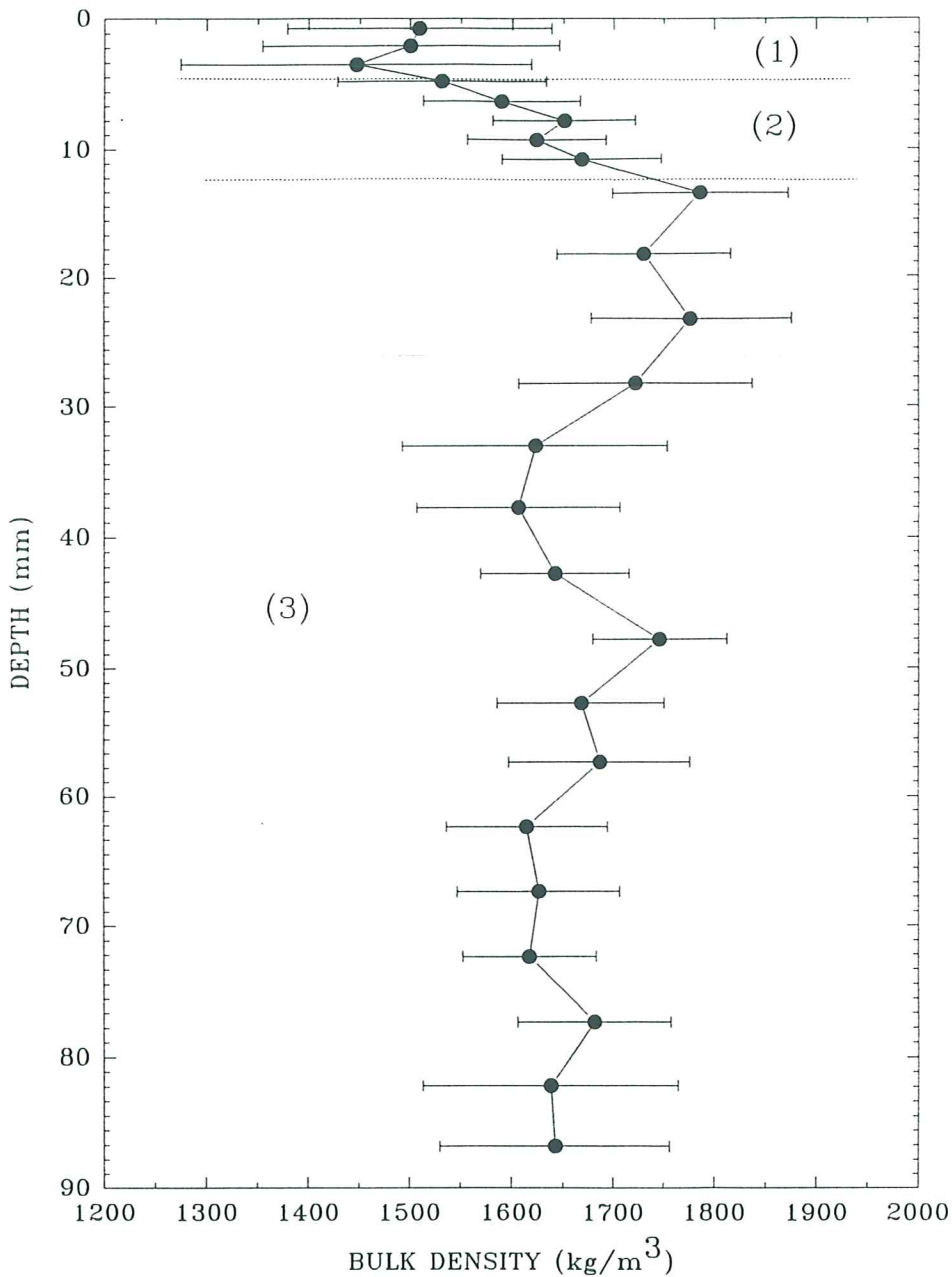


Figure 6.2.3.1. A log of the wet-weight bulk density derived from a Catscan analysis of a syringe core collected at site B. Three layers are evident: (1) a surface layer of relatively low density (4 mm thick); (2) a transitional layer of rapidly increasing density (8 mm thick); and (3) the denser substrate.

SEA CAROUSEL – LISPUK10 (Humber estuary)

SITE B/C – 13 APRIL, 1995

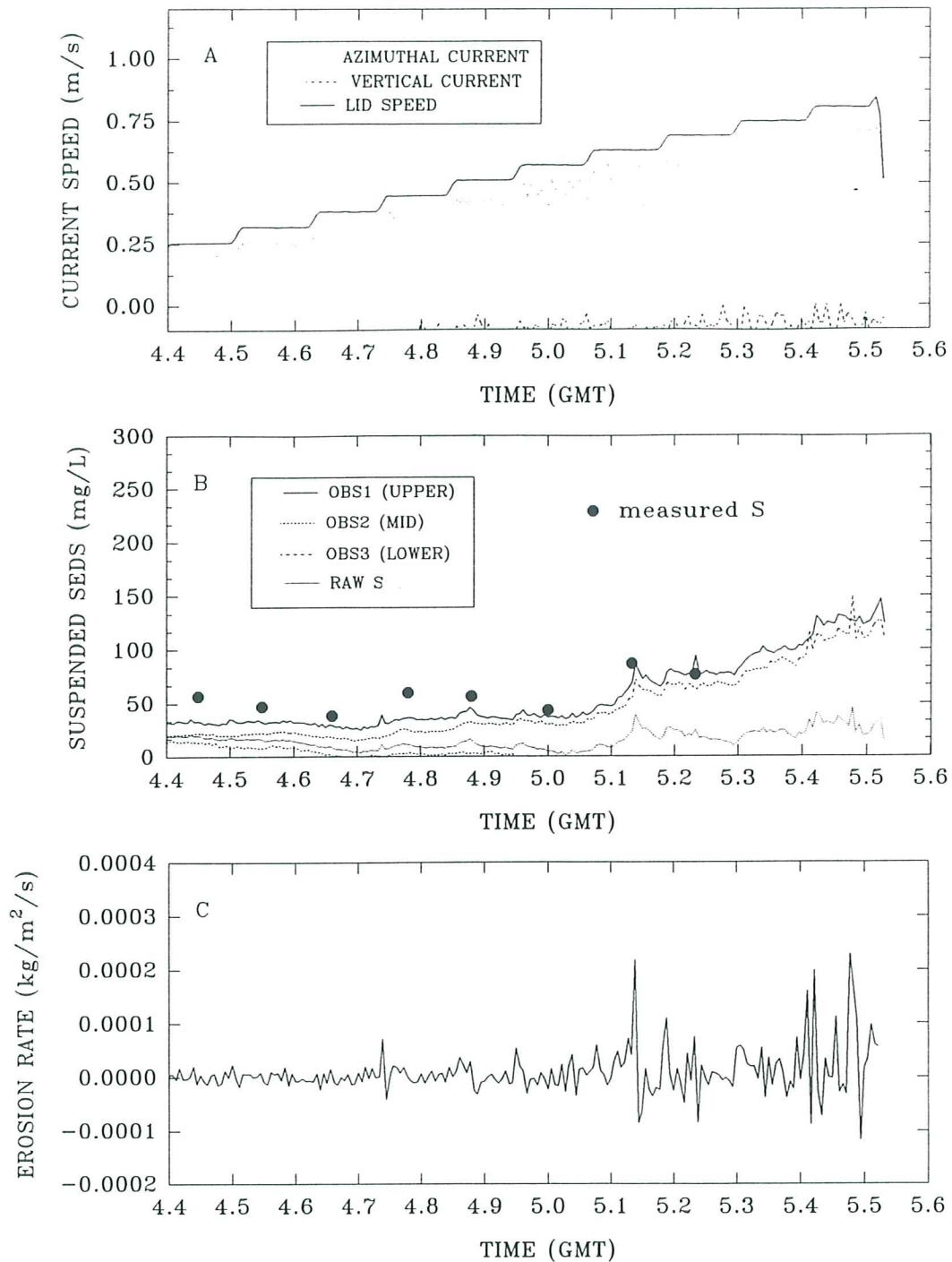


Figure 6.3.1.1. A time-series plot of results from Sea Carousel recorded at site B/C (LISPUK10) on 13 April, 1995. (A) lid speed and azimuthal and vertical currents at the reference height (0.18 m); (B) suspended sediment concentrations from the three OBS sensors (OBS1 and OBS3 are internal, OBS2 is external), and from pumped samples; and (C) erosion rate. No clear trends in erosion are evident in this time-series.

SEA CAROUSEL – LISPUK11 (Humber estuary)

SITE B/C – 13 APRIL, 1995

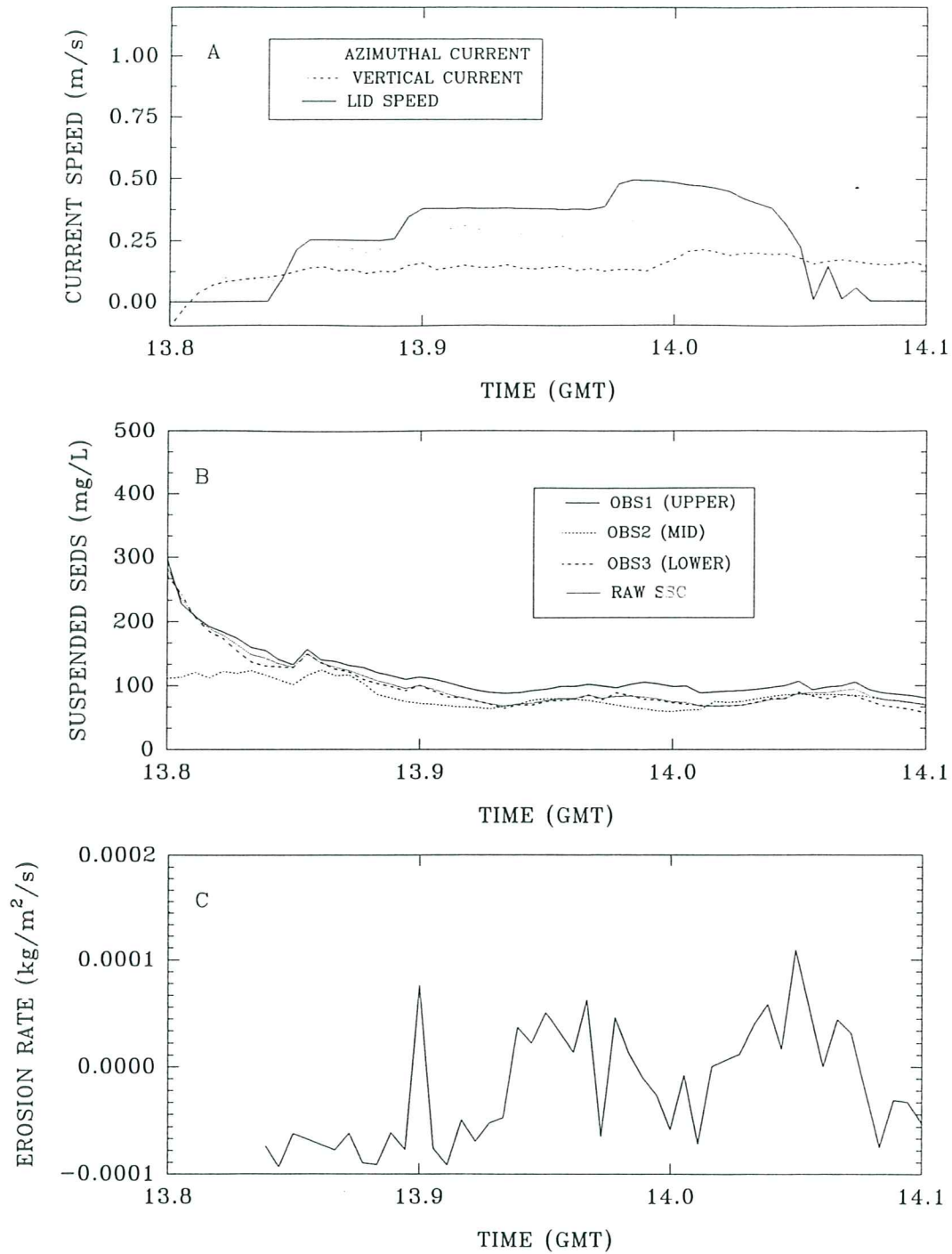


Figure 6.3.1.2. A time-series plot of results from Sea Carousel recorded at site B/C (LISPUK11) on 13 April, 1995. (A) lid speed and azimuthal and vertical currents at the reference height (0.18 m); (B) suspended sediment concentrations from the three OBS sensors (OBS1 and OBS3 are internal, OBS2 is external); and (C) erosion rate. The site was abandoned early due to drifting. Also notice the trends in sediment concentration which show the passage of a flood tide turbidity maximum.

SEA CAROUSEL – LISPUK12 (Humber estuary)

SITE B/C – 13 APRIL, 1995

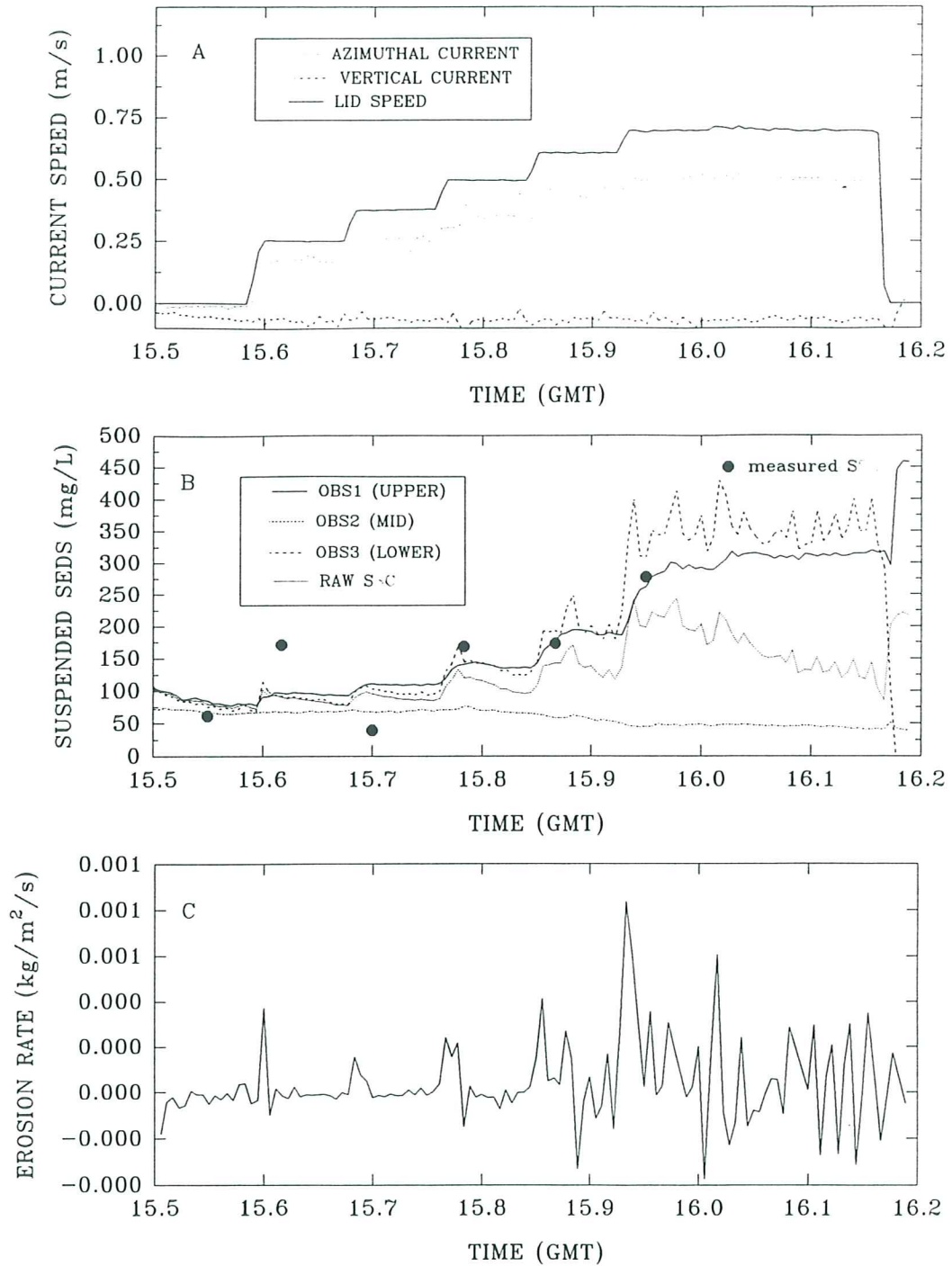


Figure 6.3.1.3. A time-series plot of results from Sea Carousel recorded at site B/C (LISPUK12) on 13 April, 1995. (A) lid speed and azimuthal and vertical currents at the reference height (0.18 m); (B) suspended sediment concentrations from the three OBS sensors (OBS1 and OBS3 are internal, OBS2 is external), and from pumped samples; and (C) erosion rate. The erratic nature of erosion is likely due to lower sensor response to intermittent burial.

STATION LISPUK10, SITE B/C - 13 APRIL, 1995

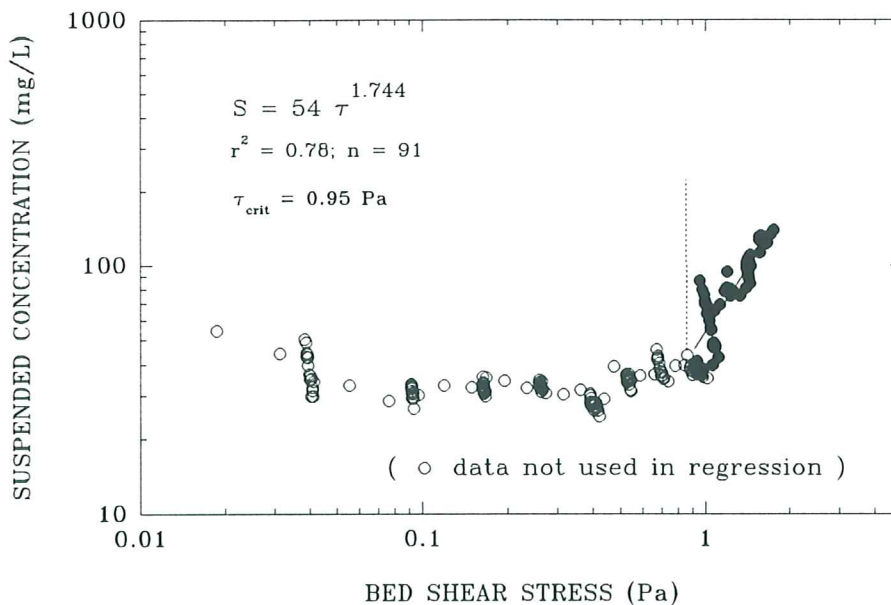
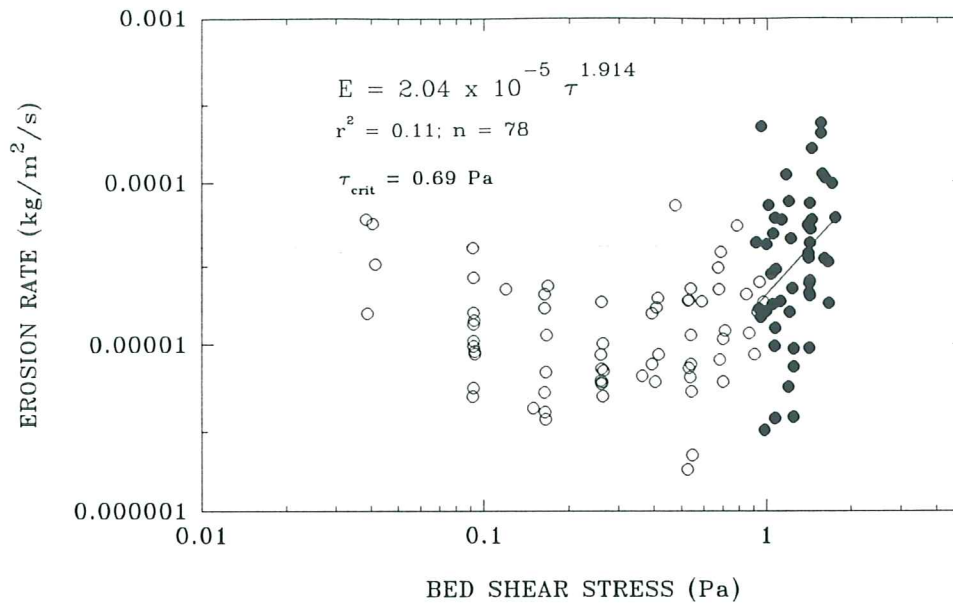


Figure 6.3.1.4. Estimates of the erosion threshold for deployment LISPUK10, site B/C. The upper panel shows that erosion rate is a power function of applied bed stress; the estimated erosion threshold is 0.69 Pa. The lower panel shows that suspended sediment concentration increases as a power function of applied bed shear stress; the threshold is equated with the stress at ambient concentration and yields a value of 0.95 Pa.

STATION LISPUK12, SITE B/C - 13 APRIL, 1995

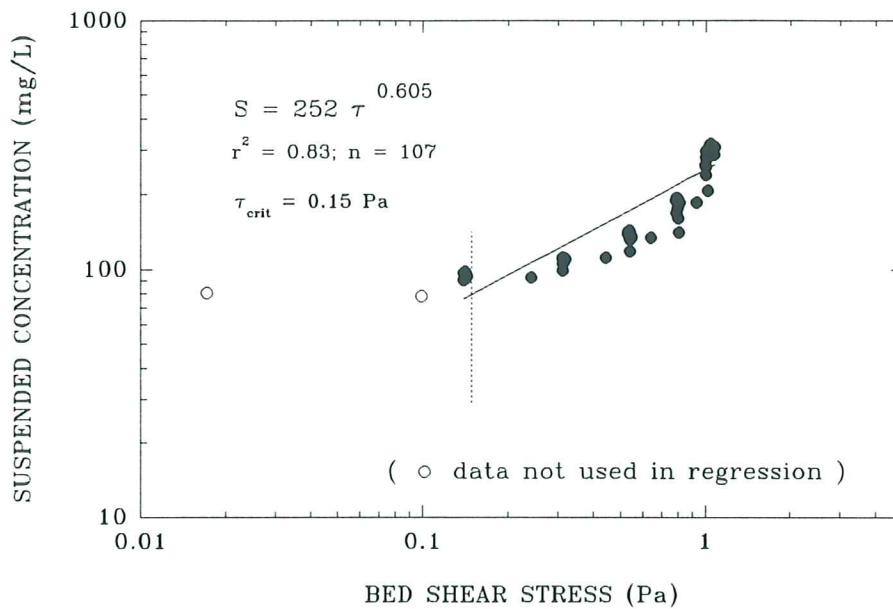
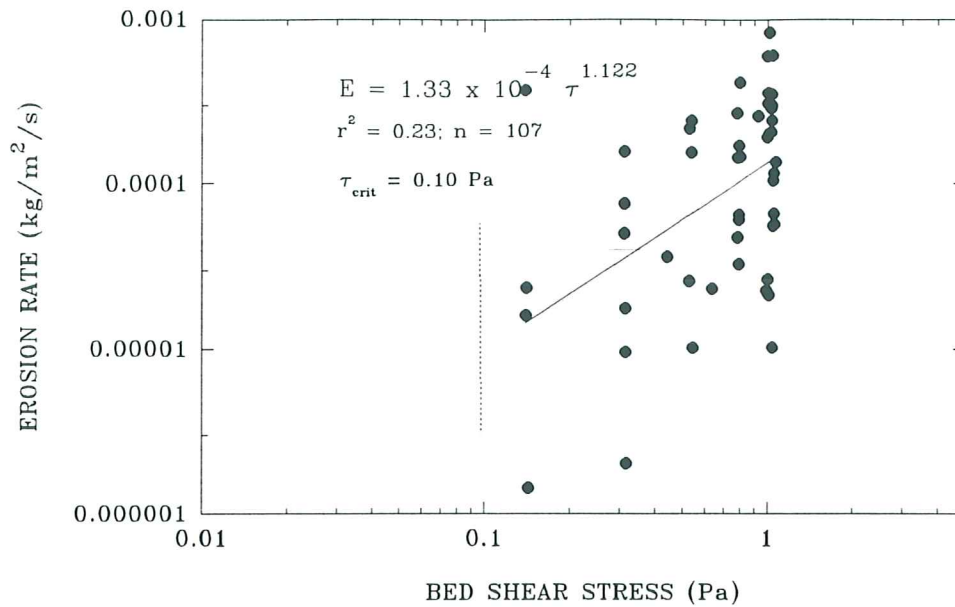


Figure 6.3.1.5. Estimates of the erosion threshold for deployment LISPUK12, site B/C. The upper panel shows that erosion rate is a power function of applied bed stress; the estimated erosion threshold is 0.10 Pa. The lower panel shows that suspended sediment concentration increases as a power function of applied bed shear stress; the threshold is equated with the stress at ambient concentration and yields a value of 0.15 Pa.

LAB CAROUSEL – LISPUK (Humber estuary)

SITE B/C (LABEXP8) – 16 APRIL, 1995

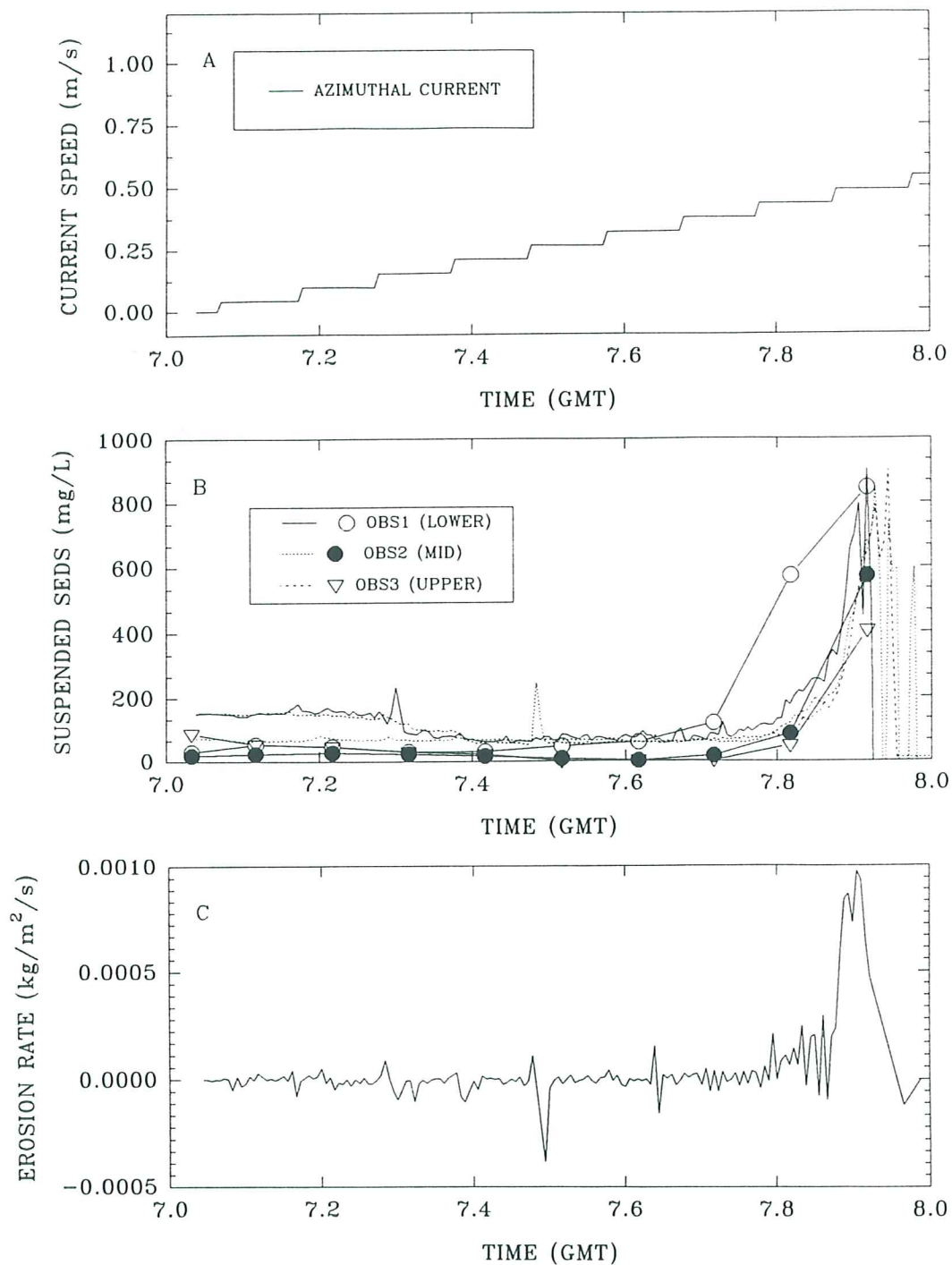


Figure 6.3.2.1. A time-series of Lab Carousel experiment (Labexp8) on a site B/C bulk sample. (A) the azimuthal reference current for a height of 0.18 m above the bed (based on lid rotation); (B) suspended sediment concentration from three OBS's and pumped samples at heights of 0.03, 0.10, and 0.20 m above the base; and (C) erosion rate.

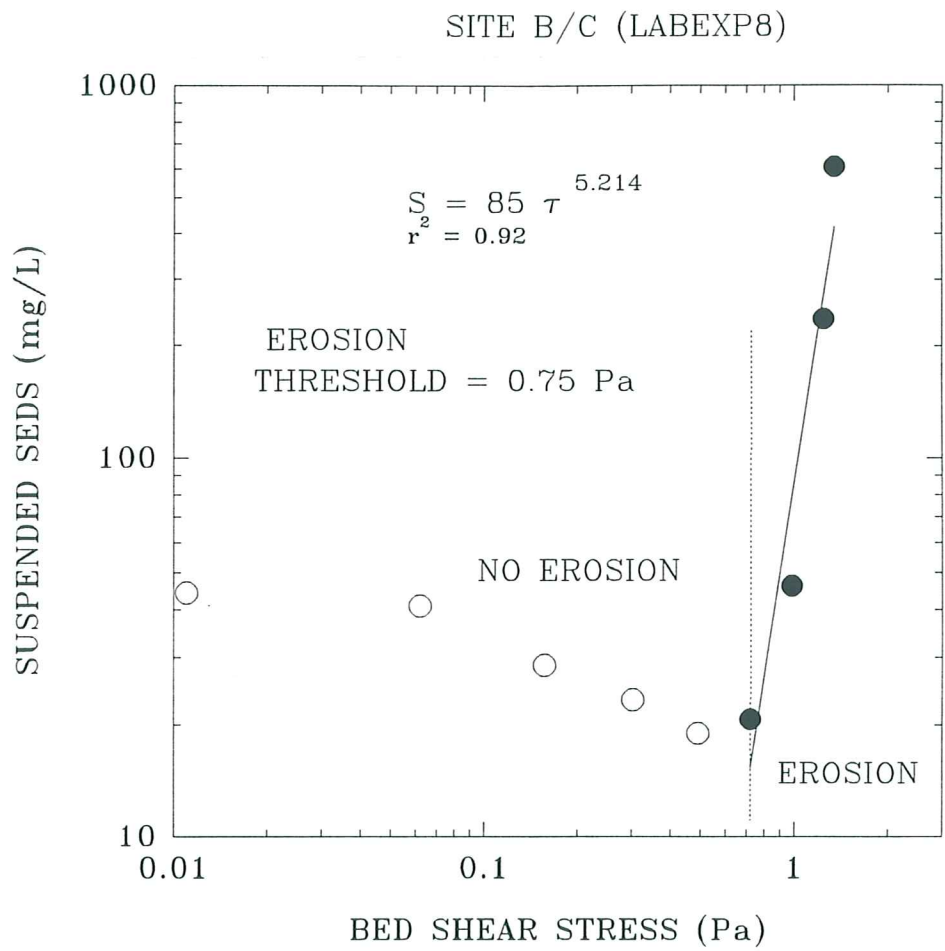


Figure 6.3.2.2. A plot of measured suspended sediment concentration (from pumped samples) versus applied bed shear stress in Lab Carousel for experiment Labexp8 (site B/C) . Notice the onset of erosion at 0.75 Pa which is based on the extrapolation of concentration to ambient levels.

LISPUK – SITE B/C, Humber estuary

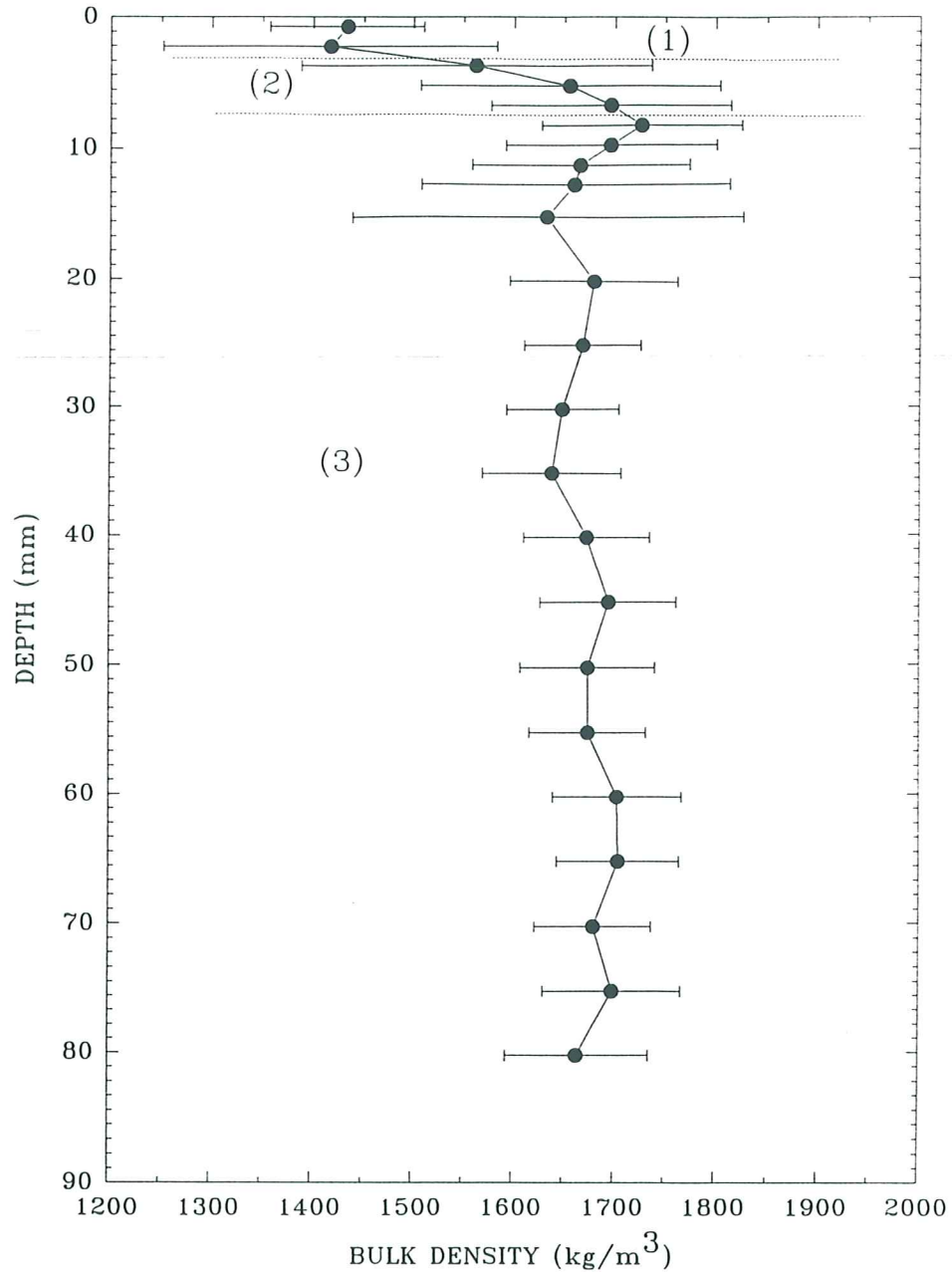


Figure 6.3.3.1. A log of the wet-weight bulk density derived from a Catscan analysis of a syringe core collected at site B/C. Three layers are evident: (1) a surface layer of relatively low density (3 mm thick); (2) a transitional layer of rapidly increasing density (5 mm thick); and (3) the denser substrate.

SEA CAROUSEL – LISPUK05 (Humber estuary)

SITE C – 11 APRIL, 1995

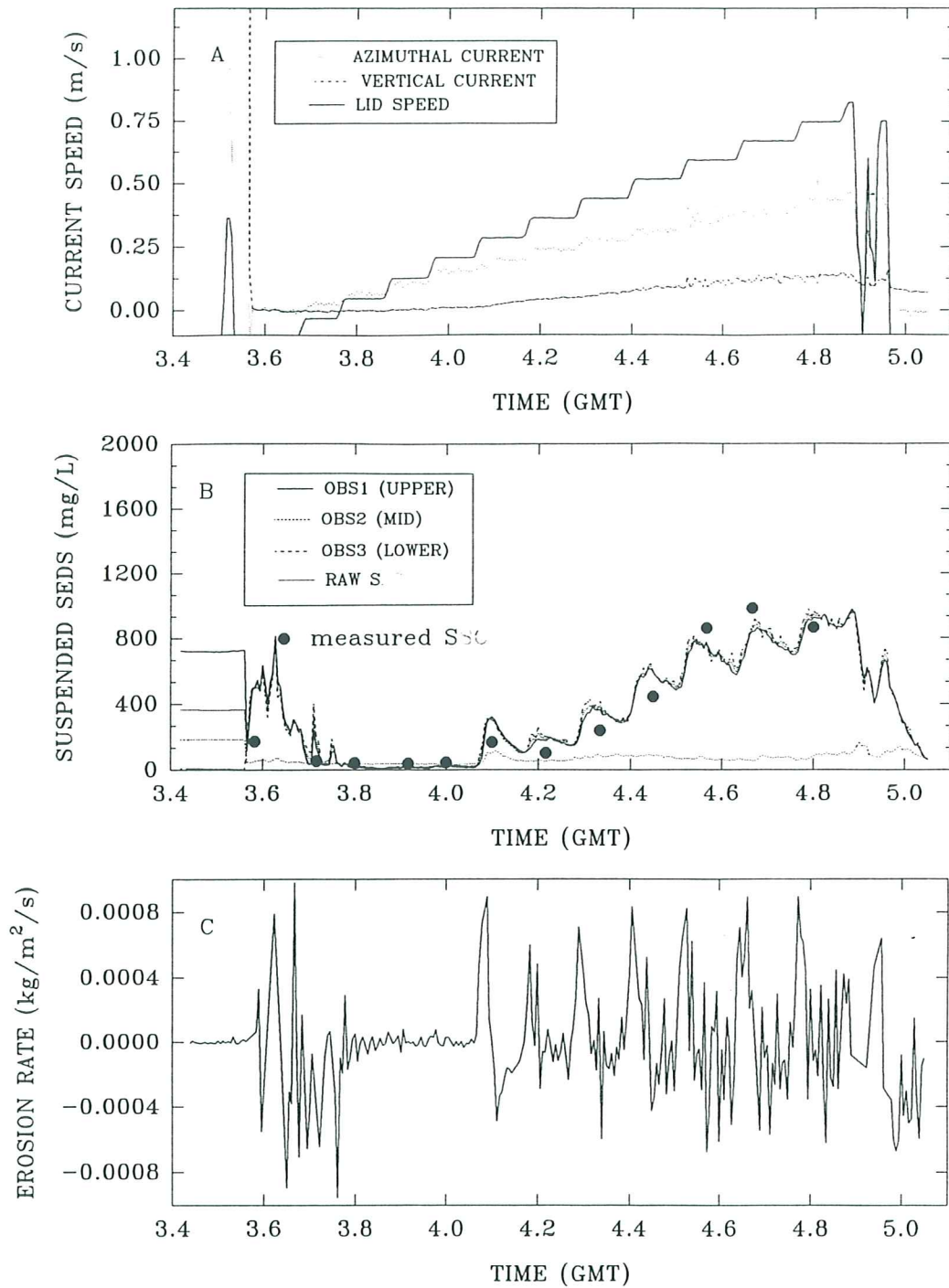


Figure 6.4.1.1. A time-series plot of results from Sea Carousel recorded at site C (LISPUK5) on 11 April, 1995. (A) lid speed and azimuthal and vertical currents at the reference height (0.18 m); (B) suspended sediment concentrations from the three OBS sensors (OBS1 and OBS3 are internal, OBS2 is external), and from pumped samples; and (C) erosion rate. The erosion is Type I in form in the early stages.

SEA CAROUSEL – LISPUK06 (Humber estuary)

SITE C – 11 APRIL, 1995

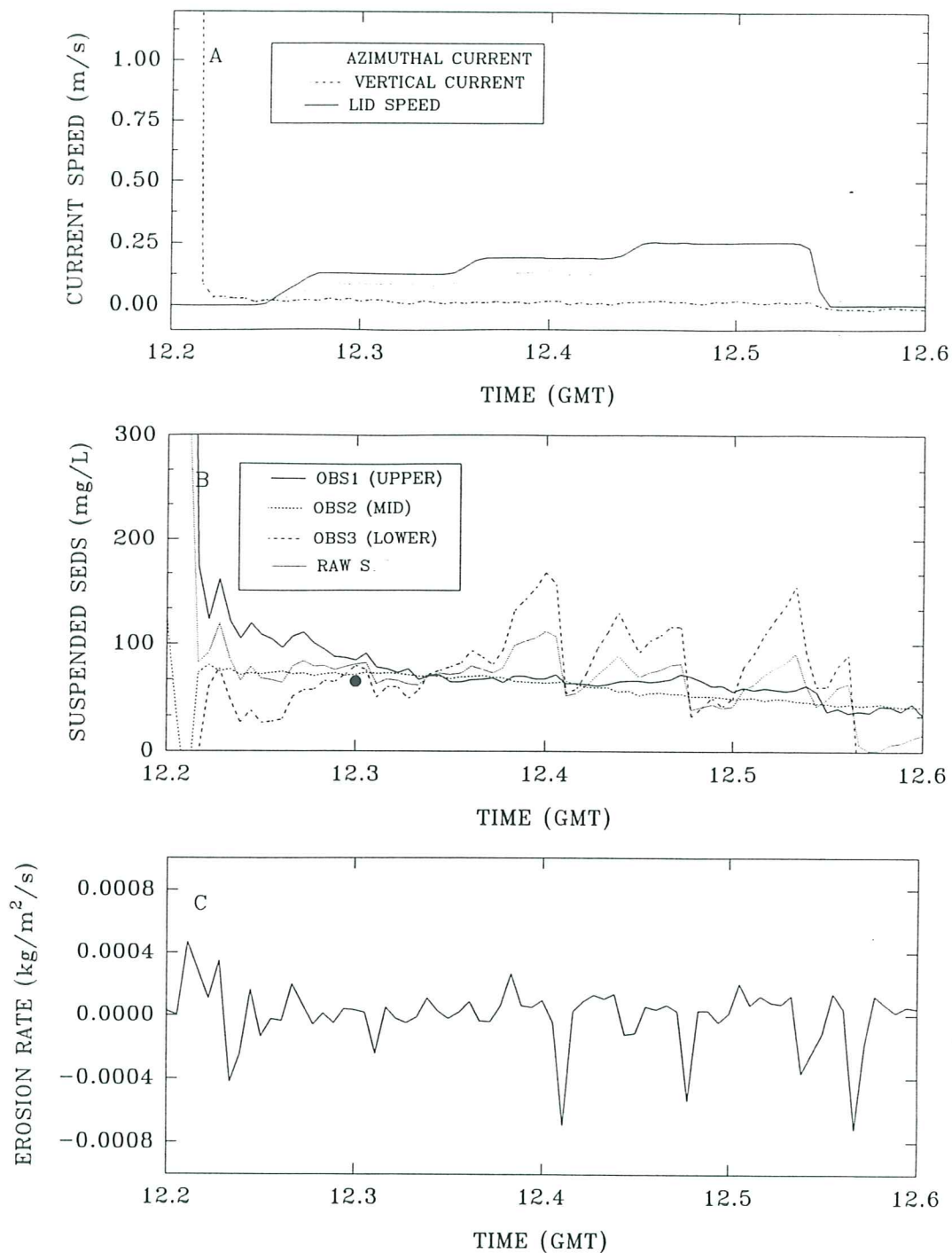


Figure 6.4.1.2. A time-series plot of results from Sea Carousel recorded at site C (LISPUK6) on 11 April, 1995. (A) lid speed and azimuthal and vertical currents at the reference height (0.18 m); (B) suspended sediment concentrations from the three OBS sensors (OBS1 and OBS3 are internal, OBS2 is external), and from one pumped sample; and (C) erosion rate. The station was abandoned prematurely due to boat drift.

STATION LISPUK5, SITE C - 11 APRIL, 1995

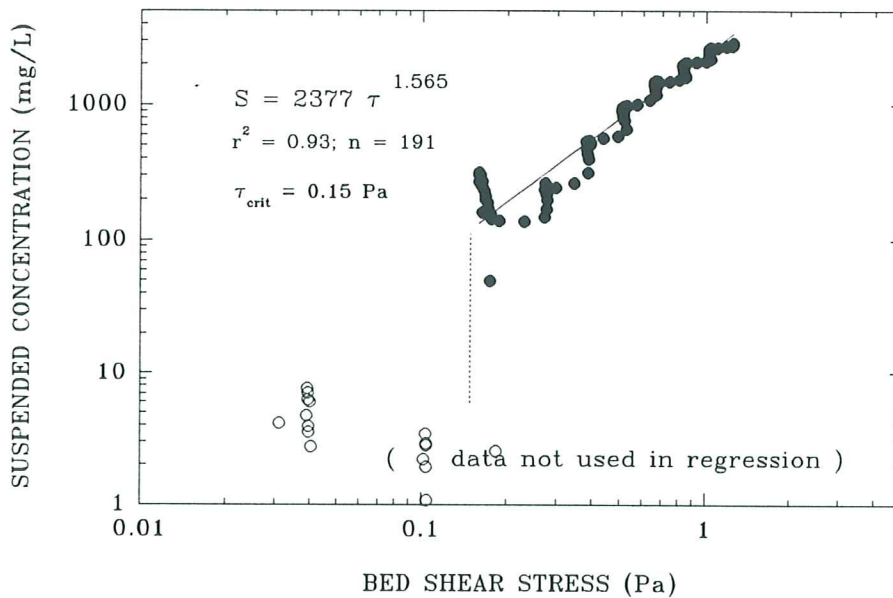
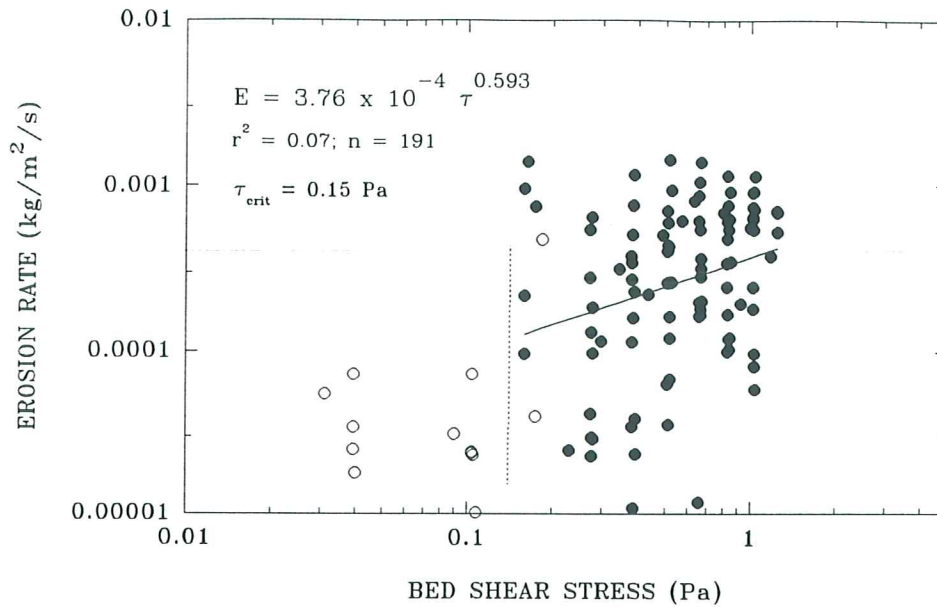


Figure 6.4.1.3. Estimates of the erosion threshold for deployment LISPUK5, site C. The upper panel shows that erosion rate is a power function of applied bed stress; the estimated erosion threshold is 0.15 Pa. The lower panel shows that suspended sediment concentration increases as a power function of applied bed shear stress; the threshold is equated with the stress at ambient concentration and yields a value of 0.15 Pa.

LAB CAROUSEL – LISPUK (Humber estuary)

SITE C (LABEXP7) – 14 APRIL, 1995

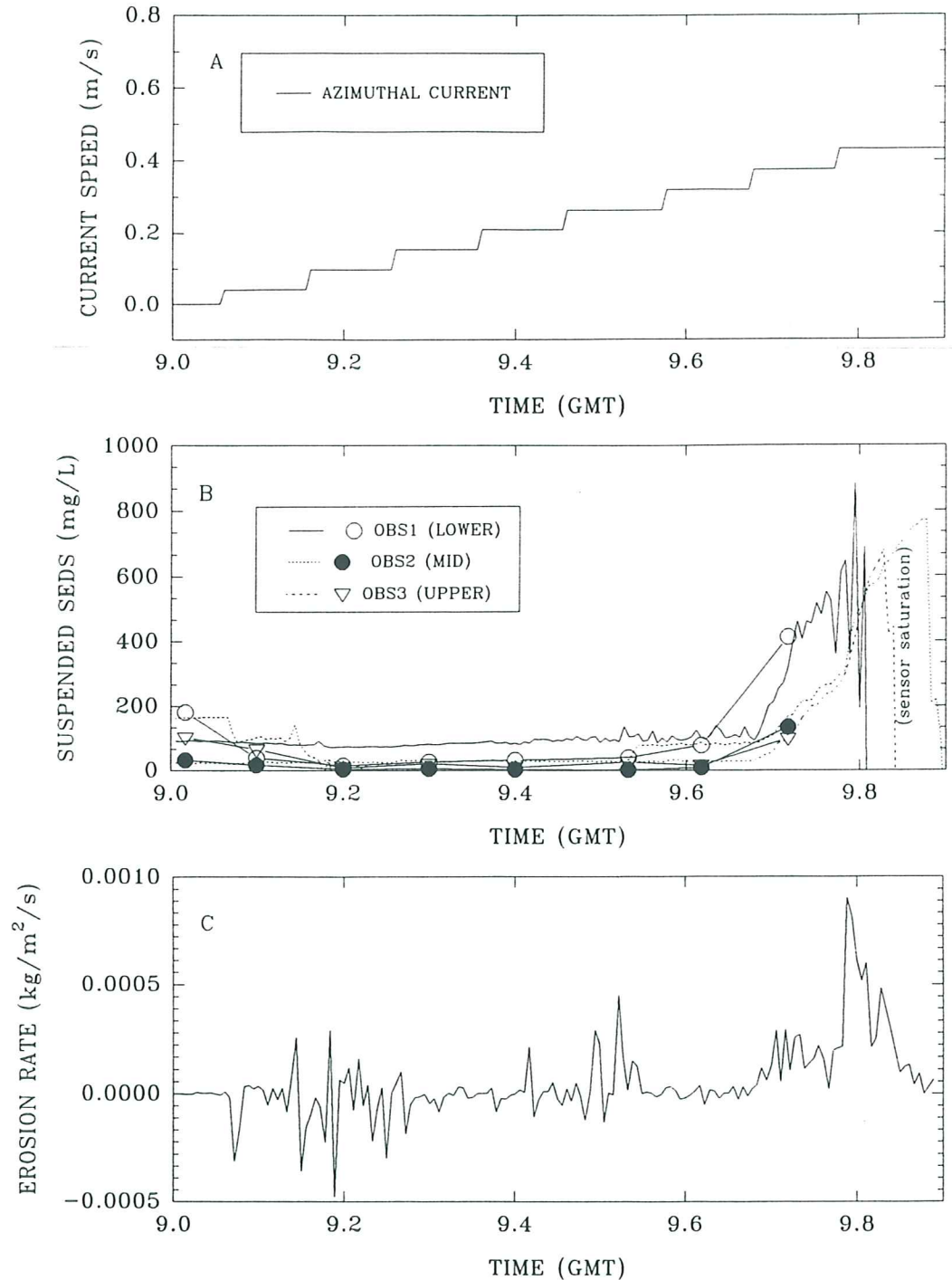


Figure 6.4.2.1. A time-series of Lab Carousel experiment (Labexp7) on a site C bulk sample. (A) the azimuthal reference current for a height of 0.18 m above the bed (based on lid rotation); (B) suspended sediment concentration from three OBS's and pumped samples at heights of 0.03, 0.10, and 0.20 m above the base; and (C) erosion rate.

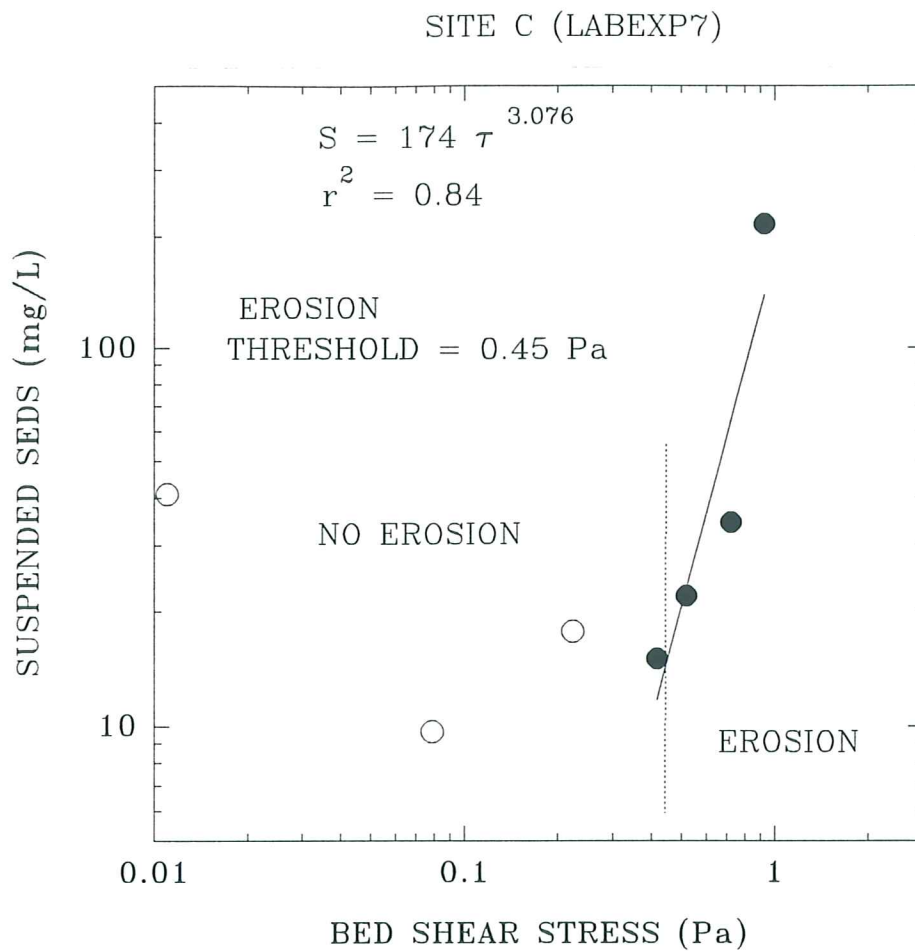


Figure 6.4.2.2. A plot of measured suspended sediment concentration (from pumped samples) versus applied bed shear stress in Lab Carousel for experiment Labexp7 (site C) . Notice the onset of erosion at 0.45 Pa which is based on the extrapolation of concentration to ambient levels.

LISPUK - SITE C, Humber estuary

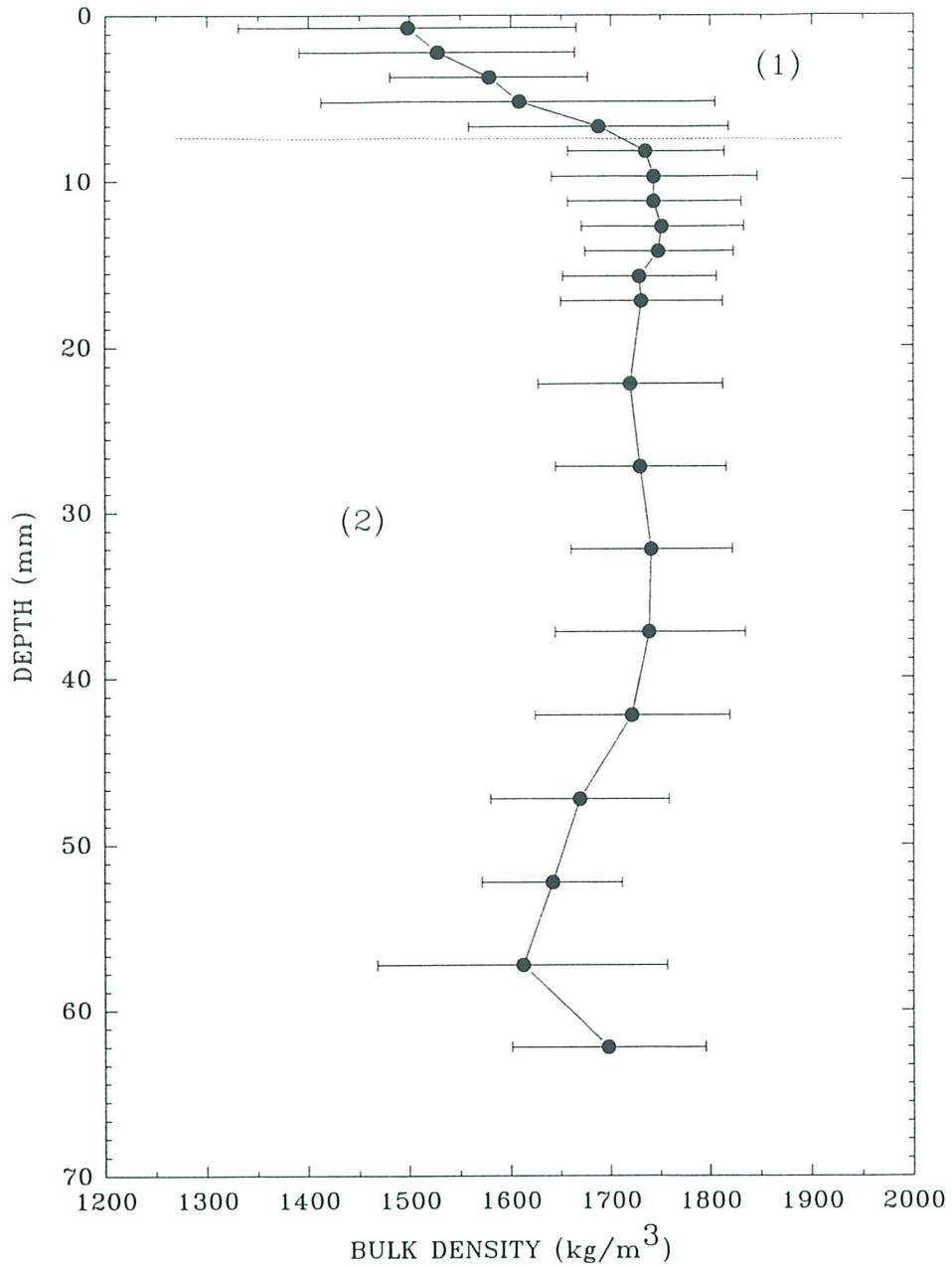


Figure 6.4.3.1. A log of the wet-weight bulk density derived from a Catscan analysis of a syringe core collected at site C. Two layers are evident: (1) a surface layer of rapidly increasing density (8 mm thick); and (2) the denser substrate.

SEA CAROUSEL – LISPUK07 (Humber estuary)

SITE CD – 10 APRIL, 1995

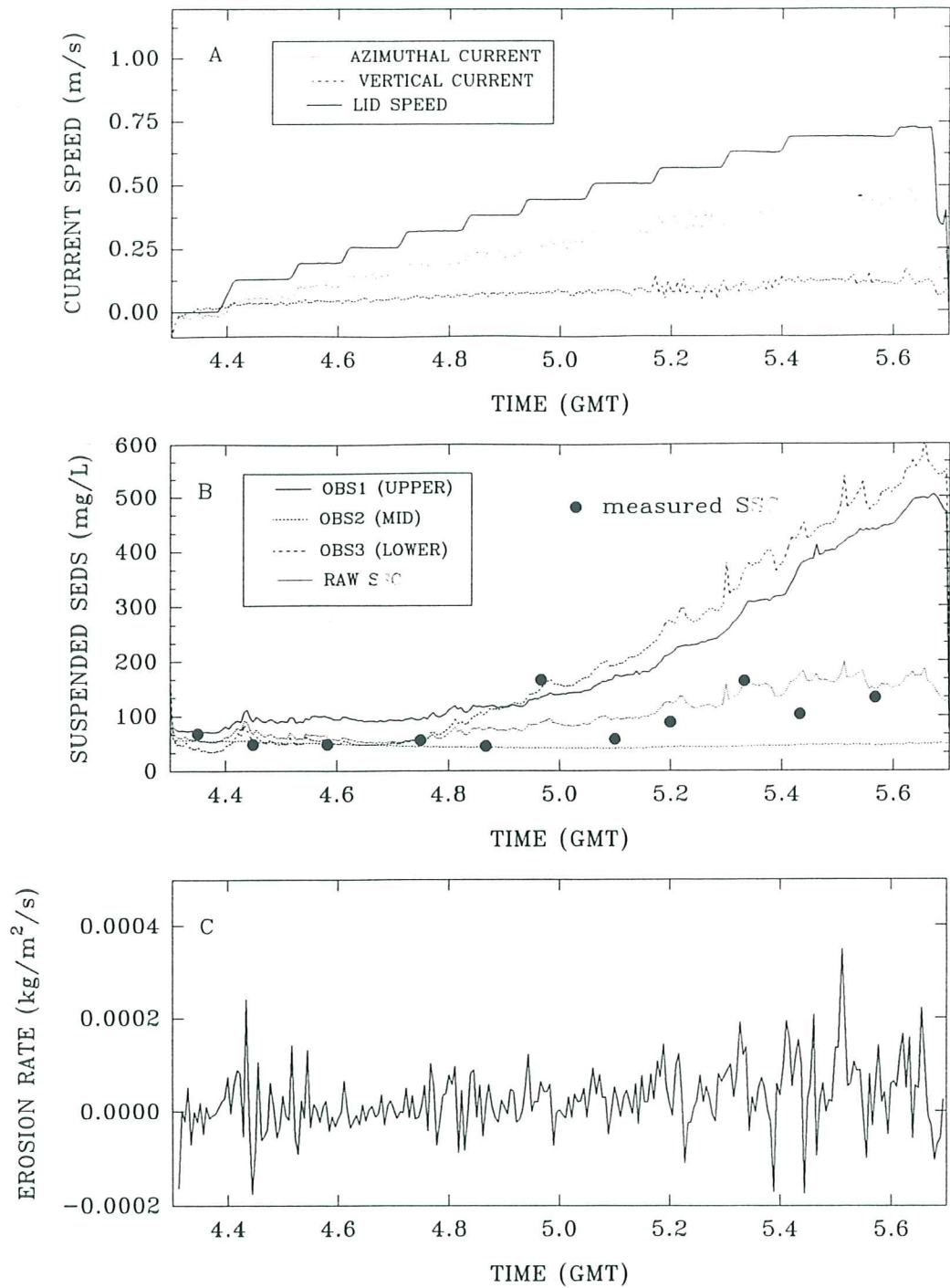


Figure 6.5.1.1. A time-series plot of results from Sea Carousel recorded at site C/D (LISPUK7) on 10 April, 1995. (A) lid speed and azimuthal and vertical currents at the reference height (0.18 m); (B) suspended sediment concentrations from the three OBS sensors (OBS1 and OBS3 are internal, OBS2 is external), and from pumped samples; and (C) erosion rate.

SEA CAROUSEL - LISPUK08 (Humber estuary)

SITE CD - 12 APRIL, 1995

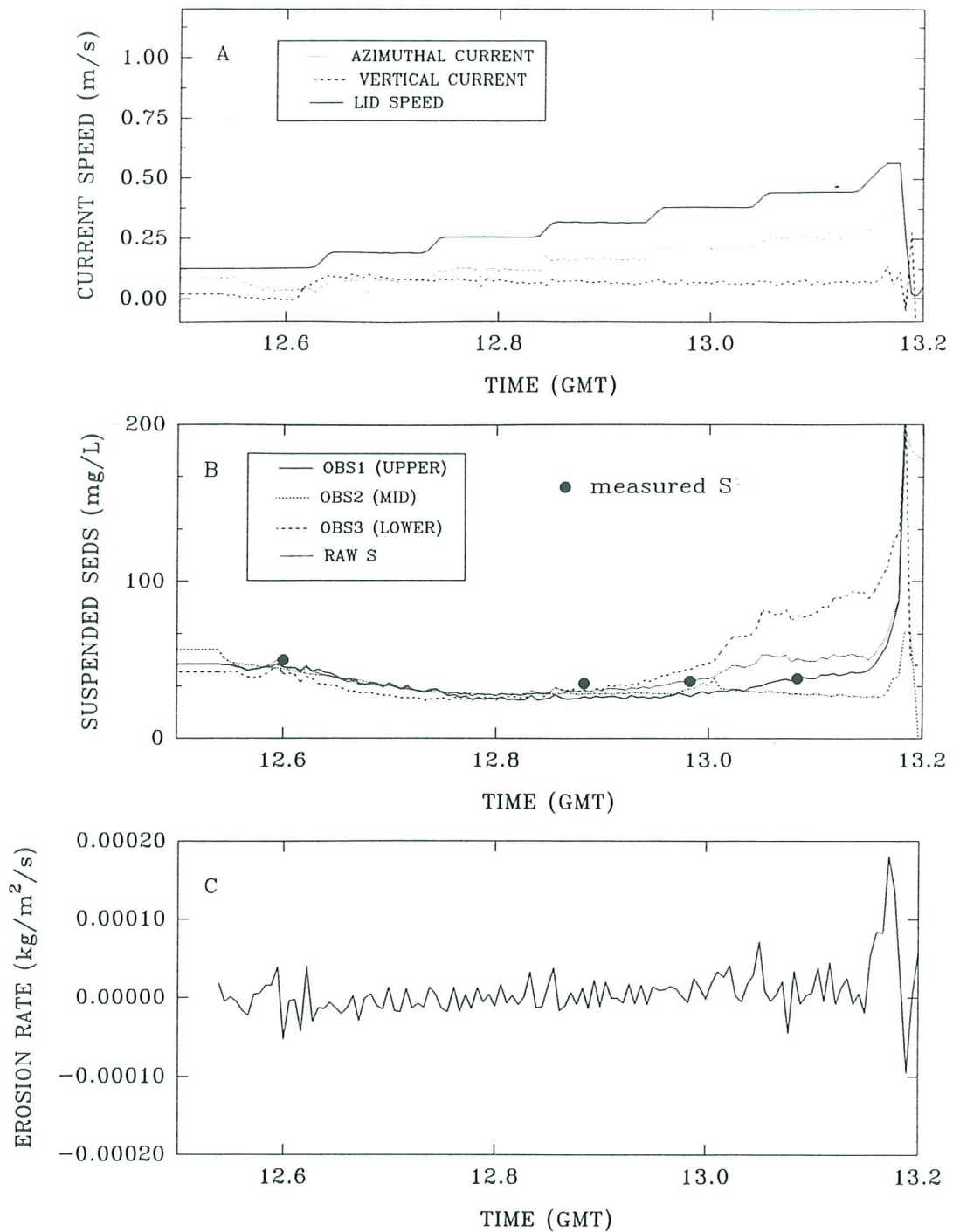


Figure 6.5.1.2. A time-series plot of results from Sea Carousel recorded at site C/D (LISPUK8) on 12 April, 1995. (A) lid speed and azimuthal and vertical currents at the reference height (0.18 m); (B) suspended sediment concentrations from the three OBS sensors (OBS1 and OBS3 are internal, OBS2 is external), and from pumped samples; and (C) erosion rate.

STATION LISPUK7, SITE C/D - 10 APRIL, 1995

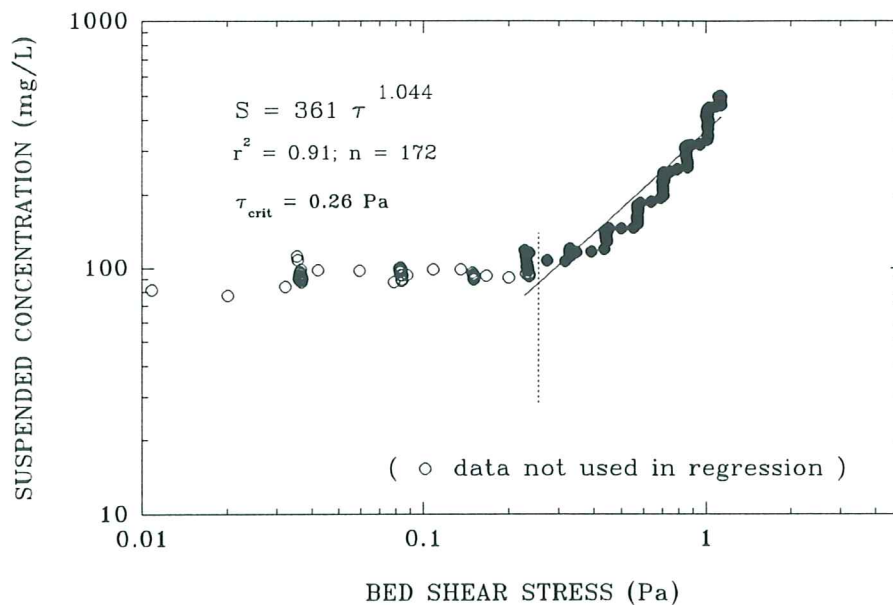
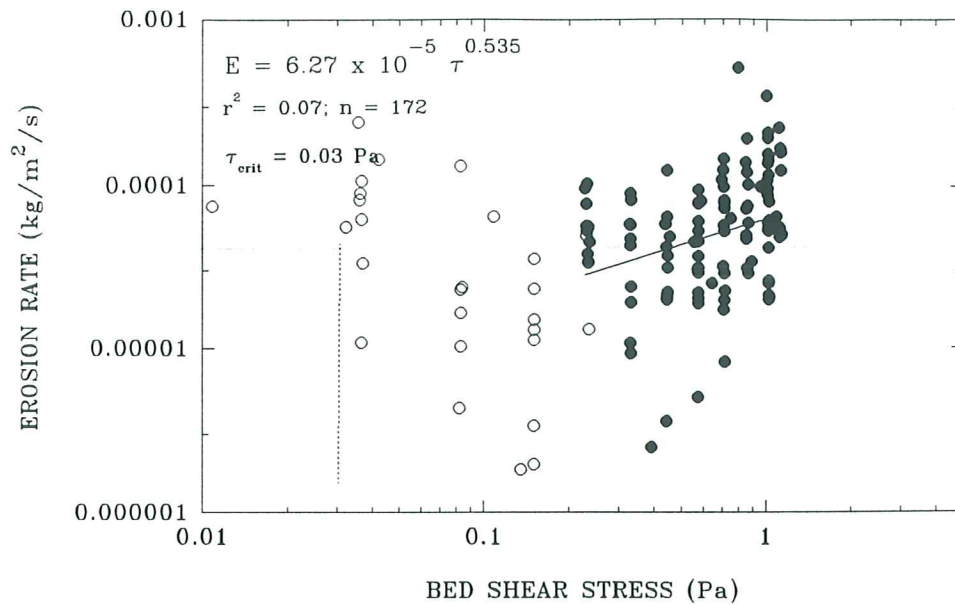


Figure 6.5.1.3. Estimates of the erosion threshold for deployment LISPUK7, site C/D. The upper panel shows that erosion rate is a power function of applied bed stress; the estimated erosion threshold is 0.03 Pa. The lower panel shows that suspended sediment concentration increases as a power function of applied bed shear stress; the threshold is equated with the stress at ambient concentration and yields a value of 0.26 Pa.

STATION LISPUK8, SITE C/D - 10 APRIL, 1995

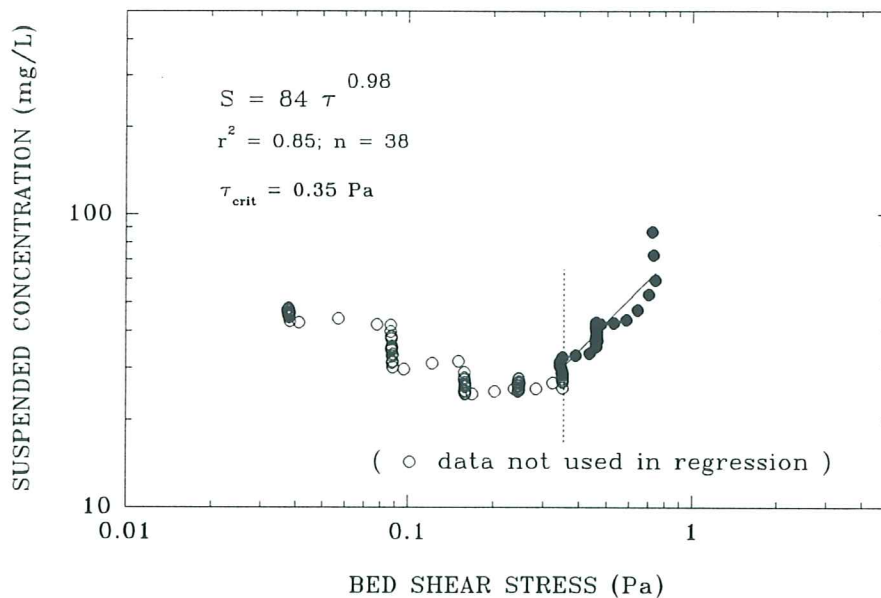
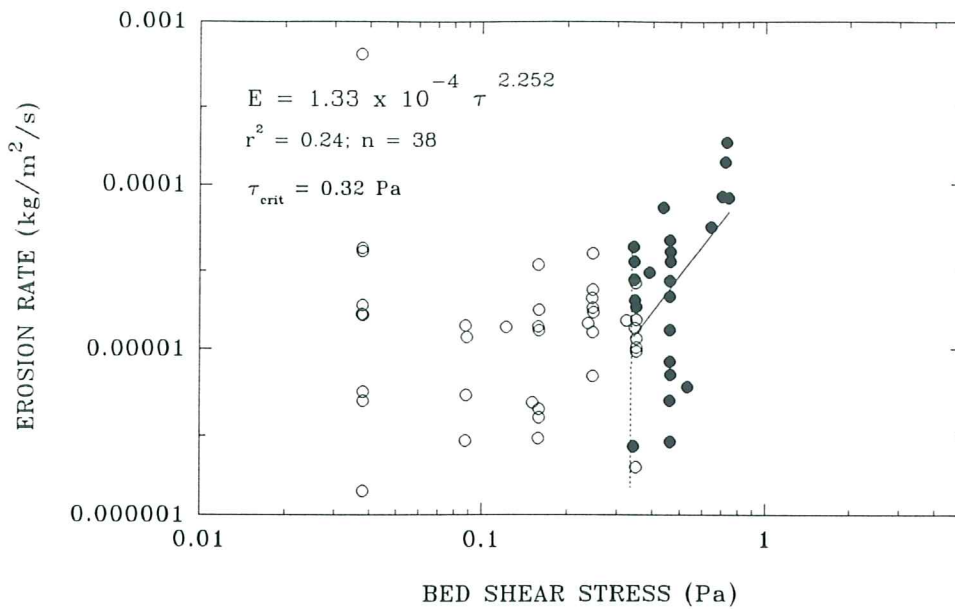


Figure 6.5.1.4. Estimates of the erosion threshold for deployment LISPUK8, site C/D. The upper panel shows that erosion rate is a power function of applied bed stress; the estimated erosion threshold is 0.32 Pa. The lower panel shows that suspended sediment concentration increases as a power function of applied bed shear stress; the threshold is equated with the stress at ambient concentration and yields a value of 0.35 Pa.

LISPUK - SITE C/D, Humber estuary

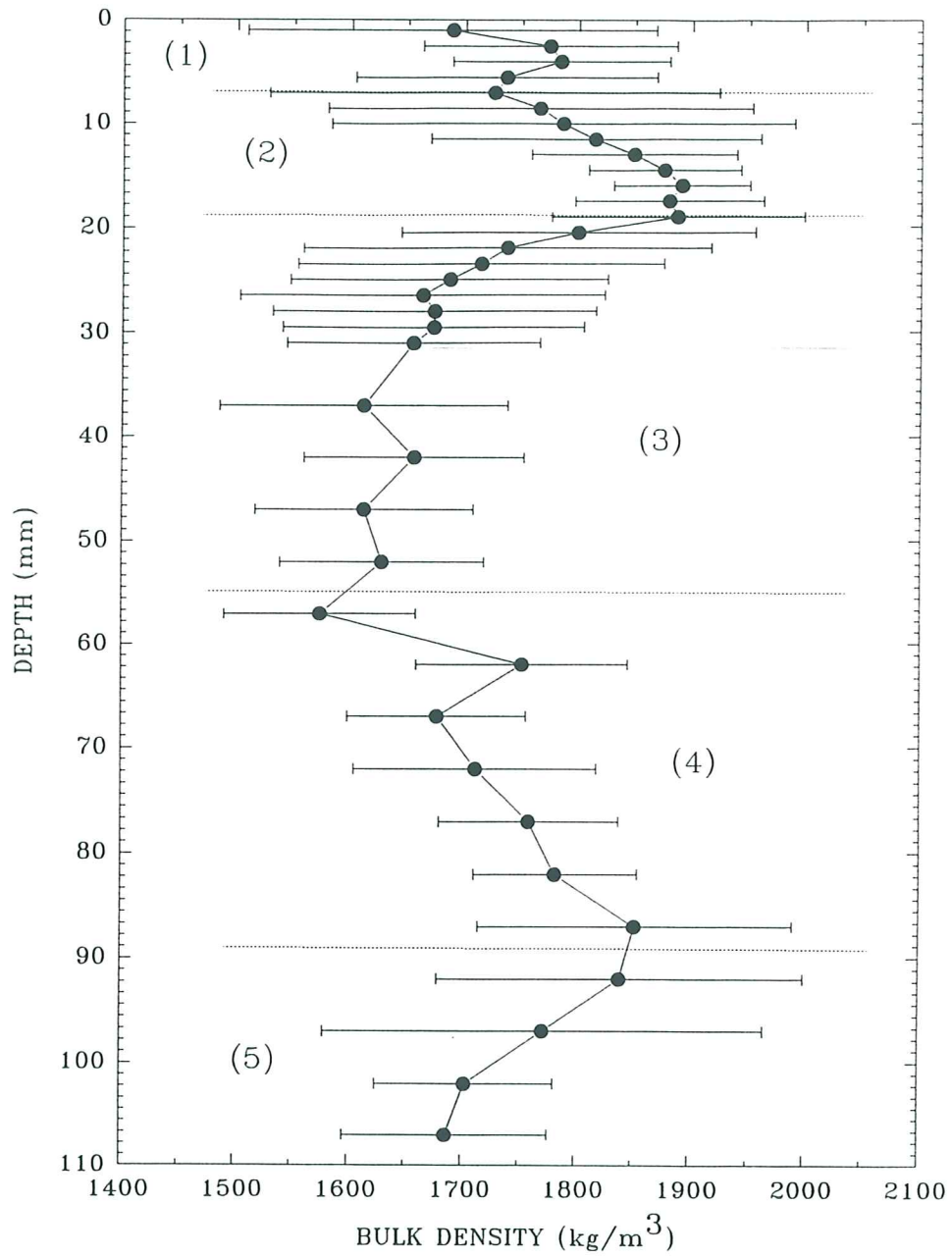


Figure 6.5.2.1. A log of the wet-weight bulk density derived from a Catscan analysis of a syringe core collected at site C/D. Five layers are evident reflecting layering of the substrate.

SEA CAROUSEL – LISPUK01 (Humber estuary)

SITE D – 8 APRIL, 1995

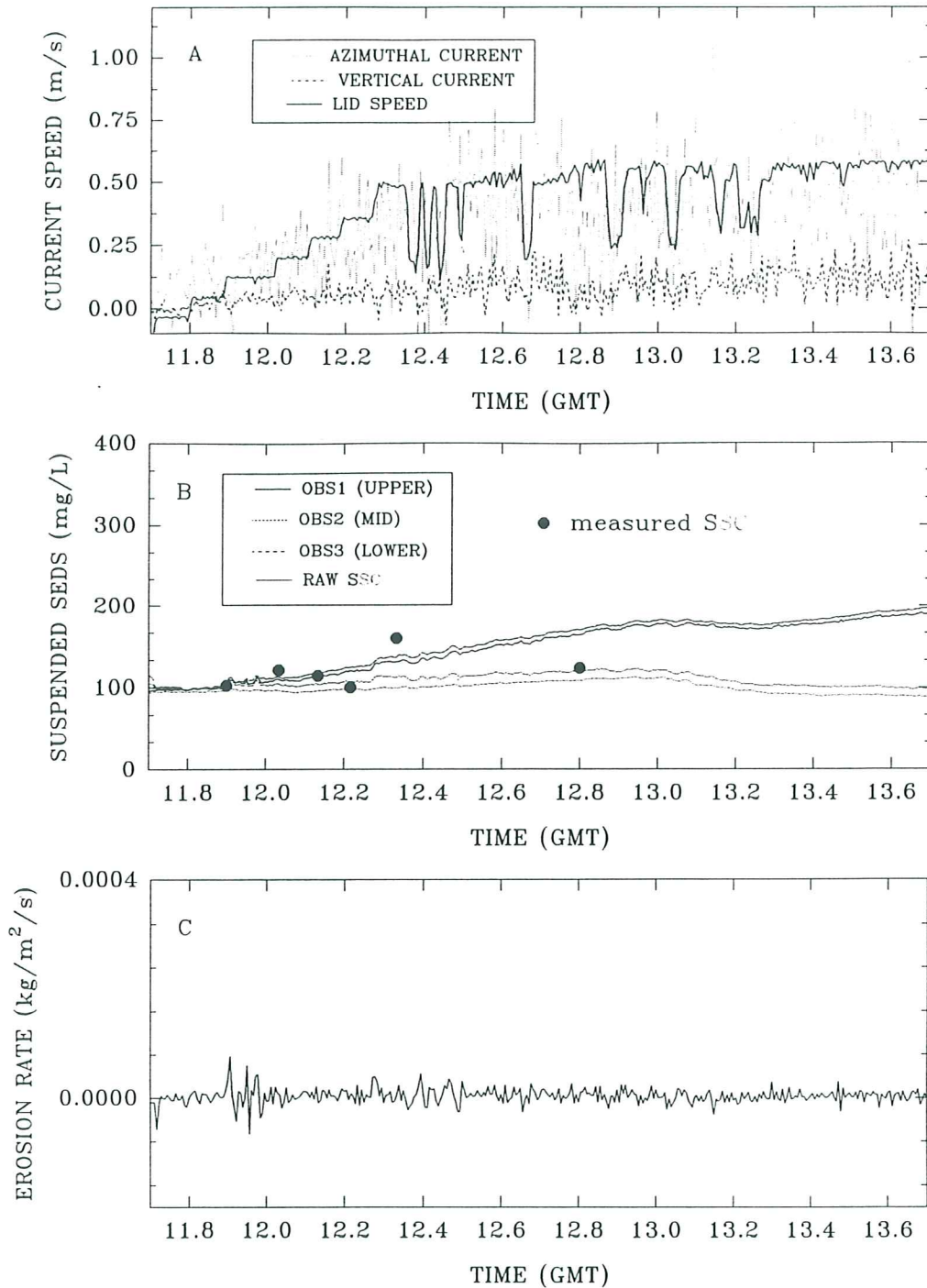


Figure 6.6.1.1. A time-series plot of results from Sea Carousel recorded at site D (LISPUK1) on 8 April, 1995. (A) lid speed and azimuthal and vertical currents at the reference height (0.18 m); (B) suspended sediment concentrations from the three OBS sensors (OBS1 and OBS3 are internal, OBS2 is external), and from pumped samples; and (C) erosion rate. This station was on the side of a creek at a high angle, hence the scatter in the results.

SEA CAROUSEL – LISPUK02 (Humber estuary)

SITE D – 8 APRIL, 1995

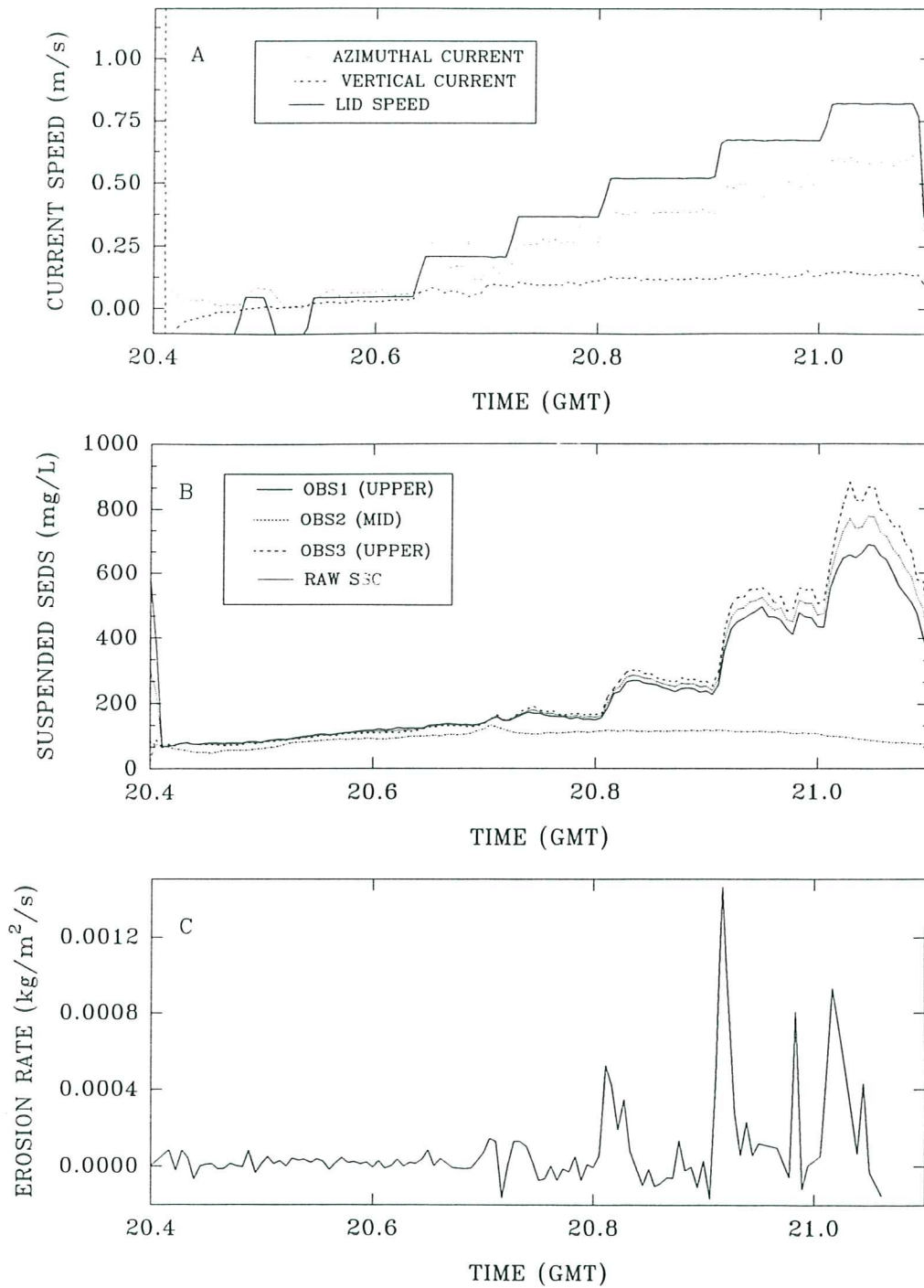


Figure 6.6.1.2. A time-series plot of results from Sea Carousel recorded at site D (LISPUK2) on 8 April, 1995. (A) lid speed and azimuthal and vertical currents at the reference height (0.18 m); (B) suspended sediment concentrations from the three OBS sensors (OBS1 and OBS3 are internal, OBS2 is external); and (C) erosion rate. Notice the Type I erosion rates.

SEA CAROUSEL – LISPUK03 (Humber estuary)

SITE D – 10 APRIL, 1995

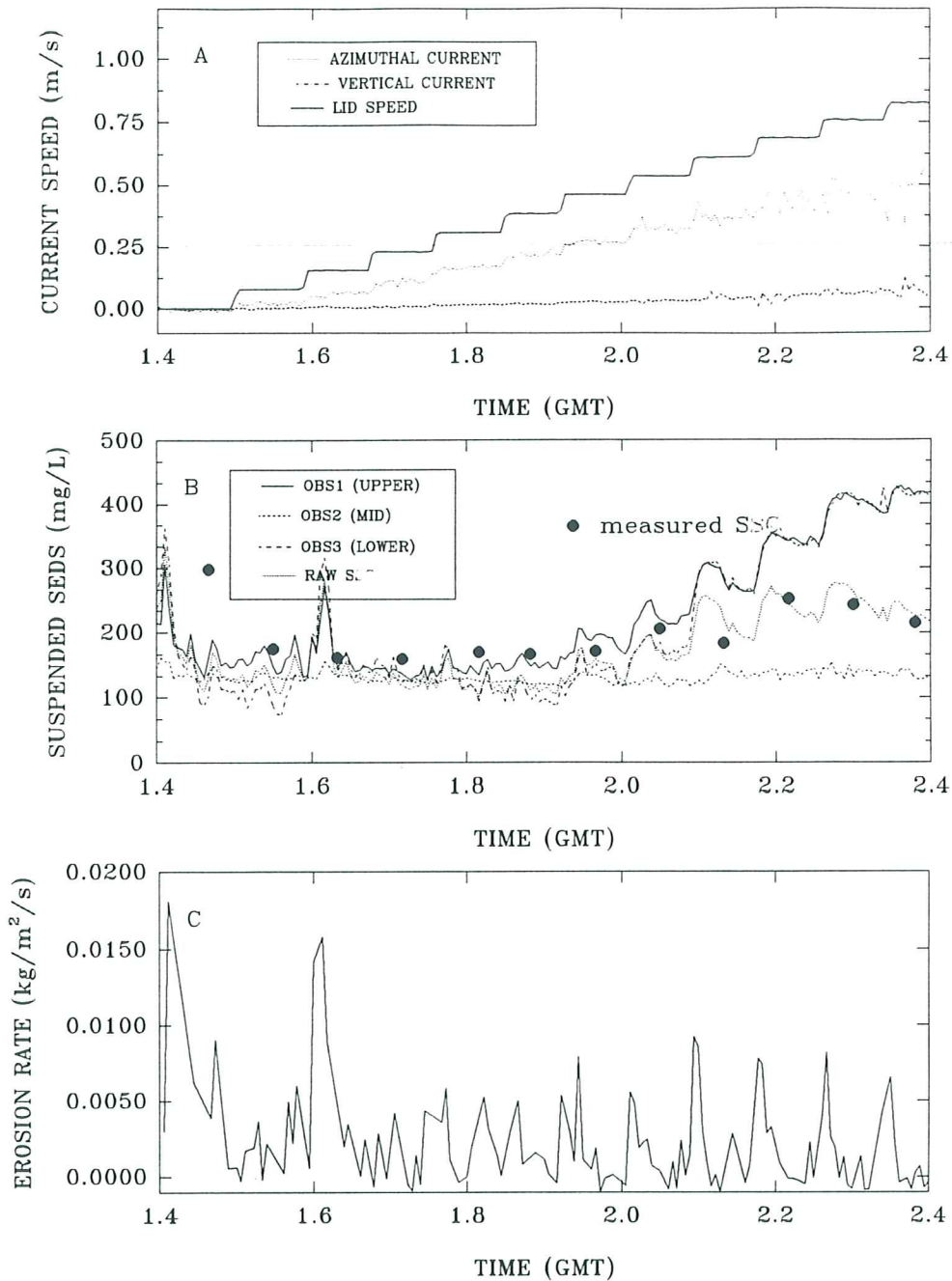


Figure 6.6.1.3. A time-series plot of results from Sea Carousel recorded at site D (LISPUK3) on 10 April, 1995. (A) lid speed and azimuthal and vertical currents at the reference height (0.18 m); (B) suspended sediment concentrations from the three OBS sensors (OBS1 and OBS3 are internal, OBS2 is external), and from pumped samples; and (C) erosion rate. Type I erosion is prevalent throughout the erosion phase.

SEA CAROUSEL – LISPUK04 (Humber estuary)

SITE D – 10 APRIL, 1995

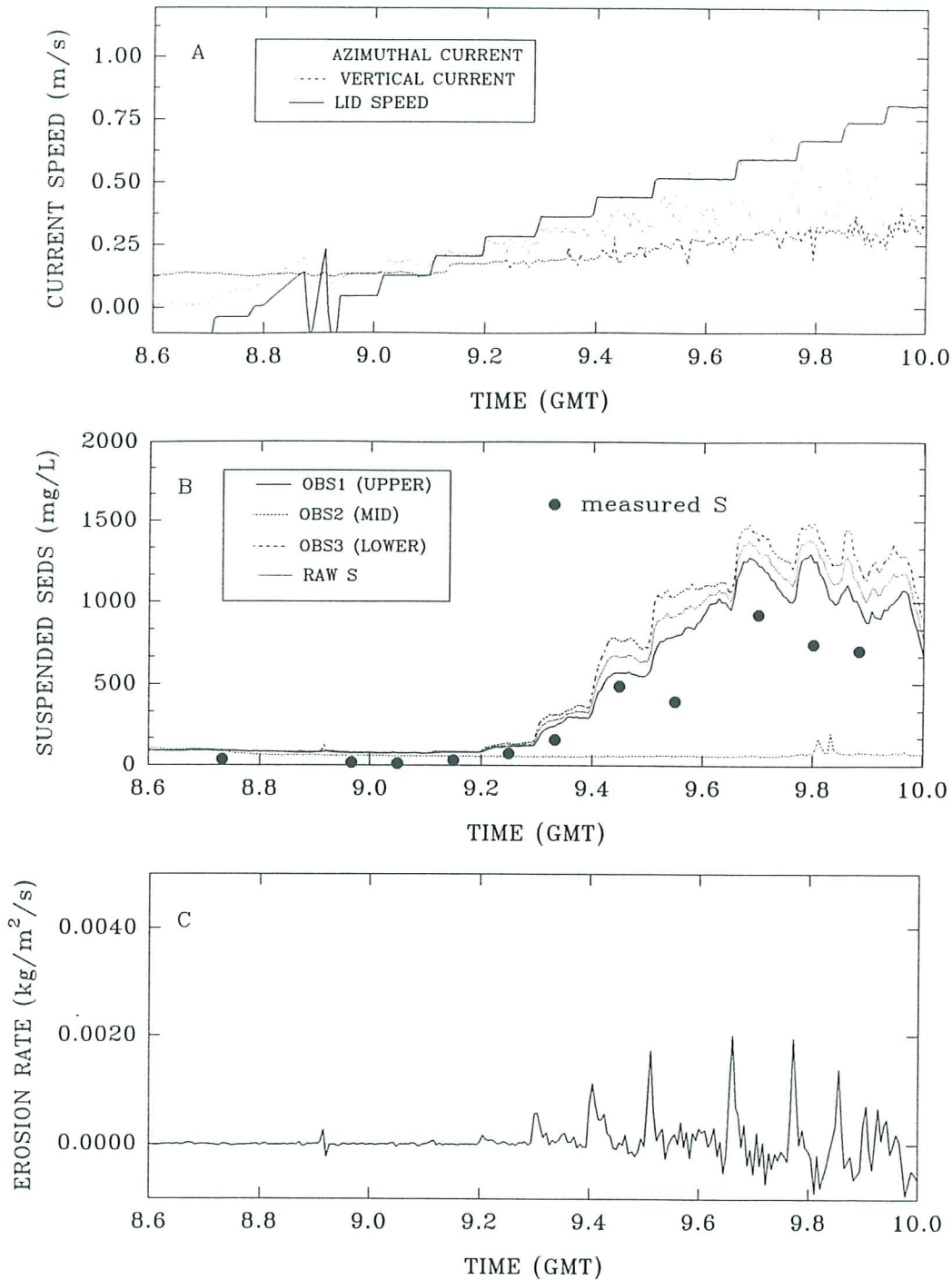


Figure 6.6.1.4. A time-series plot of results from Sea Carousel recorded at site D (LISPUK3) on 10 April, 1995. (A) lid speed and azimuthal and vertical currents at the reference height (0.18 m); (B) suspended sediment concentrations from the three OBS sensors (OBS1 and OBS3 are internal, OBS2 is external), and from pumped samples; and (C) erosion rate. Type I erosion is prevalent throughout the erosion phase.

STATION LISPUK2, SITE D – 8 APRIL, 1995

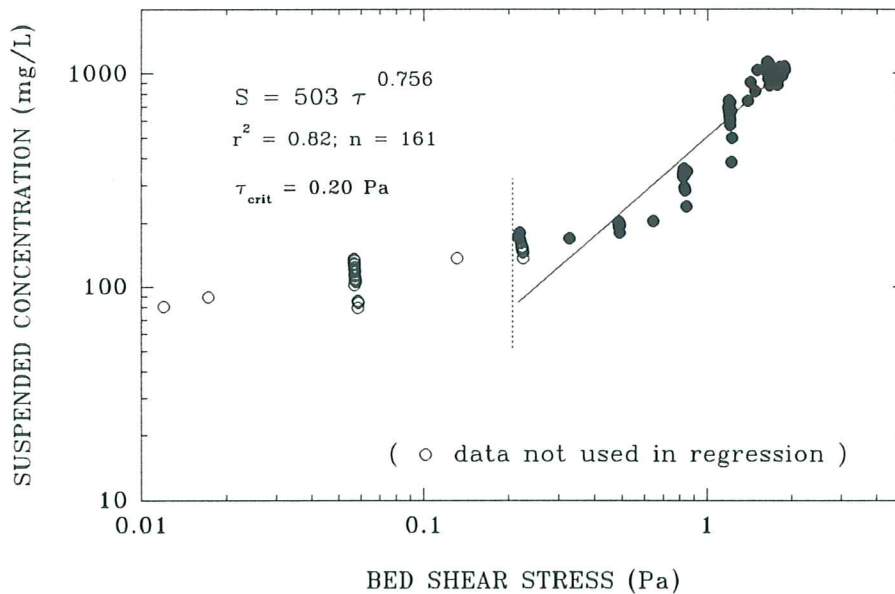
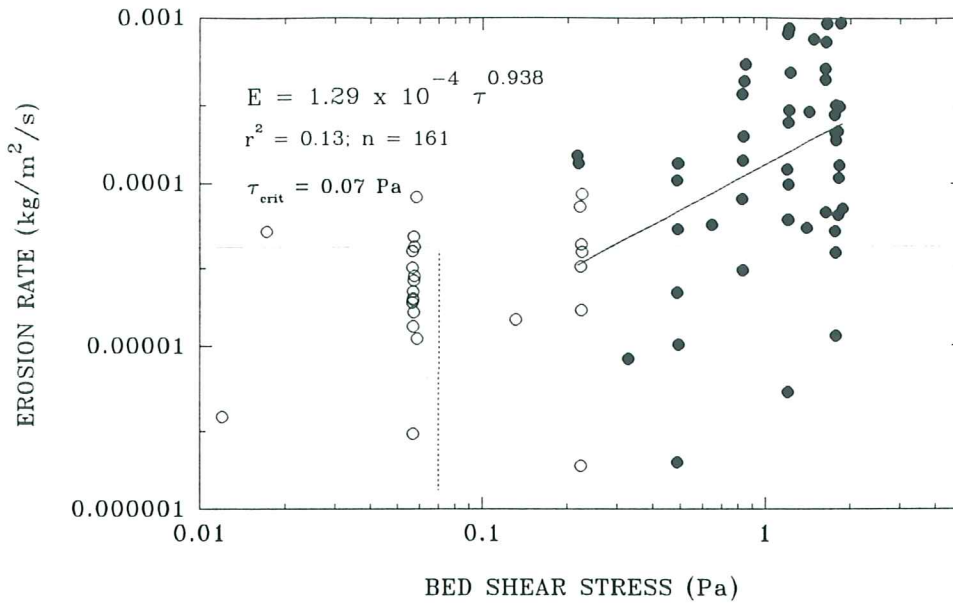


Figure 6.6.1.5. Estimates of the erosion threshold for deployment LISPUK2, site D. The upper panel shows that erosion rate is a power function of applied bed stress; the estimated erosion threshold is 0.07 Pa. The lower panel shows that suspended sediment concentration increases as a power function of applied bed shear stress; the threshold is equated with the stress at ambient concentration and yields a value of 0.20 Pa.

STATION LISPUK3, SITE D - 10 APRIL, 1995

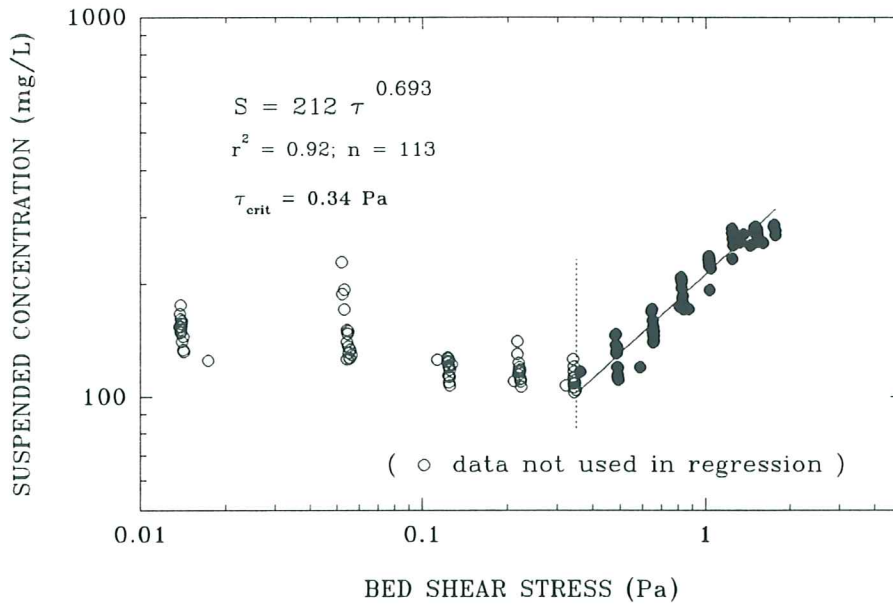
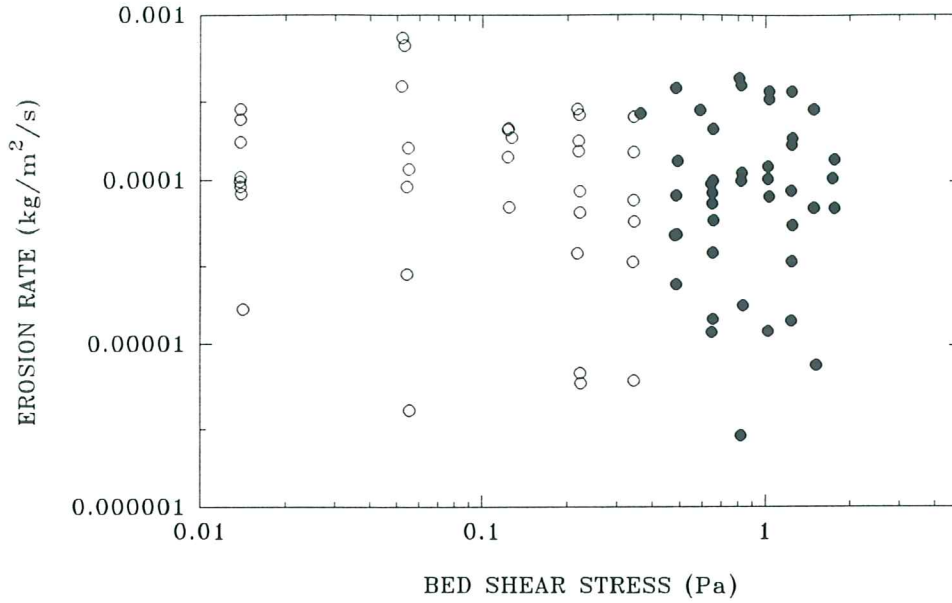


Figure 6.6.1.6. Estimates of the erosion threshold for deployment LISPUK2, site D. The upper panel shows that erosion rate is a power function of applied bed stress; it is not possible to estimate erosion threshold from this plot. The lower panel shows that suspended sediment concentration increases as a power function of applied bed shear stress; the threshold is equated with the stress at ambient concentration and yields a value of 0.34 Pa.

STATION LISPUK4, SITE D - 10 APRIL, 1995

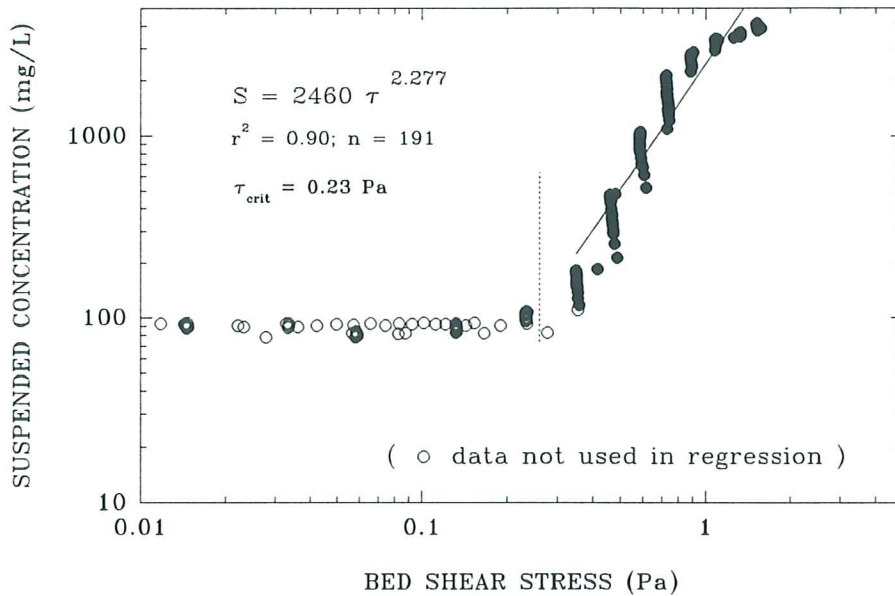
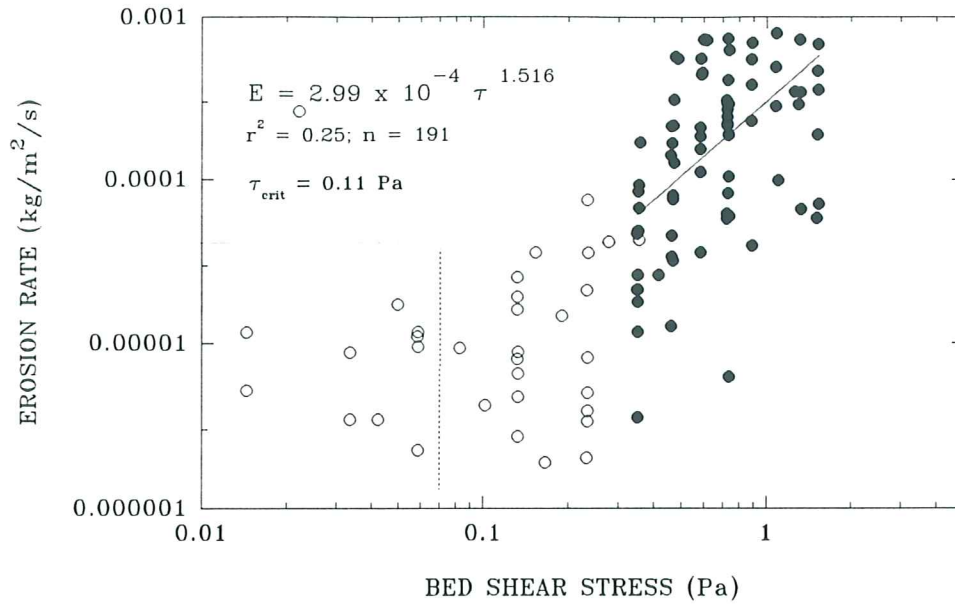


Figure 6.6.1.7. Estimates of the erosion threshold for deployment LISPUK4, site D. The upper panel shows that erosion rate is a power function of applied bed stress; the estimated erosion threshold is 0.11 Pa. The lower panel shows that suspended sediment concentration increases as a power function of applied bed shear stress; the threshold is equated with the stress at ambient concentration and yields a value of 0.23 Pa.

LAB CAROUSEL – LISPUK (Humber estuary)

SITE D (LABEXP6) – 13 APRIL, 1995

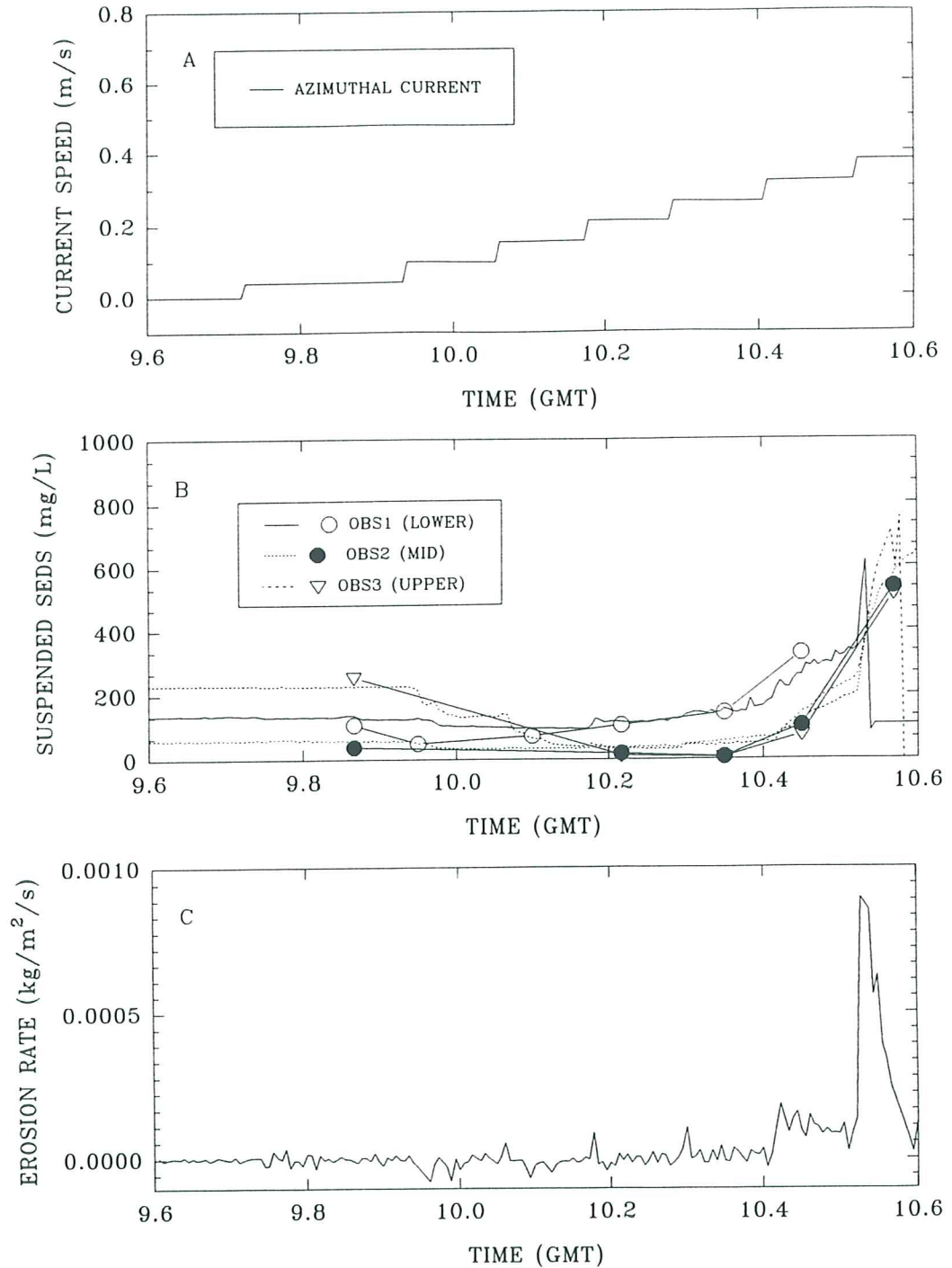


Figure 6.6.2.1. A time-series of Laboratory Carousel experiment (Labexp6) on a site D bulk sample. (A) the azimuthal reference current for a height of 0.18 m above the bed (based on lid rotation); (B) suspended sediment concentration from three OBS's and pumped samples at heights of 0.03, 0.10, and 0.20 m above the base; and (C) erosion rate.

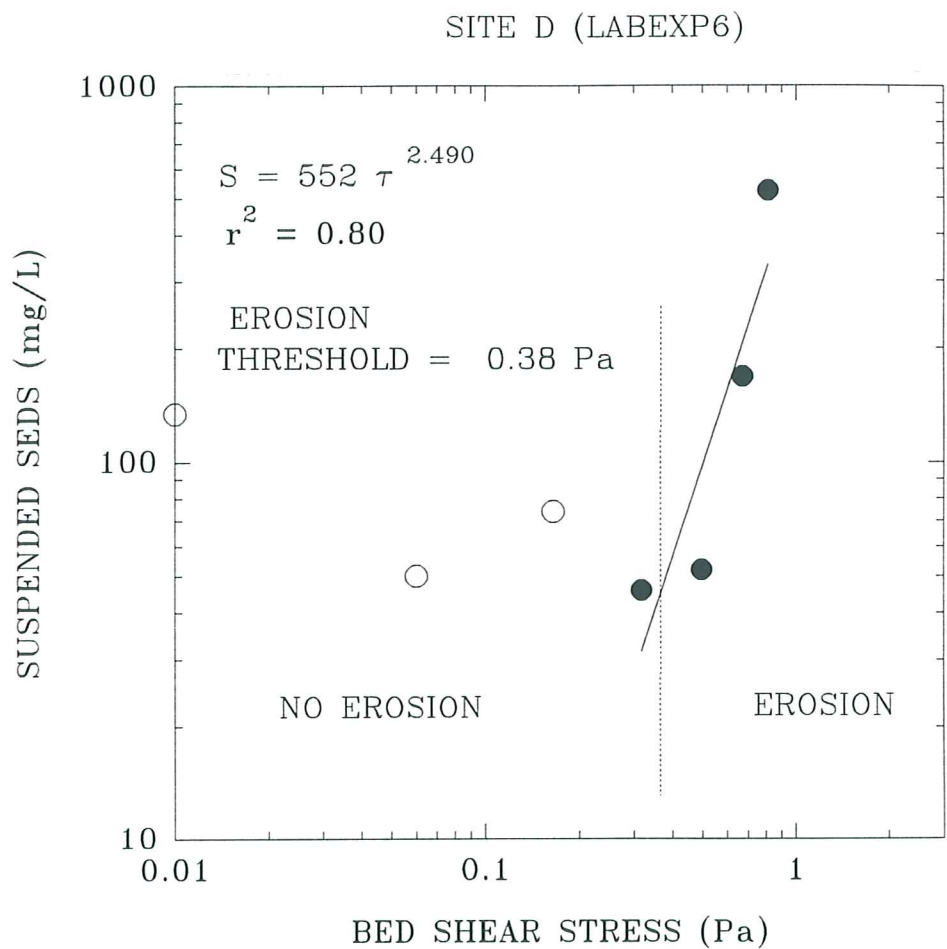


Figure 6.6.2.2. A plot of measured suspended sediment concentration (from pumped samples) versus applied bed shear stress in Lab Carousel for experiment Labexp6 (site D) . Notice the onset of erosion at 0.38 Pa which is based on the extrapolation of concentration to ambient levels.

LISPUK - SITE D, Humber estuary

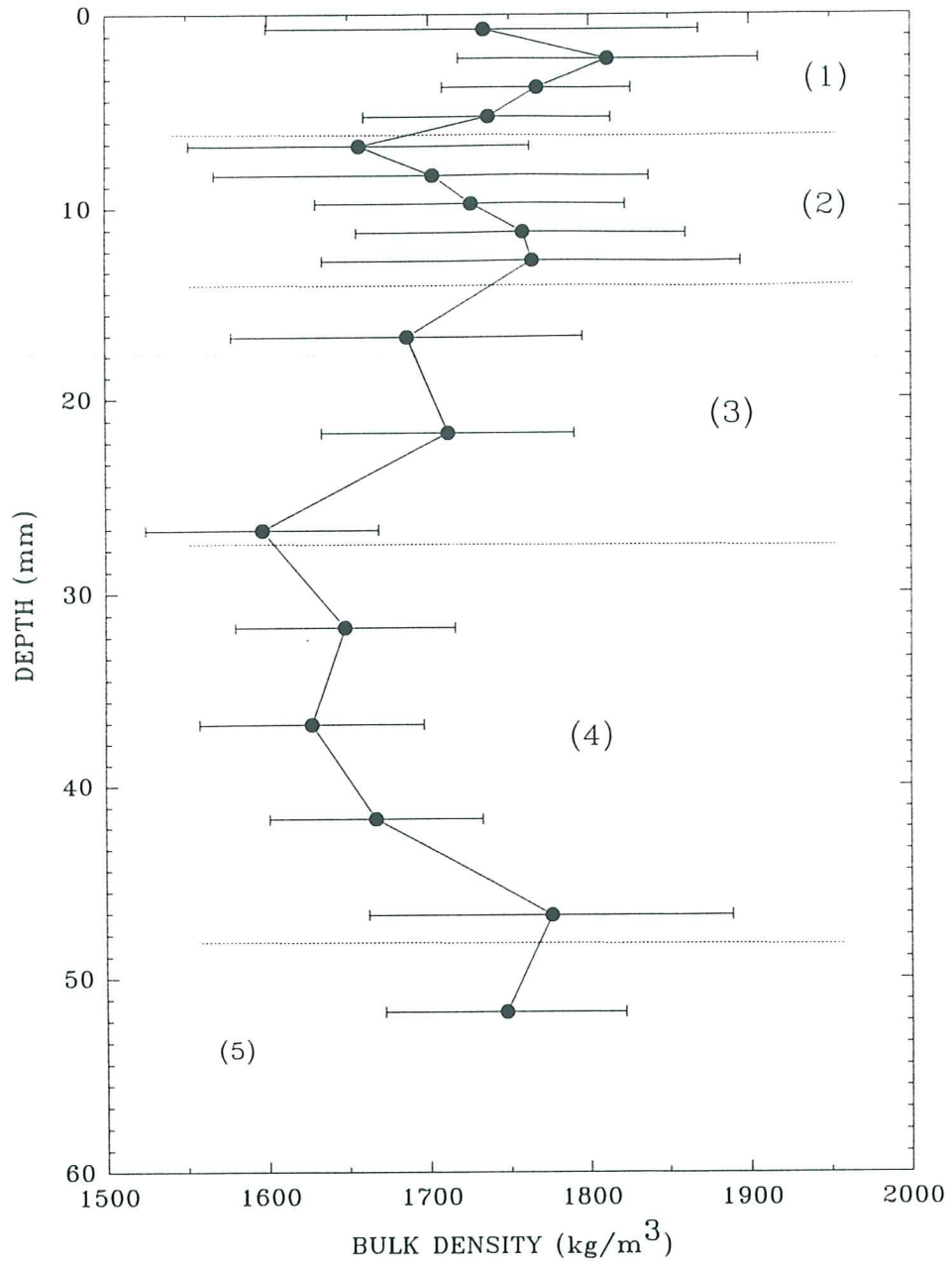


Figure 6.6.3.1. A log of the wet-weight bulk density derived from a Catscan analysis of a syringe core collected at site C/D. Five layers are evident reflecting layering of the substrate. Notice the general reduction in density with depth.

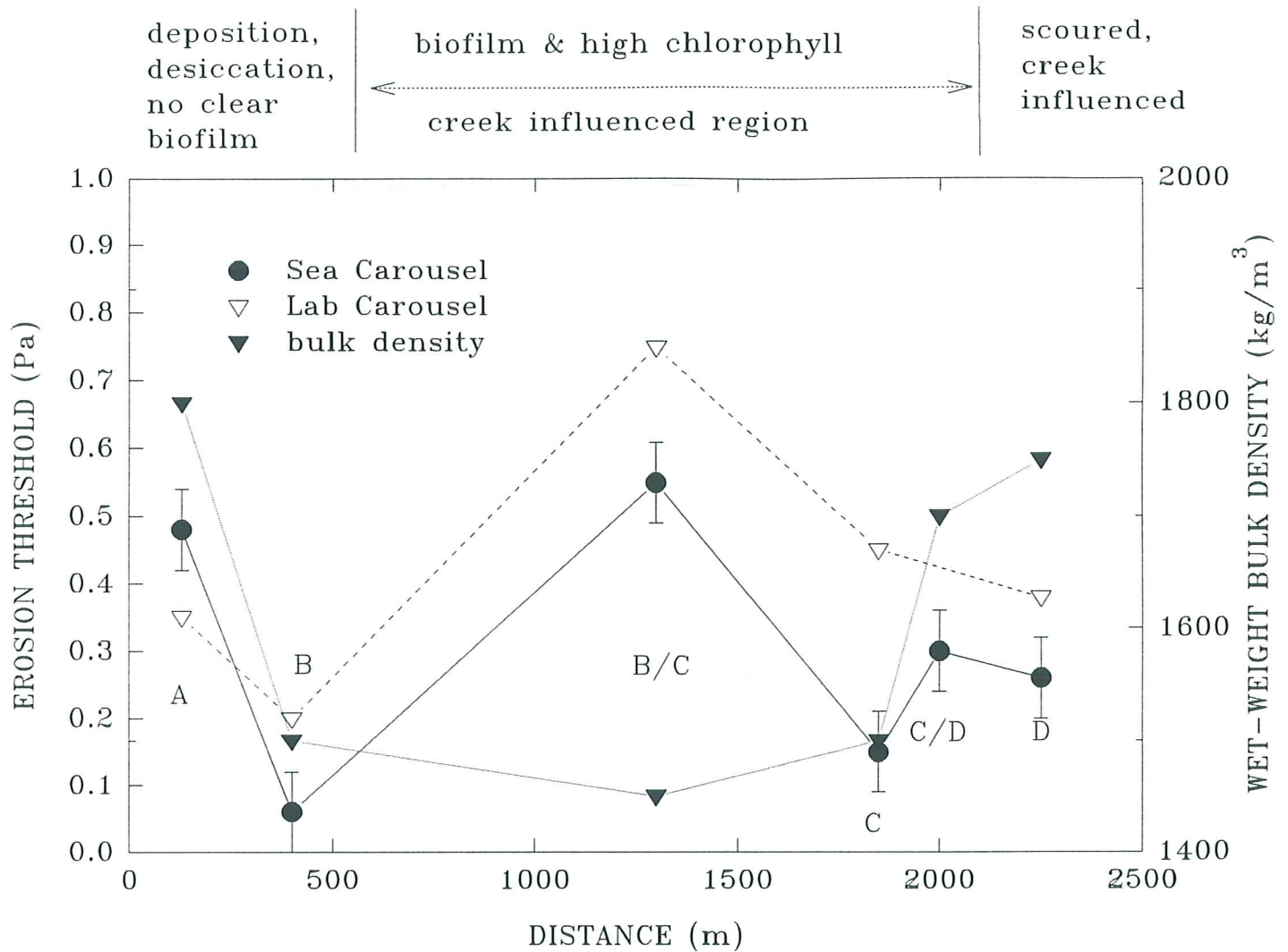


Figure 7.1.1. A summary plot showing erosion threshold from Sea Carousel and surface wet-weight bulk density against distance across the mudflat transect. Notice the three maxima: the largest on the central mudflat (site B/C); the second on the inner mudflat (site A); and the third on the outer mudflat (site D).

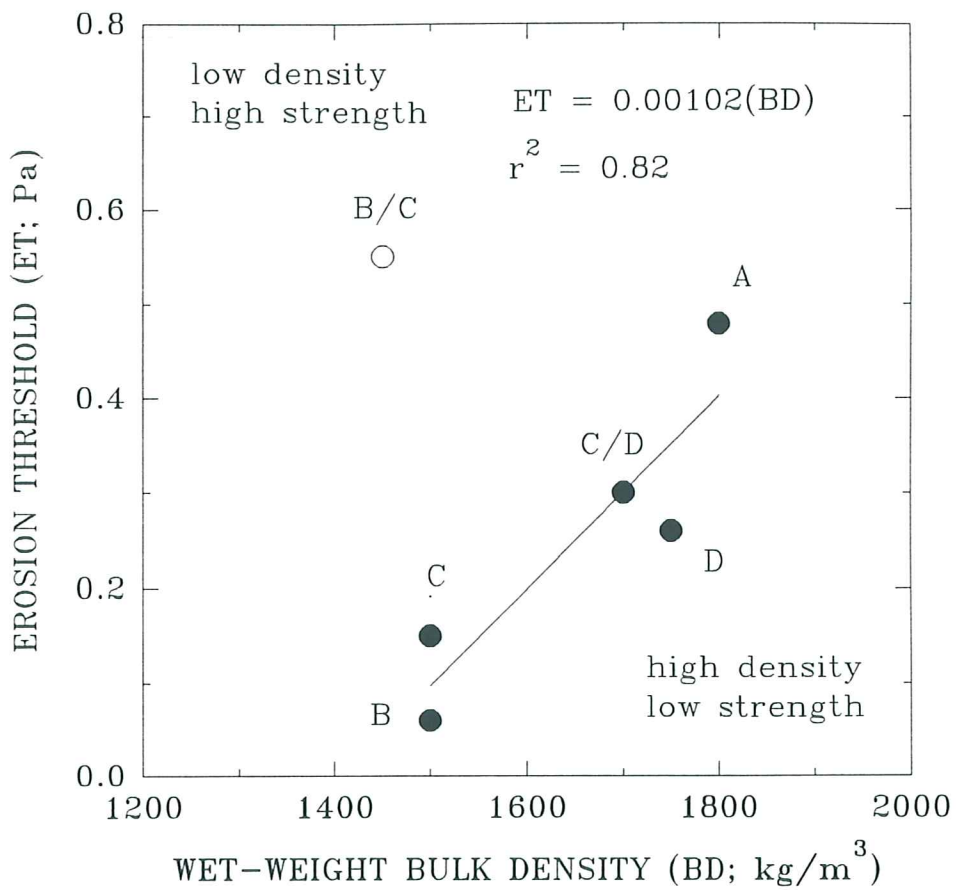


Figure 7.1.2. A scattergram of wet-weight bulk density and erosion threshold from Sea Carousel for the six sites of this study. Notice that site B/C is anomalously stable, presumably due to biostabilization.

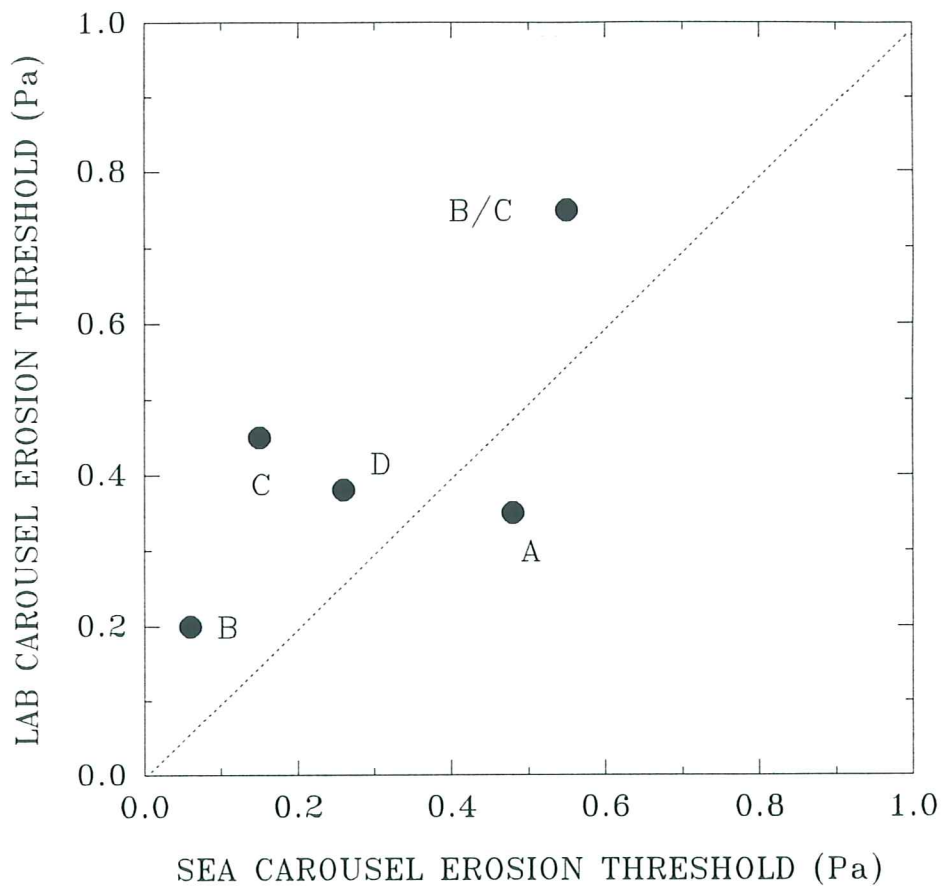


Figure 7.2.1. A comparison between erosion thresholds derived from the Sea Carousel and Lab Carousel for the six sites examined in this study. In general Lab Carousel yielded higher values than Sea Carousel. The exception is site B/C where biostabilization dominated the field signal.

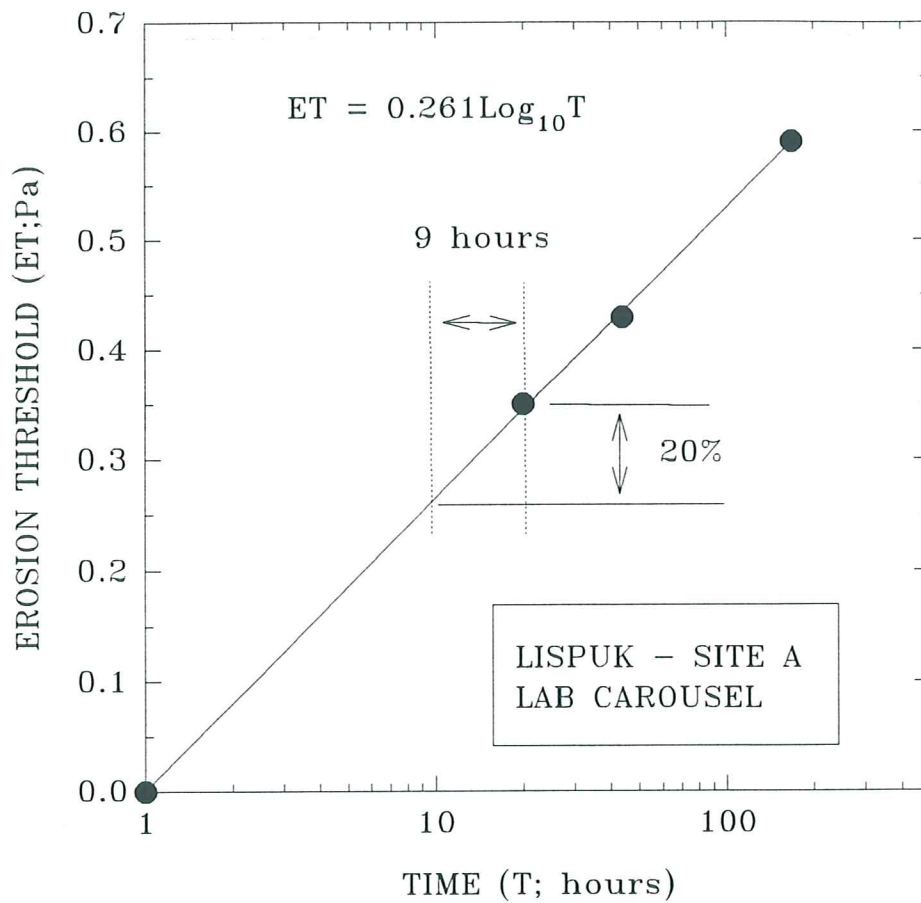


Figure 7.2.2. The effect of consolidation time on erosion threshold of site A sediment deposited in Lab Carousel. The figures shows that a 20% reduction in threshold would result if the time of consolidation was reduced from 24 to 11 hours.

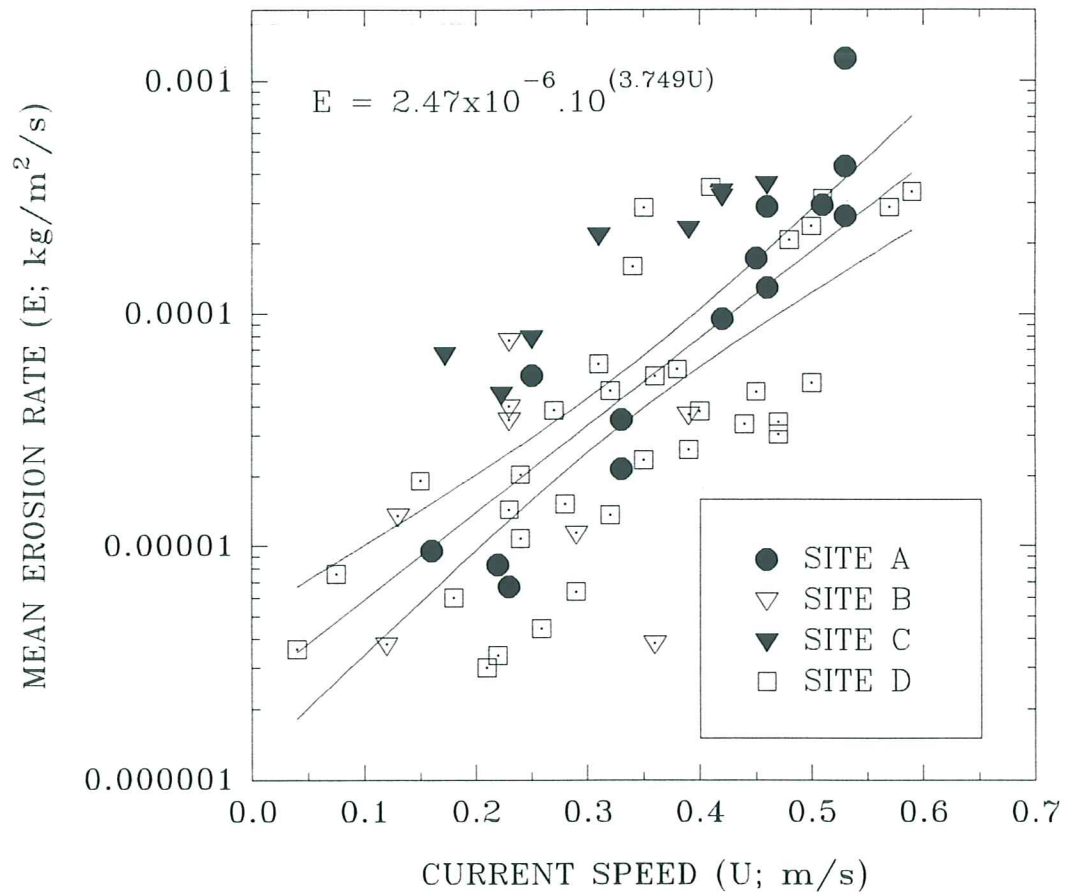


Figure 7.3.1. A regression analysis of mean erosion rate on current speed from data obtained from Sea Carousel. Results show that a single exponential function suffices for all sites.

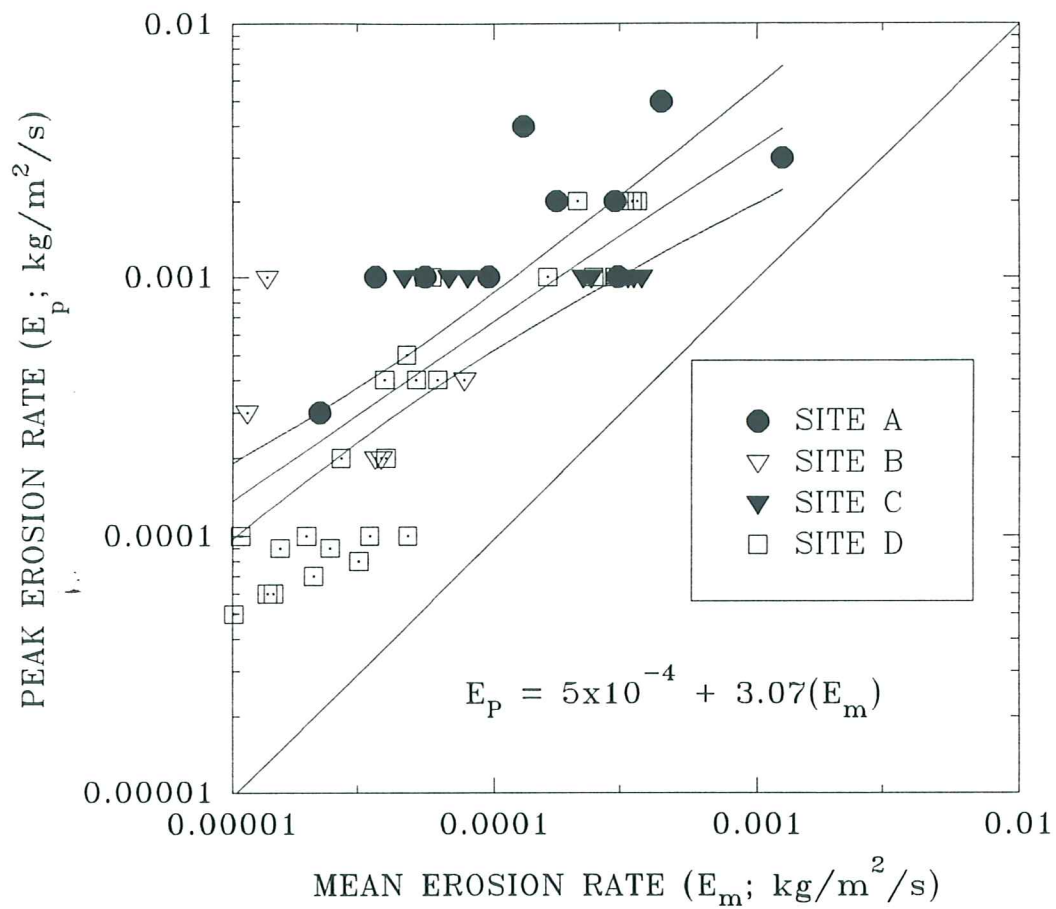


Figure 7.3.2. A correlation between mean erosion rate and peak erosion rate derived from Sea Carousel. Results show that all sites show a similar relationship which can be expressed by a simple linear equation.

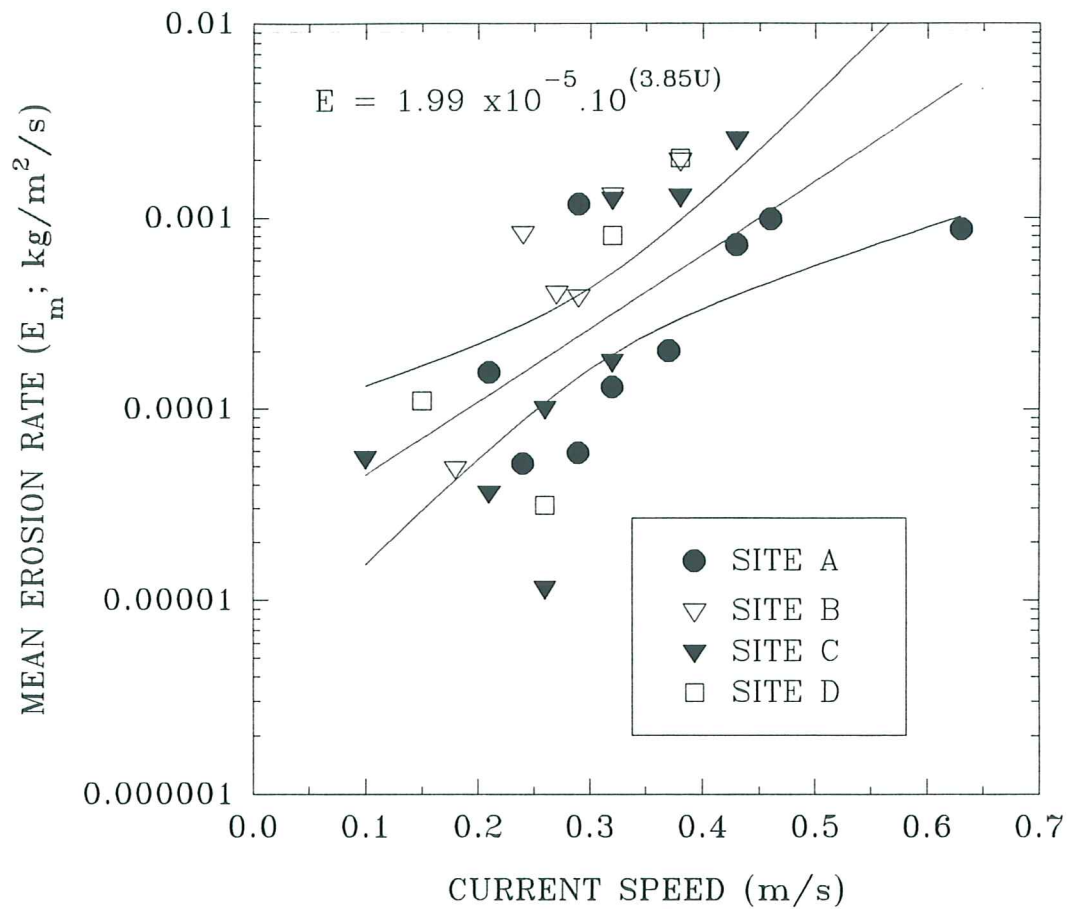


Figure 7.4.1. A regression analysis of mean erosion rate on current speed from data obtained from Lab Carousel. Results show that a single exponential function suffices for all sites. The equation is similar to that derived for Sea Carousel (see Figure 7.3.1) though more scatter prevails.

APPENDIX 1
GRAVITY CORE LOGS



Plate 6.1.1.1. Photographs of the erosion scar left by Sea Carousel at site A (inner mudflat).



Plate 6.1.1.2. Photographs of the details of scouring left by Sea Carousel at site A. Notice the abundance of shell debris, aggregates and granules that forms a lag surface, and the undisturbed mudflat either side of the erosion scar (flow was from left to right).

**LITTORAL MUDFLAT STABILITY MONITORING, THE HUMBER ESTUARY,
SOUTH YORKSHIRE - LISPUK, APRIL, 1995**

by

Carl L. Amos
Geological Survey of Canada
Bedford Institute of Oceanography
P.O. Box 1006, Dartmouth
Nova Scotia, CANADA, B2Y 4A2

Mike Brylinsky
Acadia Centre for Estuarine Research
Acadia University, Wolfville
Nova Scotia, CANADA, B0P 1X0

and

Sarah Lee and Damon O'Brien
Department of Earth Sciences
University of Wales, Cardiff
Wales, CF1 3YE

Geological Survey of Canada Open File Report # 3214
August, 1995

EXECUTIVE SUMMARY

Thirteen successful Sea Carousel deployments were undertaken on a mudflat off Skeffling, S. Yorkshire, in the Humber estuary. Six sites were occupied on a transect of the mudflat. Initial results showed that the variability between triplicates at any site was less than the variability along the transect. So, the observed, dominant trend is shore normal. The trend of erosion threshold is complex, showing three maxima: one on the inner mudflat (0.48 Pa); one on the outer mudflat (0.30 Pa); and the greatest on the central mudflat (0.55 Pa). We ascribe these maxima to three causes: (1) desiccation of parts of the inner mudflats (which would increase the surface strength); (2) storm scouring of the outer mudflats, which would exhume resistant material; and (3) biostabilization by algae on the central flats. Our results suggest that of these three factors, biostabilization was the dominant one at the time of the study.

The mean erosion rates (E_m) as a function of current speed (U_y) were similar for all sites and may be defined by the exponential function: $E_m = 2.47 \times 10^{-6} \cdot 10^{(3.749U_y)} \text{ kg/m}^2/\text{s}$. *In situ* mean particle settling rates (W_s) were up to $2.46 \times 10^{-3} \text{ m/s}$, which is up to an order of magnitude faster than has been measured in other estuaries at similar sediment concentrations (such as the Bay of Fundy).

The stability and erodibility of surface material collected at each mudflat site were evaluated in Lab Carousel, which was located at Spurn Head. Results showed that after only 20 hours consolidation, the erosion thresholds were about 20% higher than those monitored *in situ*, using Sea Carousel but spatial trends were the same. Mean erosion rates showed a similar exponential relationship with current speed to that determined from Sea Carousel. This function has the form: $E_m = 1.99 \times 10^{-5} \cdot 10^{(3.85U_y)} \text{ kg/m}^2/\text{s}$. Lab-derived values of W_s varied between 4.3×10^{-4} and $4.9 \times 10^{-3} \text{ m/s}$. The lowest rates were from the innermost site; the highest rates were from the central mudflats. This range in W_s encompasses those determined from the innermost site using Sea Carousel.

The threshold for deposition was defined only from Lab Carousel measurements, and varied between 0.03 and 0.32 Pa. This threshold varied in proportion to the erosion threshold. The variation appears to be the result of a time-varying settling rate, brought about by differential settling of a wide range in sizes of suspended material.

Catscan analysis of syringe cores collected at each mudflat site showed a tripartite division with sediment depth. That is: (1) a surface veneer (up to 5 mm thick), exhibiting low and constant density and high heterogeneity; (2) a layer of transition (5 mm thick), characterised by a rapid increase in bulk density and decrease in heterogeneity (due to collapse of pore spaces); and (3) the substratum, showing variations in density reflecting bedding at cm scale.

ACKNOWLEDGEMENTS

This study is a direct consequence of the work undertaken by the LISPUK steering committee, under the guidance of Drs. G.R. Daborn (ACER, Acadia University) and D. Paterson (Gatty Marine Labs., St. Andrews University). We acknowledge the efforts made by Dr. Paterson in bringing together the LISP team, and in providing the complex and wide-ranging infrastructure for the study. The selflessness of the St. Andrew's group is applauded, and is a model for the future. On-site logistics, background information, communication, and field support was provided by Dr. K. Black, and his contribution to this study is appreciated. Further field support was provided by Dr. P. Jonas (National Rivers Authority).

The contributions to the study made by Dr. A. Cramp (Department of Earth Sciences, Cardiff University) have been profound, particularly in regards to field logistics, in laboratory analysis of mudflat samples, and in the funding of S. Lee and D. O'Brien. Partial funding for DOB was made available through ACER Environmental, Cwmbran.

The logistical support in preparing for shipment of the container from Canada was largely provided by A. Robertson. The equipment used in the study is jointly owned by Geological Survey of Canada and Acadia University, and was provided to the study at no cost. Customs clearance in UK was coordinated through the Gatty Marine Labs.

Technical support to the study was provided by B. Wile (Geological Survey of Canada - Atlantic). His participation in this study, and overall recommendations were invaluable.

Funding for much of the on-site expenses was provided under a Land Ocean Interaction Study (LOIS) grant to the Littoral Investigation of Sediment Properties (LISP) UK group. All funds for Canadian travel, shipping of the container, and data analysis was provided under a RODAC grant from Environment Canada to Geological Survey of Canada Atlantic.

This report was reviewed by I. Droppo (Environment Canada) and M.Z. Li (Martec Limited). We appreciate their contributions to this manuscript.

FIELD PROGRAM SUMMARY SHEET

VESSEL..... Scott H

LOCATION..... Skeffling mudflats, Humber estuary, Yorkshire, U.K.

FIELD DATES..... 2 - 21 April, 1995

SCIENTIFIC STAFF..... C.L. Amos (GSCA; Program leader)
B. Wile (GSCA; Electronics)
M. Brylinsky (ACER; biological sampling)
S. Lee (Cardiff Uni; Lab Carousel and curation)
D. O'Brien (Cardiff Uni; Sea Carousel and sampling)

RESULTS

- ▶ Three (3) Sea Carousel deployments at site A.
- ▶ Two (2) Sea Carousel deployments at site B.
- ▶ Two (2) Sea Carousel deployments at site B/C.
- ▶ One (1) Sea Carousel deployment at site C.
- ▶ Two (2) Sea Carousel deployments at site C/D.
- ▶ Three (3) Sea Carousel deployments at site D.
- ▶ Bulk samples, syringe cores, and gravity cores from each site.
- ▶ Lab Carousel runs for sites A, A/B, B, B/C, C, and D.

LIST OF CONTENTS

	PAGE
EXECUTIVE SUMMARY	2
ACKNOWLEDGEMENTS	3
FIELD PROGRAM SUMMARY SHEET	4
1. BACKGROUND	7
1.1 The Littoral Investigation of Sediment Properties (LISP) concept	7
1.2 The study region	8
1.3 A definition of erodibility and sedimentation character	10
2. OBJECTIVES	11
3. SEA CAROUSEL	12
4. LAB CAROUSEL	14
5. SAMPLING AND SAMPLE ANALYSIS	14
6. RESULTS	16
6.1 SITE A	
6.1.1 Sea Carousel	21
6.1.2 Lab Carousel	24
6.1.3 Sample analysis	26
6.2 SITE B	
6.2.1 Sea Carousel	27
6.2.2 Lab Carousel	28
6.2.3 Sample analysis	28
6.3 SITE B/C	
6.3.1 Sea Carousel	30
6.3.2 Lab Carousel	30
6.3.3 Sample analysis	31
6.4 SITE C	
6.4.1 Sea Carousel	32
6.4.2 Lab Carousel	33
6.4.3 Sample analysis	33
6.5 SITE C/D	
6.5.1 Sea Carousel	34
6.5.2 Sample analysis	35

LIST OF CONTENTS(Cont.)

	PAGE
6.6 SITE D	
6.6.1 Sea Carousel	36
6.6.2 Lab Carousel	37
6.6.3 Sample analysis	38
7. GENERAL INTERPRETATIONS AND INITIAL CONCLUSIONS	39
7.1 The variation in erosion threshold with distance along transect	39
7.2 A comparison between Lab Carousel and Sea Carousel erosion thresholds	41
7.3 In situ erosion rates	42
7.4 Lab Carousel erosion rates	42
7.5 Settling rates and depositional thresholds	43
7.6 Relationship between biological parameters and bed erosion	43
7.7 Bed stability and gravity core physical properties	43
8. REFERENCES	44
9. ITINERARY	45
10. APPENDIXES	
Appendix 1 - Gravity core logs	
Appendix 2 - Water content analyses of gravity cores	
Appendix 3 - X-ray diffraction analyses of gravity cores samples	
Appendix 4 - Vane shear strength measurements of gravity cores	
Appendix 5 - Grain size analyses of surface sediments	

1. BACKGROUND

1.1 The Littoral Investigation of Sediment Properties (LISP) concept: LISP-UK is a multidisciplinary, multi-organizational program of research that has its roots in the highly-successful LISP-Minas Basin study (Daborn *et al.* 1989). The central theme of LISP has been the study of factors that influence the stability, growth and productivity of littoral tidal flats. The original precepts of LISP were:

- ▶ the integration of field effort for tidal flat monitoring at common space and time scales;
- ▶ the recognition that tidal flat attributes are variable in time and space;
- ▶ the factors that influence tidal flat evolution vary widely due to atmospheric exposure, tidal inundation, and biological production;
- ▶ the absolute need for synoptic, *in situ* measurements; and
- ▶ the integration of manipulative experimentation with field monitoring.

The focus of LISP-Minas Basin was the links and transforms between physical, biological, geological, and chemical attributes of tidal flats and the effects of these links on tidal flat evolution. A second purpose of LISP was to stimulate interaction between scientists in differing disciplines, and to stimulate the design of experimental procedures, practises and technologies for *in situ* monitoring.

LISP was not designed to characterise or map the environment within which it was carried out, but rather to occupy sites where fundamental and universal principals governing tidal flat stability could be discovered and tested.

Canadian involvement in LISPUK has been long-standing and began with the initial scoping of the study. The study was ultimately funded by LOIS and a field location was chosen by them in

the Humber estuary, S. Yorkshire, UK (Figure 1.1).

1.2 The study region: The site for LISPUK was immediately west of Spurn Head, Yorkshire on the Skeffling mudflats (Lat: 53° 37' N; Lon: 0° 05'E). It is a broad tidal flat (3600 m wide) on the northern margin of the estuary. The inner salt marsh is about 50 m wide. It was artificially introduced to fringe a reclamation dyke to landward. The adjacent mudflat (where our stations were established) is 3000 m wide and slopes seawards at 1:1000 to MSL. The innermost 200 m of mudflat is smooth; the remainder is furrowed by shore-normal drainage runnels (0.2 m deep and 1-2 m in width) and is crossed by an intricate network of deep creeks. The surface roughness of the mudflats increases seawards to MSL, where the mudflat gives way to an extensive sandflat to low water. The sandflat has a width of 900 m and occupies the steepest part of the intertidal transect (1:100). The orientation of the mudflat transect was 200° true. Six reference sites were established along this transect (Figure 1.2). A summary of the position and elevation of these sites is given in Table 1.1

SITE	APPROX DISTANCE (m)	APPROX ELEVATION (m)
A	130	5.1
B	400	4.9
B/C	1300	4.5
C	1750	4.0
C/D	1900	3.7
D	2250	3.4

Table 1.1 The approximate distances (from shore) and elevations (above chart datum) of the sites occupied in this study.

The following are brief descriptions of the six sites occupied during this study:

site A - situated adjacent to the salt marsh on the inner mudflat. This site was composed of a

bioturbated clayey silt. It was largely free of runnels and creeks and appeared to be characterised by net deposition. The surface (at the time of this study) comprised a surface veneer of very soft mud over denser silt;

site B - situated in a region of small (0.1 m deep) runnels that were oriented shore normal. The site was landward of a scarp separating this site from site B/C. Above the scarp, material appeared more heavily consolidated, dryer and absent of creeks. The surface roughness was about 2 mm and was the result of worm tubes, bird feeding, and tidal current scouring;

site B/C - situated within the drainage area of a large creek system that crosses the profile. The mudflat was furrowed and scoured by shore-normal runnels, and showed a well-developed biofilm (algal mats) on very soft clayey silt. The bases of the runnels were saturated; the ridges between were dryer;

site C - situated in a creek system on the central mudflat below the scarp. The site was covered by shore-normal runnels (0.2 m deep). The ridges and runnels were about 2 m in spacing and were more pronounced than at landward stations. Eroded sections of the ridges showed accretionary lamination, which suggests they were depositional, rather than erosive, features. The surface was highly irregular due to bioturbation, scouring, and bird feeding;

site C/D - situated on a highly eroded mudflat that had become covered by a veneer of algal material. The ridges and runnels were very pronounced and were cut by drainage channels feeding a major creek that cut through the region;

site D - situated adjacent to a large creek system on the outer mudflat. The site was covered by deep shore-normal runnels, by creek levée deposits and heterolithic point bar deposits. The site had the appearance of general erosion, due to the abundance of circular shallow depressions and

the absence of a discernible biofilm.

1.3 A definition of erodibility and sedimentation character

Confusion often arises regarding the definition of “erodibility” and “sedimentation” character.

They are not purely synonyms for “erosion threshold” and “mass settling rate”, but rather define the attributes that control mudflat response to the stabilizing and destabilizing forces at play over a mudflat. For present purposes, we define erodibility in terms of:

- ▶ the erosion threshold (cohesion) at the sediment surface, $\tau_c(0)$ (in Pa);
- ▶ the erosion threshold as a function of sediment depth, $\tau_c(z)$ (in Pa);
- ▶ the friction coefficient, ϕ (in degrees);
- ▶ the peak rate of erosion, E_p , as a function of applied bed shear stress and eroded depth (in $\text{kg/m}^2/\text{s}$);
- ▶ the mean rate of erosion, E_m , as a function of applied bed shear stress and eroded depth (in $\text{kg/m}^2/\text{s}$);
- ▶ the rate of erosion as a function of time (erosion Type) at a constant applied bed shear stress (in $\text{kg/m}^2/\text{s}$).
- ▶ the size spectra and modes of transport of material eroded from the bed; and
- ▶ the effect of consolidation time on the erosion threshold (Pa/s).

We define sedimentation character in terms of:

- ▶ the critical shear stress for the onset of deposition, τ_d (in Pa);
- ▶ the mass deposition rate, $\delta M/\delta t$ ($\text{kg/m}^2/\text{s}$);
- ▶ the still-water mass settling rate, W_s (m/s);

2. OBJECTIVES

The main strengths that we bring to the project revolve around the technologies developed for *in situ* monitoring of seabed stability (Sea Carousel, Lab Carousel, INSIST, Excalibur, RALPH, SOBS, etc; see Amos *et al.* 1994, for a review). This study was, therefore, centred around the measurement of tidal flat erodibility across the Skeffling transect, in this case using Sea Carousel, and the variability of erodibility with (1) distance along the transect, (2) within any site on the transect, and (3) with time.

A second objective was to determine the factors that control erodibility. This was evaluated through comparison of erodibility with analyses of gravity cores, bulk samples, syringe cores, biological parameters, and pumped water samples collected at each site. In the longer term, erosion thresholds will be compared with bulk density, grain size, chlorophyll content, dissolved carbohydrate content, and sediment microfabric and macrofabric.

A third objective was to determine the value of on-site flume experiments in studies of mudflat stability. We argue that the use of “fresh” local seawater, and sediment which is hours old, will likely yield better results than conventional laboratory experiments. If reliable, we will determine thresholds for deposition and the mass settling rates using the Lab Carousel. (We cannot accurately determine this threshold using Sea Carousel at present). Results will be compared with still-water settling rates determined *in situ* by Sea Carousel (which can be determined with some accuracy).

3. SEA CAROUSEL

Sea Carousel is a benthic annular flume designed for field use in intertidal and subtidal settings. The carousel is 1.0 m in radius with an annulus 0.15 m wide and 0.30 m high. It weighs approximately 150 kg in air and 40 kg in water and is made entirely of aluminium. Flow in the annulus is induced by rotating a movable lid that is driven by a 0.35 hp DC, digital stepping motor powered from the surface. Eight small paddles, spaced equidistantly beneath the lid, induce a flow of water in the annulus. The Carousel is equipped with three optical backscatter sensors (OBS's; Downing, 1983). Two of these are located non-intrusively on the inner wall of the annulus at heights of 0.03 and 0.18 m above the skirt (the skirt is a horizontal flange situated around the outer wall of the annulus 0.04 m above the base; it was designed to standardize penetration of the flume into the seabed). The third OBS detects ambient suspended sediment concentration (S) outside the annulus, or it may be used to detect internal sediment concentration at an intermediate height between the other two. The OBS sensors give linear responses to particle concentration (of a constant size) for both mud and sand over a concentration range of 0.1 to 50 g/L (Downing and Beach, 1989). A sampling port, through which water samples may be drawn, is situated in the outer wall of the annulus at a height of 0.2 m above the skirt. It is used to calibrate the three sensors under well mixed conditions.

Mean tangential lid rotational speeds are detected through a shaft end-coder resting on the lid. Tangential (U_y) and vertical (U_w) current speeds are detected by a Marsh-McBirney® EM flow meter (model 513) situated *circa* 0.18 m above the bed. Controller boards for each sensor and necessary power (12 VDC) are derived from an underwater pod located above the

annulus. Output voltages from all sensors are digitized and transformed to scientific units on a Campbell Scientific® CR10 data logger and stored on a Campbell Scientific® SM192 storage module (storage capacity of 96,000 data values), also located in the underwater pod. The data logger is interrogated and programmed from the surface using a microcomputer linked to the data logger through an RS232 interface. Maximum sampling rate of all channels is approximately 2 Hz, whereas U_y and U_w may be logged at rates up to 10 Hz. All channels may be monitored and displayed on the surface computer allowing the operator to control the experiment interactively. Bed shear stress is varied in time by varying the power supplied to the underwater motor up to 350 Watts via a surface power supply. The data stored from each deployment may be downloaded remotely through the RS232 cable at the end of each experiment and the storage module re-initialized.

A window is located in the inner flume wall for purposes of observing and recording the mechanics of bed failure. Under clear ambient conditions, visual observations are made using a Sony® Handycam 8 mm video recorder model CCD-V11 held in an Amphibico®, Amphibian V11 underwater housing. Light is provided by two 100-Watt underwater lights powered from the surface. The housing has a lens that corrects for underwater geometric distortions and so is suitable for accurate image scaling. The camera images a standard 30 frames/s. A co-axial cable connects the camera to a surface monitor for real-time detection. Sequential video images are digitized for particle trajectories at varying heights above the bed. From these, velocity profiles are constructed. From such profiles, thicknesses of the logarithmic part of the benthic boundary layer are determined and friction velocities computed. These latter values may then be compared with laboratory measures.

4. LAB CAROUSEL

Lab Carousel is an annular flume designed to examine the erosion and settling of natural marine sediments under controlled conditions. It has the exact same dimensions as Sea Carousel and so is directly comparable in terms of flow character and bed shear stress distribution. The flume is 2 m in diameter (OD), 0.15 m wide, and is filled to a height of 0.30 m. The flume is made of clear acrylic so that flow conditions and bed erosion can be clearly observed. Flow is induced by a lid suspended over the water surface from a central shaft. Eight paddles are fixed equidistantly beneath the lid to induce flow. The shaft is turned by a 0.75 Hp Industrial Drive® motor that is driven by a Focus® controller. A digital display ensures that voltage settings (and lid speed) are consistent from experiment to experiment. Three optical backscatter sensors (OBS's) are situated at heights of 0.03, 0.10 and 0.20 m above the flume base, and provide information on the presence and concentration of suspended particulate matter. A Marsh-McBirney® electro-magnetic flow meter is also located in the flume at a height of 0.18 m above the flume bed and gives measures of the vertical and azimuthal components of flow.

The OBS and EM flow meter data are logged on a Campbell Scientific® CR10 data logger and stored on a PC hard-drive. A Sony® Hi8 video camera is situated near the flume base in order to record the erosion and settling process during each experiment. Images are recorded on SVHS and displayed on a 15 inch Panasonic®, high-resolution, colour monitor.

5. SAMPLING AND SAMPLE ANALYSIS

Three types of samples were collected from each of the sites occupied by Sea Carousel. These were:

(1) short gravity cores of the topmost 30 - 50 cm of the mudflat. These samples were collected

using a Benthos® gravity corer that was ballasted with 200 lbs of lead. The core samples were sealed in wax, maintained vertical, and stored at a temperature less than 10⁰ C. The cores were split, logged, photographed, and analysed (by Department of Earth Sciences, Cardiff University) for:

- water content;
- bulk density;
- Atterburg limits;
- vane shear strength;
- grain size; and
- clay mineralogy;

(2) an Eckman grab sample of the sediment surface, from which were collected:

- two syringe cores that were frozen for (1) SEM analysis of microfabric (to be analysed by Gatty Marine Labs, St. Andrew's University), and (2) Catscan analysis for bulk density; (after Amos *et al.*, in press).
- 100 g surface scrape for grain size analysis; and
- four 1.5 cm diameter, 3 mm deep syringe cores for analysis of water content, organic content, sediment chlorophyll α , dissolved carbohydrates and bacterial numbers (analysed by Acadia Centre for Estuarine Research, Acadia University); and
- one 1.5 cm diameter, 10 cm deep syringe core for the analysis of sediment nematode numbers. and

(3) a large-sample (5-10 kg) surface scrape for use in Lab Carousel.

6. RESULTS

The Scott H, a powered barge with a container aboard, was used throughout the study between 4 and 20 April, 1995. The 1 m draft of the vessel was ideally suited for work on the tidal flat and for beaching on the flats. For each visit to the flats, the barge was sailed from Grimsby Docks across the Humber estuary on the flooding tidal and anchored on site during tidal inundation of the flats. A four point anchoring arrangement usually sufficed to prevent drift. Typically, two stations were undertaken during each visit to the flats. The first station of each visit was undertaken during the ebbing tide. The duration of these deployments were restricted by mudflat exposure. The second deployment was undertaken during the flooding phase of the subsequent tide. The duration of deployments was restricted by dangers of barge drift once free of the bottom, and by access to Grimsby Dock before lock gate closure. The exact position (with respect to creeks and runnels) of the Sea Carousel could not be determined for deployments on the falling tide and some data was lost as a result. By contrast, the instrument could be precisely located on the flats prior to inundation by the rising tide.

A total of nineteen (19) Sea Carousel deployments were attempted during the course of this study (LISPUK1 - LISPUK19). Good results were obtained from thirteen. Of these, three came from site A, two from site B, two from site B/C, one from site C, two from site C/D, and three from site D. A summary of the results obtained from these stations and tentative interpretations are given in Table 6.1.

STATION #	SITE	EROSION THRESHOLD (Pa)	FRICTION COEFF (ϕ)	BULK DENSITY (kg/m^3)
LISPUK1	D(f)	--	--	1700-1800

STATION #	SITE	EROSION THRESHOLD (Pa)	FRICTION COEFF (ϕ)	BULK DENSITY (kg/m^3)
LISPUK2	D(r)	0.20	34	1700-1800
LISPUK3	D(f)	0.34	64	1700-1800
LISPUK4	D(r)	0.23	10	1700-1800
LISPUK5	C(f)	0.15	3	1500-1700
LISPUK6	C(r)	--	--	--
LISPUK7	C/D(f)	0.26	77	1600-1800
LISPUK8	C/D(r)	0.35	63	1600-1800
LISPUK9	--	--	--	--
LISPUK10	B/C(f)	0.95	51	1400-1700
LISPUK11	B/C(r)	--	--	--
LISPUK12	B/C(r)	0.15	12	1400-1700
LISPUK13	A(f)	0.42	6	1800
LISPUK14	A(r)	0.58	11	1800
LISPUK15	A(r)0.45	0.45	11	1800
LISPUK16	--	--	--	--
LISPUK17	B(f)	0.01	--	1500-1700
LISPUK18	B(f)	0.11	26	1500-1700
LISPUK19	B(r)	--	--	--

Table 6.1. A summary of Sea Carousel stations occupied in this study. Also given are the derived surface erosion thresholds, the computed friction coefficients, and the range of wet-weight sediment bulk densities determined from Catscan analyses of syringe cores (f - falling tide; r - rising tide).

The Carousel at site LISPUK1 was perched on the side of a major creek with the base exposed; these results are, therefore, unreliable. Erosion trends during LISPUK6, LISPUK11, and LISPUK19 time-series were masked by the passage of the flood-tide turbidity maximum;

LISPUK9 was aborted due to boat drift; and LISPUK16 was aborted due to a broken Hyab® crane. Nevertheless satisfactory results were eventually obtained from all sites. The deployment procedure for each station was held as constant as possible. That is, each experiment was initiated with a 10-minute still-water period, followed by seven increments of lid speed each lasting approximately 5 minutes. The lid speed increments were: 0.16; 0.32; 0.47; 0.63; 0.78; 0.84; 0.90 m/s. These corresponded to reference azimuthal current speeds (U_v) of: 0.09; 0.18; 0.26; 0.35; 0.44; 0.47; 0.50 m/s. Speed control was good at lower levels and lid rotation was constant. At highest levels, however, lid speed was erratic as the motor was at its limit of power output. This erratic nature of lid speed is reflected in the macroturbulence of the reference current within the Sea Carousel. Consequently, results from these faster-flowing intervals must be treated as suspect. Water samples (500 ml in volume) were pumped from the Sea Carousel about 3 minutes into each increment of lid speed. These samples provided overall control as well as calibration for the OBS sensors, measures of eroded chlorophyll, and particulate organic and inorganic contents. A 10-minute period of still-water settling would normally be carried out after each erosion phase if time permitted. Unfortunately this was possible only for stations LISPUK13, and LISPUK14 (site A) and LISPUK5 (site C).

Eight Lab Carousel experiments were carried out on bulk samples (surface scrapes) collected from the intertidal transect at Skeffling. A summary of these experiments is given in Table 6.2.

EXPERIMENT	SITE	THRESHOLD (Pa)	
		DEPOSITION	EROSION
LABEXP2	SITE A (24 hours settling)	--	0.35
LABEXP3	SITE A (44 hours settling)	--	0.43

EXPERIMENT	SITE	THRESHOLD (Pa)	
		DEPOSITION	EROSION
LABEXP4	SITE B	0.03	0.20
LABEXP5	SITE A (7 days settling)	--	0.59
LABEXP6	SITE D	0.23	0.38
LABEXP7	SITE C	--	0.45
LABEXP8	SITE B/C	0.32	0.75
LABEXP9	SITE A/B	0.07	0.19

Table 6.2. A summary of Lab Carousel experiments on bulk samples taken from the Skeffling transect. Unless otherwise stated, the samples were allowed to consolidate for 20 hours.

The analysis of physical properties of the gravity cores collected at each site are presented in Appendixes 1 - 5. We found no clear trends linking erosion threshold to any of the parameters measured. The strongest link to erodibility came from bulk density, although even this parameter was over-shadowed by the effects of biostabilization.

The results of sample analysis for biological parameters are listed in Table 6.3 and in Figure 6.1 by site and in Figure 6.2 by Sea Carousel station. Sediment organic contents ranged between 4.3 and 10.2%. There were no obvious consistent trends in sediment organic content across the mudflat. Sediment chlorophyll *a* concentrations were quite high at some sites and there was a trend of decreasing chlorophyll *a* concentration towards low water. Dissolved carbohydrate concentrations generally followed the same trend as sediment chlorophyll *a*. Bacteria numbers were within the range normally reported for marine sediments, but showed no obvious relationship to either sediment organic, chlorophyll *a* or dissolved carbohydrate concentrations. Nematode numbers varied greatly and were generally highest between sites within the middle intertidal. The results of particulate organic and inorganic content analyses, as well as

Table 6.3. Biological sediment characteristics at each Sea Carousel deployment site.

Sea Carousel Station	Site	Water Content (%)	Organic Content (%)	Chlorophyll <i>a</i> ($\mu\text{gm} / \text{gm dry sed.}$)	Dissolved Carbohydrates ($\text{mg} / \text{gm dry sed.}$)	Bacteria Numbers ($10^3 / \text{gm dry sed.}$)	Nematode Numbers ($/ \text{gm dry sed.}$)
1	D	-	-	1.9	0.042	358,394	298
3	D	32.4	4.3	4.7	0.034	166,182	280
4	D	34.0	6.2	4.1	0.042	339,247	162
5	C	34.9	8.4	10.4	0.066	310,280	197
6	C	45.2	9.4	6.6	0.068	608,240	573
7	CD	32.8	5.4	25.2	0.107	623,544	933
8	CD	27.6	4.6	8.0	0.069	705,537	106
9	BC	27.9	4.3	26.4	0.188	-	580
13	A	28.7	6.0	12.0	0.087	244,319	69
14	A	35.3	5.9	12.3	0.094	584,067	92
17	B	41.1	10.2	12.9	0.045	511,057	60
19	B	31.1	8.3	19.4	0.051	670,538	104

chlorophyll *a* concentration, from samples pumped from Sea Carousel are still under analysis.

6.1 SITE A

6.1.1 SEA CAROUSEL

Good results were obtained from three stations at site A (LISPUK13, LISPUK14, and LISPUK15). The site was flat, smooth and ideal for Sea Carousel deployment. Plate 6.1.1.1 shows the eroded annulus of experiments LISPUK13 and LISPUK14. Close ups of the eroded mudflat are shown in Plate 6.1.1.2. Erosion appears consistent around the annulus as well as radially across it. Notice, however, the presence of a coarse substrate exposed by the annulus, which elsewhere is covered by a thin veneer of very soft, brown mud. Also notice the irregular nature of the eroded surface, and the presence of large aggregates concentrated along the inside wall that we interpret as being rip-up clasts that moved mainly as bedload.

The calibration between OBS voltage output from Sea Carousel and dry weight *S* was linear over the range in *S* although considerable scatter was evident (Figure 6.1.1.1). Consequently, calibrations were determined for each station. The calibrated, time-series plots of results from the site A stations are shown in Figures 6.1.1.2 to 6.1.1.4. Panel A in each Figure illustrates lid speed and azimuthal and vertical current speeds at the reference height (0.18 m). In panel B, the calibrated OBS outputs are plotted together with the dry-weight *S*'s determined from the pumped samples. OBS1 and 3 are inside the annulus of the Carousel and show trends of increasing *S* in harmony with the current time-series of panel A. OBS2, however, shows little change with time as it is outside the annulus and monitors ambient *S*. Raw *S* is uncorrected for dispersion (leakage) and should agree with the pumped samples (solid dots). OBS1 and OBS3 have been corrected for dispersion (based on a method outlined in Amos *et al.* (1992)). Panel C illustrates

the erosion rate time-series determined from the changes in corrected S with time. The peaks in erosion (E_p) clearly correspond to the beginnings of each increment of lid speed and are relatively short-lived events. This typifies Type I erosion, wherein bed erosion ceases approximately 1 minute after application of the eroding flow. Due to high ambient turbidity, we were unable to video-record the erosion process in Sea Carousel and so the nature of the mechanical failure of the bed is unknown.

The overall increases in S with time illustrated that bed erosion took place. The surface threshold for erosion ($\tau_c(0)$) was evaluated in two ways: (1) from plots of applied bed shear stress versus erosion rate; and (2) from applied bed shear stress against S (see Figures 6.1.1.5 to 6.1.1.7). The derived threshold values from the two methods for estimating erosion threshold are summarised in Table 7.1.1. Due to the wide scatter of data in method (1), only results from method (2) are used for comparisons with Sea Carousel. Results from the three deployments showed variability within the site ($\tau_c(0) = 0.42 - 0.58$ Pa) but reasonable coherence with the Sea Carousel results. Synthetic cores were produced illustrating bed strength by plotting the applied shear stress (τ_o) against the erosion threshold when erosion ceases (τ_c) at depth z, which is a measure of the sediment strength (τ_d) at that depth. The friction coefficient (Φ) is the arctan of the increase in bed strength (τ_d) with increasing geostatic load (σ): $\Phi = \tan^{-1}(\tau_d/\sigma)$. Conversely, the erosion threshold at any depth, z, may be determined from: $\tau_c(z) = \sigma \cdot \tan(\Phi) + \tau_c(0)$.

Values of Φ are summarised in Table 6.1. The wide range in Φ indicates that the structure of the surface sediment was complex and highly variable in space. A positive friction coefficient conforms to a normal-loaded bed; a near-zero friction coefficients implies no consolidation and perhaps the existence of a gel (LISPUK13); and a negative friction coefficient implies the

possible presence of a surface biofilm with weaker material beneath (not found in this study).

The friction coefficients from site A were the lowest recorded from the transect and suggest recent deposition with lack of consolidation.

Erosion rates are expressed in two ways: (1) the mean erosion rate (E_m) - that is, the net eroded mass over the duration of the increment of an applied flow; and (2) the peak erosion rate (E_p) - that is, the maximum erosion rate evident over an applied flow (usually associated with the start of the applied speed increment). The mean erosion rate (E_m) has been computed for each speed increment. It shows positive correlation with current speed in the exponential form:

$$E_m = 9.12 \times 10^{-7} \cdot 10^{(5.047U_y)} \text{ kg/m}^2/\text{s}, \quad r^2 = 0.86; \quad n = 20$$

The mean still-water mass deposition rate ($\delta M/\delta t$) has been derived from the rate of change in S within Sea Carousel, and is the product of suspended sediment concentration S(t) and the mean particle settling rate (W_s): $\delta M/\delta t = W_s \cdot S(t)$. Thus we may derive $W_s = \delta M/\delta t \cdot 1/S(t)$. The computed mean values of W_s are presented in Table 6.1.1.1.

STATION	MEAN S (mg/L)	W_s (m/s)
LISPUK13	135	1.94×10^{-3}
LISPUK14	110	1.52×10^{-3}
LISPUK15	391	2.46×10^{-3}

Table 6.1.1.1. Calculated values of mean settling velocity W_s for site A stations.

These settling velocities are very high for estuarine muds and suggest strong flocculation and the transport of rip-up clasts within the Carousel. Also, there is a general increase in W_s with mean S, perhaps suggesting the release of large aggregates (rip-up clasts with high settling rates) from the bed during periods of high bed stress.

6.1.2 LAB CAROUSEL

A bulk sample from site A was mixed with seawater collected from the Spurn Head pier, and settled in the Lab Carousel under still-water conditions, at 9° C, for 24 hours (Labexp2), and then for 44 hours (Labexp3). As well, insert trays were filled with the remoulded bulk material and set aside in seawater for a period of 7 days (Labexp5) in order to examine the effects of consolidation time on the erosion threshold. The insert trays were 0.30 x 0.15 m and were curved to fit into the base of the flume in purpose-made recesses. A bulk sample from a site midway between sites A and B (site A/B; Labexp 9) was also tested, as described above. It is included as part of site A for convenience.

Lid speed was increased in a series of 5-minute steps ($U_y = 0.1; 0.7; 0.12; 0.18; 0.24; 0.29; 0.35; 0.40; 0.46$ m/s) until the OBS sensors became saturated. Saturation took place above $S \approx 800$ mg/L which effectively restricted the experiments to lid speeds less than about 0.4 m/s. (The output range of the sensors have now been changed to provide an operating range beyond 2000 mg/L). At each increment of lid speed, 0.5 L water samples were collected from three ports at the heights of the three OBS's. All samples were analysed for S, chlorophyll and particulate organic and inorganic matter.

Time-series plots of the erosional part of experiments on site A material are shown in Figures 6.1.2.1 to 6.1.2.4. Increases in S illustrate that the erosion threshold was exceeded in all cases. Also, the erosion rate time-series (Figure 6.1.2.2) show that Type I erosion prevailed at early stages of the erosion process, with the well-defined, short-lived peaks in erosion rate. Notice also the prevalence of Type II erosion (continuous) in the later stages of erosion (Figure 6.1.2.3). S has been plotted against applied bed shear stress in Figures 6.1.2.5 to 6.1.2.8. The erosion

threshold has been based on the extrapolation of trends in S to background values. Synthetic cores for these experiments could not be derived as we had no measure of the bulk density of the artificially-created beds. The mean erosion thresholds for Labexp2 and Labexp3 were 0.35 and 0.43 Pa (which is within the range derived from Sea Carousel). The threshold for the more consolidated material from site A was higher (0.59 Pa; Figure 6.1.2.7). The erosion threshold for site A/B, by contrast, was amongst the lowest of those tested ($\tau_c(0) = 0.19$ Pa; Figure 6.1.2.8).

STATION	EROSION THRESHOLD (Pa)	EQUATION
LABEXP2 (site A)	0.35	$S = 472 + 593\text{Log}_{10}\tau$
LABEXP3 (site A)	0.43	$S = 422 + 743\text{Log}_{10}\tau$
LABEXP5 (site A)	0.59	$S = 184\tau^{0.383}$
LABEXP9 (site A/B)	0.19	$S = 2773\tau^{2.464}$

Table 6.1.2.1. A summary of the surface erosion thresholds determined from the Lab Carousel experiments on bulk samples from sites A and A/B.

E_p bore no obvious relationship to either applied stress or current speed in either absolute or excess form. The critical threshold for onset of deposition (τ_d) may be determined from Krone's (1961) relationship: $\delta M/\delta t = S(t)W_s(1 - \tau_o/\tau_d)$, where τ_o is the applied shear stress. By measuring mass settling rate ($\delta M/\delta t$) at a known and finite stress (for $\tau_o < \tau_d$), we may determine τ_d as: $\tau_d = \tau_o / (1 - \{\delta M/\delta t \cdot 1/S(t) \cdot W_s\})$. The S time-series for this part of each experiment are shown in Figure 6.1.2.9. Notice that for Labexp5 (site A) $\tau_o > \tau_d$, so no settling took place. For remaining experiments, a measurable settling rate was apparent. Still water settling rate (W_s) was determined from Labexp3 and Labexp5. The results are presented in Table 6.1.2.2. Notice that these settling rates show considerable scatter but span those derived from the Sea Carousel. The threshold for deposition was evaluated for Labexp9 only, and yielded a value of 0.07 Pa. This

value is about 30% of $\tau_c(0)$ for this station.

STATION	W_s (m/s)
LABEXP3 (site A)	7.98×10^{-3}
LABEXP5 (site A)	6.64×10^{-4}
LABEXP9 (site A/B)	1.64×10^{-3}

Table 6.1.2.2. Mean still-water settling rates determined from a bulk sample from site A that was deposited and eroded in Lab Carousel.

6.1.3 SAMPLE ANALYSIS

The bulk density profiles of the surface sediment has been evaluated through Catscan analysis of syringe cores taken from each Sea Carousel site. The method of analysis is given in Appendix 1. Results are plotted in Figure 6.1.3.1. Three layers were recognised: (1) a surface layer, 2-3 mm thick of relatively high bulk density; (2) a transitional layer (2-3 mm thick) of rapidly changing bulk density; and (3) a uniform sub-stratum, exhibiting slowly-varying physical properties with depth. The high density of layer (1) may result from desiccation of surface sediment through solar heating, which occurred during tidal exposure at the time of sampling. Also, the constant density of layer (3) suggests that the process of self-weight consolidation has not taken place. The scatter in bulk density values (horizontal bars around each data point) reflects the heterogeneity at each depth interval, not the error in detection. This scatter is large throughout the core, and may reflect the presence of either bioturbation or poorly-sorted material.

The gravity core collected from site A consists of two sediment types - a silty clay with a bioturbated region at the top and sand (Appendix 1). The core which has a length of 0.26 m, is mottled with both black and dark organic-rich clay. Water content of the core varies between 32

and 42%. The vane shear strength (S_u) increases downcore as would be expected, from 6.4 kPa at 0.005 m to 17.8 kPa at 0.25 m. 25% of the surface sample taken consists of sand, 45% is silt, whilst 26% is clay. The surface of the core is illite rich, containing 47%. 27% consists of kaolinite, 22% chlorite, and the remainder consists of calcite.

Biological sediment samples at site A were collected at Sea Carousel stations LISPUK13 and LISPUK14. Site A was characterized by intermediate levels of chlorophyll α , dissolved carbohydrates and bacteria numbers, and low numbers of nematodes. The latter may be related to the water content of the sediments which was also low and which supports the interpretation of the Catscan analysis suggesting desiccation of the surface sediment layer.

6.2 SITE B

6.2.1 SEA CAROUSEL

Sea Carousel experiments LISPUK17, LISPUK18, and LISPUK19 were carried out at site B. Time-series plots of these stations are shown in Figures 6.2.1.1 to 6.2.1.3. All stations were subject to rapidly changing ambient S . This was the result of the passage of turbidity maxima during either the last stage of the ebb tide (Figure 6.2.1.2) or the first phase of the flood tide (Figure 6.2.1.3). At station LISPUK19, the change in S inside Sea Carousel was dominated by the passage of a turbidity maximum during the first flood of the tide. The S peaked at *circa* 3000 mg/L and dropped steadily to 300 mg/L over the subsequent 20 minutes.

Consequently, only the results from stations LISPUK17 and LISPUK18 will be discussed further. Both of these stations showed similar results. That is, well-defined peaks in erosion rate (E_p) associated with the onset of each increment of flow (above threshold): Type I erosion. Also, we found a well-defined surface erosion threshold of 0.3 - 0.6 Pa. The topmost 0.03 mm was

rapidly eroded (Figure 6.2.1.5A) whereas beneath, a substrate of steadily increasing strength with depth was found ($\Phi = 26^\circ$).

There was no clear relationship between peak erosion rate (E_p) and bed shear stress or current speed (as evident in earlier experiments). The mean erosion rate (E_m) showed only a poor relationship to flow (Figures 6.2.1.4 and 5). No still-water settling was carried out at this site.

6.2.2 LAB CAROUSEL

Labexp4 was carried out on a site B bulk sample. As in previous experiments of this kind, sensor saturation truncated the results early in the lid speed range (Figure 6.2.2.1). Type I erosion prevailed throughout with peak erosion rates of $3 \times 10^{-4} \text{ kg/m}^2/\text{s}$ (the scatter is due to intermittent saturation of sensor 1). The measured S , when plotted against applied bed shear stress, showed an erosion threshold of 0.20 Pa (Figure 6.2.2.2). The significance of this value is low, given the limited number of samples on which the threshold is based. The mean erosion rate (E_m) showed a positive correlation to flow of the exponential form:

$$E_m = 4.86 \times 10^{-6} \cdot 10^{(7.212Uy)} \text{ kg/m}^2/\text{s} \quad r^2 = 0.74; \quad n = 25$$

The still-water mean particle settling rate (W_s) was $2.07 \times 10^{-3} \text{ m/s}$, and the deposition threshold stress (τ_d) was evaluated as 0.03 Pa. The ratio $\tau_c(0):\tau_d$ is therefore 6.6.

6.2.3 SAMPLE ANALYSIS

The Catscan analysis of a syringe core taken from site B is shown in Figure 6.2.3.1. As at site A, three layers may be defined: (1) a surface layer (0.5 cm thick) of relatively low density (1500-1520 kg/m^3), and high heterogeneity. The density decreases with depth, and is least at the base of the layer (this may reflect either desiccation or bioturbation); (2) a layer of transition, wherein the density increases linearly with depth to about 1800 kg/m^3 at a depth of 1.4

cm. The heterogeneity of this layer decreases with depth, possibly due to the compression of pore spaces and animal tubes; and (3) the mudflat substrate, demonstrating a general decrease in density with depth, superimposed by systematic fluctuations in density and heterogeneity at the cm scale. The overall decrease in bulk density with sediment depth in this layer is opposite to that expected of a normally-consolidated sediment and may reflect a change in grain size.

Logs of the gravity core collected at site B are shown in Appendix 1. Site B has a heavily bioturbated near-surface. The top 0.075 m of the gravity core consists of a silty clay with sand and black organic-rich clay mottles. The rest of the core consists of layers of sand and black and dark organic-rich clay. At the base, a coarse sand is found. Water content at the surface is 56% and shows a drop to 31% at 0.29 m. Vane shear strength shows a drop from 13.9 kPa at 0.05 m, to 9.3 kPa at 0.1 m, whereon it increases to 32.7 kPa at 0.29 m. The surface sample taken from this site was extremely clay rich. Only 4% sand is present, with 48% silt and 46% clay. The modal grain size is 13 microns, with 4% of the mass being of this size. Illite is the dominant clay mineral, making up 57% of the surface clay mineralogy. 29% of the total clay is kaolinite, 11% is chlorite, and calcite forms the remainder.

Sediment samples for biological analyses at site B were collected at Sea Carousel stations LISPUK17 and LISPUK19. Site B had intermediate levels of chlorophyll *a* and bacteria numbers and relatively low levels of dissolved carbohydrates and nematodes.

6.3 SITE B/C

6.3.1 SEA CAROUSEL

Three experiments were carried out at site B/C: LISPUK10, LISPUK11, and LISPUK12. Time-series of these experiments are given in Figures 6.3.1.1 to 6.3.1.3 respectively. LISPUK11 was short-lived due to technical difficulties. Consequently, only the results from the remaining two stations will be discussed further. The eroded mass from site B/C was generally very low. Furthermore, the erosion rate time-series appeared erratic with no obvious trends with time. The trends in S during station LISPUK12 suggest that erosion was Type I. However, the ambient values of S varied on a scale of the changes resulting from the erosion process itself (Figure 6.3.1.3C). Furthermore, systematic fluctuations in the lower OBS (the origin of which are unknown) masked the erosion trends. A threshold for erosion is thus difficult to define. The surface erosion threshold derived from plots of E_m and S versus τ_o is ambiguous. E_m shows considerable scatter and yields unreliable estimates of the erosion threshold. S by contrast appears to increase as a smooth power function of τ_o and good estimates of the erosion threshold have been derived. These are 0.05 and 0.15 Pa for stations LISPUK10 and 11 respectively. The large difference between the two stations may result from the influences of the barge Scott H which profoundly reworked many of the sites upon landing. Nevertheless, large differences were also detected in the friction coefficient (12 - 51°) which suggests natural heterogeneity as the cause at least in part.

6.3.2 LAB CAROUSEL

Material from site B/C was evaluated in Labexp8. Our results show that there was clear and strong erosion (Figure 6.3.2.1) and a well-defined erosion threshold at 0.75 Pa

(Figure 6.3.2.2). The mean sediment concentration (S) showed a positive correlation with bed shear stress of the power form: $E_m = 85\tau_o^{5.214}$ kg/m²/s. The still-water settling rate (W_s) for this site was 4.90×10^{-3} m/s, which was the highest of the Lab Carousel estimates. $\delta M/\delta t$ for an applied stress of 0.13 Pa was 1.71×10^{-3} kg/m²/s, which yielded a deposition threshold (τ_d) of 0.32 Pa. The ratio $\tau_c(0) : \tau_d$ was 2.3.

6.3.3 SAMPLE ANALYSIS

The Catscan analysis of the syringe core from site B/C is shown in Figure 6.3.3.1. Similar to the two landward sites, three distinct layers were recognised: (1) a surface layer of low bulk density (1440 kg/m³) and high heterogeneity, that was *circa* 3 mm thick. There was no clear change in density with depth in this layer; (2) a layer of transition, wherein the density increased rapidly to a maximum of 1750 kg/m³. The heterogeneity of bulk density decreases with depth in this layer, possibly due to the consolidation (and elimination) of pore spaces; and (3) the substrate, which shows fluctuations in bulk density at the cm scale. Note, the heterogeneity in this layer is large at the top (where shell debris prevails), then drops abruptly to a near-constant value.

Core logs for the gravity core taken at site B/C are illustrated in Appendix 1. Fine laminations of silty clay and sand and of dark, organic-rich clay and sand dominate the substrate of this site. The top of the gravity core does not appear to be bioturbated as the others are, but a burrow can be seen 0.25 metres down the core. A number of erosion surfaces are present, including one at 0.22 m, another at 0.26 m and another at 0.54 m. Water content is 44% at the surface, and after a slight increase, it falls to 39% at 0.4 m. Following this, it shows a general increase to 76% at 0.6 m, whereon it decreases to 26% at the base of the core. Vane shear strength mirrors the water

content well, and varies between 10.0 and 16.5 kPa. 14.1% of the surface sample is made up of sand, 57% silt, and 22% clay. Site B/C contains the most illite of any site - 66%. Whilst 16% of the clay mineralogy is chlorite, this site contains the least amount of kaolinite (13%).

Sediment samples for biological analysis at site B/C were collected at Sea Carousel station LISPUR9. Site B/C was the highest in dissolved carbohydrates, chlorophyll *a* concentration and nematode numbers (unfortunately we did not obtain data on bacteria numbers for this site).

6.4 SITE C

6.4.1 SEA CAROUSEL

Sea Carousel experiments LISPUR5 and LISPUR6 were carried out at site C. Time-series plots of these two deployments are shown in Figures 6.4.1.1 and 6.4.1.2. Results from the first deployment were excellent, and form the basis of this interpretation. LISPUR6 was abandoned due to boat drift. Results from LISPUR5 show a well-defined threshold followed by Type I erosion. Peak erosion rates were relatively constant at $8 \times 10^{-4} \text{ kg/m}^2/\text{s}$. Onset of erosion was characterised by a rapid increase in *S* (Figure 6.4.1.3). The surface erosion threshold is clearly seen to be 0.15 Pa; a relatively low value for the transect. Mean erosion rates are amongst the highest in the survey and show a positive correlation with applied bed shear stress and current speed of the exponential form:

$$E_m = 1.45 \times 10^{-5} \cdot 10^{(3.166U_y)} \text{ kg/m}^2/\text{s} \quad r^2 = 0.88; n = 12$$

The still-water settling rate (W_s) recorded at this site ($9.07 \times 10^{-3} \text{ m/s}$) was the highest value recorded in the survey, and was approximately 3 times larger than the values for site A. The friction coefficient for site C was extremely low (3°) and is diagnostic (in this context) of recent deposition.

6.4.2 LAB CAROUSEL

Labexp7 was carried out on a site C bulk sample. The time-series for this experiment is shown in Figure 6.4.2.1. A clear peak in erosion was evident at early stages of erosion, and bed failure was largely Type II; erosion rates reached values of $9 \times 10^{-4} \text{ kg/m}^2/\text{s}$. The erosion threshold was clearly seen in a plot of S versus bed shear stress (Figure 6.4.2.2), and was estimated to be 0.45 Pa. This value is considerably higher than that determined from Sea Carousel. Mean erosion rate showed only a poor relationship to flow in the following exponential form:

$$E_m = 3.12 \times 10^{-6} \cdot 10^{(6.268U^y)} \text{ kg/m}^2/\text{s} \quad r^2 = 0.66; n = 14$$

This relationship is similar to those derived from sites A and B. Note the similarity in erosion trends between the lab and the field data. Curiously, the lab sample appears to be more erosion resistant than the field site.

The still-water settling rate (W_s) for this experiment was $3.97 \times 10^{-3} \text{ m/s}$ (the highest value except for site B/C). Curiously, $\delta M/\delta t$ for still water settling was less than that for an applied stress of 0.05 Pa. (We attribute this to differential settling of a range of sizes of suspended aggregates). As a result, we were unable to define τ_d .

6.4.3 SAMPLE ANALYSIS

The Catscan analysis of the syringe core collected from site C is shown in Figure 6.4.3.1. In this example it appears that the surface, recently-deposited layer is absent, and only the two lowermost layers remain. These are: (1) an upper layer, 8 mm thick, that shows a rapidly increasing density from 1500 and 1730 kg/m^3 (this layer is equated with the transitional layer of landward sites); also, the heterogeneity of the density is very large; and (2) the substrate,

characterised by a near-constant bulk density with depth, modulated at the cm scale. The heterogeneity is low and constant with depth reflecting a lack of distinct stratification. The gravity core log, shown in Appendix 1, demonstrates that site C was heavily bioturbated in the near-surface. The top 0.10 m of the core consist of a silty clay with sandy mottles. Laminations are an important feature in this core and consist of either sand and silty clay or sand and black organic-rich clay. There are a number of erosion surfaces evident, at 0.22 m and 0.27 m, and black organic-rich clay is quite extensive. Water content is 43% at the top of the core and decreases to 37% at the base of the core, varying quite considerably (Appendix 2). 49% of the surface sample consists of illite, whilst 15% is chlorite and 36% kaolinite (Appendix 3). Vane shear strength varies significantly from 16.0 kPa at the surface to 8.9 kPa at a depth of 0.65 m (Appendix 4). The surface was extremely silty, containing 59% silt. 22% consists of sand, whilst clay makes up 16%. The modal grain size is 44 microns, with 8% of the mass of this grain size (Appendix 5).

Biological sediment samples at site C were collected at Sea Carousel stations LISPUK5 and LISPUK6. This site had intermediate values for all the biological characteristics measured.

6.5 SITE C/D

6.5.1 SEA CAROUSEL

Two experiments were carried out at site C/D: LISPUK7 and LISPUK8. Plots of the time-series of these experiments are shown in Figures 6.5.1.1 and 6.5.1.2. Station LISPUK8 was terminated prematurely due to dangers of boat drift. Nevertheless, the erosion process had begun and so a well-defined threshold could be defined. Bed failure took place early in both experiments and was manifested by a continuous release of bed material typical of Type II

erosion. This was apparent at all applied bed shear stresses above the critical. The erosion thresholds for the two sites were intermediate in magnitude (Figures 6.5.1.3 and 6.5.1.4) and were between 0.26 and 0.35 Pa; values equivalent to that from site D. The friction coefficients were the highest recorded from the transect (63 - 77°).

6.5.2 SAMPLE ANALYSIS

The Catscan analysis of a syringe core collected at site C/D is shown in Figure 6.5.2.1. The tripartite division of the bed (seen at landward sites) was not apparent. Rather five distinct layers have been defined: (1) a 3 mm surface layer of steadily increasing bulk density (1680 - 1780 kg/m³) and decreasing heterogeneity; (2) a layer of transition, showing a steady increase in bulk density to a maximum of 1890 kg/m³, and an associated decrease in heterogeneity; and (3) - (5) strata showing small variations in bulk density (1600 - 1850 kg/m³) and systematic modulations in heterogeneity. The values of bulk density are equivalent to those landward, though the scale in variation has increased.

The gravity core collected at this site (Appendix 1) is dominated by fine laminations. A coarse, bioturbated sand is present at the top containing black organic-rich mottles. Erosion surfaces are also evident. Water content at this site is 40% at the surface and is the lowest surface value of all the cores. Vane shear strength mirrors the water content. 53% of the surface sample consists of silt, with 33% clay and 12% sand. The modal grain size is 44 microns - 7% of the total mass is of this size. Illite is dominant, taking up 46% of the surface clay mineralogy. 36% of the surface sample consists of kaolinite whilst 14% consists of chlorite.

Sediment samples for biological analyses at site C/D were collected at Sea Carousel stations LISPUK7 and LISPUK8. This site appeared more heterogeneous than the other sites. Station

LISPUK7 was among the highest in sediment chlorophyll α , dissolved carbohydrates, and bacteria and nematode numbers. In contrast, LISPUK8 was amongst the lowest in these same parameters except for bacteria numbers which were intermediate.

6.6 SITE D

6.6.1 SEA CAROUSEL

Sea Carousel experiments LISPUK1, LISPUK2, LISPUK3, and LISPUK4 were carried out at site D. The time-series for these deployments are shown in Figures 6.6.1.1 to 6.6.1.4. Station LISPUK1 was sited on a steep wall of a major creek that traversed the region. As a consequence, the Carousel base was unsealed in parts. This effect is clearly seen in the erratic nature of lid rotation, current speed, and S. LISPUK2 was located on a smooth creek levée that showed evidence of scouring. LISPUK3 was sited on 0.1 m high erosion furrows, and leakage from the base of the Carousel is suspected. LISPUK4 was sited at the base of the major creek which was composed of fully-saturated, soft sandy material. The erosion of creek levée material produced well-defined asymptotes in S diagnostic of Type I erosion (Figure 6.6.1.2). Peak erosion rates were very high; up to 10^{-2} kg/m²/s. The threshold for erosion is well-defined and intermediate in value (0.20 - 0.34 Pa).

The furrowed mudflat also eroded in Type I fashion (Figure 6.6.1.3), although the decreases in corrected S at each speed increment suggests losses from the base of the Carousel (not accounted for in the estimation of dispersion, which considers losses from the top only). The erosion threshold for this material ($\tau_c(0) = 0.34$ Pa; Figure 6.6.1.6) is higher than at the levée suggesting that the levée was forming at the time. The friction coefficient of the furrowed mudflat is also higher ($\Phi = 64^\circ$) than adjacent to the creek, with an apparently in-erodible substrate at a depth of

0.03 mm that may be diagnostic of compacted exhumed sediment.

The creek bed exhibited an erosion pattern that was transitional between Type I and Type II; that is an initial peak was evident, yet erosion continued measurably throughout each increment of applied stress (Figure 6.6.1.4B and C). The peak erosion rates were lower than at other stations (up to 10^{-3} kg/m²/s) but was continuous. The erosion threshold was also intermediate ($\tau_c(0) = 0.23$ Pa; Figure 6.6.1.7) as a consequence of the soft, saturated nature of the bed material. The friction coefficient was much lower than that of the creek levée ($\Phi = 10^\circ$) reflecting the highly saturated mobile sand creek bed. Mean erosion rates showed exponential trends with flow similar to landward sites, though the scatter in results was large:

$$E_m = 1.99 \times 10^{-6} \cdot 10^{(3.601U_y)} \text{ kg/m}^2/\text{s} \quad r^2 = 0.59; n = 42$$

6.6.2 LAB CAROUSEL

Labexp6 was carried out on a bulk sample from site D. The time-series of this experiment is shown in Figure 6.6.2.1. As in previous experiments, sensors saturated early after erosion began. Peak erosion rates were, however, comparable to those from Sea Carousel (10^{-3} kg/m²/s). The erosion threshold ($\tau_c(0)$) was well-defined and had a value of 0.38 Pa (Figure 6.6.2.2). This falls within the range derived from Sea Carousel from this site. The mean erosion rate (E_m) may be defined in terms of the flow in the following exponential form:

$$E_m = 5.56 \times 10^{-6} \cdot 10^{(6.102U_y)} \text{ kg/m}^2/\text{s} \quad r^2 = 0.53; n = 7$$

The high exponents demonstrate that this material is more susceptible to erosion than the natural site. This relationship shows the second highest erosion rate increase (as a function of applied stress) of all the samples tested from the transect (after site B), perhaps reflecting lower cohesion and consolidation of the relatively sandy samples. The still-water settling rate was evaluated to

be 2.47×10^{-3} m/s, which is approximately three times higher than sites A and A/B (again, reflecting the sandy nature of the bed material). Furthermore, the mean threshold for deposition was 0.23 Pa thus the ratio $\tau_c(0) : \tau_d$ was 1.65 which is close to a value of 2 that is often assumed in modelling.

6.6.3 SAMPLE ANALYSIS

The Catscan analysis of a syringe core taken from the vicinity of the levée (site D) is shown in Figure 6.6.3.1. As at site C/D, no clear tripartite sub-division of the bed could be made. Rather, 5 layers have been defined on the basis of the systematic fluctuations in bulk density and heterogeneity of material. These fluctuations are on the order of cm in scale and show variations in density between 1600 and 1810 kg/m². No soft surface veneer was present, nor was the transitional layer evident. This supports the on-site observations, that the bed appeared scoured, and absent of a biofilm.

The top of the gravity core from this site is bioturbated. The remainder consists mainly of interbedded sands, silty clay and black and dark organic-rich clay. Water content decreases from 66% at the surface to 30% at the base (in keeping with compaction). Yet site D has the highest surface water content. Vane shear strength also increases with depth from 4.3 to 8.1 kPa. The surface of the core is silt rich (46%). Clay makes up 39% of the surface composition, with sand making up the remainder. Site D contains the least amount of illite, at only 42%, but the most kaolinite at 38%. Chlorite is also greater here than at all the other sites apart from site A.

Biological sediment samples at site D were collected at Sea Carousel stations LISPUK1, LISPUK3 and LISPUK4. The surface heterogeneity at this site made sampling difficult and all samples were collected from the creek bottom. This site had relatively low values of chlorophyll

α , dissolved carbohydrates and bacteria. Nematode numbers were also low.

7. GENERAL INTERPRETATIONS AND INITIAL CONCLUSIONS

7.1 The variation of erosion threshold with distance along transect

The variation of surface erosion threshold showed no systematic trends, but rather three distinct maxima were evident (Figure 7.1.1). The variation at any site was less than the variation across the mudflat, so the spatial trends that we describe appear real. The highest threshold was found on the central mudflat in a region of abundant chlorophyll, carbohydrate production, and biofilm development. The second maximum was found at the innermost site (A), reflecting the possible effects of solar radiation. The third maximum was found at the outer site (D) reflecting the effects of scouring.

Recent deposition was evident at site A, yet the bulk density values were higher than on the middle mudflats perhaps due to desiccation (Table 7.1.1). The lowest erosion thresholds detected by Lab and Sea Carousels were at site B. This is perhaps reflected in the low surface bulk density detected at this site, which may reflect recent deposition. Site B/C shows a high erosion threshold in contrast to the lowest bulk density of the transect. Here we suspect the dominating role of biostabilization; an interpretation supported by the near-surface structure. This site also has an anomalously high sand content (Black, unpublished data).

SITE	WET BULK DENSITY (kg/m ³)	POROSITY (%)	DRY BULK DENSITY (kg/m ³)	$\tau(0)1$ (Pa)	$\tau(0)2$ (Pa)
SITE A	1800	53	1255	0.48	0.35
SITE B	1500	71	769	0.06	0.20
SITE B/C	1450	74	688	0.55	0.75
SITE C	1500	71	769	0.15	0.45

SITE	WET BULK DENSITY (kg/m ³)	POROSITY (%)	DRY BULK DENSITY (kg/m ³)	τ(0) 1 (Pa)	τ(0)2 (Pa)
SITE C/D	1700	60	1093	0.30	--
SITE D	1750	56	1174	0.26	0.38

Table 7.1.1. A summary of sediment physical properties determined from the Catscan analyses, and erosion threshold ($\tau(0)$) determined for (1) the Sea Carousel, and (2) Lab Carousel.

Sites C and C/D, located on the central mudflat, show intermediate erosion thresholds despite being on the scoured (dense) outer mudflat. The high erosion threshold at site D reflects observations of scouring at this site, and the absence of a surface layer of recently deposited material. This site had the highest sand content of the entire transect.

There is a good relationship between wet-weight bulk density (ρ_b) and erosion threshold (ET) of the form $ET = 0.00102 (\rho_b)$; $r^2 = 0.82$ (where ρ_b is in kg/m^3), provided we exclude results from site B/C (Figure 7.1.2). This is because of the outlier created by site B/C. We interpret this outlier to be the result of biostabilization by a biofilm which was apparent only at this site. In the absence of the biofilm, the higher is the bulk density, the higher the erosion threshold. The wet- and dry-weight bulk densities of surface material may be compared with the erosion thresholds in Table 7.1.1. Porosity (P) is also defined, and has been derived from the formula: $P = (1 - V_s)$, where $V_s = (\text{wet-weight bulk density} - \text{water density})/\text{sediment buoyant density}$.

The scatter in results reflects several problems with the survey. Firstly, Sea Carousel was unsuited to the furrowed topography of the mudflat and leakage from the base must be considered a possible source of error. Secondly, reworking of the mudflat by the barge props was severe, and largely unavoidable. We noted that LISPUK6 was carried out in the prop wash scour of Scott H from an earlier visit. It must be assumed that resuspension of any soft surface layer

would have taken place beneath the props (a possibility at site B/C) yielding unrealistically high values of bed stability. Thirdly, the whole mudflat had been subjected to intense reworking by late winter storms. So, the mudflat profile may not be in equilibrium with depositional processes, but rather with erosional ones prevalent in storms. Perhaps we have recorded a “winter equilibrium mudflat profile” rather than the more conventional “summer profile”; the latter expected to be more controlled by sedimentation and biological effects.

7.2 A comparison between Lab and Sea Carousels erosion thresholds

The erosion thresholds derived from the Lab and Sea Carousels compare reasonably well (Figure 7.2.1). Curiously, the Lab Carousel thresholds appear higher than those determined in situ by about 20%. The reason for this may be in the consolidation time in the Lab Carousel. We found that erosion threshold of site A samples increased in proportion with consolidation time (T, in hours) in the form $ET = 0.261\text{Log}_{10}(T)$. In Figure 7.2.2 we see that a 20% reduction in ET (for material consolidated for 20 hours) would result if the consolidation time was reduced by 9 hours. As the consolidation time for lab experiments was typically 20 hours we would suppose that closest agreement to Sea Carousel would have occurred had we consolidated material for only 11 hours. This is about equivalent to one tidal inundation of the mudflat, and may indicate that the in situ material reflects consolidation of material deposited by the immediately preceding tidal inundation. Thus it appears that the weak surface layer, observed in many syringe cores from the Skeffling transect, was deposited by the still-stand immediately prior to sampling. The exception was found at site A. Here, the in situ measurements were higher than the Lab Carousel results indicating solar radiation (which was intense at the time of the in situ survey) may have significantly increased the erosion threshold of the inner mudflat.

7.3 In situ erosion rates

Mean erosion rates (E_m) for all sites appear to follow the same relationship to applied current speed (U). This relationship takes the exponential form:

$$E_m = 2.47 \times 10^{-6} \cdot 10^{(3.749Uy)} \text{ kg/m}^2/\text{s}; \quad r^2 = 0.55; \quad n = 100$$

Figure 7.3.1 shows the best-fit regression line with the 95% confidence limits. Considering the diversity of sites, the correspondence of results is notable. For modelling purposes, the above equation would be a reasonable representation of the entire mudflat.

There appears to be a link between peak and mean erosion rates with the former being about an order of magnitude greater than the latter (Figure 7.3.2). Yet we could find no consistent trends in the factors controlling E_p . We need to examine further the link between instantaneous bed erosion and bed properties in order to understand this phenomenon.

7.4 Lab Carousel erosion rates

The mean erosion rates derived from each site in Lab Carousel appear to show reasonable correspondence with current speed. The best-fit regression of all sites is shown in Figure 7.4.1.

The form of the fit is as follows:

$$E_m = 1.99 \times 10^{-5} \cdot 10^{(3.85Uy)} \text{ kg/m}^2/\text{s}; \quad r^2 = 0.38; \quad n = 52$$

This equation is very similar to that determined from in situ monitoring and suggests that the material properties were similar. However, the scatter in the Lab Carousel results is higher than that from Sea Carousel and erosion rates were generally higher. The fact that the Lab Carousel samples were remoulded would favour higher erosion rates due to the breakdown of in situ bed strength.

7.5 Settling rates and depositional thresholds

Settling rates determined from Sea Carousel were limited to site A. Here we found rates which were comparable to those observed in Lab Carousel, but an order of magnitude greater than values reported from other estuarine sites by Amos and Mosher (1985). Lab Carousel experiments showed that settling rates were lowest at site A, were at a maximum at site B/C and generally decreased in a seaward direction. Thus settling rate mimics the trends in erosion threshold. This may not be surprising if we assume that flocculation, which enhances settling, is itself enhanced by organic matter.

7.6. Relationship between biological parameters and bed erosion.

With the exception of a relatively weak correlation between dissolved carbohydrate and chlorophyll *a* concentration, there were no obvious strong correlations between any of the biological parameters measured. With the exception that site B/C had the highest erosion threshold and the highest chlorophyll *a* and dissolved carbohydrate concentration, there was little relationship between biological characteristics at each site and sediment erodibility parameters.

The lack of any consistent trends in biological parameters along the mudflat transect may be a result of the time of the study. If it were carried out during the late spring or summer, when biological processes would be more active, a clearer relationship between biology and sediment stability may have been observed.

7.7 Bed stability and gravity core physical properties

We found no clear relationship between the physical properties measured in gravity cores and erodibility. Site B had the lowest erosion threshold of all the sites and also the lowest sand and

highest clay contents, which is opposite to the trend one would expect. We found that site A had the highest sand content, which conflicts with results from samples collected the previous summer (see Figure 1.2). As a result, one might expect site A to show the lowest erosion threshold of the transect. However, this is not the case. Site B/C, which had the highest erosion threshold, was intermediate in terms of sediment texture. Illite, which exhibits strong cohesion, was highest at this site and so may play a role in stabilizing the surface in association with biostabilization. Water content does not seem to have any bearing on the erodibility of the sediments. Site D had the highest water content along with a high percentage of clay, but it had the same erosion threshold as site C which had one of the lowest water contents.

A good positive correlation was found between bulk density and erosion threshold provided site B/C was removed from the data set. This suggests that erosion threshold may be predicted by bulk physical properties in abiotic situations, but in natural settings, this relationship can be overshadowed by the effects of biofilms.

8. REFERENCES

Amos, C.L., Sutherland, T.F., Radzjewski, B. And Doucette, M. (In press). A rapid technique to determine bulk density of fine-grained sediments by X-ray computed tomography. *Geo-Marine Letters*.

Amos, C.L., Christian, H.A., Heffler, D.A. and MacKinnon, W. (1994). Instrumentation for *in situ* monitoring of marine sediment geodynamics. *Science Review 1992 & '93*. Publ. Department of Fisheries and Oceans: 55-59.

Amos, C.L., Grant, G.R., Daborn, G.R., and Black, K. (1992). Sea Carousel - a benthic annular flume. *Estuarine Coastal and Shelf Science* 34: 557-577.

Amos, C.L. and Mosher, D.A. (1985). Erosion and deposition of fine-grained sediments from the Bay of Fundy. *Sedimentology* 32: 815-832.

Downing, J.P. (1983). An optical instrument for monitoring suspended particulates in ocean and laboratory *in Proceedings of Oceans '83*: 199-202.

Downing, J.P. and Beach, R.A. (1989). Laboratory apparatus for calibrating optical suspended solids sensors. *Marine Geology* 86: 243-249.

9. ITINERARY

<u>DATE/TIME</u>	<u>OPERATION</u>
2 APRIL	arrive at Hull from Canada
3 APRIL	container arrives Spurn Head
4 APRIL	mobilizing lab Carousel/lab container
5 APRIL	collection of sample A/lab Carousel
6 APRIL	Labexp1 (site A); Sea Carousel motor inoperational
7 APRIL	Labexp2 (site A); new motor arrives from Canada
8 APRIL	Sea Carousel deployments 1 & 2 (LISPUK1 & 2; site D)
9 APRIL	Labexp3 (site A)
10 APRIL	Sea Carousel deployments 3 & 4 (LISPUK3 & 4; site D)
11 APRIL	Sea Carousel deployments 5 & 6 (LISPUK5 & 6; site C); labexp4 (site B)
12 APRIL	Sea Carousel deployments 7 & 8 (LISPUK7 & 8; site C/D) Labexp5 (site A tray; 7 days consolidation)
13 APRIL	Sea Carousel deployments 10, 11 & 12 (LISPUK10, 11 & 12; site B/C); Labexp6 (site D)
14 APRIL	Sea Carousel deployments 13, 14 & 15 (LISPUK13, 14 & 15; site A) Labexp7 (site C)
15 APRIL	Data processing/Easter weekend
16 APRIL	Labexp8 (site B/C)/Easter Sunday
17 APRIL	Hyab crane strut broken/Sea Carousel deployment LISPUK16 aborted
18 APRIL	Sea Carousel deployments 17 & 18 (LISPUK17 & 18; site B)
19 APRIL	Sea Carousel deployment 19 (site B) abandoned due to drifting Labexp9 (site A/B); labexp10 (site A tray; 14 days consolidation)
20 APRIL	demobilization
21 APRIL	ship container to Canada; leave Hull

FIGURE CAPTIONS

Figure 1.1. A location diagram of the study region, Humber estuary, S. Yorkshire, England. The intertidal transect was located across the mudflats off Skeffling on the northern flank of the estuary.

Figure 1.2. A transect of the Skeffling mudflat profile. The stations occupied in this study are marked to show distance from the shoreline and elevation relative to Chart Datum (CD). The sand content of seabed samples taken along the transect is also shown (after K. Black, unpublished data).

Figure 6.1. Summary plots of the biological parameters (water content, % organic content, chlorophyll α , dissolved carbohydrates (DCHO), bacteria numbers and nematode numbers) plotted versus site.

Figure 6.2. Summary plots of the biological parameters (listed in Figure 6.1) plotted versus station number.

Plate 6.1.1.1. Photographs of the erosion scar left by Sea Carousel at site A (inner mudflat).

Plate 6.1.1.2. Photographs of the details of scouring left by Sea Carousel at site A. Notice the abundance of shell debris, aggregates and granules that forms a lag surface, and the undisturbed mudflat either side of the erosion scar (flow was from left to right).

Figure 6.1.1.1. A calibration plot of OBS output voltage from Sea Carousel versus dry-weight suspended sediment concentration. The calibration is for site A and B samples combined.

Figure 6.1.1.2. A time-series plot of results from Sea Carousel recorded at site A (LISPUK13) on 14 April, 1995. (A) lid speed and azimuthal and vertical currents at the reference height (0.18 m); (B) suspended sediment concentrations from the three OBS sensors (OBS1 and OBS3 are internal, OBS2 is external) and from pumped samples; and (C) erosion rate. Notice the prevalence of Type I erosion.

Figure 6.1.1.3. A time-series plot of results from Sea Carousel recorded at site A (LISPUK14) on 14 April, 1995. (A) lid speed and azimuthal and vertical currents at the reference height (0.18 m); and (B) suspended sediment concentrations from the three OBS sensors (OBS1 and OBS3 are internal, OBS2 is external) and from pumped samples; and (C) erosion rate.

Figure 6.1.1.4. A time-series plot of results from Sea Carousel recorded at site A (LISPUK15) on 14 April, 1995. (A) lid speed and azimuthal and vertical currents at the reference height (0.18 m); and (B) suspended sediment concentrations from the three OBS sensors (OBS1 and OBS3 are internal, OBS2 is external) and from pumped samples; and (C) erosion rate.

Figure 6.1.1.5. Estimates of the erosion threshold for deployment LISPUK13, site A. The upper panel shows erosion rate versus applied bed stress; the threshold ($\tau_c(0)$) is equated with the stress for a base erosion of 3×10^{-5} kg/m²/s and yields a value of 0.20 Pa. The lower panel shows

suspended sediment concentration versus applied bed shear stress; the threshold is equated with the stress at ambient concentration and yields a value of 0.42 Pa.

Figure 6.1.1.6. Estimates of the erosion threshold for deployment LISPUK14, site A. The upper panel shows erosion rate versus applied bed stress; it is not possible to derive the threshold from this plot. The lower panel shows that suspended sediment concentration increases as a power function of applied bed shear stress; the threshold is equated with the stress at ambient concentration and yields a value of 0.58 Pa.

Figure 6.1.1.7. Estimates of the erosion threshold for deployment LISPUK15, site A. The upper panel shows that erosion rate is a power function of applied bed stress; the estimated erosion threshold is 0.41 Pa. The lower panel shows that suspended sediment concentration increases as a power function of applied bed shear stress; the threshold is equated with the stress at ambient concentration and yields a value of 0.45 Pa.

Figure 6.1.2.1. A time-series of Lab Carousel experiment (Labexp2) on a site A bulk sample. (A) the azimuthal reference current for a height of 0.18 m above the bed (based on lid rotation); and (B) measured dry-weight suspended sediment concentration from three sample ports at heights of 0.03, 0.10, and 0.20 m above the base.

Figure 6.1.2.2. A time-series of Lab Carousel experiment (Labexp3) on a site A bulk sample. (A) the azimuthal reference current for a height of 0.18 m above the bed (based on lid rotation); (B) measured dry-weight suspended sediment concentration from three sample ports at heights of 0.03, 0.10, and 0.20 m above the base; and (C) erosion rate. Notice the prevalence of Type I erosion at early stages of erosion and sensor saturation during later stages.

Figure 6.1.2.3. A time-series of Lab Carousel experiment (Labexp5) on a site A bulk sample. (A) the azimuthal reference current for a height of 0.18 m above the bed (based on lid rotation); (B) suspended sediment concentration from three OBS's at heights of 0.03, 0.10, and 0.20 m above the base; and (C) erosion rate. Notice the prevalence of Type II erosion.

Figure 6.1.2.4. A time-series of Lab Carousel experiment (Labexp9) on a site A/B bulk sample. (A) the azimuthal reference current for a height of 0.18 m above the bed (based on lid rotation); (B) suspended sediment concentration from three OBS's and pumped samples at heights of 0.03, 0.10, and 0.20 m above the base; and (C) erosion rate.

Figure 6.1.2.5. Suspended sediment concentration versus the log of applied bed shear stress for Labexp2, site A. The erosion threshold is evaluated at 0.35 Pa. Also shown is the functional relationship between sediment concentration (S) and bed shear stress.

Figure 6.1.2.6. Suspended sediment concentration versus the log of applied bed shear stress for Labexp3, site A. The erosion threshold is evaluated at 0.43 Pa. Also shown is the functional relationship between S and τ_o (the applied bed shear stress).

Figure 6.1.2.7. Log eroded mass (kg) versus the log of applied bed shear stress for Labexp5, site A. The erosion threshold is evaluated at 0.59 Pa.

Figure 6.1.2.8. Log suspended sediment concentration versus the log of applied bed shear stress for Labexp9, site A/B. The erosion threshold is evaluated at 0.19 Pa. Also shown is the functional relationship between S and τ_o .

Figure 6.1.2.9. Time-series plots of suspended sediment concentration (A) and applied bed shear stress (B) during the settling phase of all Lab Carousel experiments carried out in this study. Mass settling rate (W_s) and depositional threshold (τ_d) have been determined from these data.

Figure 6.1.3.1. A log of the wet-weight bulk density derived from a Catscan analysis of a syringe core collected at site A. Three layers are evident: (1) a surface layer of relatively high density (2 mm thick); (2) a transitional layer of rapidly changing density (5 mm thick); and (3) the substrate.

Figure 6.2.1.1. A time-series plot of results from Sea Carousel recorded at site B (LISPUK17) on 18 April, 1995. (A) lid speed and azimuthal and vertical currents at the reference height (0.18 m); (B) suspended sediment concentrations from the three OBS sensors (OBS1 and OBS3 are internal, OBS2 is external), and from pumped samples; and (C) erosion rate. Notice the prevalence of Type I erosion.

Figure 6.2.1.2. A time-series plot of results from Sea Carousel recorded at site B (LISPUK18) on 18 April, 1995. (A) lid speed and azimuthal and vertical currents at the reference height (0.18 m); (B) suspended sediment concentrations from the three OBS sensors (OBS1 and OBS3 are internal, OBS2 is external), and from pumped samples; and (C) erosion rate.

Figure 6.2.1.3. A time-series plot of results from Sea Carousel recorded at site B (LISPUK19) on 18 April, 1995. (A) lid speed and azimuthal and vertical currents at the reference height (0.18 m); (B) suspended sediment concentrations from the three OBS sensors (OBS1 and OBS3 are internal, OBS2 is external); and (C) erosion rate. Notice the dominant effect of the passage of the flood tide turbidity maximum on the sediment concentration signal inside the flume.

Figure 6.2.1.4. Estimates of the erosion threshold for deployment LISPUK17, site B. The upper panel shows that erosion rate is a power function of applied bed stress; it is not possible to derive erosion threshold from this plot. The lower panel shows that suspended sediment concentration increases as a power function of applied bed shear stress; the threshold is equated with the stress at ambient concentration and yields a value of 0.008 Pa.

Figure 6.2.1.5. Estimates of the erosion threshold for deployment LISPUK18, site B. The upper panel shows that erosion rate is a power function of applied bed stress; the erosion threshold is evaluated as 0.04 Pa. The lower panel shows that suspended sediment concentration increases as a power function of applied bed shear stress; the threshold is equated with the stress at ambient concentration and yields a value of 0.11 Pa.

Figure 6.2.2.1. A time-series of Lab Carousel experiment (Labexp4) on a site B bulk sample. (A) the azimuthal reference current for a height of 0.18 m above the bed (based on lid rotation); (B) suspended sediment concentration from three OBS's and pumped samples at heights of 0.03, 0.10, and 0.20 m above the base; and (C) erosion rate. The intermittent effects of sensor

saturation are clearly seen during the eroding phase.

Figure 6.2.2.2. A plot of measured suspended sediment concentration (from pumped samples) versus applied bed shear stress in Sea Carousel. Notice the onset of erosion at 0.5 Pa which is based on the extrapolation of concentration to ambient levels.

Figure 6.2.3.1. A log of the wet-weight bulk density derived from a Catscan analysis of a syringe core collected at site B. Three layers are evident: (1) a surface layer of relatively low density (4 mm thick); (2) a transitional layer of rapidly increasing density (8 mm thick); and (3) the denser substrate.

Figure 6.3.1.1. A time-series plot of results from Sea Carousel recorded at site B/C (LISPUK10) on 13 April, 1995. (A) lid speed and azimuthal and vertical currents at the reference height (0.18 m); (B) suspended sediment concentrations from the three OBS sensors (OBS1 and OBS3 are internal, OBS2 is external), and from pumped samples; and (C) erosion rate. No clear trends in erosion are evident in this time-series.

Figure 6.3.1.2. A time-series plot of results from Sea Carousel recorded at site B/C (LISPUK11) on 13 April, 1995. (A) lid speed and azimuthal and vertical currents at the reference height (0.18 m); (B) suspended sediment concentrations from the three OBS sensors (OBS1 and OBS3 are internal, OBS2 is external); and (C) erosion rate. The site was abandoned early due to drifting. Also notice the trends in sediment concentration which show the passage of a flood tide turbidity maximum.

Figure 6.3.1.3. A time-series plot of results from Sea Carousel recorded at site B/C (LISPUK12) on 13 April, 1995. (A) lid speed and azimuthal and vertical currents at the reference height (0.18 m); (B) suspended sediment concentrations from the three OBS sensors (OBS1 and OBS3 are internal, OBS2 is external), and from pumped samples; and (C) erosion rate. The erratic nature of erosion is likely due to lower sensor response to intermittent burial.

Figure 6.3.1.4. Estimates of the erosion threshold for deployment LISPUK10, site B/C. The upper panel shows that erosion rate is a power function of applied bed stress; the estimated erosion threshold is 0.69 Pa. The lower panel shows that suspended sediment concentration increases as a power function of applied bed shear stress; the threshold is equated with the stress at ambient concentration and yields a value of 0.95 Pa.

Figure 6.3.1.5. Estimates of the erosion threshold for deployment LISPUK12, site B/C. The upper panel shows that erosion rate is a power function of applied bed stress; the estimated erosion threshold is 0.10 Pa. The lower panel shows that suspended sediment concentration increases as a power function of applied bed shear stress; the threshold is equated with the stress at ambient concentration and yields a value of 0.15 Pa.

Figure 6.3.2.1. A time-series of Lab Carousel experiment (Labexp8) on a site B/C bulk sample. (A) the azimuthal reference current for a height of 0.18 m above the bed (based on lid rotation); (B) suspended sediment concentration from three OBS's and pumped samples at heights of 0.03, 0.10, and 0.20 m above the base; and (C) erosion rate.

Figure 6.3.2.2. A plot of measured suspended sediment concentration (from pumped samples) versus applied bed shear stress in Lab Carousel for experiment Labexp8 (site B/C) . Notice the onset of erosion at 1.8 Pa which is based on the extrapolation of concentration to ambient levels.

Figure 6.3.3.1. A log of the wet-weight bulk density derived from a Catscan analysis of a syringe core collected at site B/C. Three layers are evident: (1) a surface layer of relatively low density (3 mm thick); (2) a transitional layer of rapidly increasing density (5 mm thick); and (3) the denser substrate.

Figure 6.4.1.1. A time-series plot of results from Sea Carousel recorded at site C (LISPUK5) on 11 April, 1995. (A) lid speed and azimuthal and vertical currents at the reference height (0.18 m); (B) suspended sediment concentrations from the three OBS sensors (OBS1 and OBS3 are internal, OBS2 is external), and from pumped samples; and (C) erosion rate. The erosion is Type I in form in the early stages.

Figure 6.4.1.2. A time-series plot of results from Sea Carousel recorded at site C (LISPUK6) on 11 April, 1995. (A) lid speed and azimuthal and vertical currents at the reference height (0.18 m); (B) suspended sediment concentrations from the three OBS sensors (OBS1 and OBS3 are internal, OBS2 is external), and from one pumped sample; and (C) erosion rate. The station was abandoned prematurely due to boat drift.

Figure 6.4.1.3. Estimates of the erosion threshold for deployment LISPUK5, site C. The upper panel shows that erosion rate is a power function of applied bed stress; the estimated erosion threshold is 0.15 Pa. The lower panel shows that suspended sediment concentration increases as a power function of applied bed shear stress; the threshold is equated with the stress at ambient concentration and yields a value of 0.15 Pa.

Figure 6.4.2.1. Estimates of the erosion threshold for deployment LISPUK7, site C/D. The upper panel shows that erosion rate is a power function of applied bed stress; the estimated erosion threshold is 0.03 Pa. The lower panel shows that suspended sediment concentration increases as a power function of applied bed shear stress; the threshold is equated with the stress at ambient concentration and yields a value of 0.26 Pa.

Figure 6.4.2.2. A plot of measured suspended sediment concentration (from pumped samples) versus applied bed shear stress in Lab Carousel for experiment Labexp7 (site C) . Notice the onset of erosion at 0.45 Pa which is based on the extrapolation of concentration to ambient levels.

Figure 6.4.3.1. A log of the wet-weight bulk density derived from a Catscan analysis of a syringe core collected at site C. Two layers are evident: (1) a surface layer of rapidly increasing density (8 mm thick); and (2) the denser substrate.

Figure 6.5.1.1. A time-series plot of results from Sea Carousel recorded at site C/D (LISPUK7) on 10 April, 1995. (A) lid speed and azimuthal and vertical currents at the reference height (0.18 m); (B) suspended sediment concentrations from the three OBS sensors (OBS1 and OBS3 are internal, OBS2 is external), and from pumped samples; and (C) erosion rate.

Figure 6.5.1.2. A time-series plot of results from Sea Carousel recorded at site C/D (LISPUK8) on 12 April, 1995. (A) lid speed and azimuthal and vertical currents at the reference height (0.18 m); (B) suspended sediment concentrations from the three OBS sensors (OBS1 and OBS3 are internal, OBS2 is external), and from pumped samples; and (C) erosion rate.

Figure 6.5.1.3. Estimates of the erosion threshold for deployment LISPUK7, site C/D. The upper panel shows that erosion rate is a power function of applied bed stress; the estimated erosion threshold is 0.03 Pa. The lower panel shows that suspended sediment concentration increases as a power function of applied bed shear stress; the threshold is equated with the stress at ambient concentration and yields a value of 0.26 Pa.

Figure 6.5.1.4. Estimates of the erosion threshold for deployment LISPUK8, site C/D. The upper panel shows that erosion rate is a power function of applied bed stress; the estimated erosion threshold is 0.32 Pa. The lower panel shows that suspended sediment concentration increases as a power function of applied bed shear stress; the threshold is equated with the stress at ambient concentration and yields a value of 0.35 Pa.

Figure 6.5.2.1. A log of the wet-weight bulk density derived from a Catscan analysis of a syringe core collected at site C/D. Five layers are evident reflecting layering of the substrate.

Figure 6.6.1.1. A time-series plot of results from Sea Carousel recorded at site D (LISPUK1) on 8 April, 1995. (A) lid speed and azimuthal and vertical currents at the reference height (0.18 m); (B) suspended sediment concentrations from the three OBS sensors (OBS1 and OBS3 are internal, OBS2 is external), and from pumped samples; and (C) erosion rate. This station was on the side of a creek at a high angle, hence the scatter in the results.

Figure 6.6.1.2. A time-series plot of results from Sea Carousel recorded at site D (LISPUK2) on 8 April, 1995. (A) lid speed and azimuthal and vertical currents at the reference height (0.18 m); (B) suspended sediment concentrations from the three OBS sensors (OBS1 and OBS3 are internal, OBS2 is external); and (C) erosion rate. Notice the Type I erosion rates.

Figure 6.6.1.3. A time-series plot of results from Sea Carousel recorded at site D (LISPUK3) on 10 April, 1995. (A) lid speed and azimuthal and vertical currents at the reference height (0.18 m); (B) suspended sediment concentrations from the three OBS sensors (OBS1 and OBS3 are internal, OBS2 is external), and from pumped samples; and (C) erosion rate. Type I erosion is prevalent throughout the erosion phase.

Figure 6.6.1.4. A time-series plot of results from Sea Carousel recorded at site D (LISPUK3) on 10 April, 1995. (A) lid speed and azimuthal and vertical currents at the reference height (0.18 m); (B) suspended sediment concentrations from the three OBS sensors (OBS1 and OBS3 are internal, OBS2 is external), and from pumped samples; and (C) erosion rate. Type I erosion is prevalent throughout the erosion phase.

Figure 6.6.1.5. Estimates of the erosion threshold for deployment LISPUK2, site D. The upper panel shows that erosion rate is a power function of applied bed stress; the estimated erosion threshold is 0.07 Pa. The lower panel shows that suspended sediment concentration increases as

a power function of applied bed shear stress; the threshold is equated with the stress at ambient concentration and yields a value of 0.20 Pa.

Figure 6.6.1.6. Estimates of the erosion threshold for deployment LISPUK2, site D. The upper panel shows that erosion rate is a power function of applied bed stress; it is not possible to estimate erosion threshold from this plot. The lower panel shows that suspended sediment concentration increases as a power function of applied bed shear stress; the threshold is equated with the stress at ambient concentration and yields a value of 0.34 Pa.

Figure 6.6.1.7. Estimates of the erosion threshold for deployment LISPUK4, site D. The upper panel shows that erosion rate is a power function of applied bed stress; the estimated erosion threshold is 0.11 Pa. The lower panel shows that suspended sediment concentration increases as a power function of applied bed shear stress; the threshold is equated with the stress at ambient concentration and yields a value of 0.23 Pa.

Figure 6.6.2.1. A time-series of Laboratory Carousel experiment (Labexp6) on a site D bulk sample. (A) the azimuthal reference current for a height of 0.18 m above the bed (based on lid rotation); (B) suspended sediment concentration from three OBS's and pumped samples at heights of 0.03, 0.10, and 0.20 m above the base; and (C) erosion rate.

Figure 6.6.2.2. A plot of measured suspended sediment concentration (from pumped samples) versus applied bed shear stress in Lab Carousel for experiment Labexp6 (site D). Notice the onset of erosion at 0.38 Pa which is based on the extrapolation of concentration to ambient levels.

Figure 6.6.3.1. A log of the wet-weight bulk density derived from a Catscan analysis of a syringe core collected at site C/D. Five layers are evident reflecting layering of the substrate. Notice the general reduction in density with depth.

Figure 7.1.1. A summary plot showing erosion threshold from Sea Carousel and surface wet-weight bulk density against distance across the mudflat transect. Notice the three maxima: the largest on the central mudflat (site B/C); the second on the inner mudflat (site A); and the third on the outer mudflat (site D).

Figure 7.1.2. A scattergram of wet-weight bulk density and erosion threshold from Sea Carousel for the six sites of this study. Notice that site B/C is anomalously stable, presumably due to biostabilization.

Figure 7.2.1. A comparison between erosion thresholds derived from the Sea Carousel and Lab Carousel for the six sites examined in this study. In general Lab Carousel yielded higher values than Sea Carousel. The exception is site B/C where biostabilization dominated the field signal.

Figure 7.2.2. The effect of consolidation time on erosion threshold of site A sediment deposited in Lab Carousel. The figures shows that a 20% reduction in threshold would result if the time of consolidation was reduced from 24 to 11 hours.

Figure 7.3.1. A regression analysis of mean erosion rate on current speed from data obtained from Sea Carousel. Results show that a single exponential function suffices for all sites.

Figure 7.3.2. A correlation between mean erosion rate and peak erosion rate derived from Sea Carousel. Results show that all sites show a similar relationship which can be expressed by a simple linear equation.

Figure 7.4.1. A regression analysis of mean erosion rate on current speed from data obtained from Lab Carousel. Results show that a single exponential function suffices for all sites. The equation is similar to that derived for Sea Carousel (see Figure 7.3.1) though more scatter prevails.

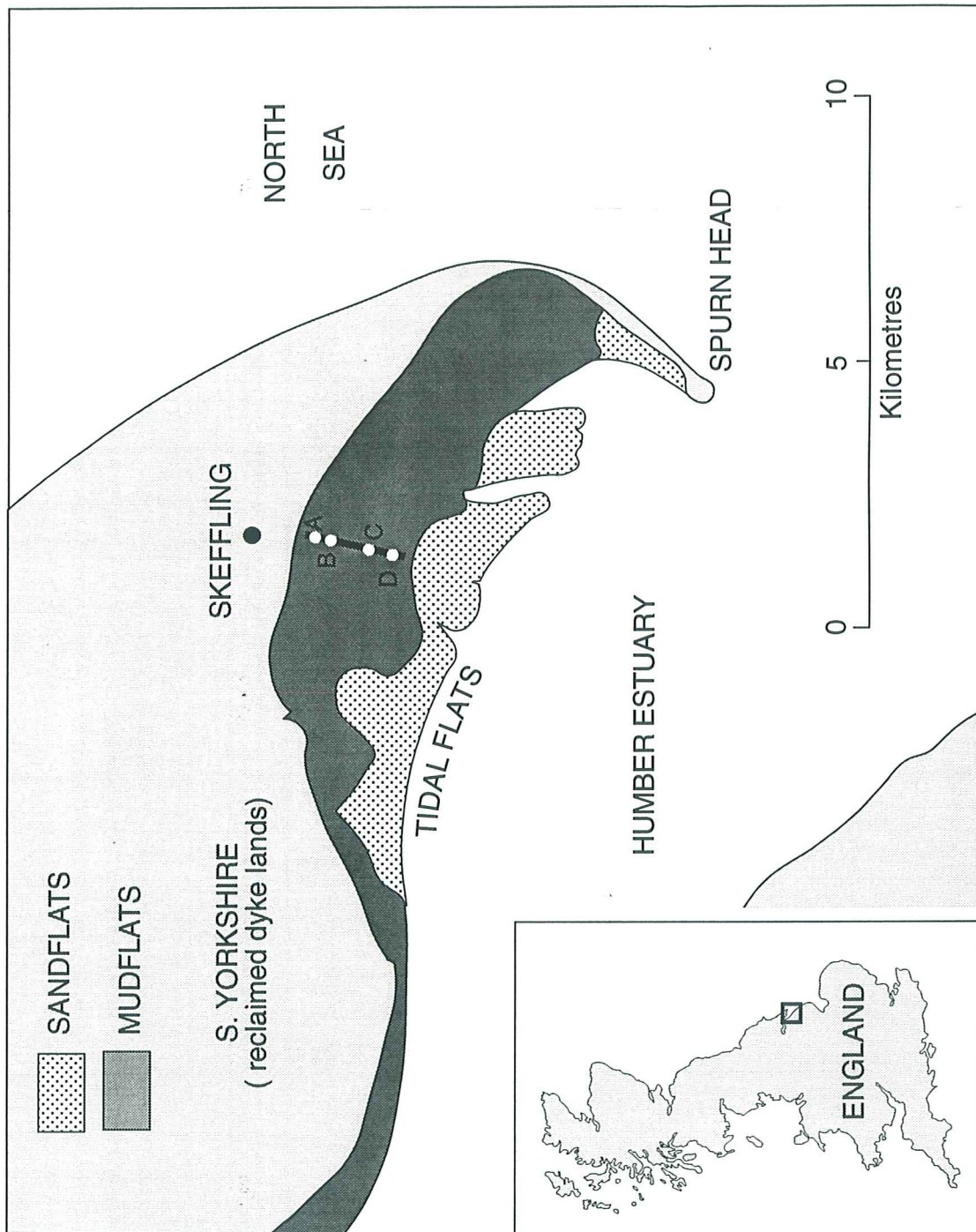


Figure 1.1. A location diagram of the study region, Humber estuary, S. Yorkshire, England. The intertidal transect was located across the mudflats off Skeffling on the northern flank of the estuary.

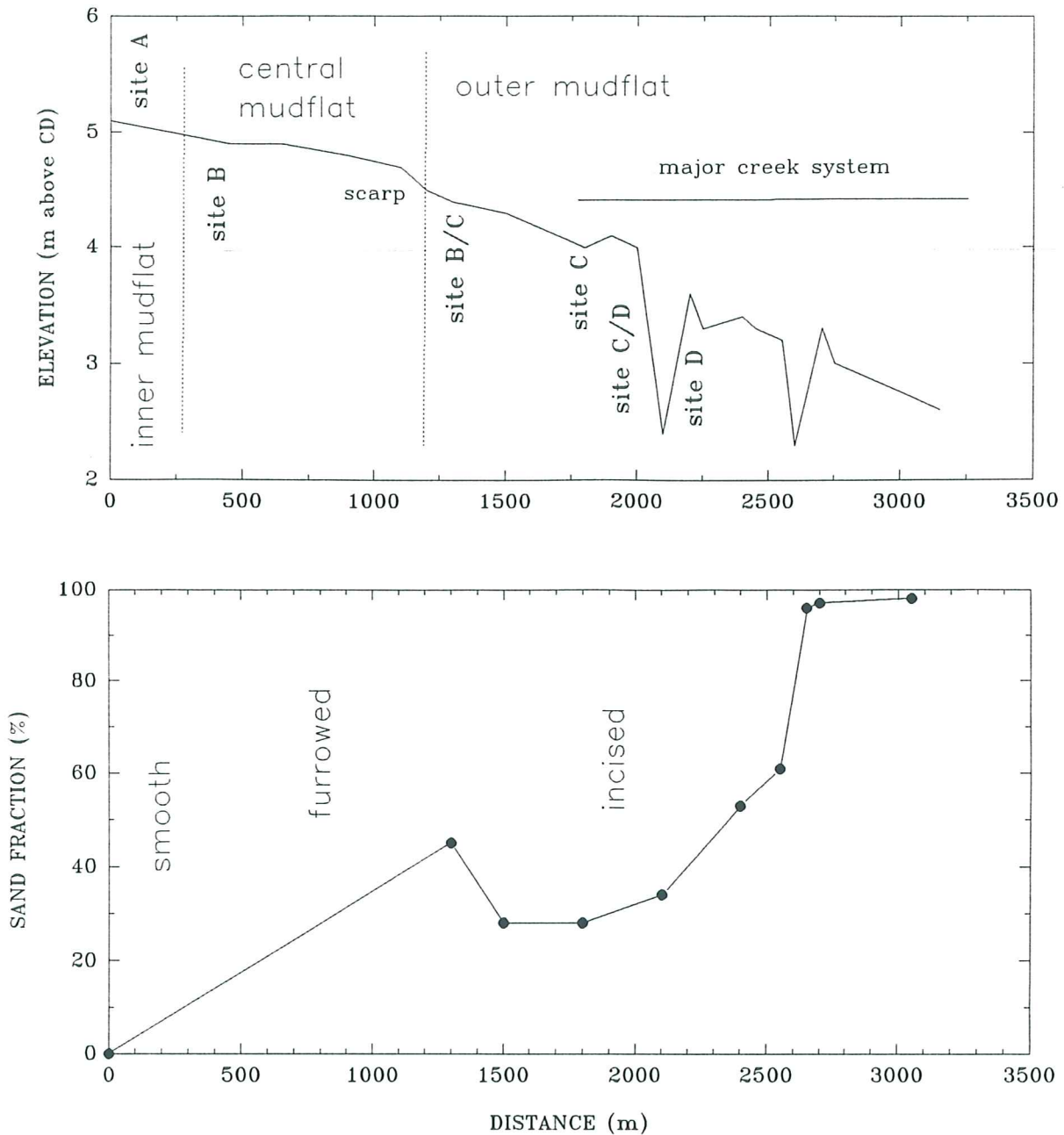


Figure 1.2. A transect of the Skeffling mudflat profile. The stations occupied in this study are marked to show distance from the shoreline and elevation relative to Chart Datum (CD). The sand content of seabed samples taken along the transect is also shown (after K. Black, unpublished data).

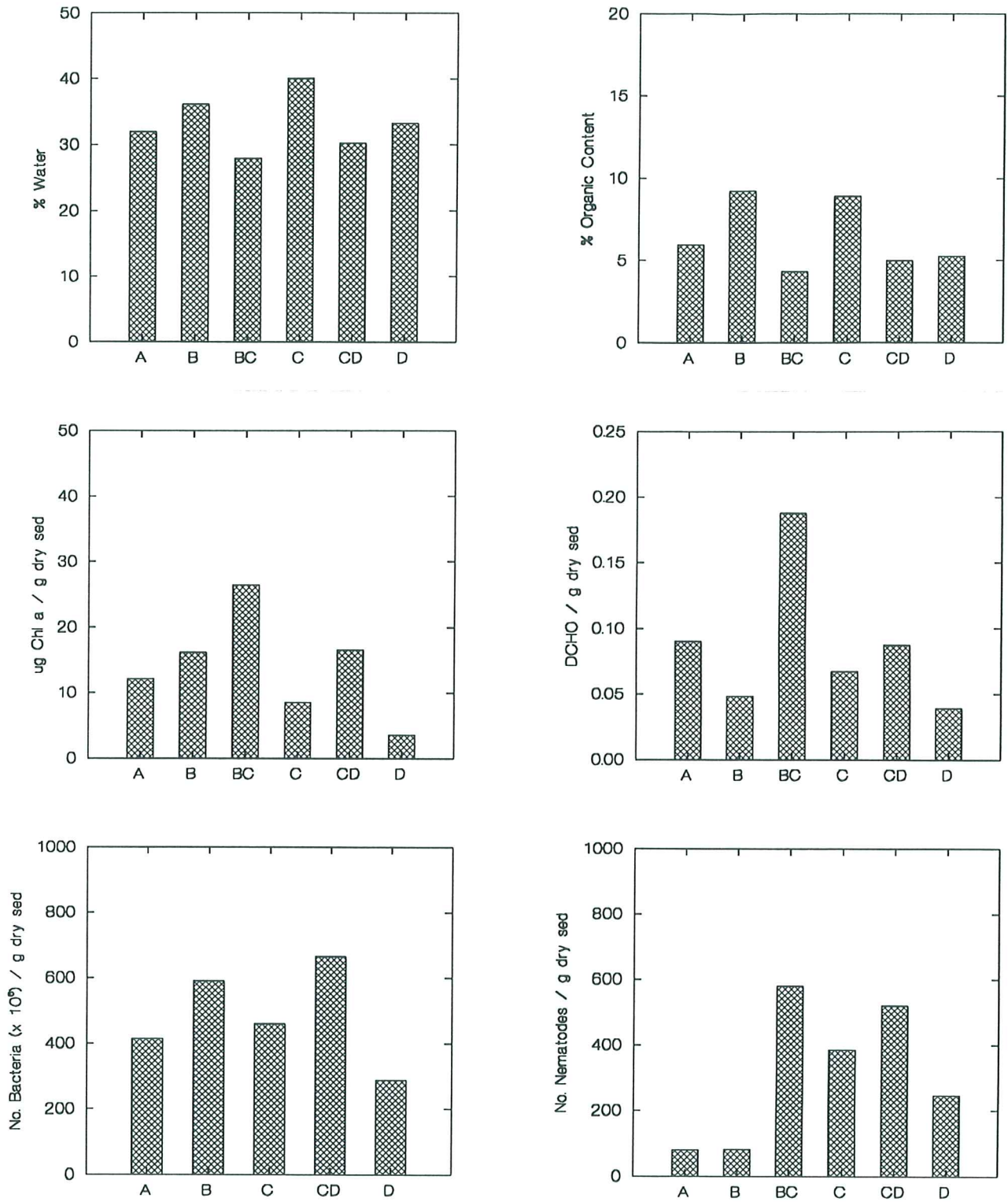


Figure 6.1. Summary plots of the biological parameters (water content, % organic content, chlorophyll α , dissolved carbohydrates (DCHO), bacteria numbers and nematode numbers) plotted versus site.

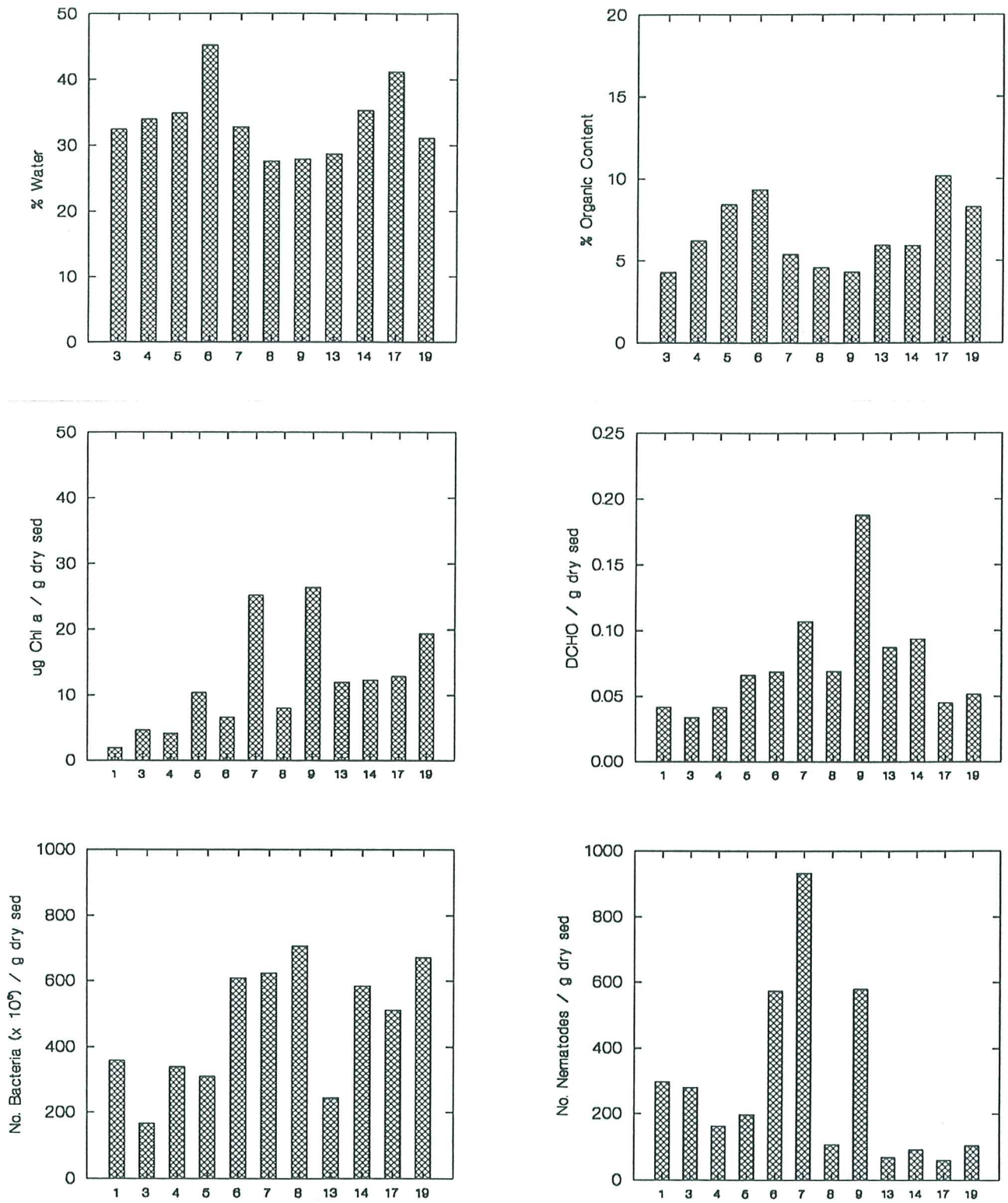


Figure 6.2. Summary plots of the biological parameters (listed in Figure 6.1) plotted versus station number.

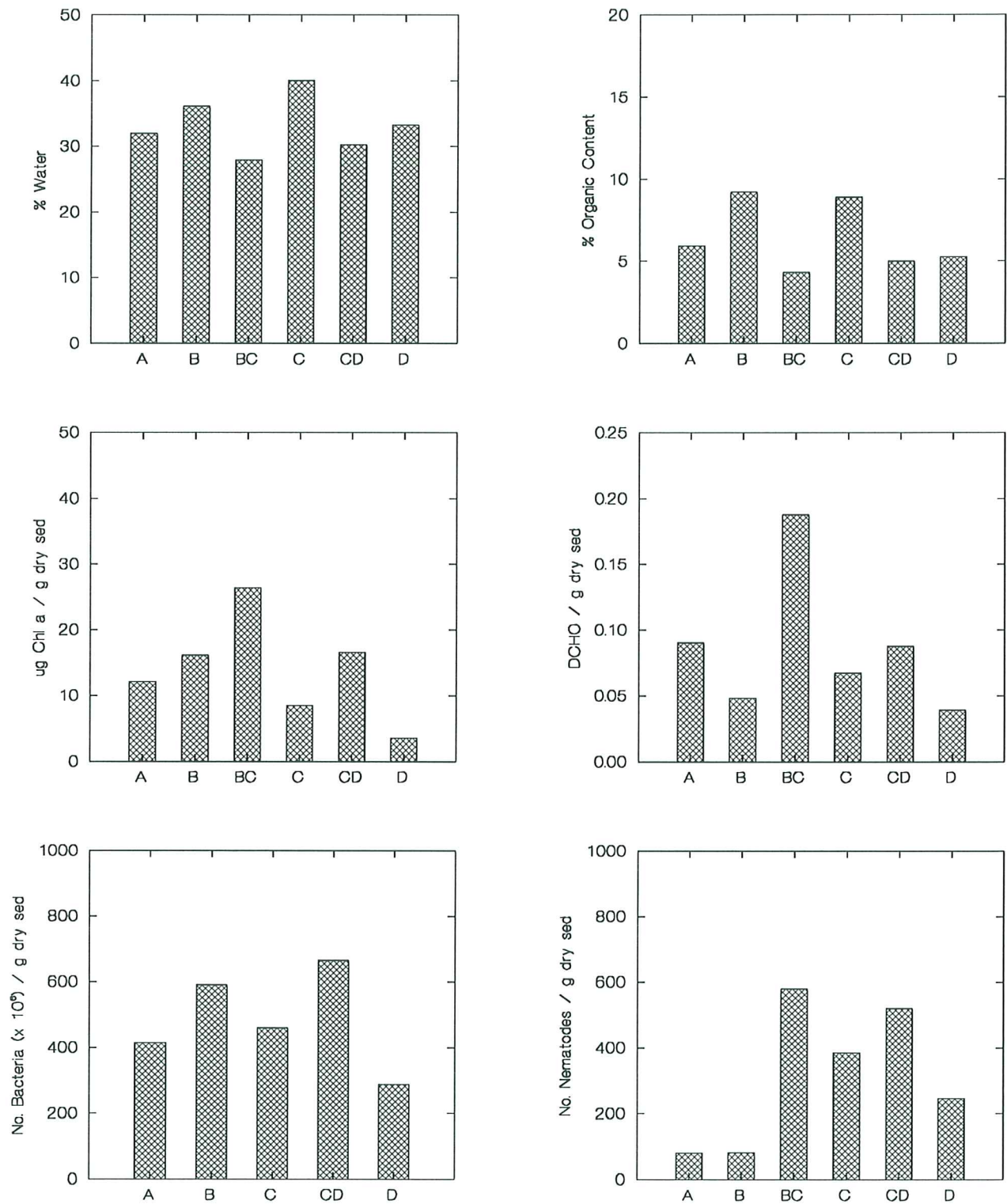


Figure 6.1. Summary plots of the biological parameters (water content, % organic content, chlorophyll *a*, dissolved carbohydrates (DCHO), bacteria numbers and nematode numbers) plotted versus site.

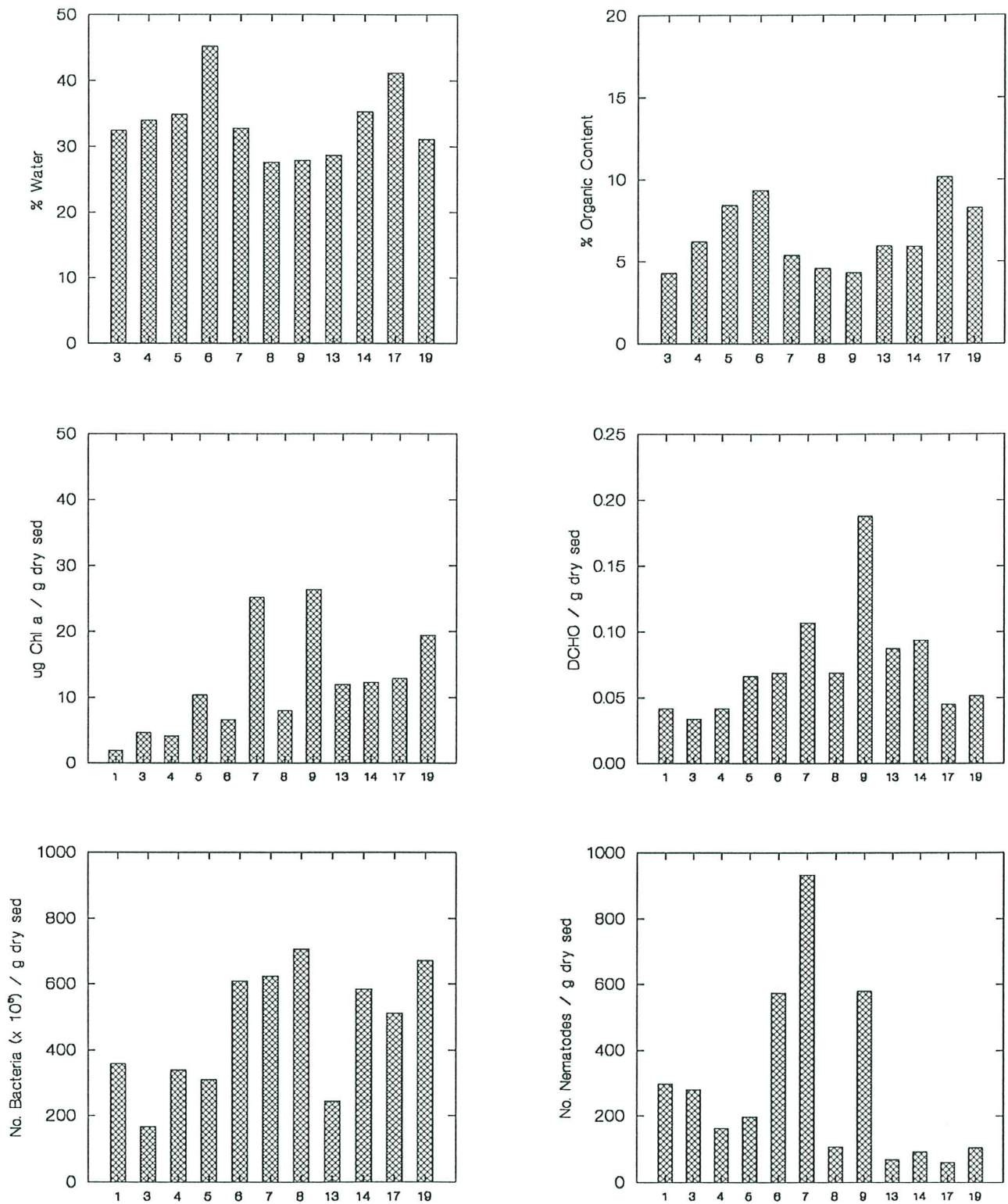


Figure 6.2. Summary plots of the biological parameters (listed in Figure 6.1) plotted versus station number.

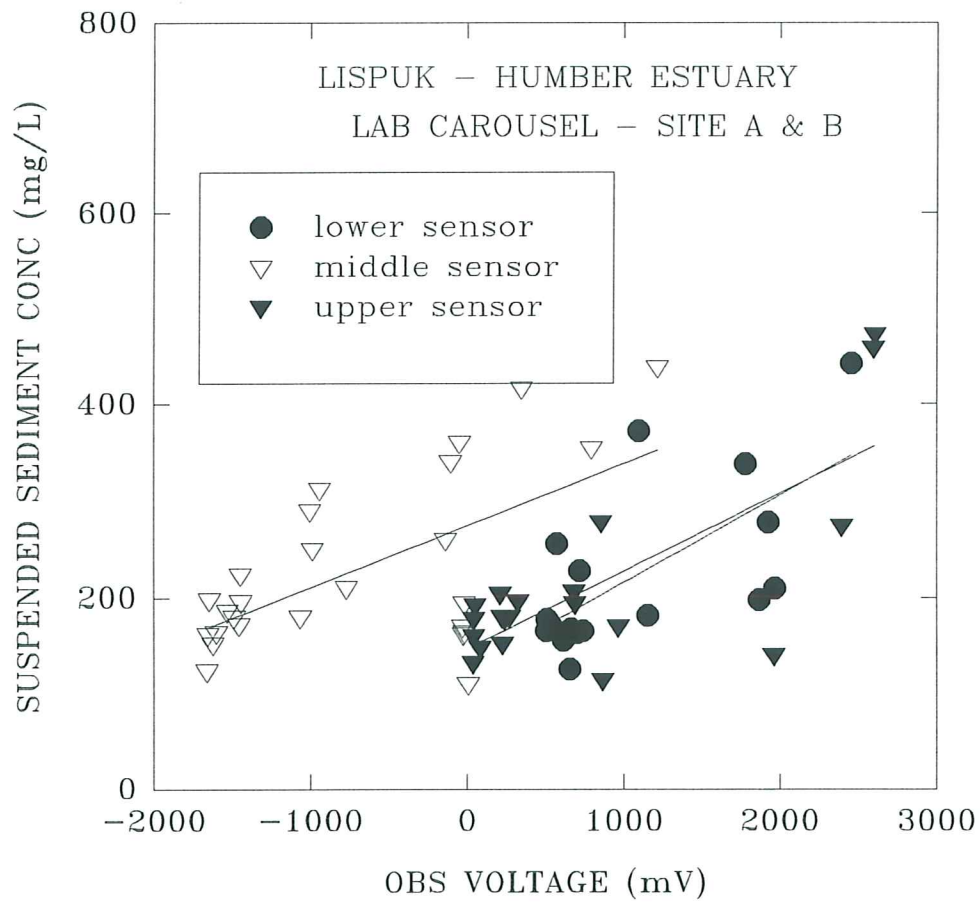


Figure 6.1.1.1. A calibration plot of OBS output voltage from Sea Carousel versus dry-weight suspended sediment concentration. The calibration is for site A and B samples combined.

SEA CAROUSEL – LISPUK13 (Humber estuary)

SITE A – 14 APRIL, 1995

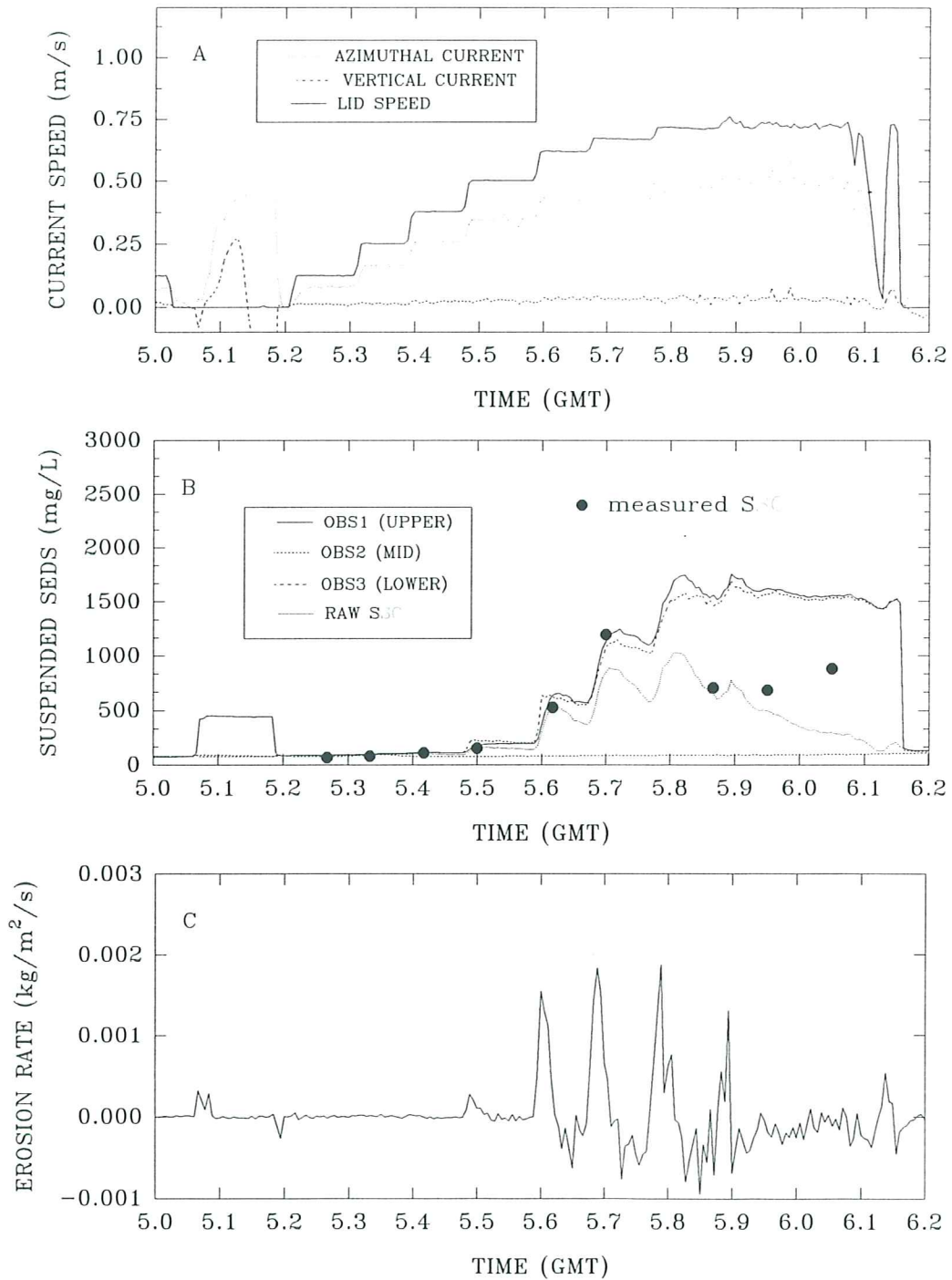


Figure 6.1.1.2. A time-series plot of results from Sea Carousel recorded at site A (LISPUK13) on 14 April, 1995. (A) lid speed and azimuthal and vertical currents at the reference height (0.18 m); (B) suspended sediment concentrations from the three OBS sensors (OBS1 and OBS3 are internal, OBS2 is external) and from pumped samples; and (C) erosion rate. Notice the prevalence of Type I erosion.

SEA CAROUSEL – LISPUK14 (Humber estuary)

SITE A – 14 APRIL, 1995

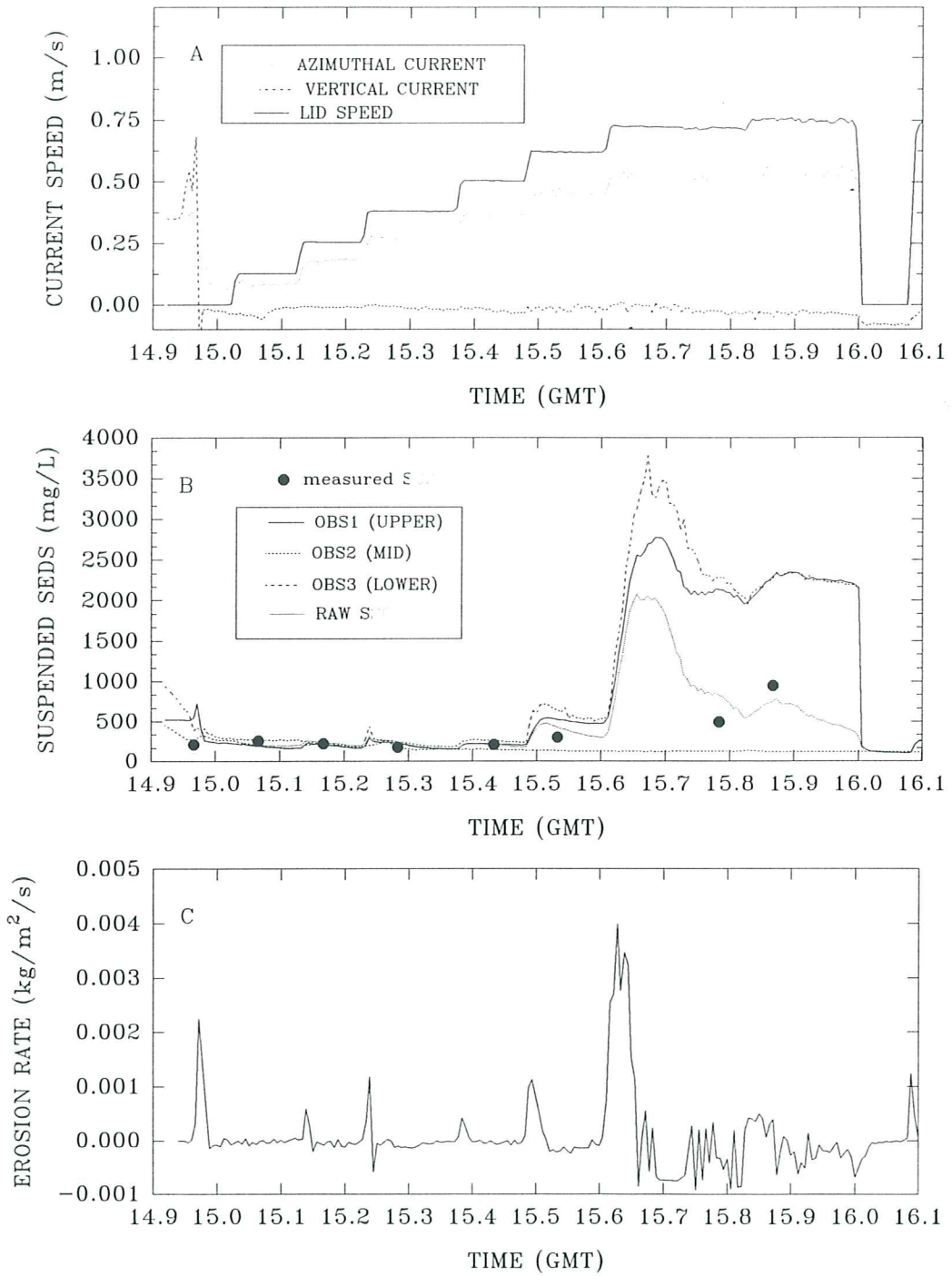


Figure 6.1.1.3. A time-series plot of results from Sea Carousel recorded at site A (LISPUK14) on 14 April, 1995. (A) lid speed and azimuthal and vertical currents at the reference height (0.18 m); and (B) suspended sediment concentrations from the three OBS sensors (OBS1 and OBS3 are internal, OBS2 is external) and from pumped samples; and (C) erosion rate.

SEA CAROUSEL – LISPUK15 (Humber estuary)

SITE A – 14 APRIL, 1995

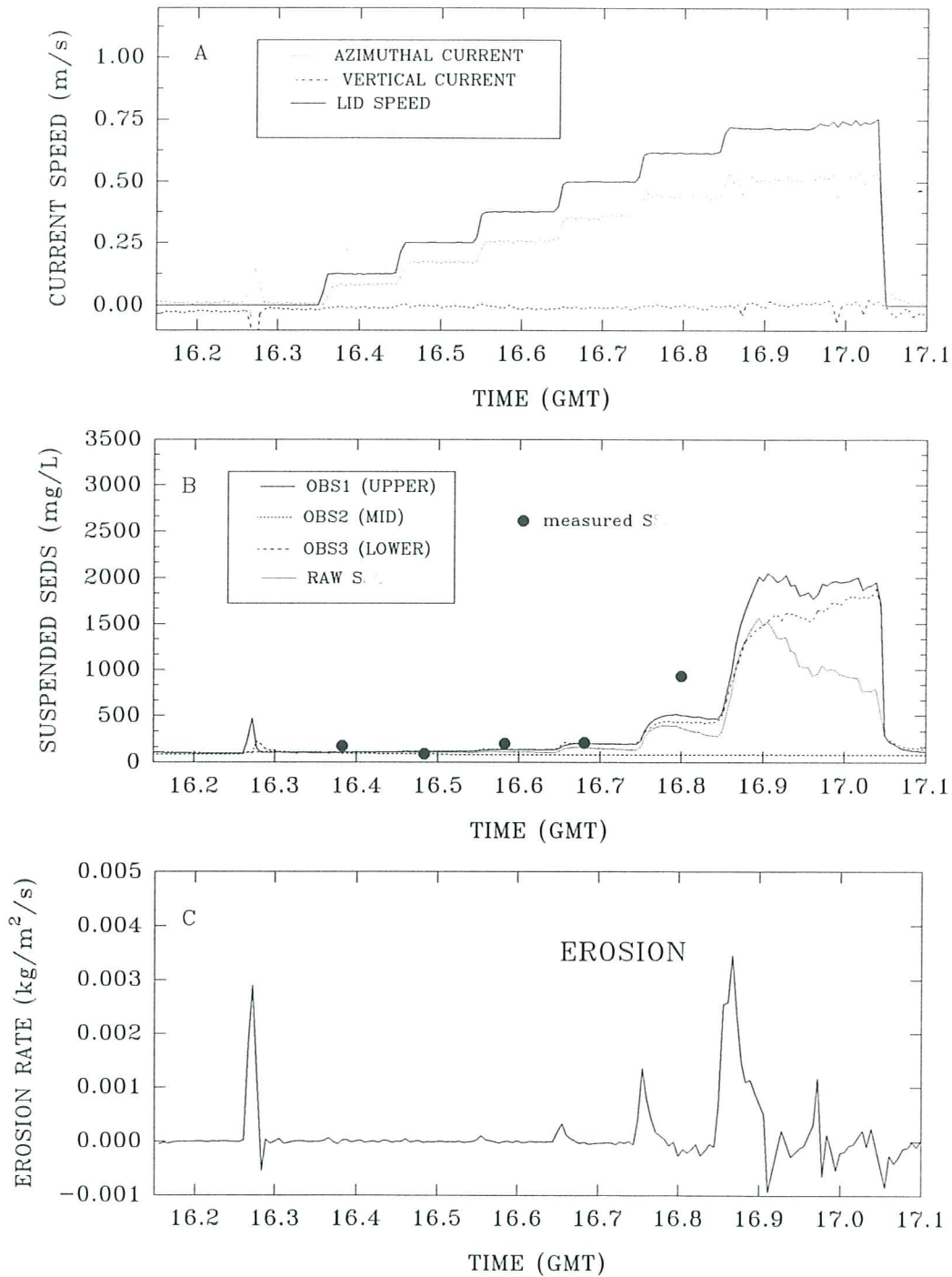


Figure 6.1.1.4. A time-series plot of results from Sea Carousel recorded at site A (LISPUK15) on 14 April, 1995. (A) lid speed and azimuthal and vertical currents at the reference height (0.18 m); and (B) suspended sediment concentrations from the three OBS sensors (OBS1 and OBS3 are internal, OBS2 is external) and from pumped samples; and (C) erosion rate.

STATION LISPUK13, SITE A - 14 APRIL, 1995

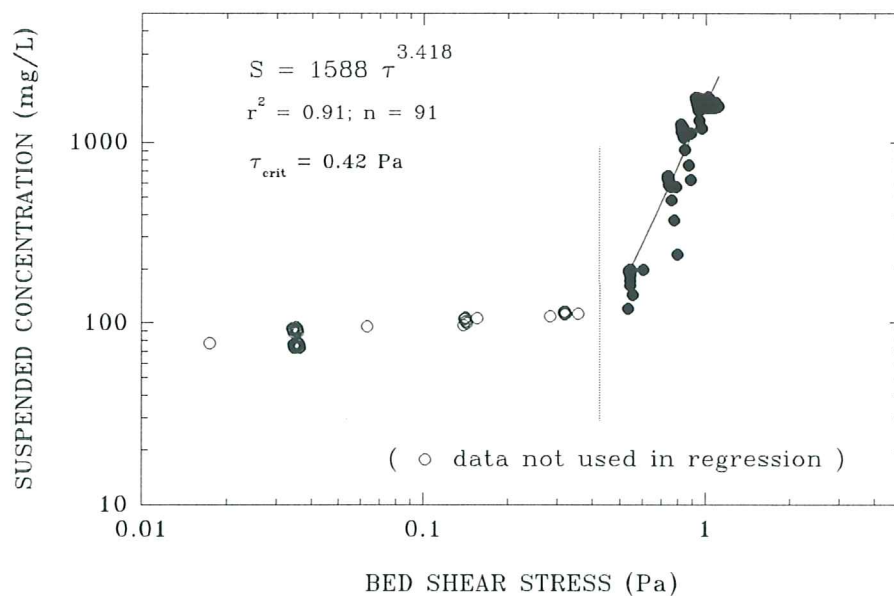
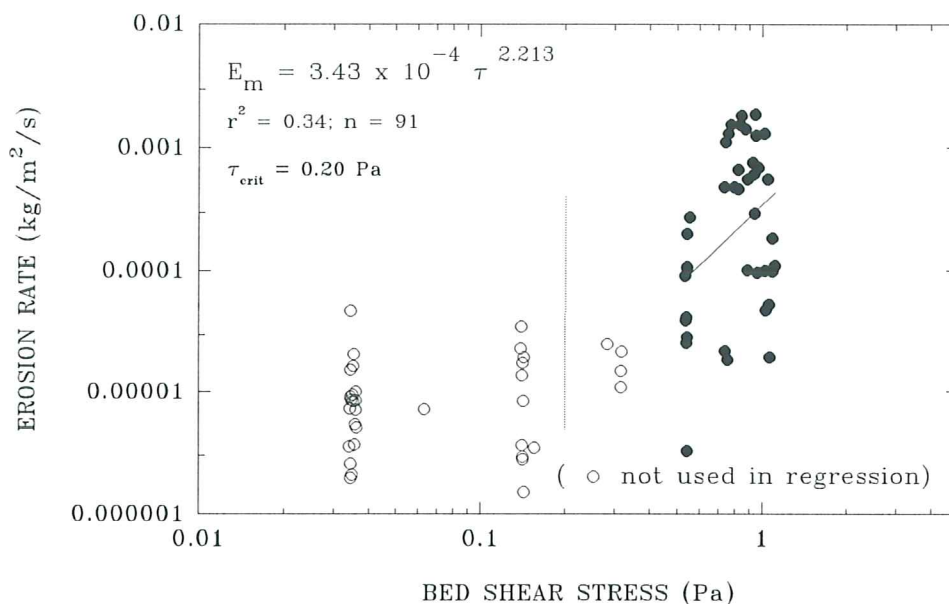


Figure 6.1.1.5. Estimates of the erosion threshold for deployment LISPUK13, site A. The upper panel shows erosion rate versus applied bed stress; the threshold ($\tau_c(0)$) is equated with the stress for a base erosion of $3 \times 10^{-5} \text{ kg}/\text{m}^2/\text{s}$ and yields a value of 0.20 Pa. The lower panel shows suspended sediment concentration versus applied bed shear stress; the threshold is equated with the stress at ambient concentration and yields a value of 0.42 Pa.

STATION LISPUK14, SITE A - 14 APRIL, 1995

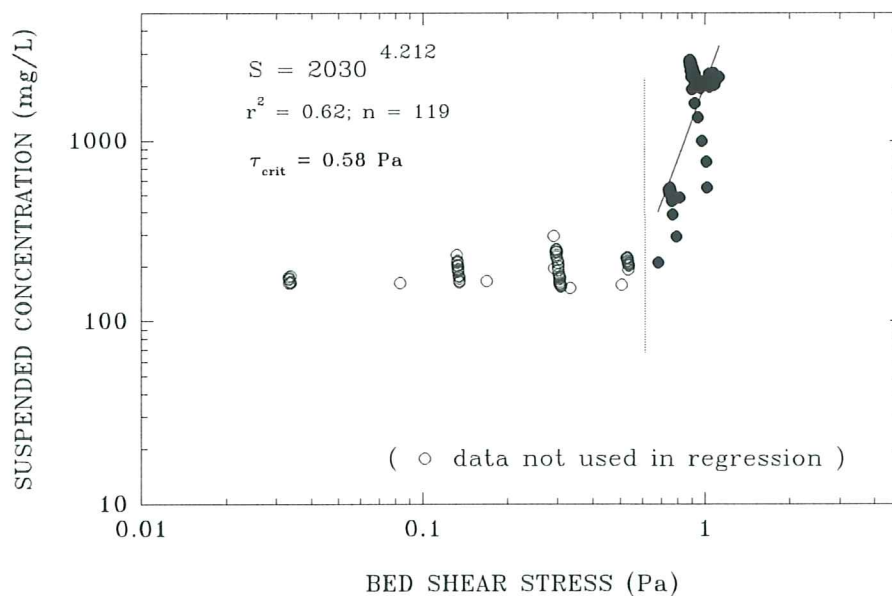
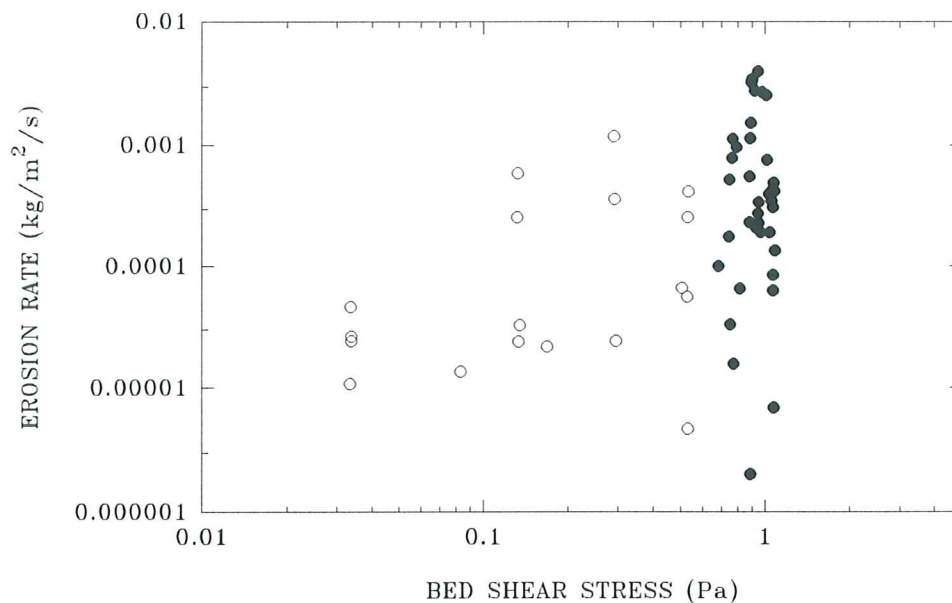


Figure 6.1.1.6. Estimates of the erosion threshold for deployment LISPUK14, site A. The upper panel shows erosion rate versus applied bed stress; it is not possible to derive the threshold from this plot. The lower panel shows that suspended sediment concentration increases as a power function of applied bed shear stress; the threshold is equated with the stress at ambient concentration and yields a value of 0.58 Pa.

STATION LISPUK15, SITE A - 14 APRIL, 1995

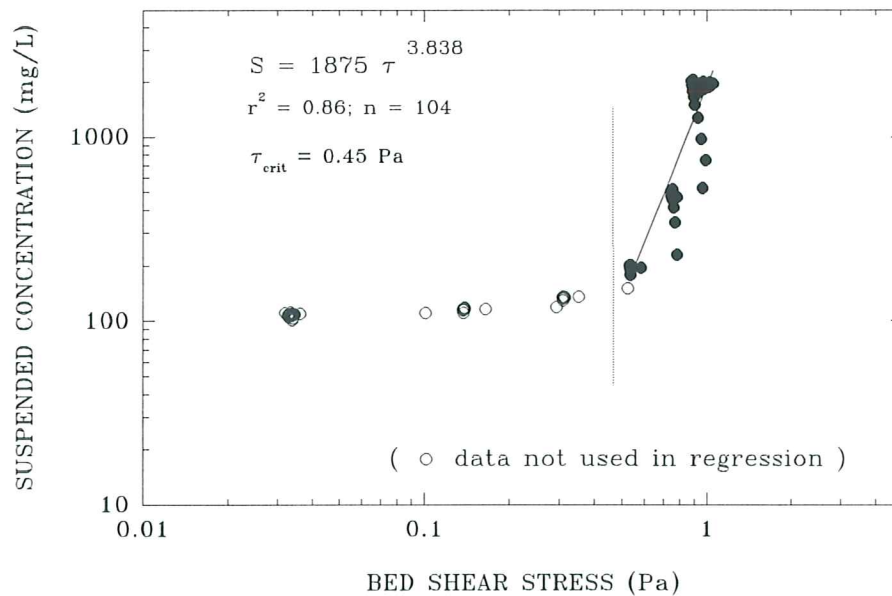
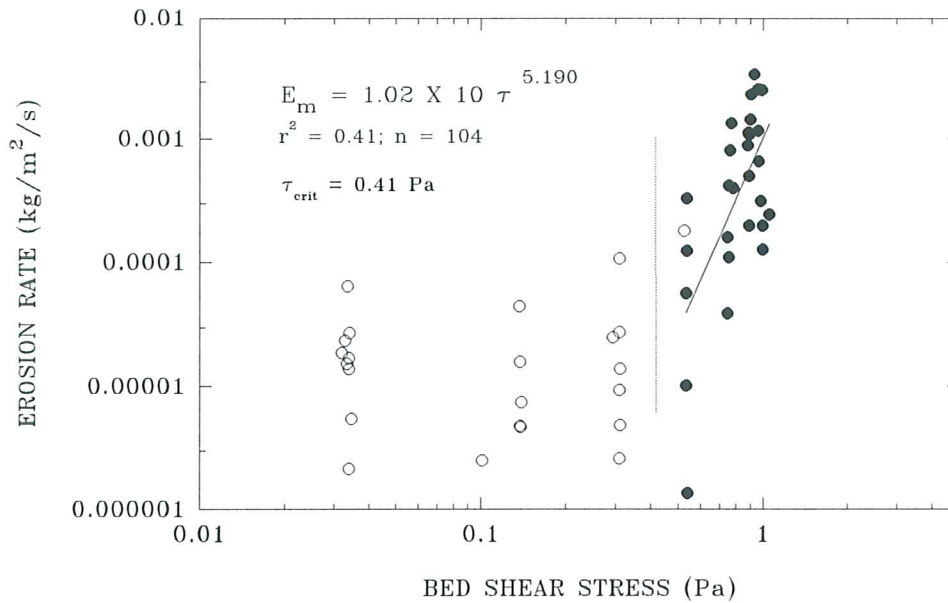


Figure 6.1.1.7. Estimates of the erosion threshold for deployment LISPUK15, site A. The upper panel shows that erosion rate is a power function of applied bed stress; the estimated erosion threshold is 0.41 Pa. The lower panel shows that suspended sediment concentration increases as a power function of applied bed shear stress; the threshold is equated with the stress at ambient concentration and yields a value of 0.45 Pa.

LAB CAROUSEL – LISPUK (Humber estuary)

SITE A (LABEXP2) – 7 APRIL, 1995

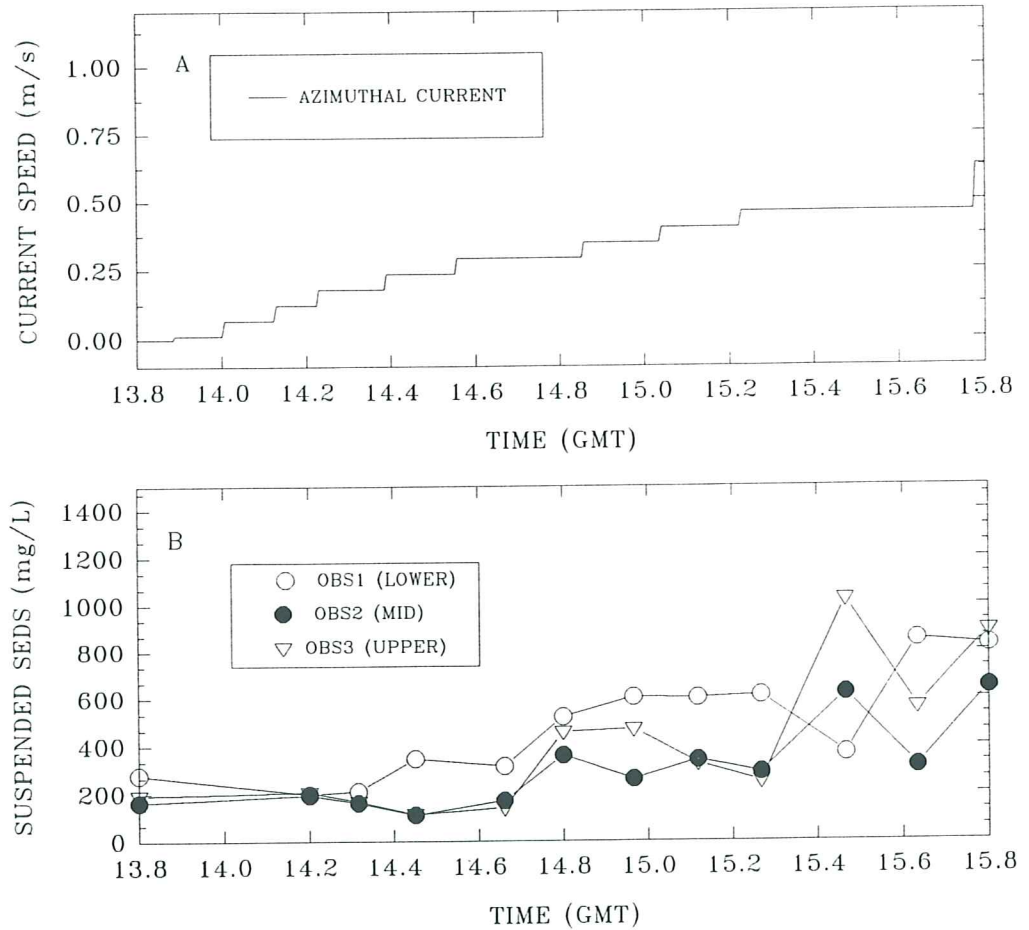


Figure 6.1.2.1. A time-series of Lab Carousel experiment (Labexp2) on a site A bulk sample. (A) the azimuthal reference current for a height of 0.18 m above the bed (based on lid rotation); and (B) measured dry-weight suspended sediment concentration from three sample ports at heights of 0.03, 0.10, and 0.20 m above the base.

LAB CAROUSEL – LISPUK (Humber estuary)

SITE A (LABEXP3) – 9 APRIL, 1995

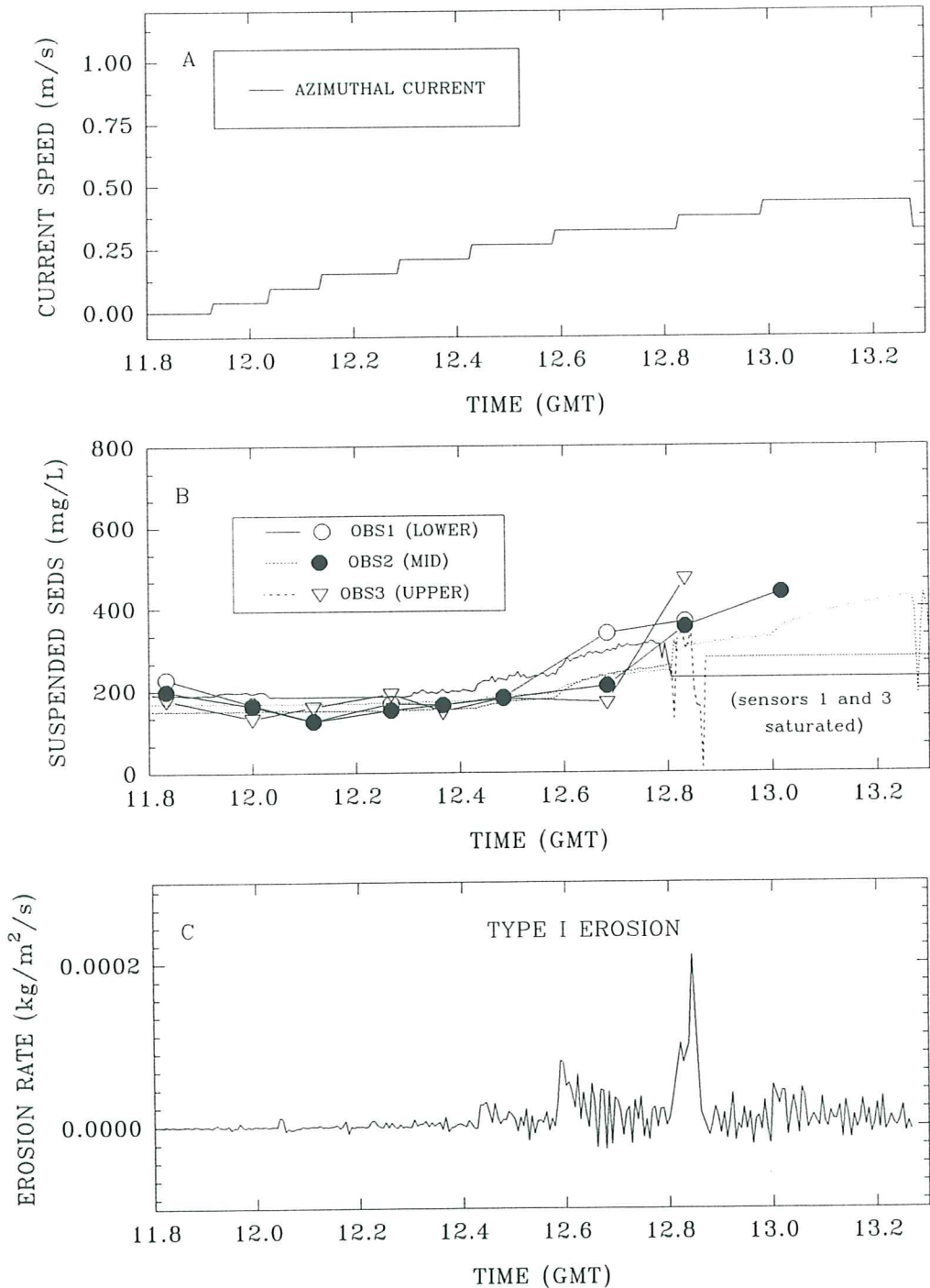


Figure 6.1.2.2. A time-series of Lab Carousel experiment (Labexp3) on a site A bulk sample. (A) the azimuthal reference current for a height of 0.18 m above the bed (based on lid rotation); (B) measured dry-weight suspended sediment concentration from three sample ports at heights of 0.03, 0.10, and 0.20 m above the base; and (C) erosion rate. Notice the prevalence of Type I erosion at early stages of erosion and sensor saturation during later stages.

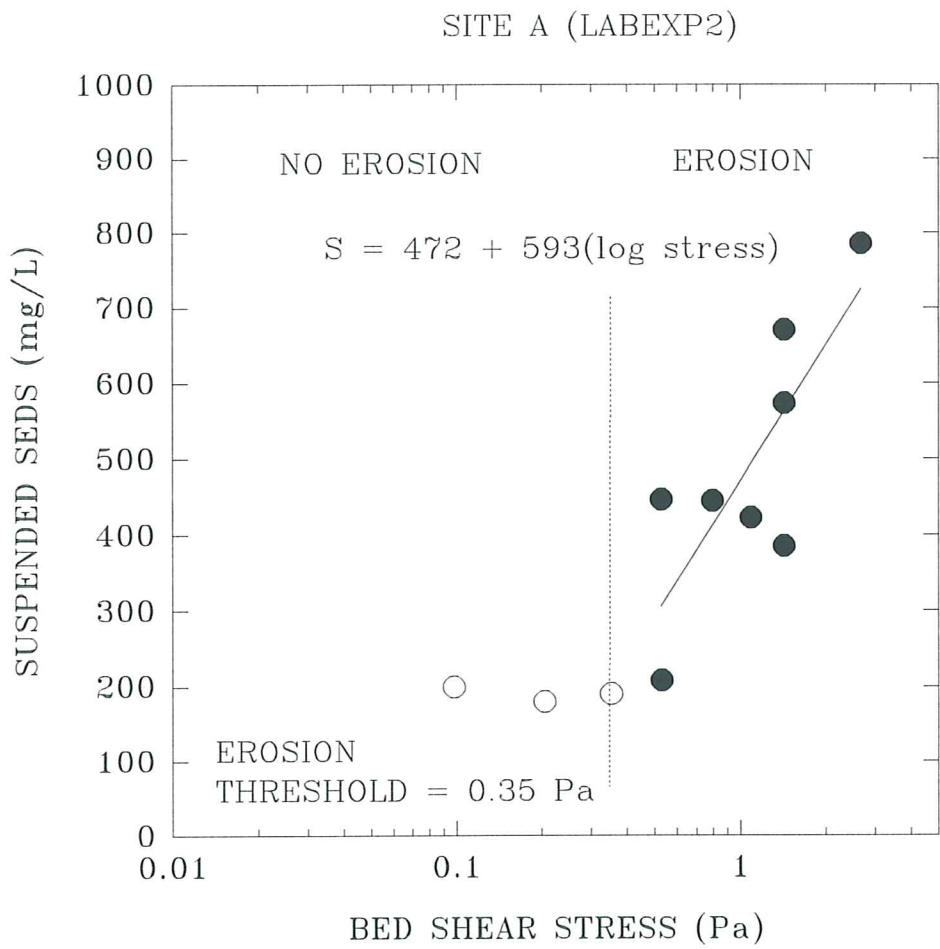


Figure 6.1.2.5. Suspended sediment concentration versus the log of applied bed shear stress for Labexp2, site A. The erosion threshold is evaluated at 0.35 Pa. Also shown is the functional relationship between sediment concentration (S) and bed shear stress.

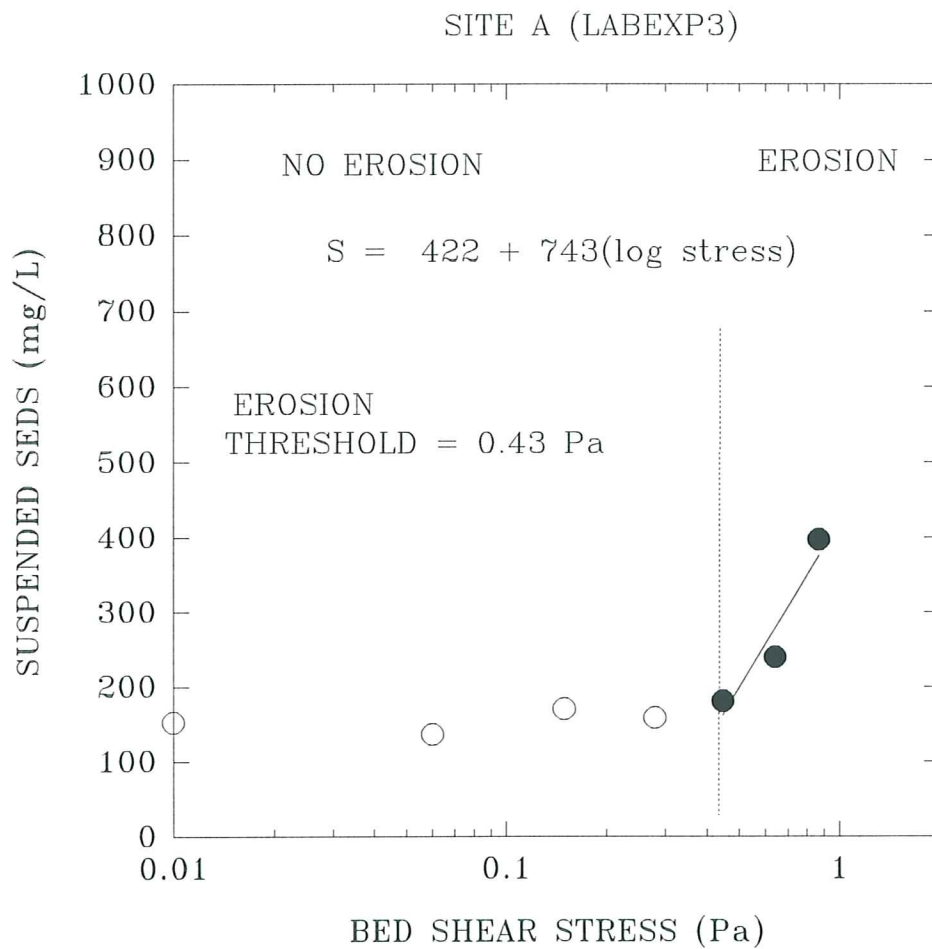


Figure 6.1.2.6. Suspended sediment concentration versus the log of applied bed shear stress for Labexp3, site A. The erosion threshold is evaluated at 0.43 Pa. Also shown is the functional relationship between S and τ_o (the applied bed shear stress).

LAB CAROUSEL – LISPUK (Humber estuary)

SITE A/B (LABEXP9) – 19 APRIL, 1995

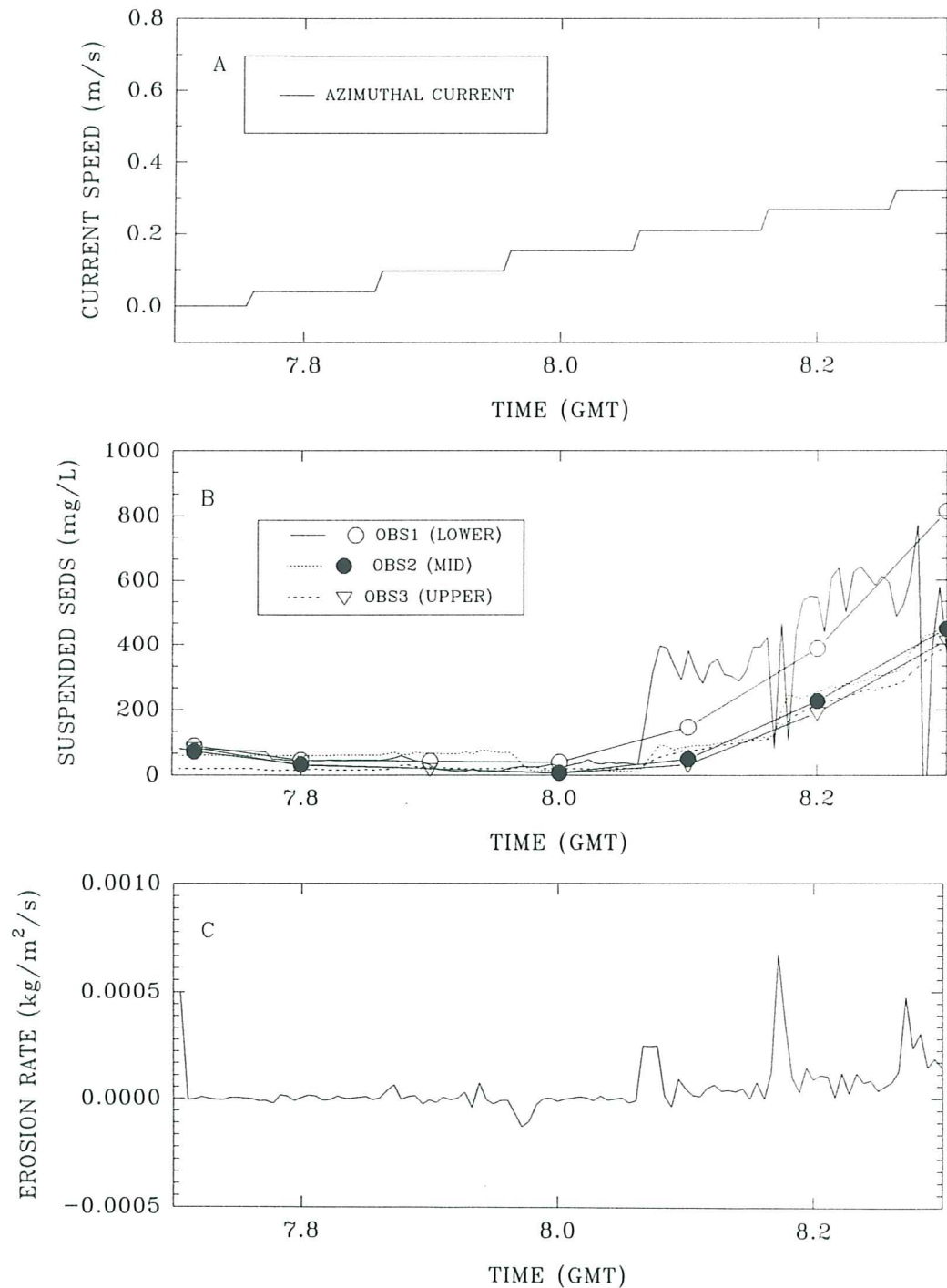


Figure 6.1.2.4. A time-series of Lab Carousel experiment (Labexp9) on a site A/B bulk sample. (A) the azimuthal reference current for a height of 0.18 m above the bed (based on lid rotation); (B) suspended sediment concentration from three OBS's and pumped samples at heights of 0.03, 0.10, and 0.20 m above the base; and (C) erosion rate.

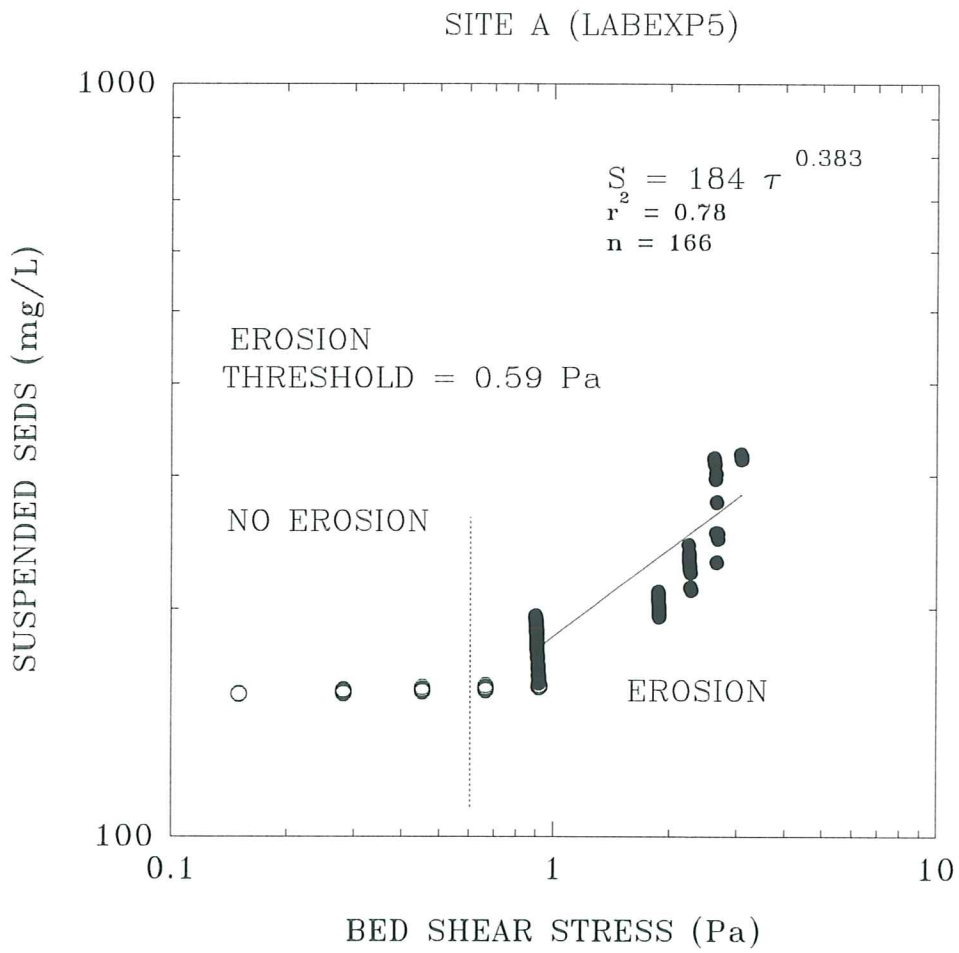


Figure 6.1.2.7. Log eroded mass (kg) versus the log of applied bed shear stress for Labexp5, site A. The erosion threshold is evaluated at 0.59 Pa.

LAB CAROUSEL – LISPUK (Humber estuary)

SITE A (LABEXP5) – 12 APRIL, 1995

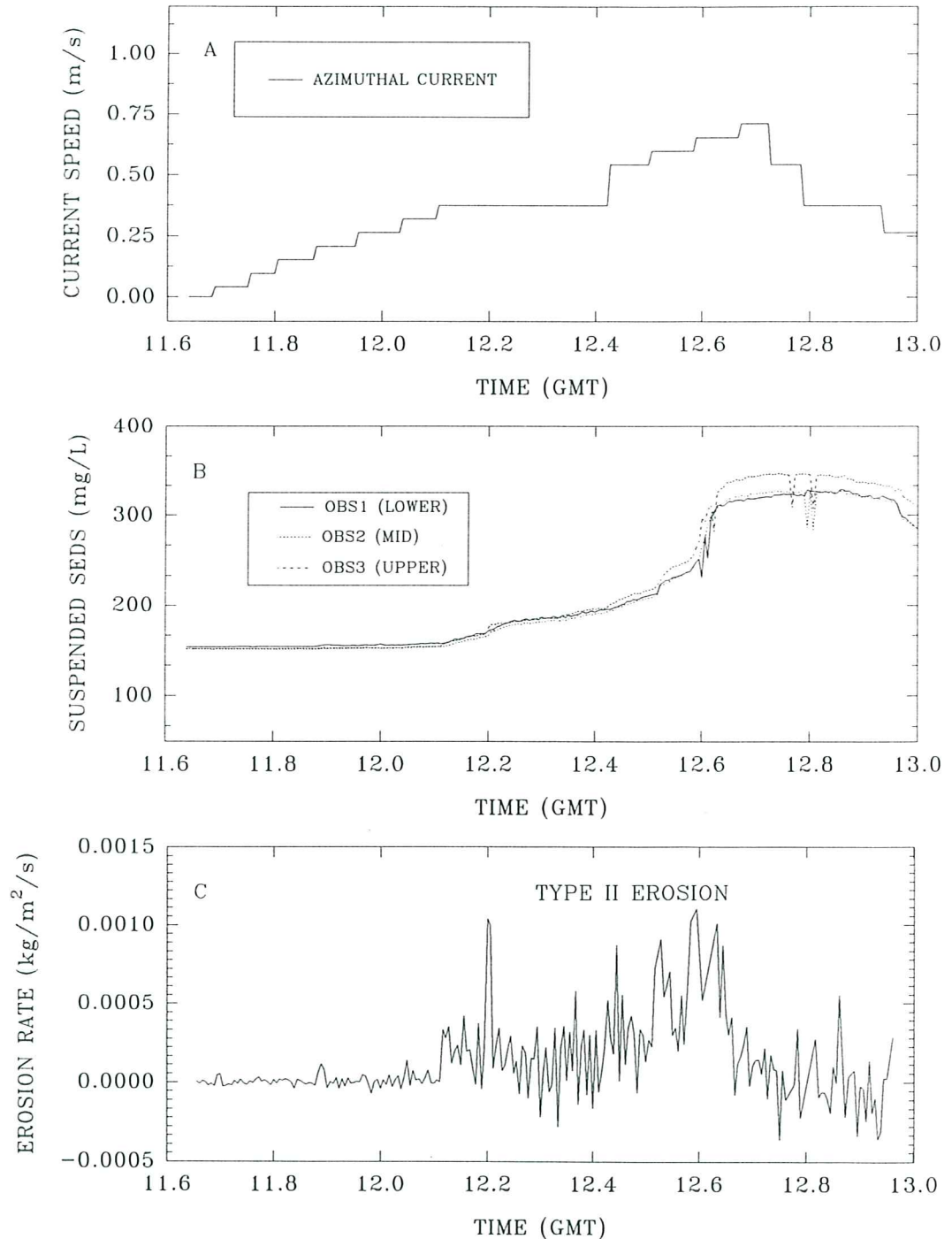


Figure 6.1.2.3. A time-series of Lab Carousel experiment (Labexp5) on a site A bulk sample. (A) the azimuthal reference current for a height of 0.18 m above the bed (based on lid rotation); (B) suspended sediment concentration from three OBS's at heights of 0.03, 0.10, and 0.20 m above the base; and (C) erosion rate. Notice the prevalence of Type II erosion.

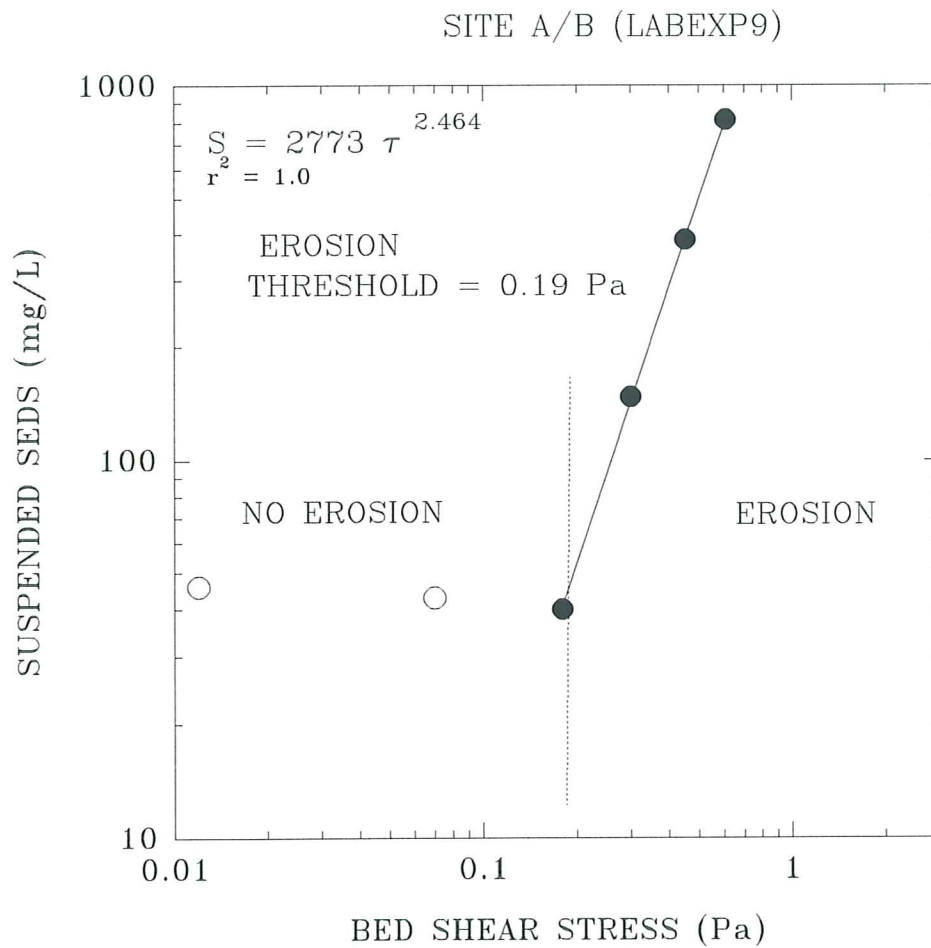


Figure 6.1.2.8. Log suspended sediment concentration versus the log of applied bed shear stress for Labexp9, site A/B. The erosion threshold is evaluated at 0.19 Pa. Also shown is the functional relationship between S and τ_o .

LISPUK LAB CAROUSEL SEDIMENT SETTLING

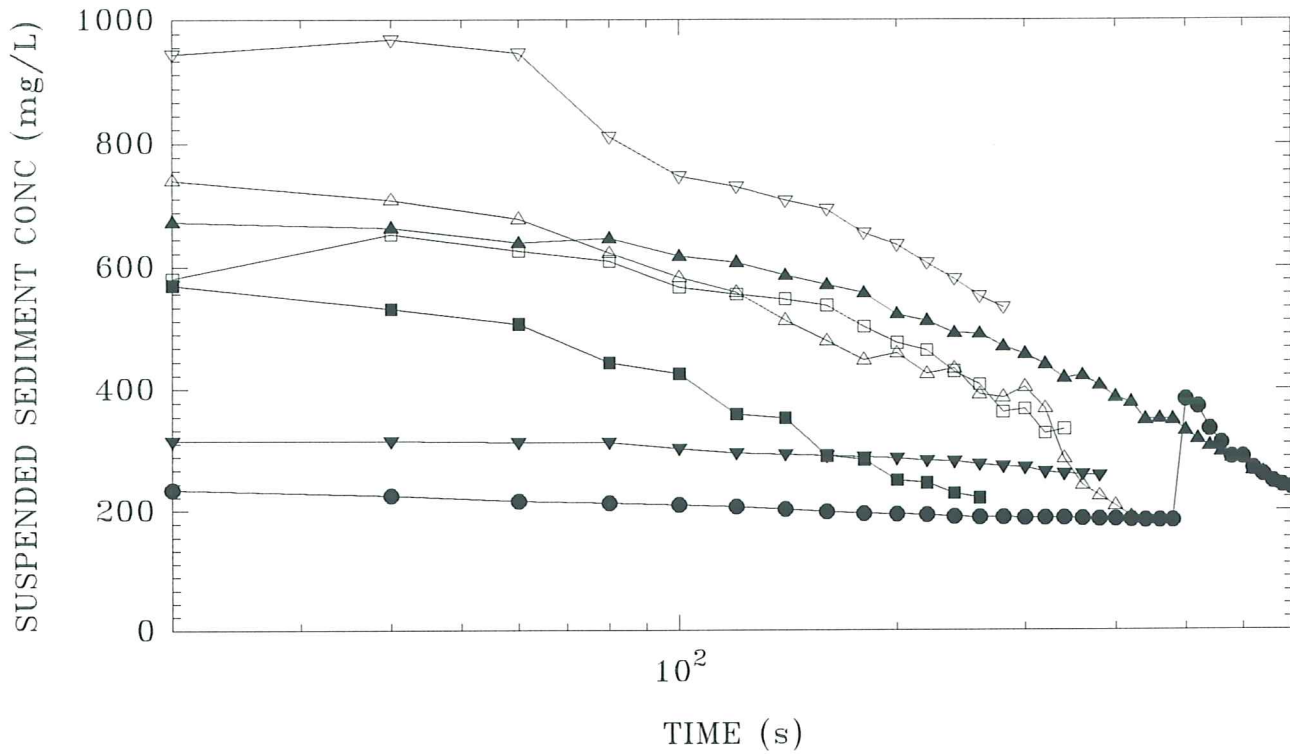
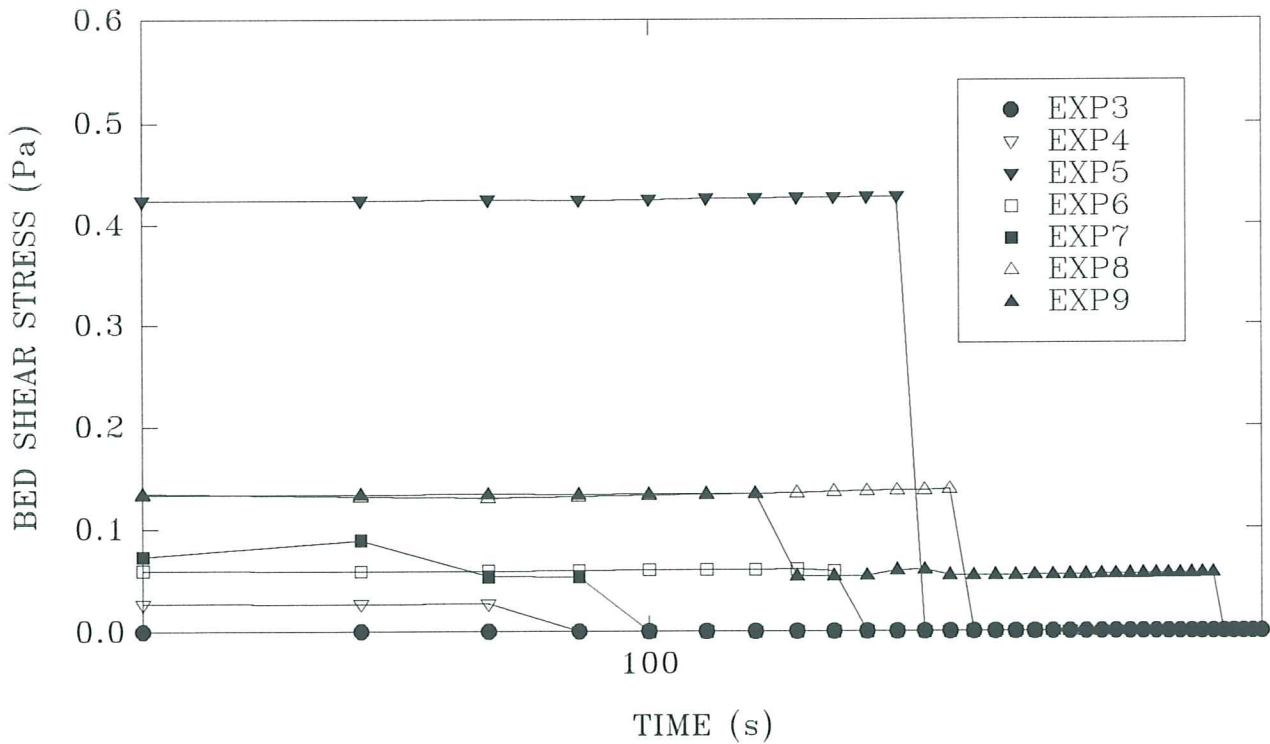


Figure 6.1.2.9. Time-series plots of suspended sediment concentration (A) and applied bed shear stress (B) during the settling phase of all Lab Carousel experiments carried out in this study. Mass settling rate (W_s) and depositional threshold (τ_d) have been determined from these data.



LISPUK - SITE A, Humber estuary

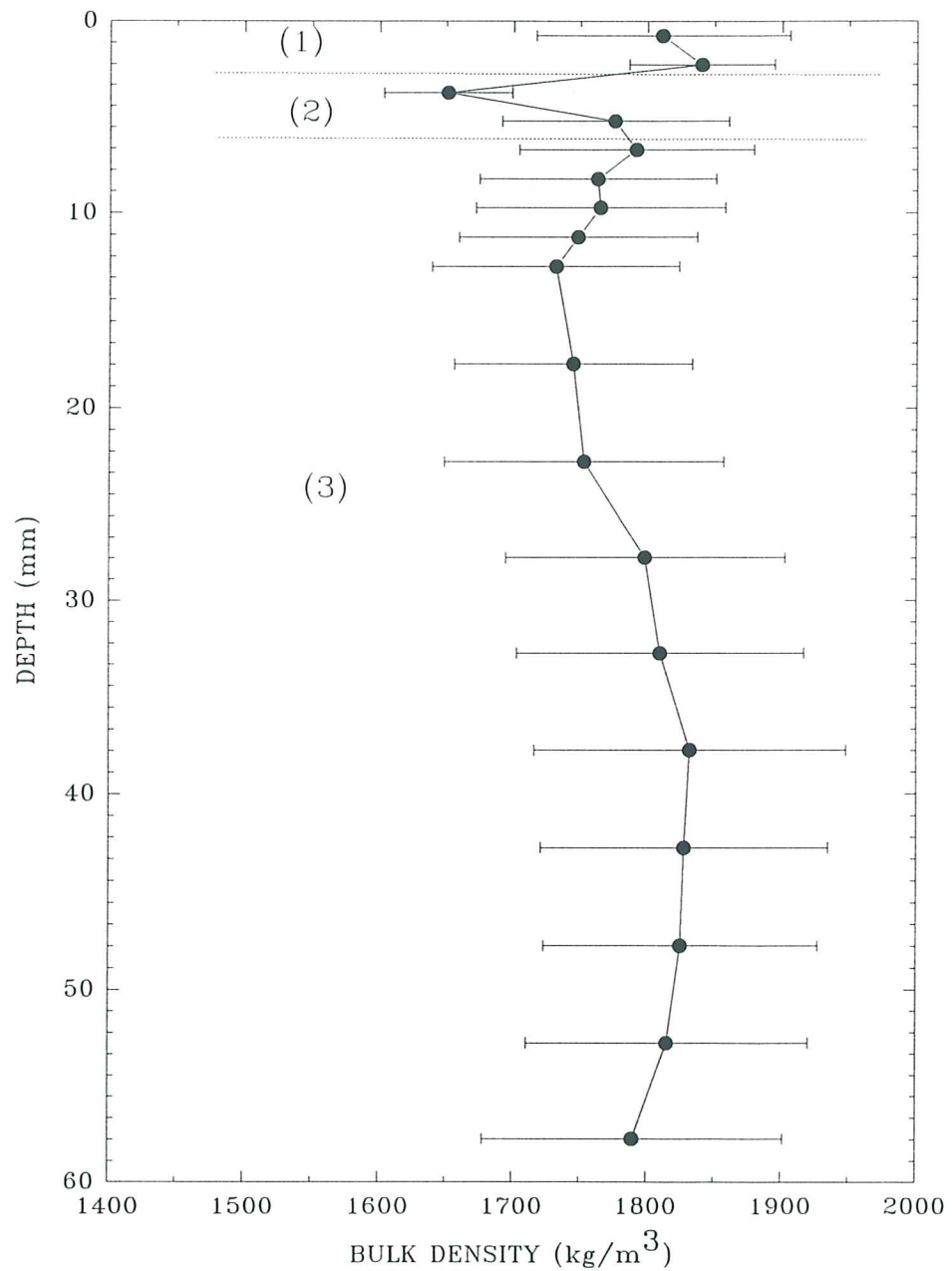


Figure 6.1.3.1. A log of the wet-weight bulk density derived from a Catscan analysis of a syringe core collected at site A. Three layers are evident: (1) a surface layer of relatively high density (2 mm thick); (2) a transitional layer of rapidly changing density (5 mm thick); and (3) the substrate.

SEA CAROUSEL – LISPUK19 (Humber estuary)

SITE B – 18 APRIL, 1995

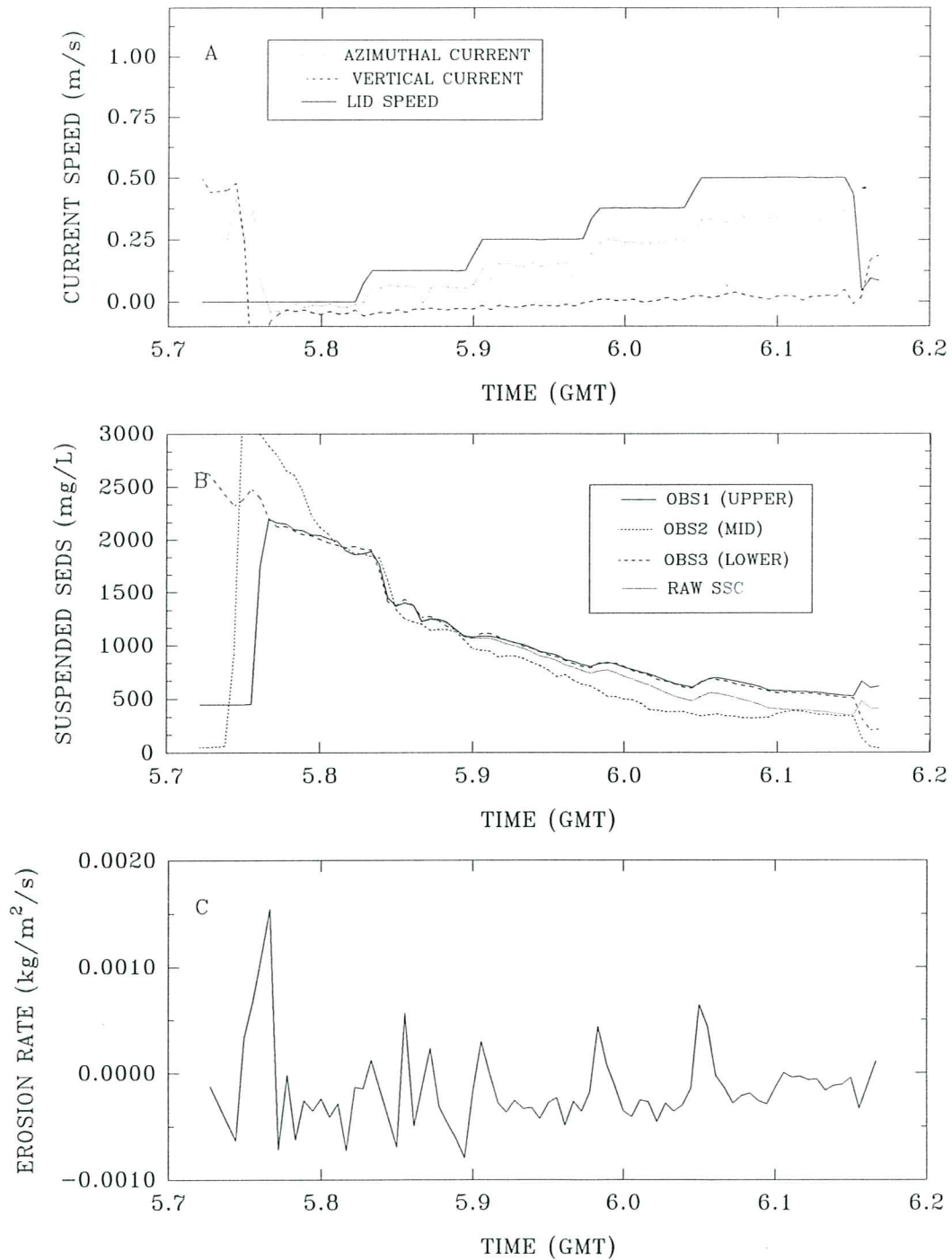


Figure 6.2.1.3. A time-series plot of results from Sea Carousel recorded at site B (LISPUK19) on 18 April, 1995. (A) lid speed and azimuthal and vertical currents at the reference height (0.18 m); (B) suspended sediment concentrations from the three OBS sensors (OBS1 and OBS3 are internal, OBS2 is external); and (C) erosion rate. Notice the dominant effect of the passage of the flood tide turbidity maximum on the sediment concentration signal inside the flume.

SEA CAROUSEL – LISPUK18 (Humber estuary)

SITE B – 18 APRIL, 1995

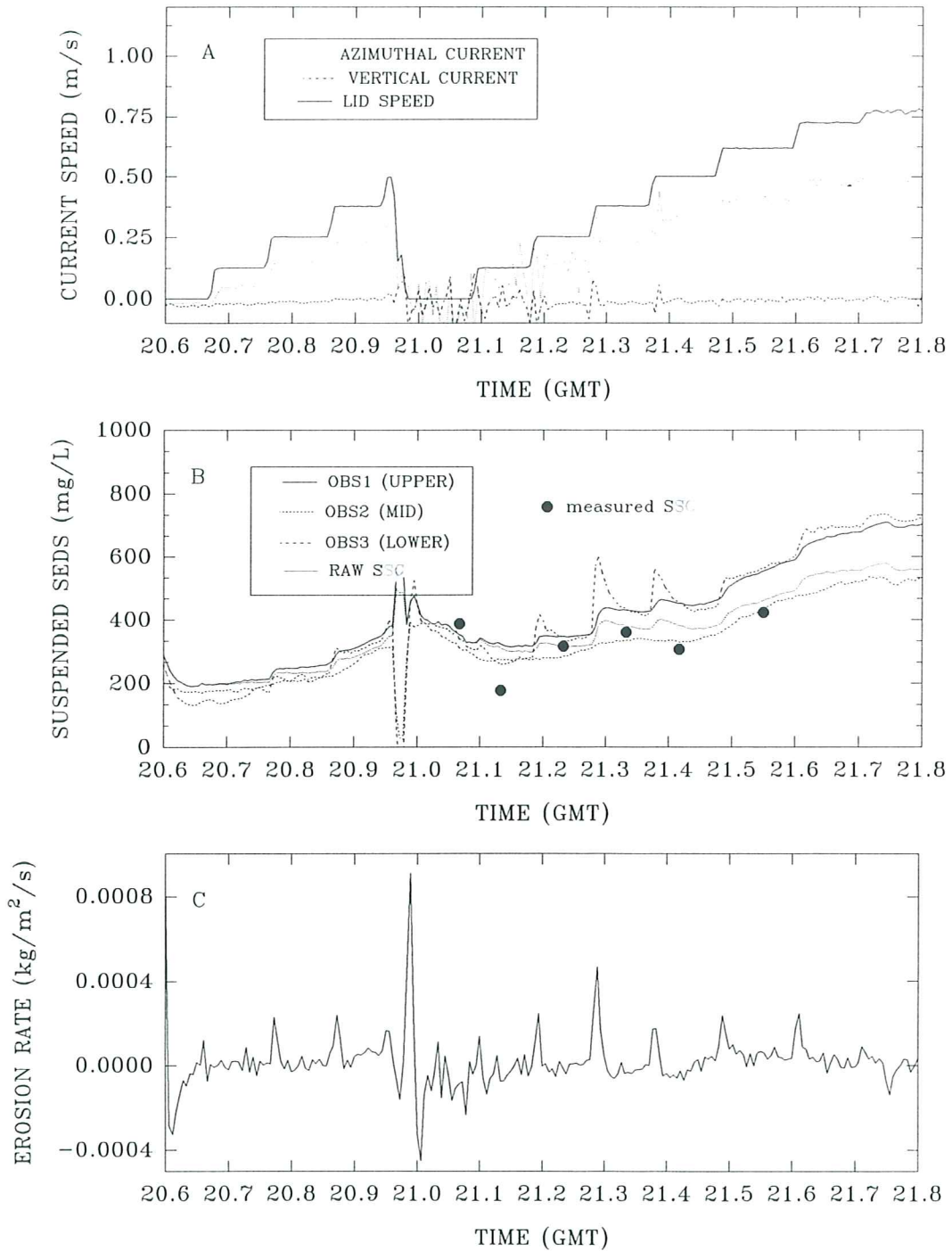


Figure 6.2.1.2. A time-series plot of results from Sea Carousel recorded at site B (LISPUK18) on 18 April, 1995. (A) lid speed and azimuthal and vertical currents at the reference height (0.18 m); (B) suspended sediment concentrations from the three OBS sensors (OBS1 and OBS3 are internal, OBS2 is external), and from pumped samples; and (C) erosion rate.

SEA CAROUSEL – LISPUK17 (Humber estuary)

SITE B – 18 APRIL, 1995

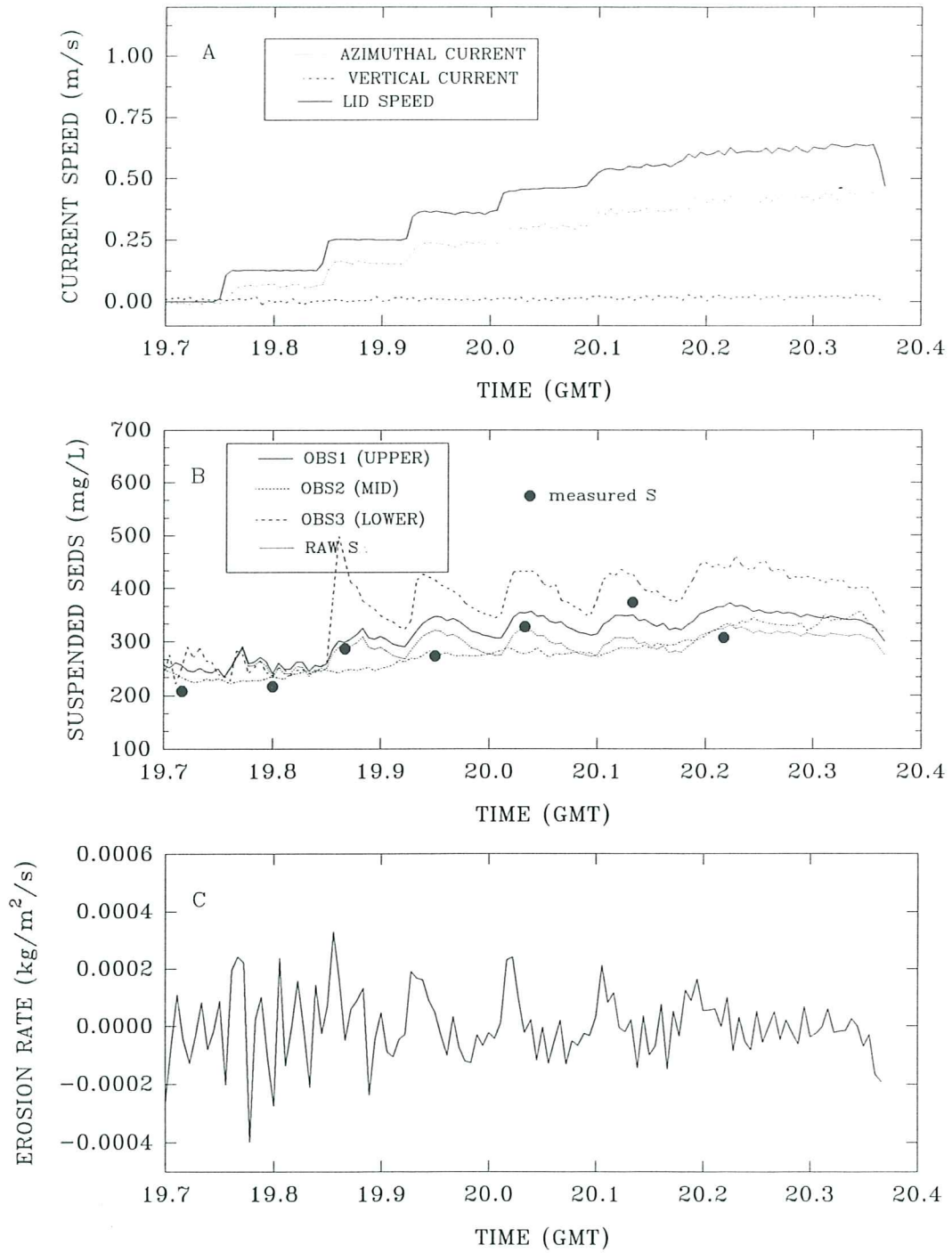


Figure 6.2.1.1. A time-series plot of results from Sea Carousel recorded at site B (LISPUK17) on 18 April, 1995. (A) lid speed and azimuthal and vertical currents at the reference height (0.18 m); (B) suspended sediment concentrations from the three OBS sensors (OBS1 and OBS3 are internal, OBS2 is external), and from pumped samples; and (C) erosion rate. Notice the prevalence of Type I erosion.

STATION LISPUK17, SITE B - 18 APRIL, 1995

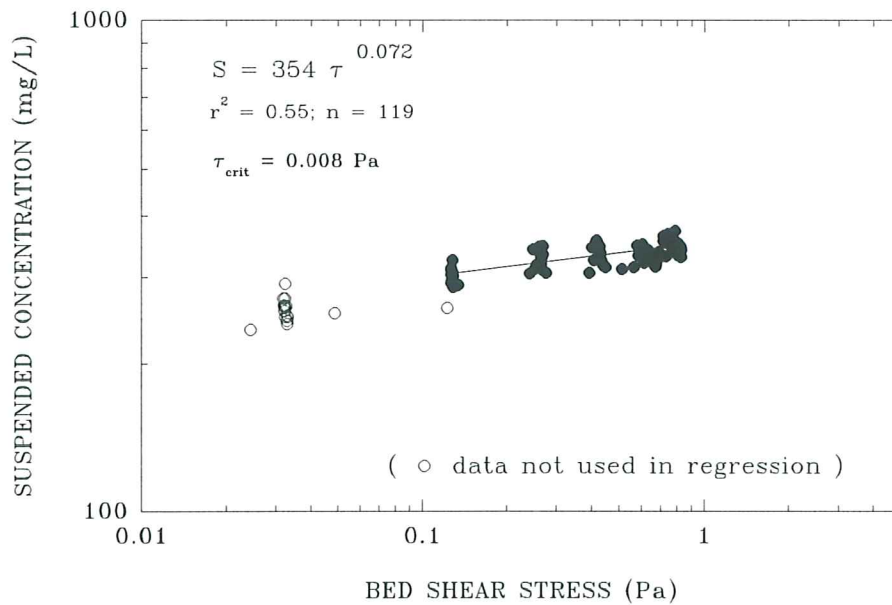
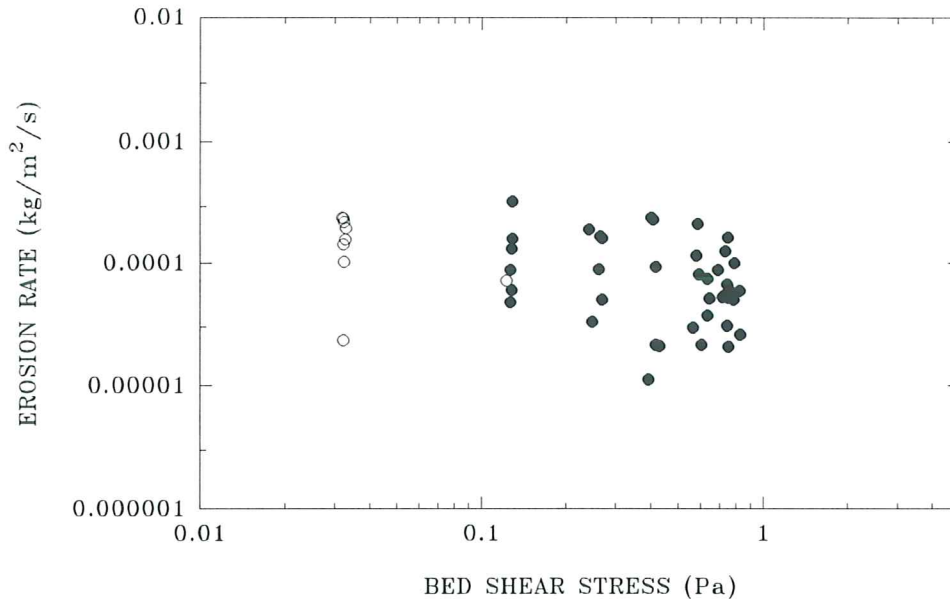


Figure 6.2.1.4. Estimates of the erosion threshold for deployment LISPUK17, site B. The upper panel shows that erosion rate is a power function of applied bed stress; it is not possible to derive erosion threshold from this plot. The lower panel shows that suspended sediment concentration increases as a power function of applied bed shear stress; the threshold is equated with the stress at ambient concentration and yields a value of 0.008 Pa.

STATION LISPUK18, SITE B - 18 APRIL, 1995

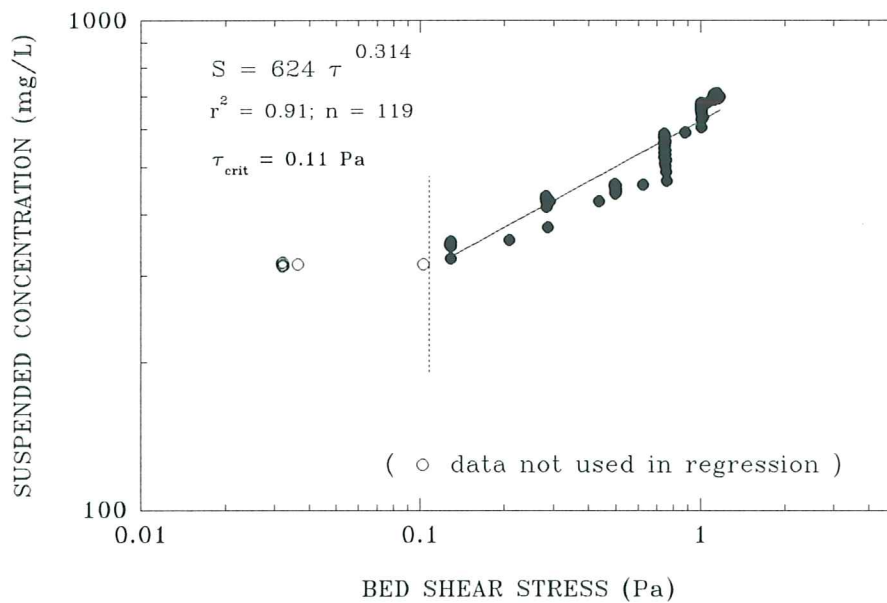
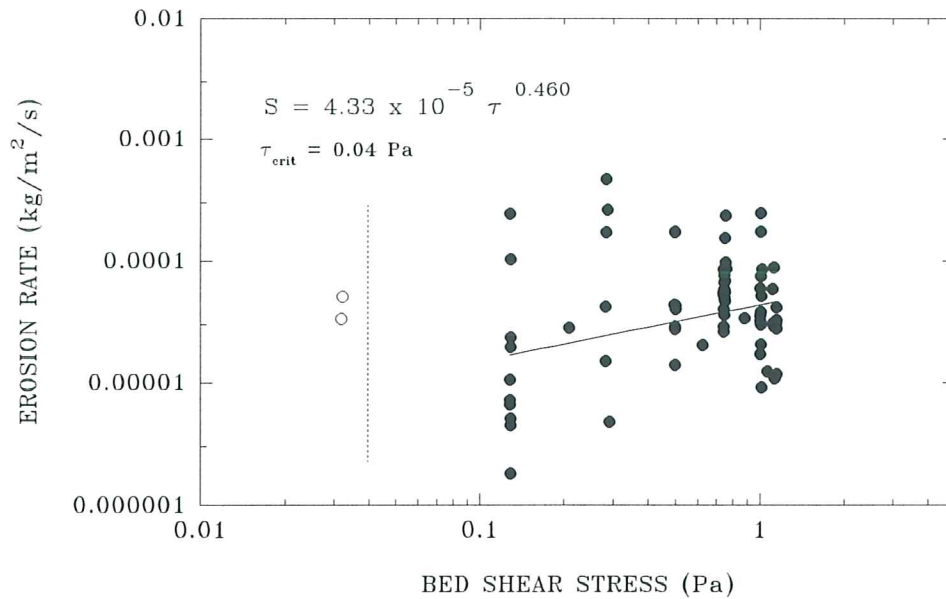


Figure 6.2.1.5. Estimates of the erosion threshold for deployment LISPUK18, site B. The upper panel shows that erosion rate is a power function of applied bed stress; the erosion threshold is evaluated as 0.04 Pa. The lower panel shows that suspended sediment concentration increases as a power function of applied bed shear stress; the threshold is equated with the stress at ambient concentration and yields a value of 0.11 Pa.

LAB CAROUSEL – LISPUK (Humber estuary)

SITE B (LABEXP4) – 11 APRIL, 1995

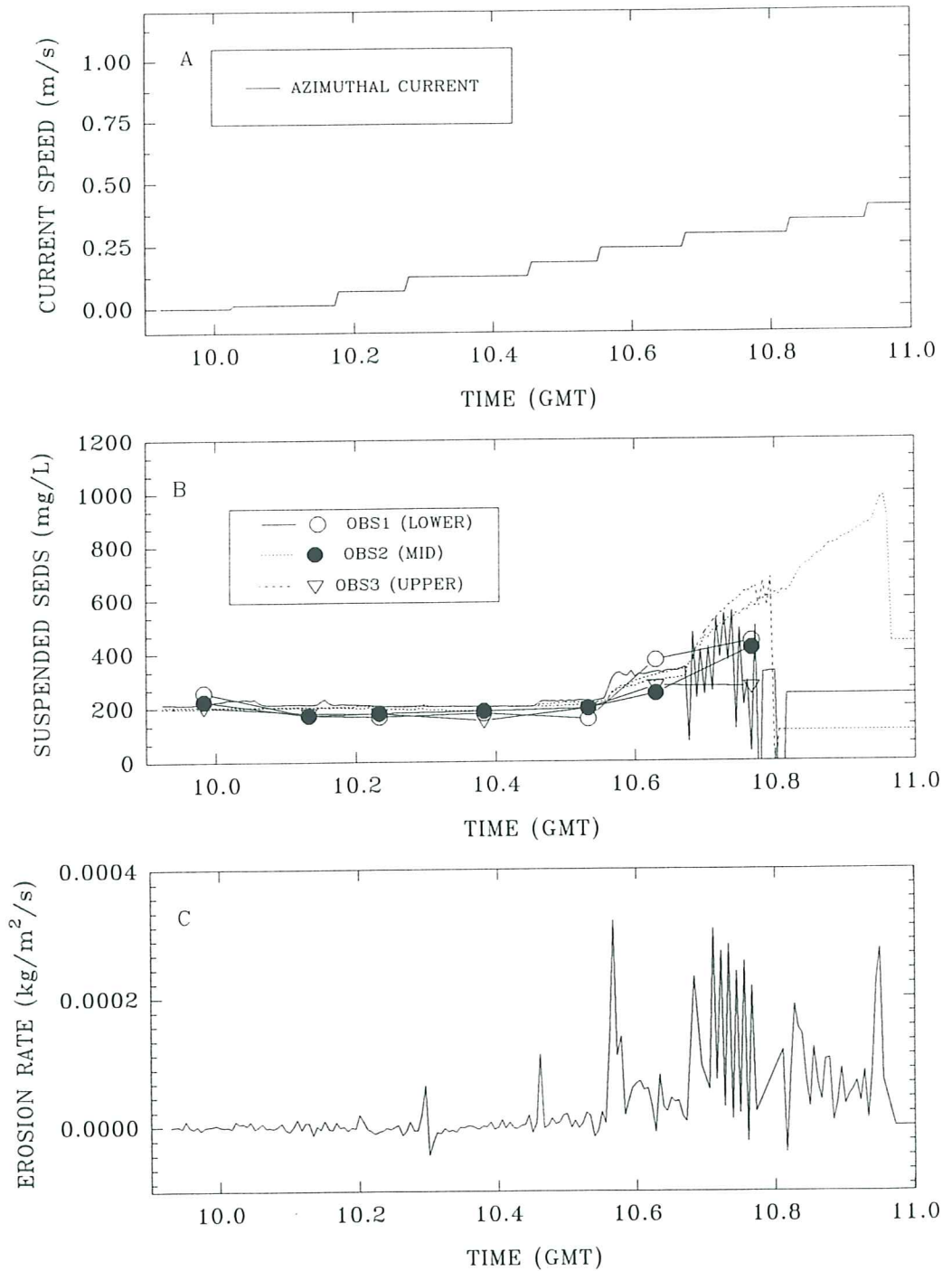


Figure 6.2.2.1. A time-series of Lab Carousel experiment (Labexp4) on a site B bulk sample. (A) the azimuthal reference current for a height of 0.18 m above the bed (based on lid rotation); (B) suspended sediment concentration from three OBS's and pumped samples at heights of 0.03, 0.10, and 0.20 m above the base; and (C) erosion rate. The intermittent effects of sensor saturation are clearly seen during the eroding phase.

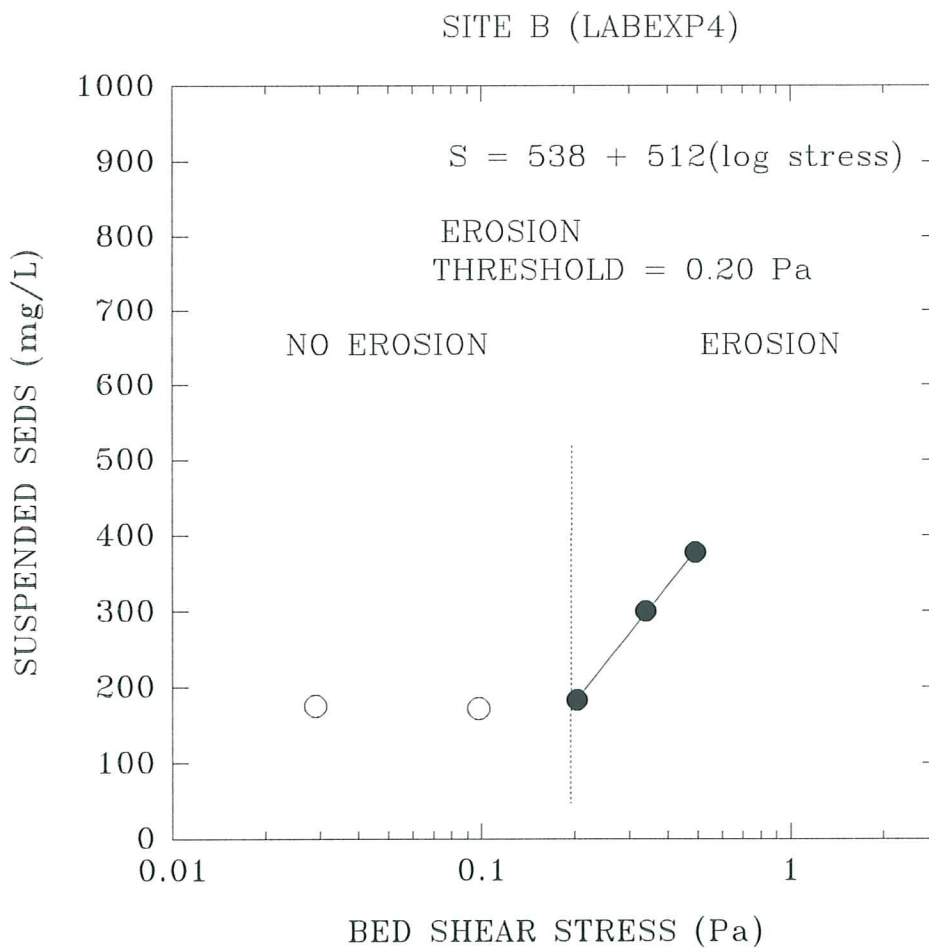


Figure 6.2.2.2. A plot of measured suspended sediment concentration (from pumped samples) versus applied bed shear stress in Sea Carousel. Notice the onset of erosion at 0.2 Pa which is based on the extrapolation of concentration to ambient levels.

LISPUK – SITE B, Humber estuary

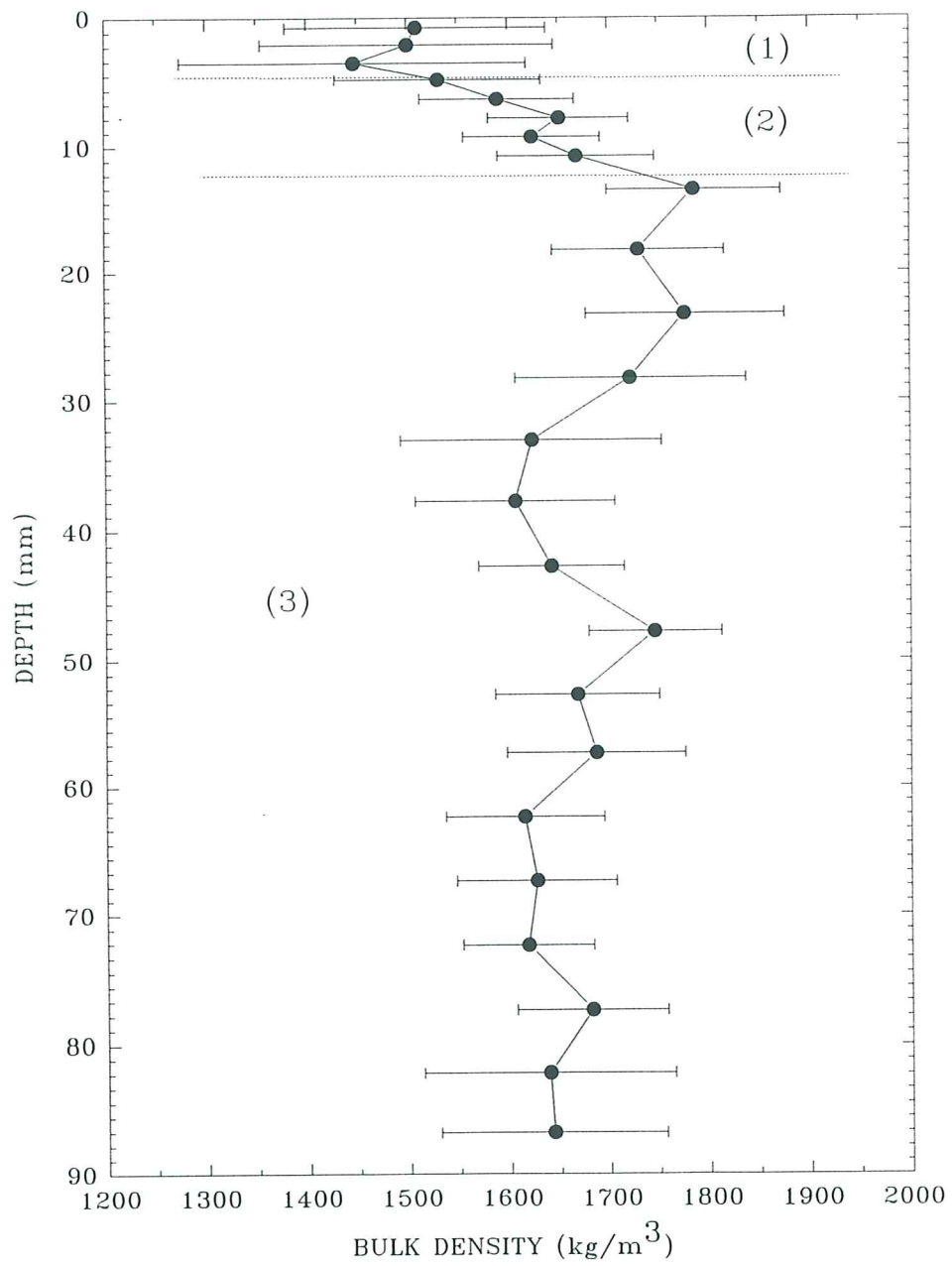


Figure 6.2.3.1. A log of the wet-weight bulk density derived from a Catscan analysis of a syringe core collected at site B. Three layers are evident: (1) a surface layer of relatively low density (4 mm thick); (2) a transitional layer of rapidly increasing density (8 mm thick); and (3) the denser substrate.

SEA CAROUSEL – LISPUK10 (Humber estuary)

SITE B/C – 13 APRIL, 1995

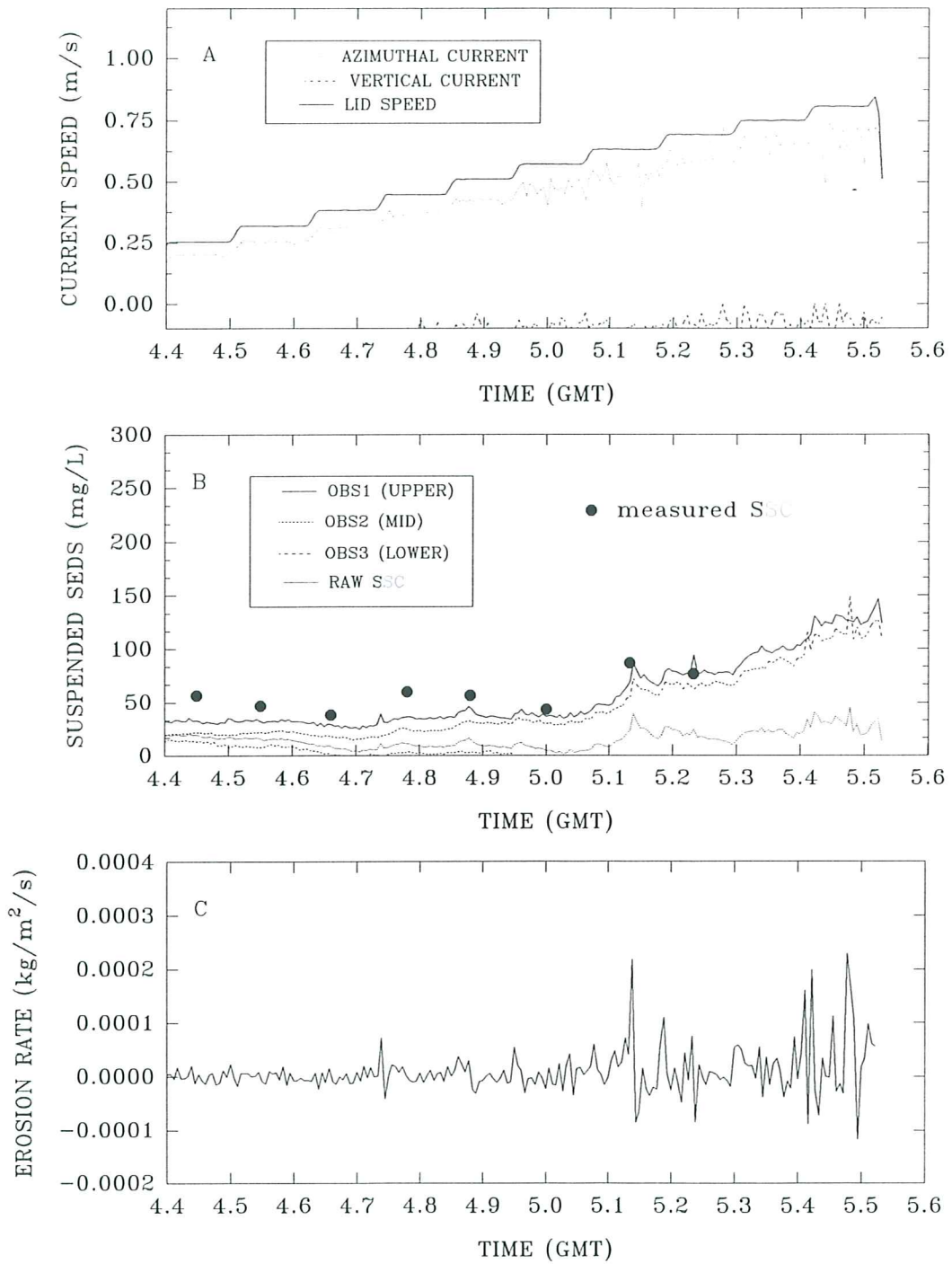


Figure 6.3.1.1. A time-series plot of results from Sea Carousel recorded at site B/C (LISPUK10) on 13 April, 1995. (A) lid speed and azimuthal and vertical currents at the reference height (0.18 m); (B) suspended sediment concentrations from the three OBS sensors (OBS1 and OBS3 are internal, OBS2 is external), and from pumped samples; and (C) erosion rate. No clear trends in erosion are evident in this time-series.

SEA CAROUSEL – LISPUK11 (Humber estuary)

SITE B/C – 13 APRIL, 1995

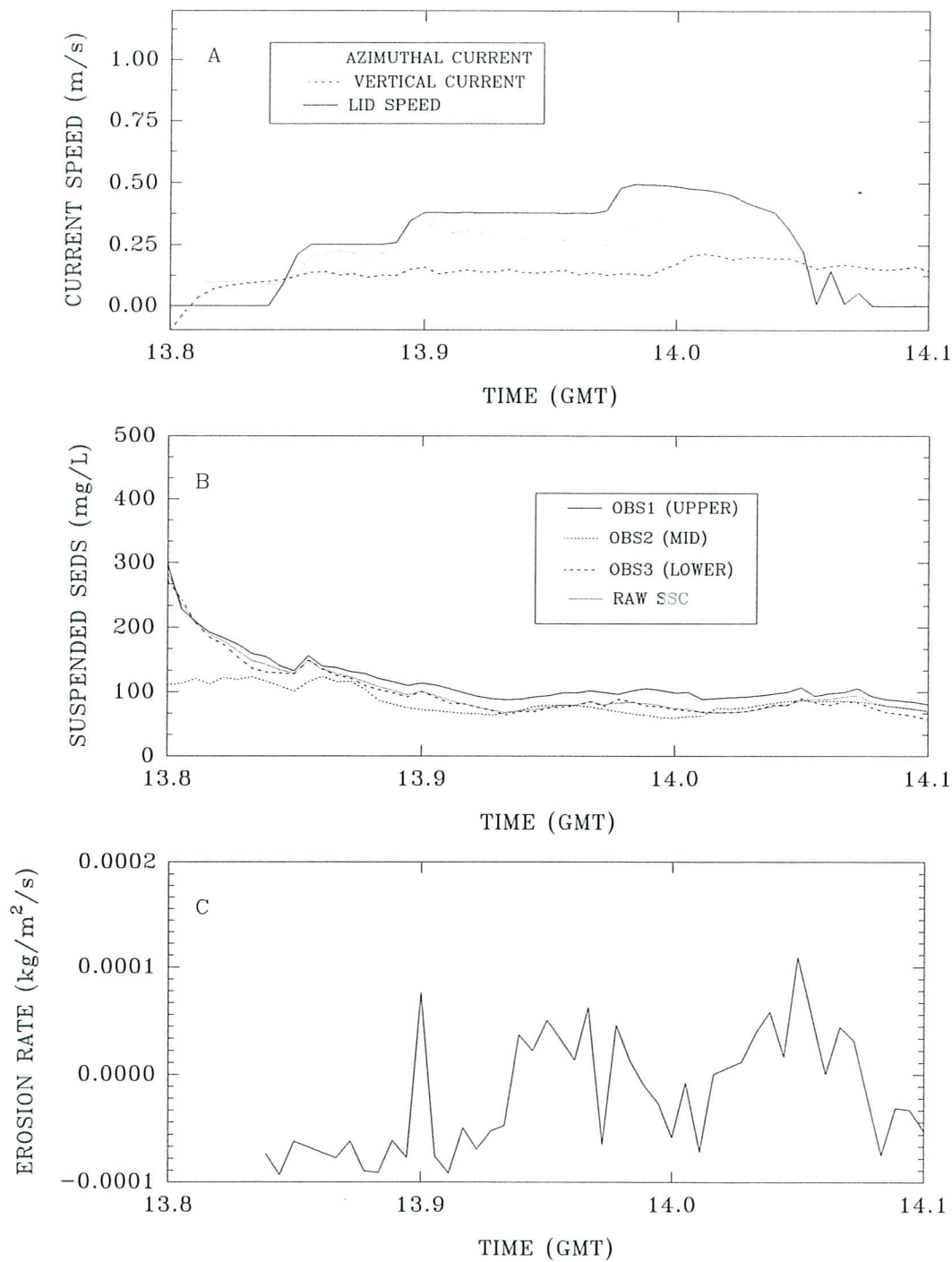


Figure 6.3.1.2. A time-series plot of results from Sea Carousel recorded at site B/C (LISPUK11) on 13 April, 1995. (A) lid speed and azimuthal and vertical currents at the reference height (0.18 m); (B) suspended sediment concentrations from the three OBS sensors (OBS1 and OBS3 are internal, OBS2 is external); and (C) erosion rate. The site was abandoned early due to drifting. Also notice the trends in sediment concentration which show the passage of a flood tide turbidity maximum.

SEA CAROUSEL – LISPUK12 (Humber estuary)

SITE B/C – 13 APRIL, 1995

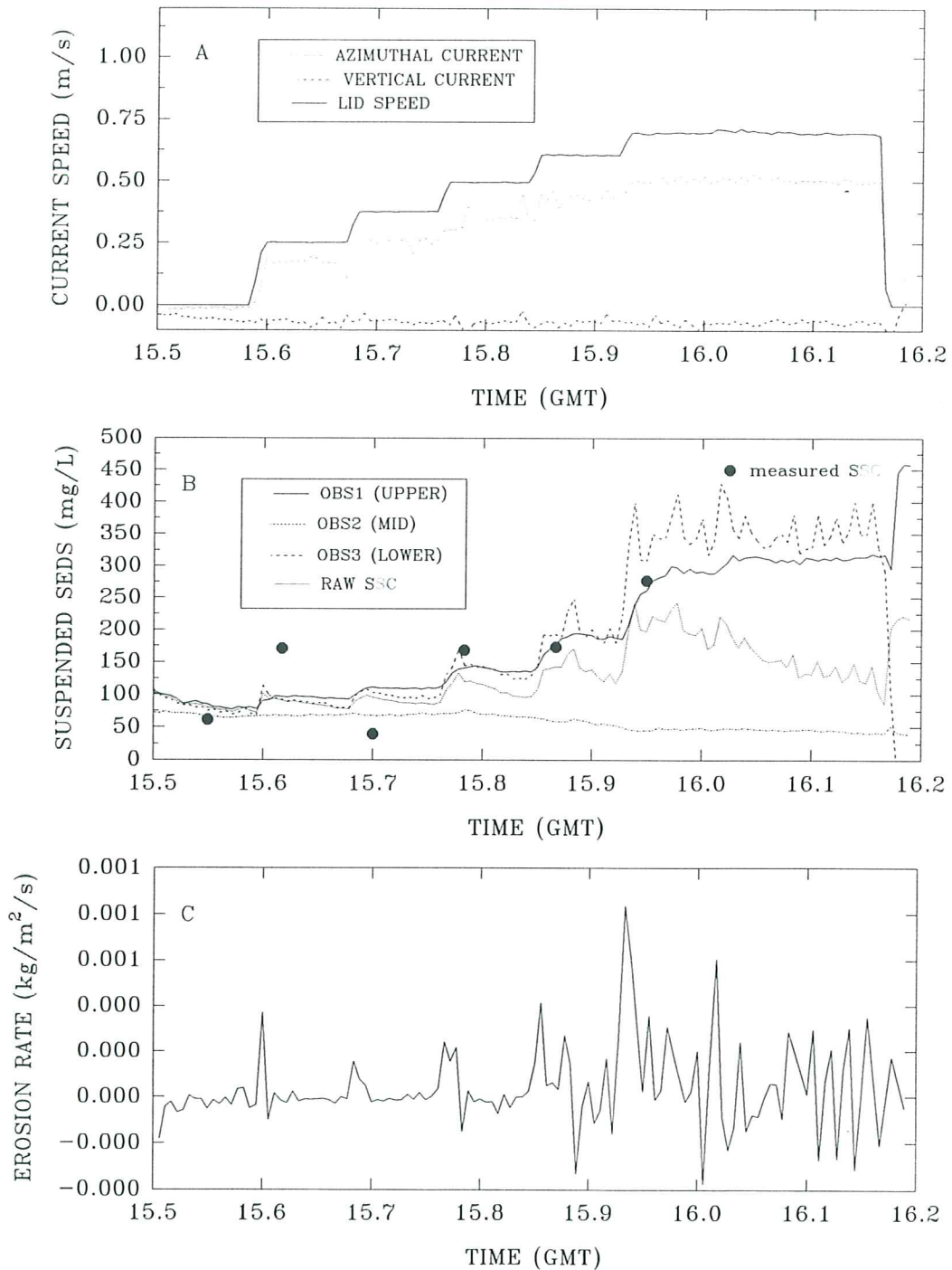


Figure 6.3.1.3. A time-series plot of results from Sea Carousel recorded at site B/C (LISPUK12) on 13 April, 1995. (A) lid speed and azimuthal and vertical currents at the reference height (0.18 m); (B) suspended sediment concentrations from the three OBS sensors (OBS1 and OBS3 are internal, OBS2 is external), and from pumped samples; and (C) erosion rate. The erratic nature of erosion is likely due to lower sensor response to intermittent burial.

STATION LISPUK12, SITE B/C - 13 APRIL, 1995

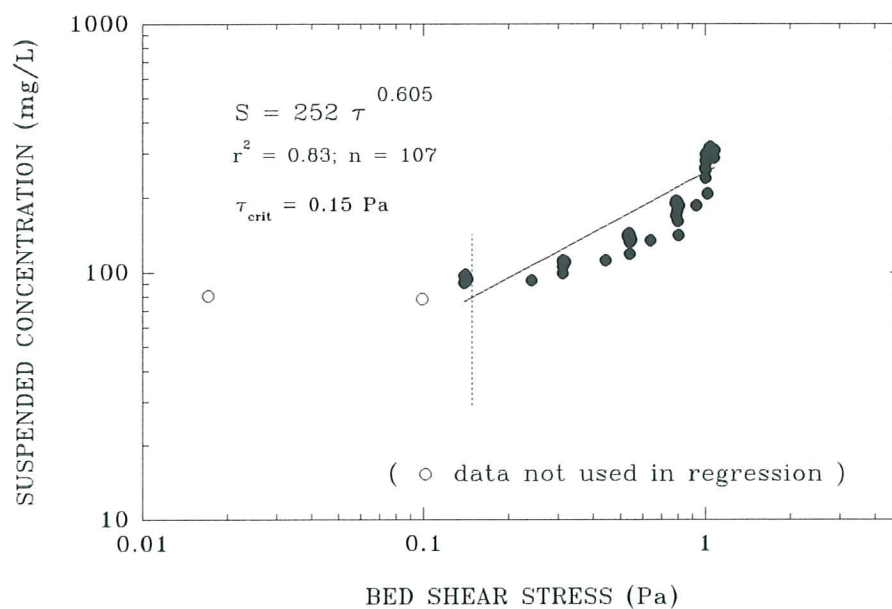
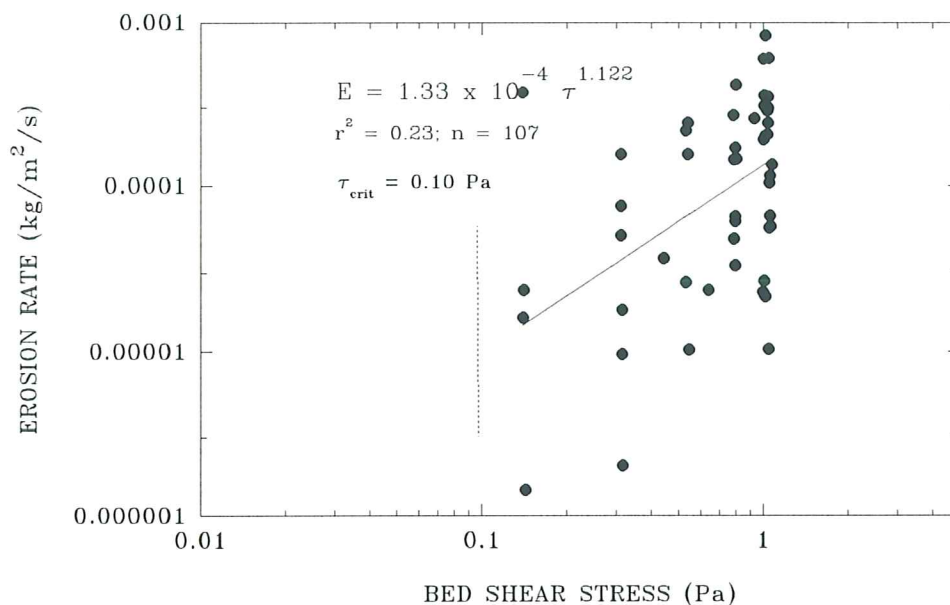


Figure 6.3.1.5. Estimates of the erosion threshold for deployment LISPUK12, site B/C. The upper panel shows that erosion rate is a power function of applied bed stress; the estimated erosion threshold is 0.10 Pa. The lower panel shows that suspended sediment concentration increases as a power function of applied bed shear stress; the threshold is equated with the stress at ambient concentration and yields a value of 0.15 Pa.

STATION LISPUK10, SITE B/C - 13 APRIL, 1995

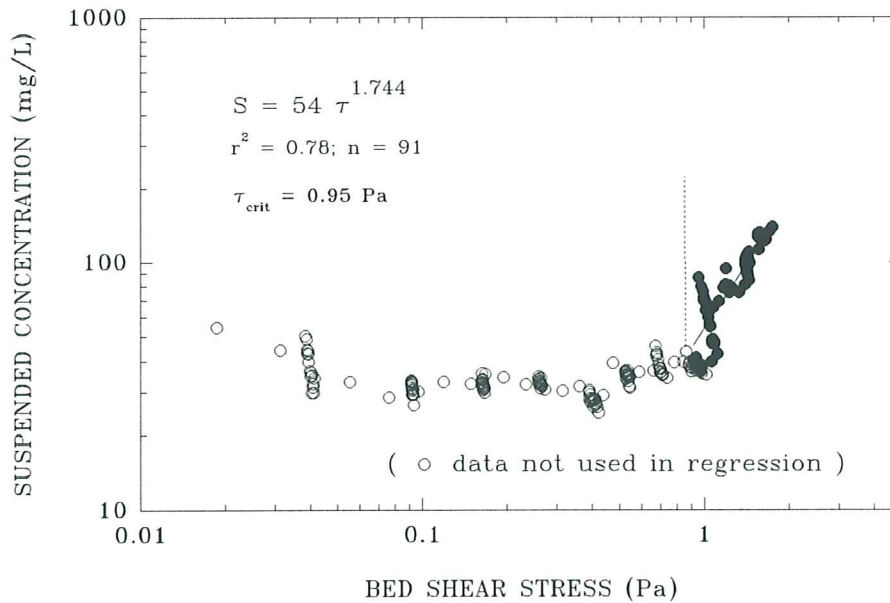
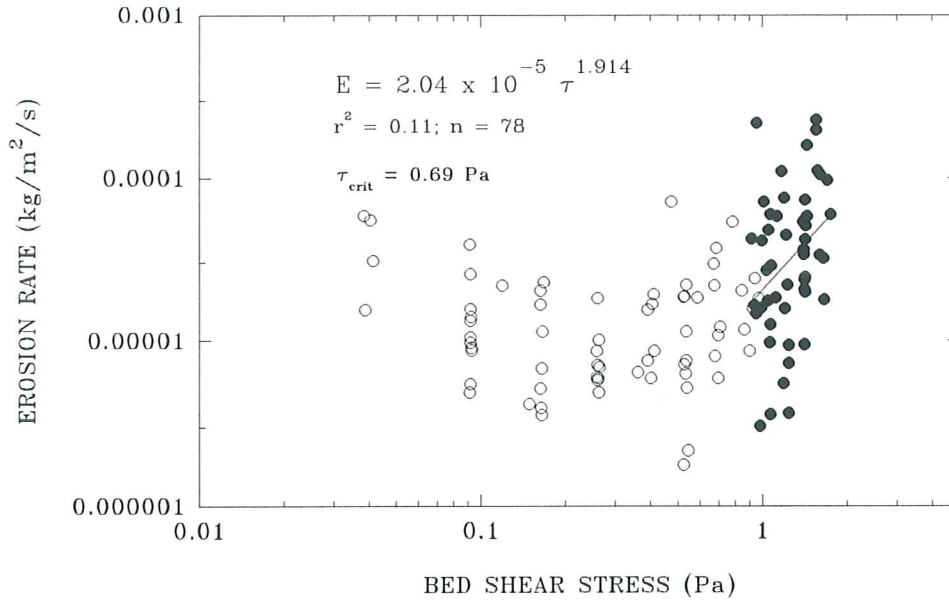


Figure 6.3.1.4. Estimates of the erosion threshold for deployment LISPUK10, site B/C. The upper panel shows that erosion rate is a power function of applied bed stress; the estimated erosion threshold is 0.69 Pa. The lower panel shows that suspended sediment concentration increases as a power function of applied bed shear stress; the threshold is equated with the stress at ambient concentration and yields a value of 0.95 Pa.

LAB CAROUSEL - LISPUK (Humber estuary)

SITE B/C (LABEXP8) - 16 APRIL, 1995

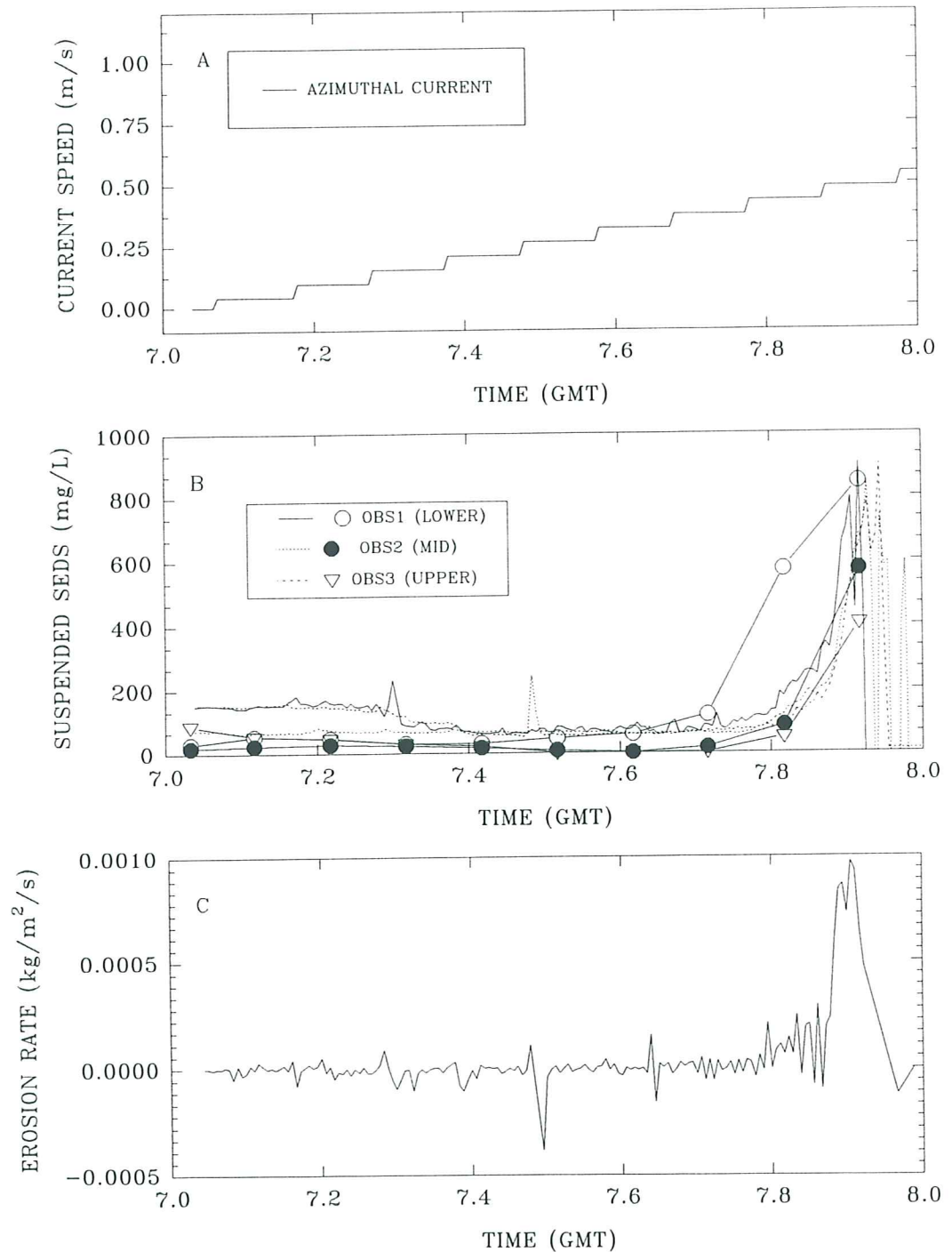


Figure 6.3.2.1. A time-series of Lab Carousel experiment (Labexp8) on a site B/C bulk sample. (A) the azimuthal reference current for a height of 0.18 m above the bed (based on lid rotation); (B) suspended sediment concentration from three OBS's and pumped samples at heights of 0.03, 0.10, and 0.20 m above the base; and (C) erosion rate.

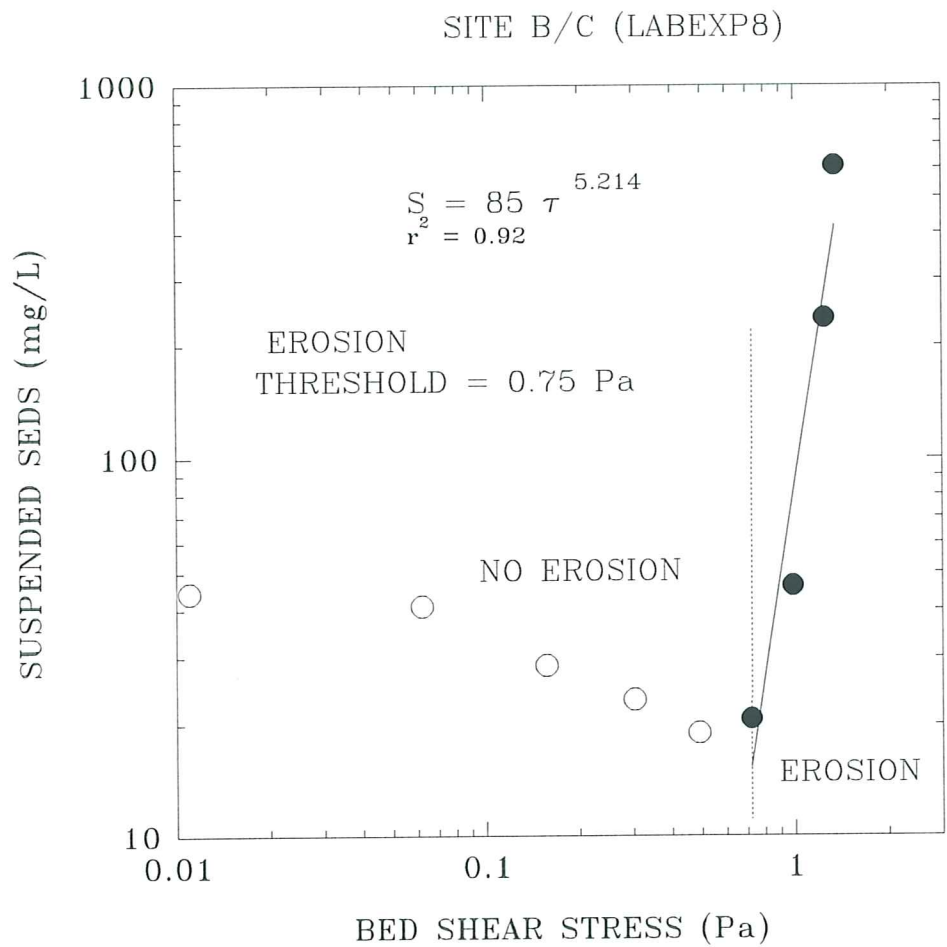


Figure 6.3.2.2. A plot of measured suspended sediment concentration (from pumped samples) versus applied bed shear stress in Lab Carousel for experiment Labexp8 (site B/C) . Notice the onset of erosion at 0.75 Pa which is based on the extrapolation of concentration to ambient levels.

LISPUK – SITE B/C, Humber estuary

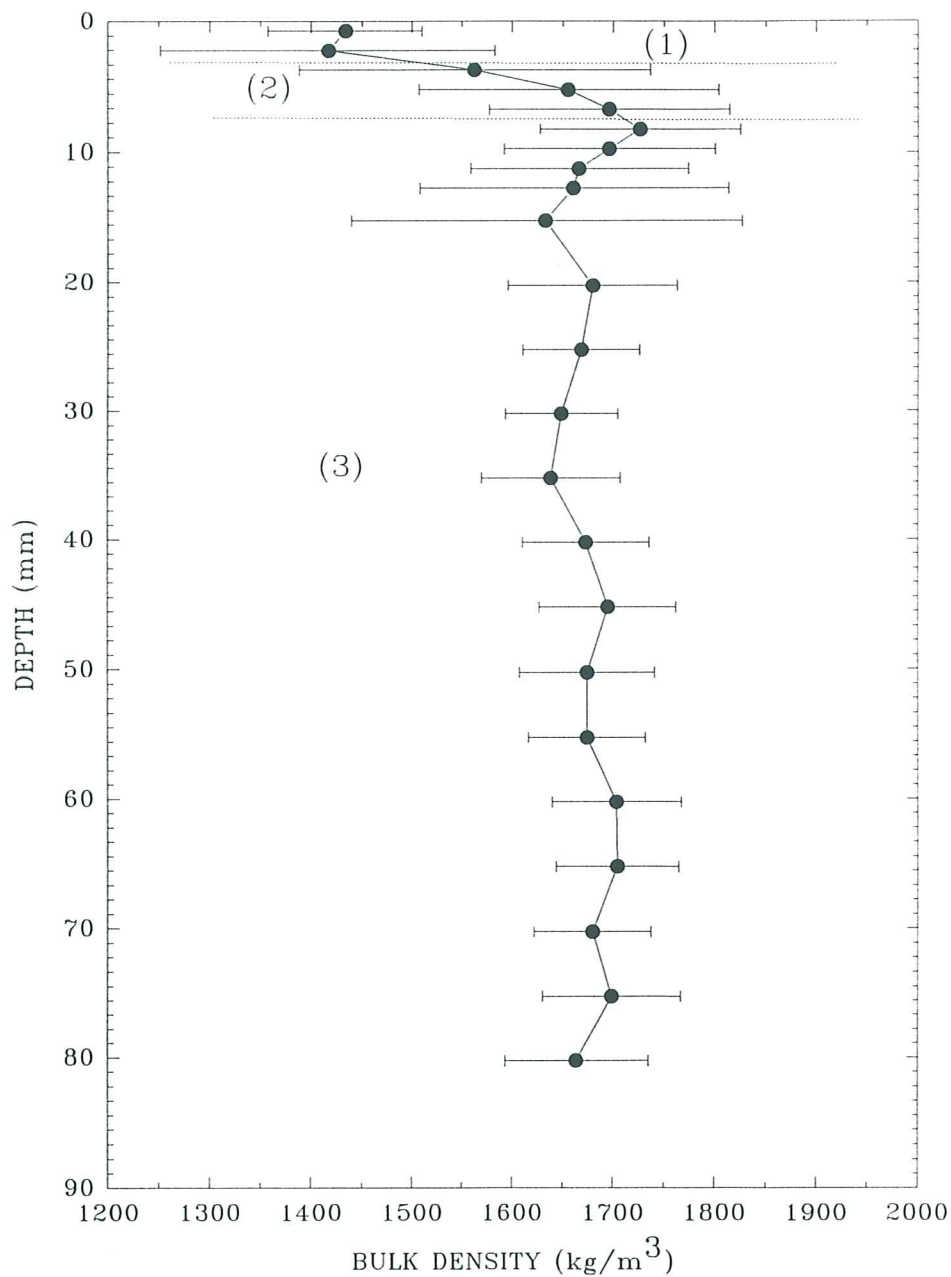


Figure 6.3.3.1. A log of the wet-weight bulk density derived from a Catscan analysis of a syringe core collected at site B/C. Three layers are evident: (1) a surface layer of relatively low density (3 mm thick); (2) a transitional layer of rapidly increasing density (5 mm thick); and (3) the denser substrate.

SEA CAROUSEL – LISPUK05 (Humber estuary)

SITE C – 11 APRIL, 1995

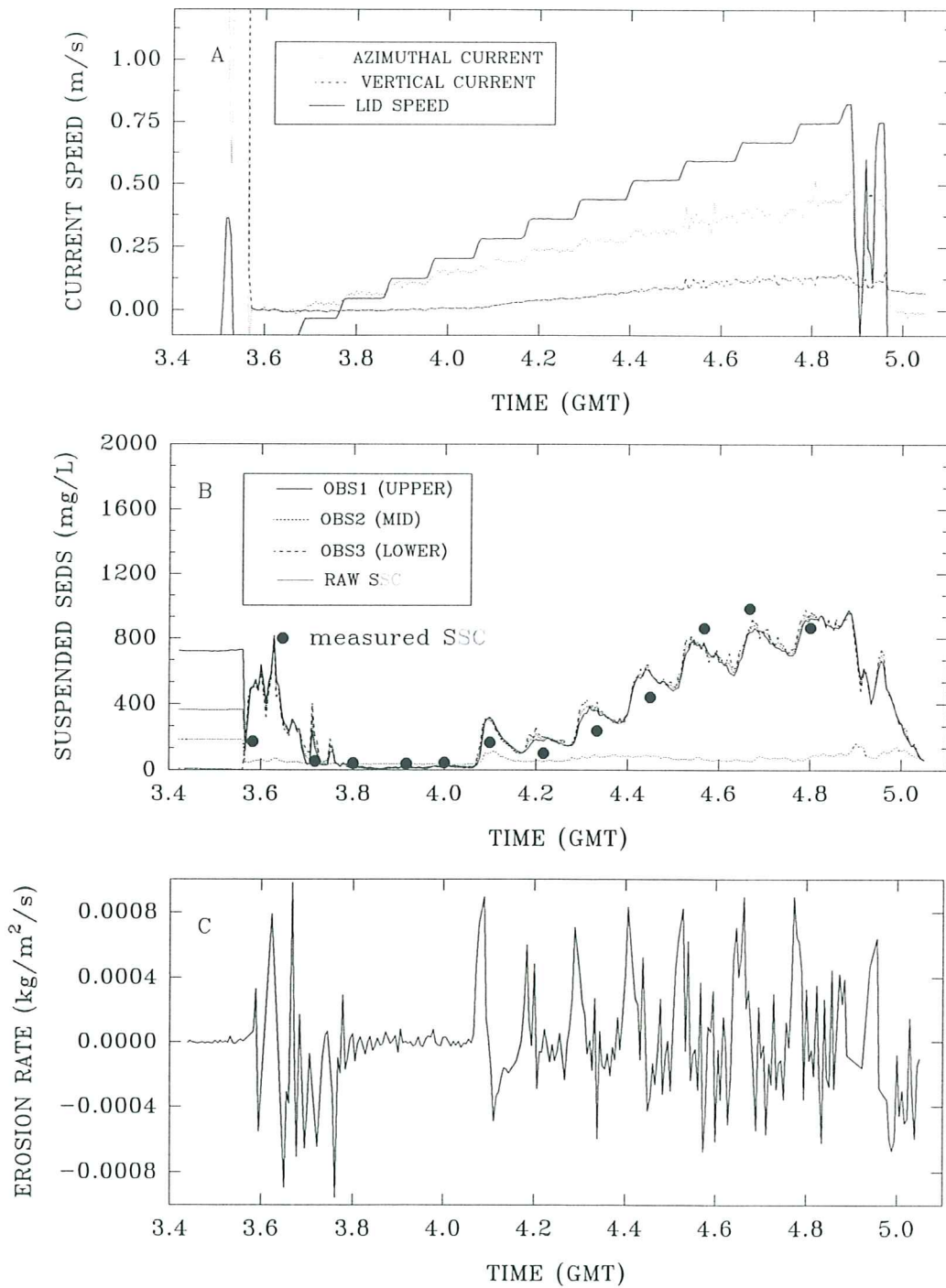


Figure 6.4.1.1. A time-series plot of results from Sea Carousel recorded at site C (LISPUK5) on 11 April, 1995. (A) lid speed and azimuthal and vertical currents at the reference height (0.18 m); (B) suspended sediment concentrations from the three OBS sensors (OBS1 and OBS3 are internal, OBS2 is external), and from pumped samples; and (C) erosion rate. The erosion is Type I in form in the early stages.

SEA CAROUSEL – LISPUK06 (Humber estuary)

SITE C – 11 APRIL, 1995

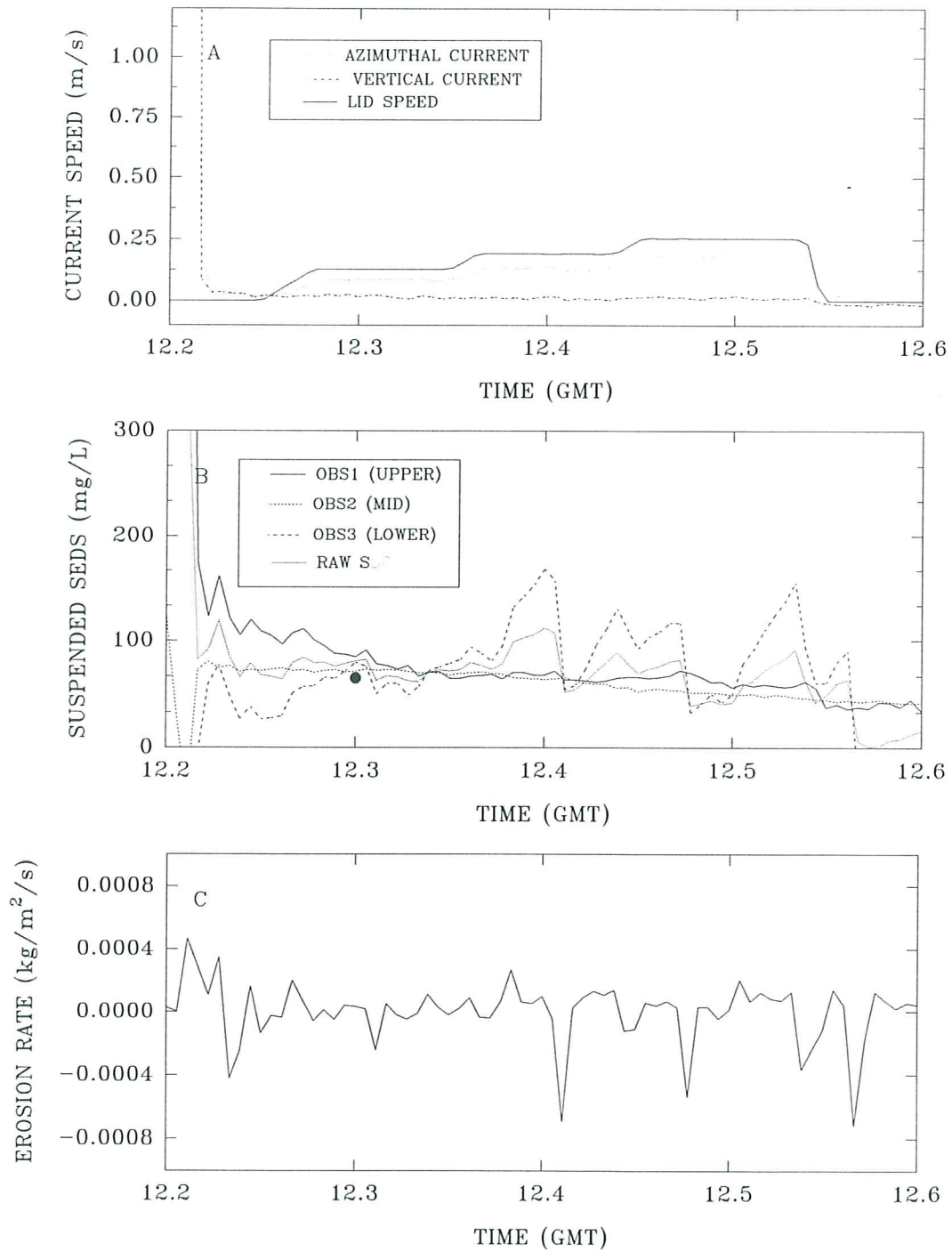


Figure 6.4.1.2. A time-series plot of results from Sea Carousel recorded at site C (LISPUK6) on 11 April, 1995. (A) lid speed and azimuthal and vertical currents at the reference height (0.18 m); (B) suspended sediment concentrations from the three OBS sensors (OBS1 and OBS3 are internal, OBS2 is external), and from one pumped sample; and (C) erosion rate. The station was abandoned prematurely due to boat drift.

STATION LISPUK5, SITE C - 11 APRIL, 1995

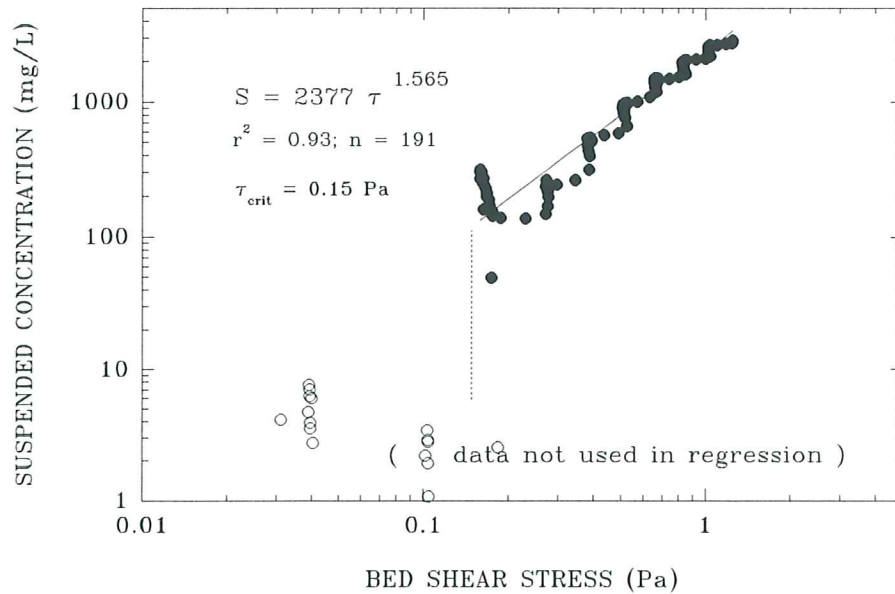
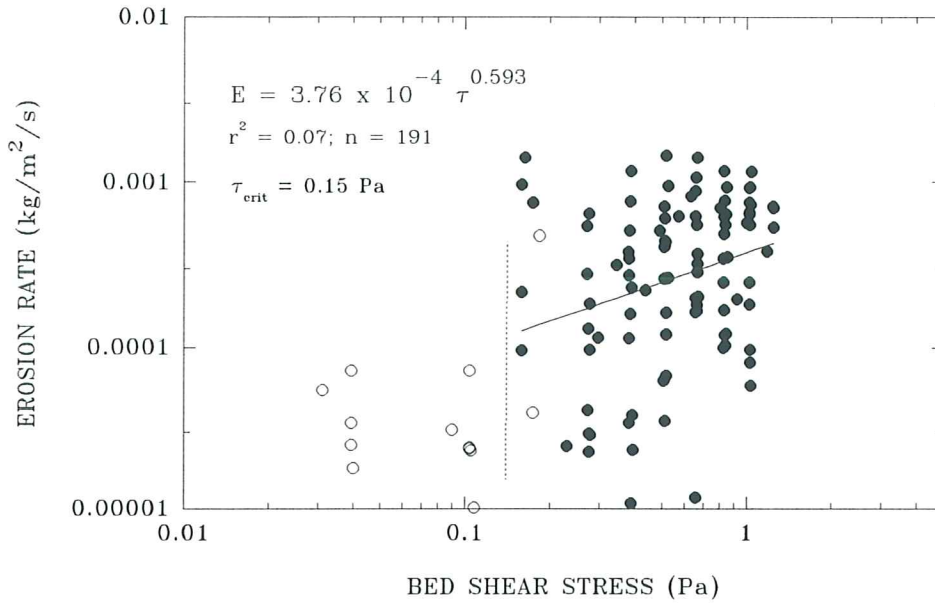


Figure 6.4.1.3. Estimates of the erosion threshold for deployment LISPUK5, site C. The upper panel shows that erosion rate is a power function of applied bed stress; the estimated erosion threshold is 0.15 Pa. The lower panel shows that suspended sediment concentration increases as a power function of applied bed shear stress; the threshold is equated with the stress at ambient concentration and yields a value of 0.15 Pa.

LAB CAROUSEL – LISPUK (Humber estuary)

SITE C (LABEXP7) – 14 APRIL, 1995

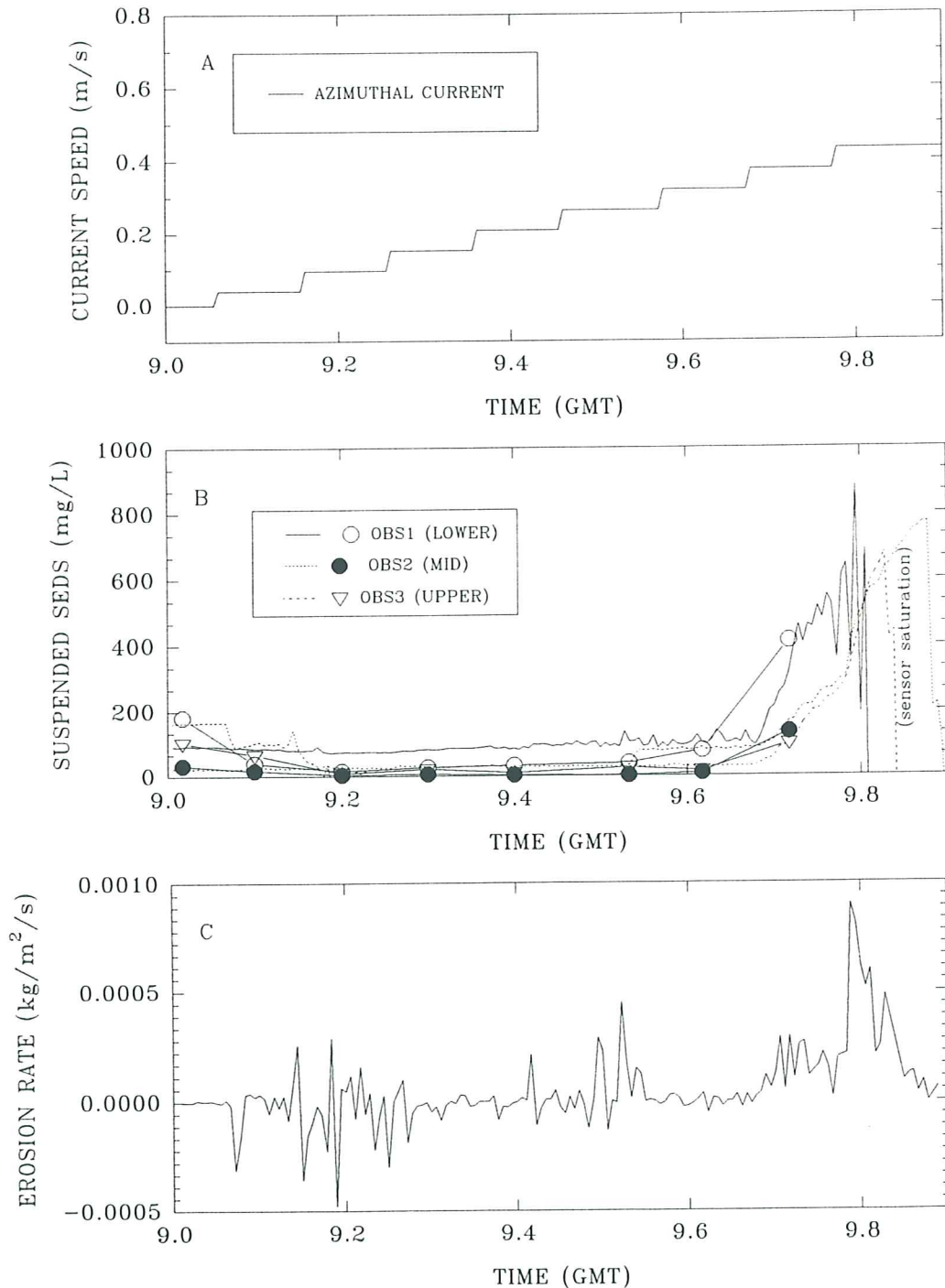


Figure 6.4.2.1. A time-series of Lab Carousel experiment (Labexp7) on a site C bulk sample. (A) the azimuthal reference current for a height of 0.18 m above the bed (based on lid rotation); (B) suspended sediment concentration from three OBS's and pumped samples at heights of 0.03, 0.10, and 0.20 m above the base; and (C) erosion rate.

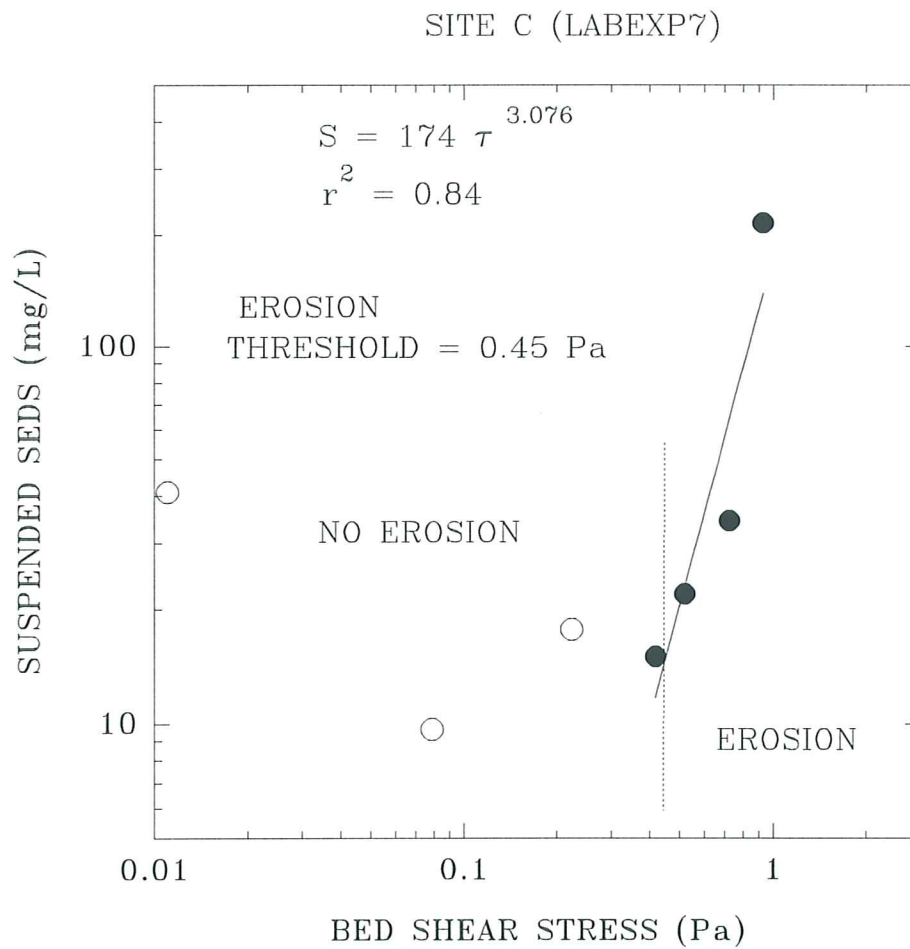


Figure 6.4.2.2. A plot of measured suspended sediment concentration (from pumped samples) versus applied bed shear stress in Lab Carousel for experiment Labexp7 (site C) . Notice the onset of erosion at 0.45 Pa which is based on the extrapolation of concentration to ambient levels.

STATION LISPUK8, SITE C/D - 10 APRIL, 1995

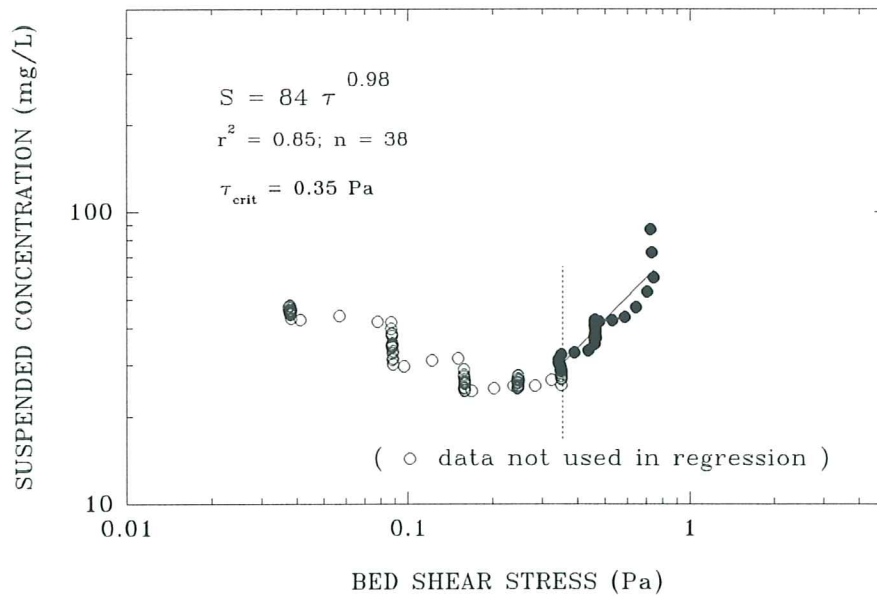
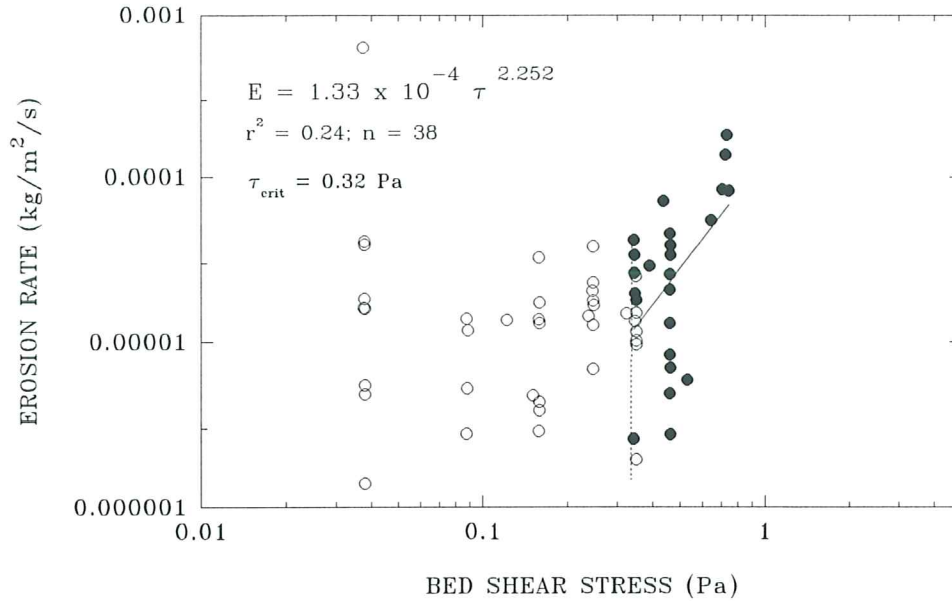


Figure 6.5.1.4. Estimates of the erosion threshold for deployment LISPUK8, site C/D. The upper panel shows that erosion rate is a power function of applied bed stress; the estimated erosion threshold is 0.32 Pa. The lower panel shows that suspended sediment concentration increases as a power function of applied bed shear stress; the threshold is equated with the stress at ambient concentration and yields a value of 0.35 Pa.

LISPUK – SITE C, Humber estuary

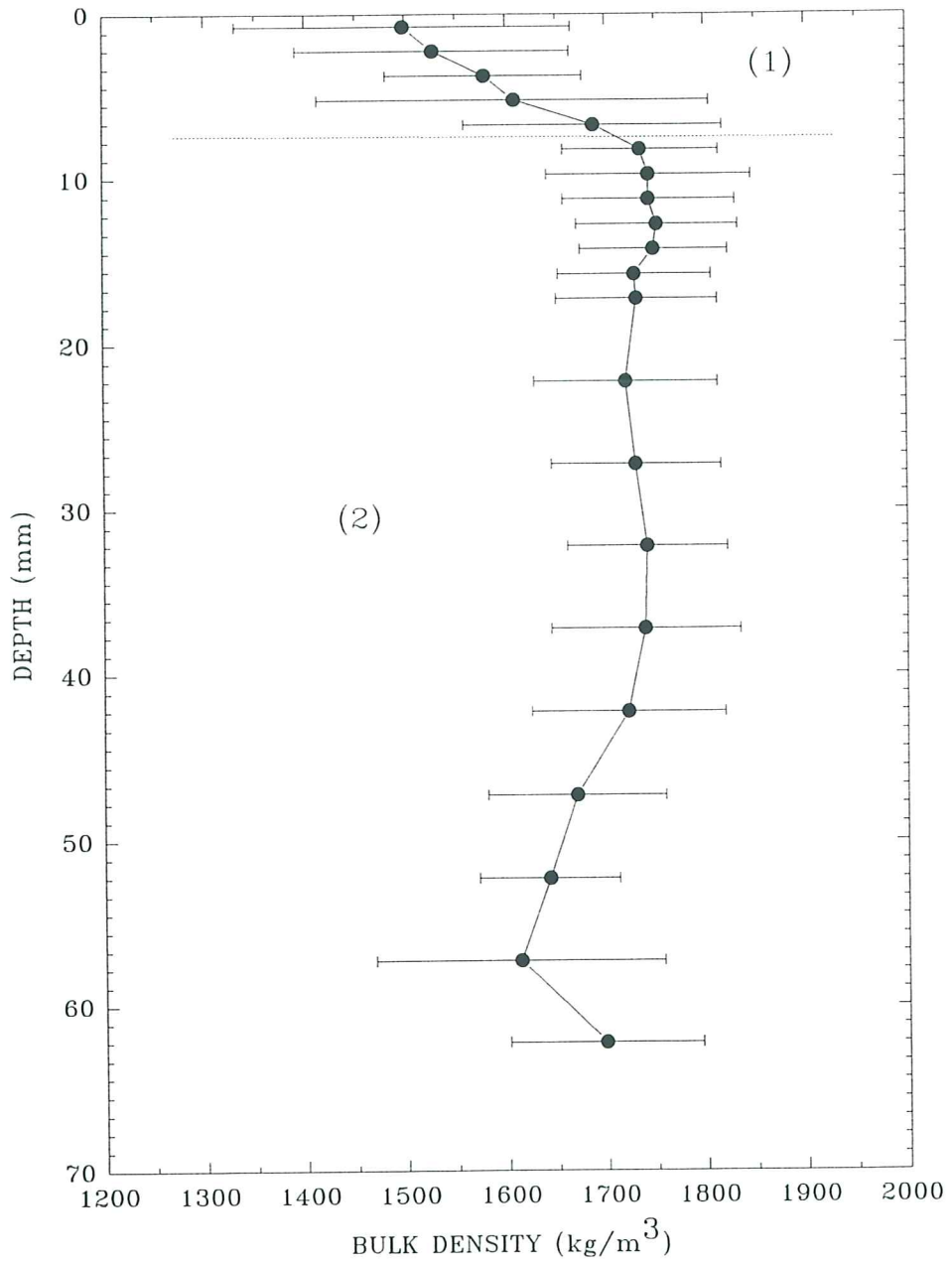


Figure 6.4.3.1. A log of the wet-weight bulk density derived from a Catscan analysis of a syringe core collected at site C. Two layers are evident: (1) a surface layer of rapidly increasing density (8 mm thick); and (2) the denser substrate.

SEA CAROUSEL – LISPUK08 (Humber estuary)

SITE CD – 12 APRIL, 1995

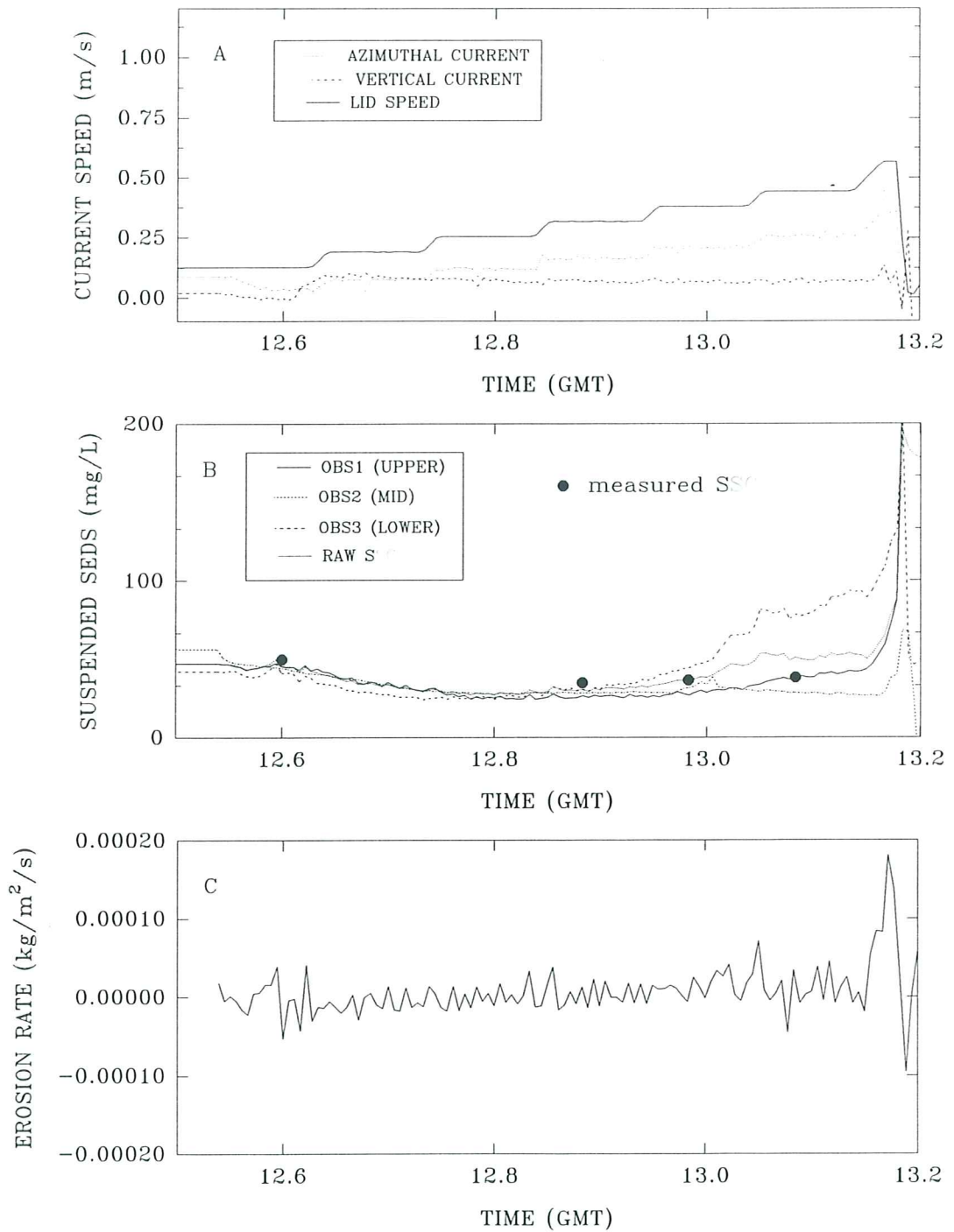


Figure 6.5.1.2. A time-series plot of results from Sea Carousel recorded at site C/D (LISPUK8) on 12 April, 1995. (A) lid speed and azimuthal and vertical currents at the reference height (0.18 m); (B) suspended sediment concentrations from the three OBS sensors (OBS1 and OBS3 are internal, OBS2 is external), and from pumped samples; and (C) erosion rate.

SEA CAROUSEL – LISPUK07 (Humber estuary)

SITE CD – 10 APRIL, 1995

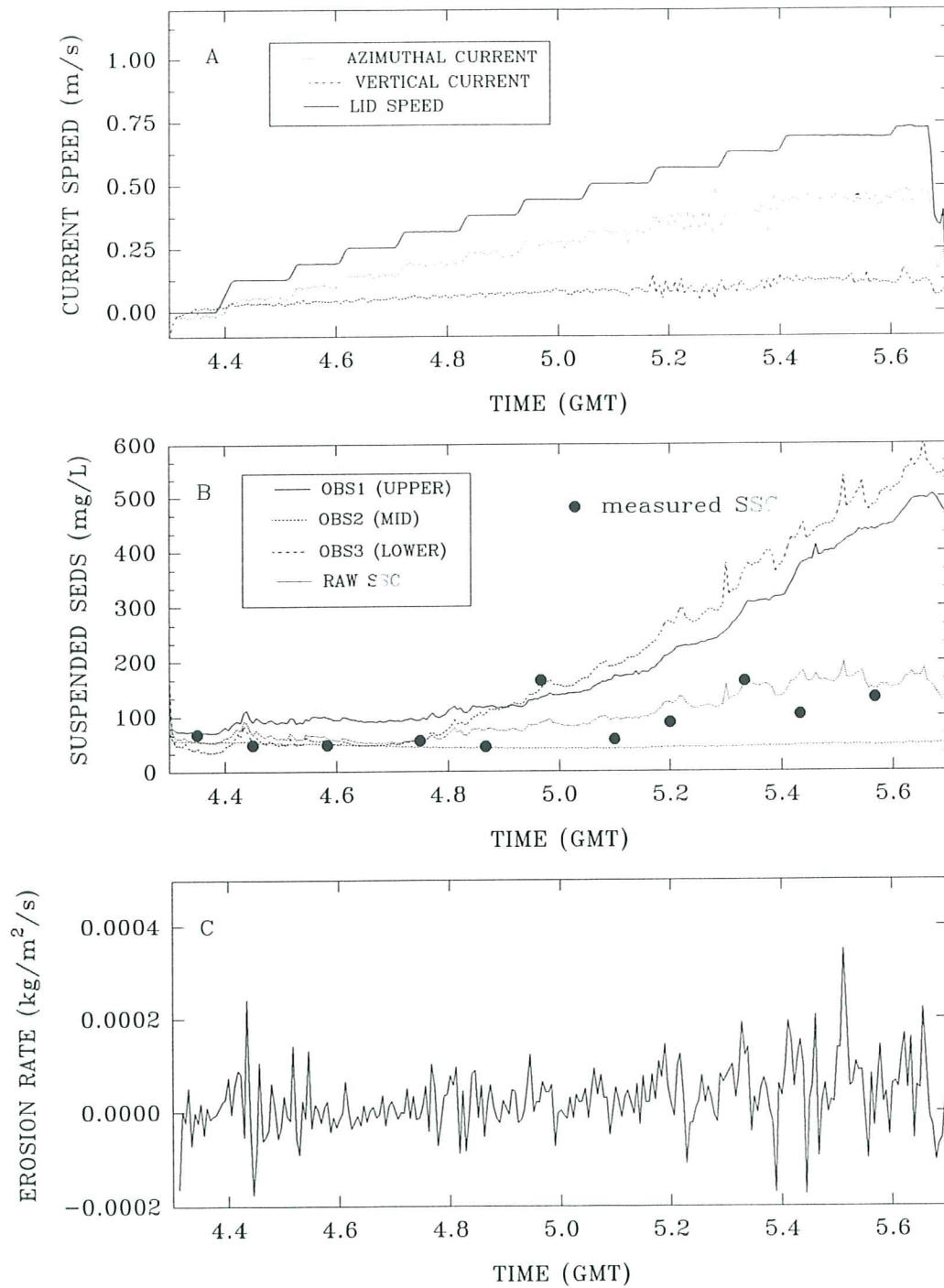


Figure 6.5.1.1. A time-series plot of results from Sea Carousel recorded at site C/D (LISPUK7) on 10 April, 1995. (A) lid speed and azimuthal and vertical currents at the reference height (0.18 m); (B) suspended sediment concentrations from the three OBS sensors (OBS1 and OBS3 are internal, OBS2 is external), and from pumped samples; and (C) erosion rate.

STATION LISPUK7, SITE C/D - 10 APRIL, 1995

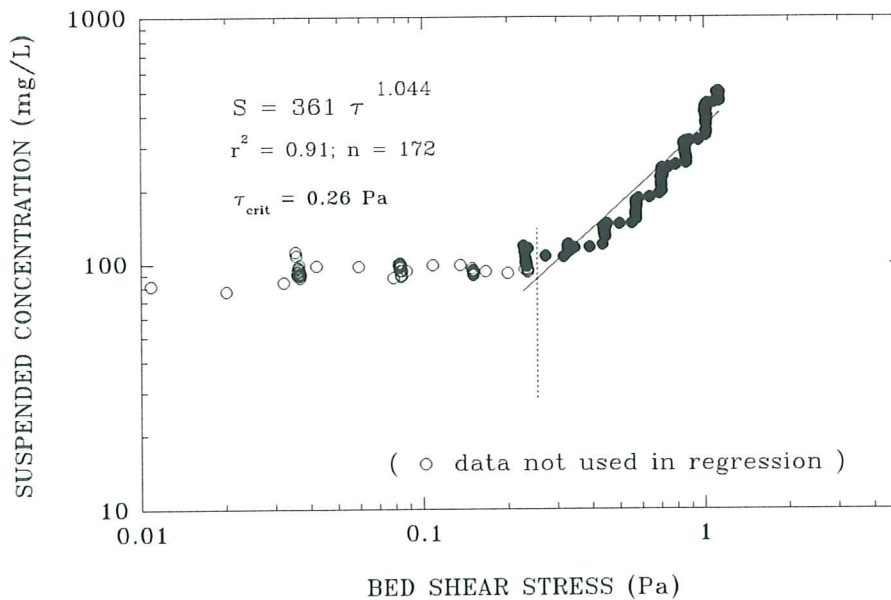
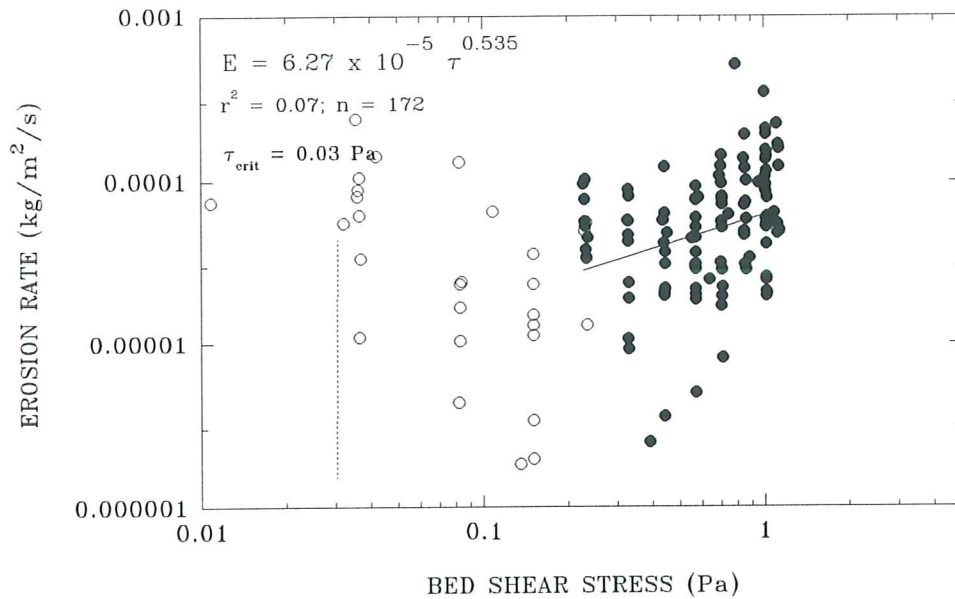


Figure 6.5.1.3. Estimates of the erosion threshold for deployment LISPUK7, site C/D. The upper panel shows that erosion rate is a power function of applied bed stress; the estimated erosion threshold is 0.03 Pa. The lower panel shows that suspended sediment concentration increases as a power function of applied bed shear stress; the threshold is equated with the stress at ambient concentration and yields a value of 0.26 Pa.

LISPUK - SITE C/D, Humber estuary

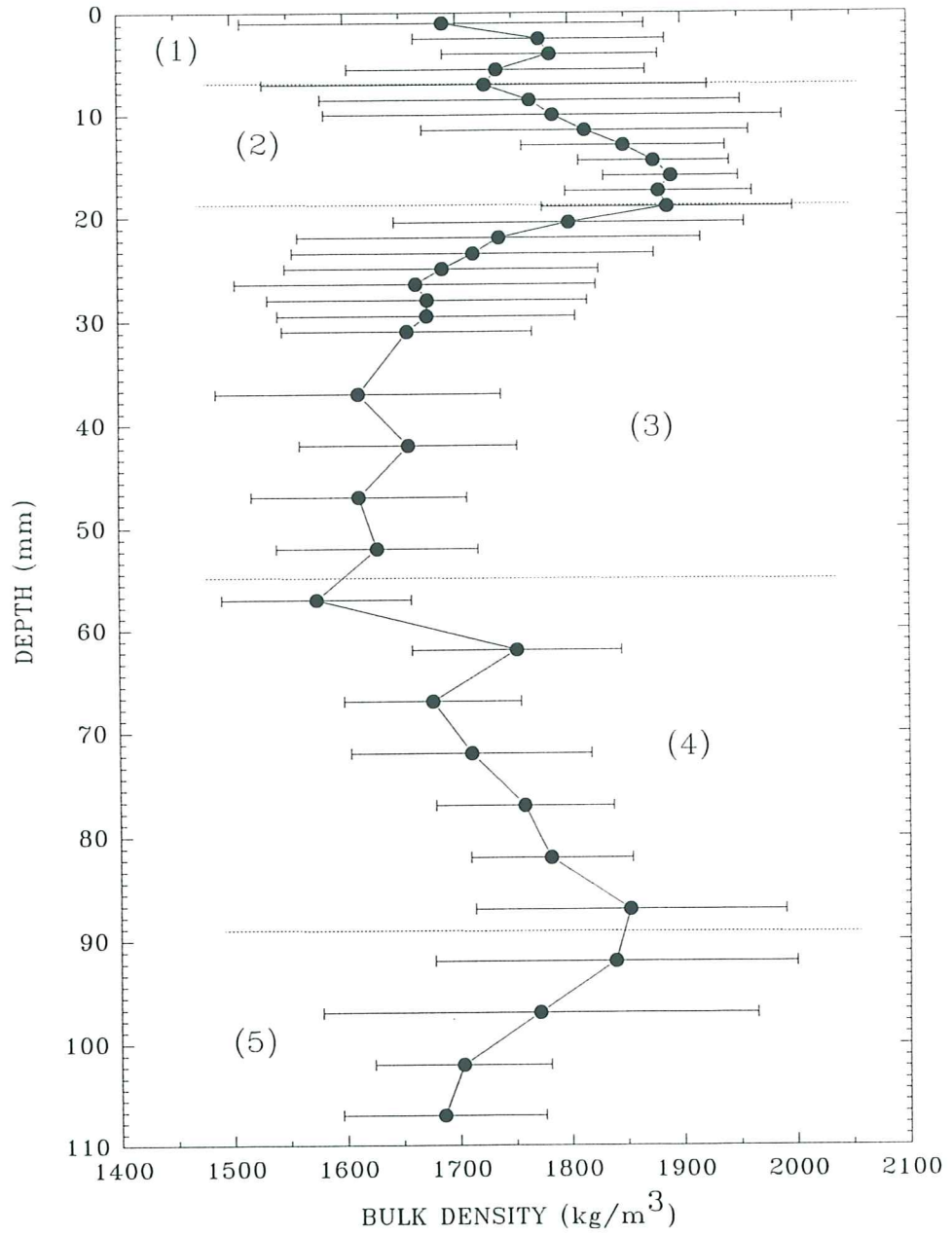


Figure 6.5.2.1. A log of the wet-weight bulk density derived from a Catscan analysis of a syringe core collected at site C/D. Five layers are evident reflecting layering of the substrate.

SEA CAROUSEL - LISPUK01 (Humber estuary)

SITE D - 8 APRIL, 1995

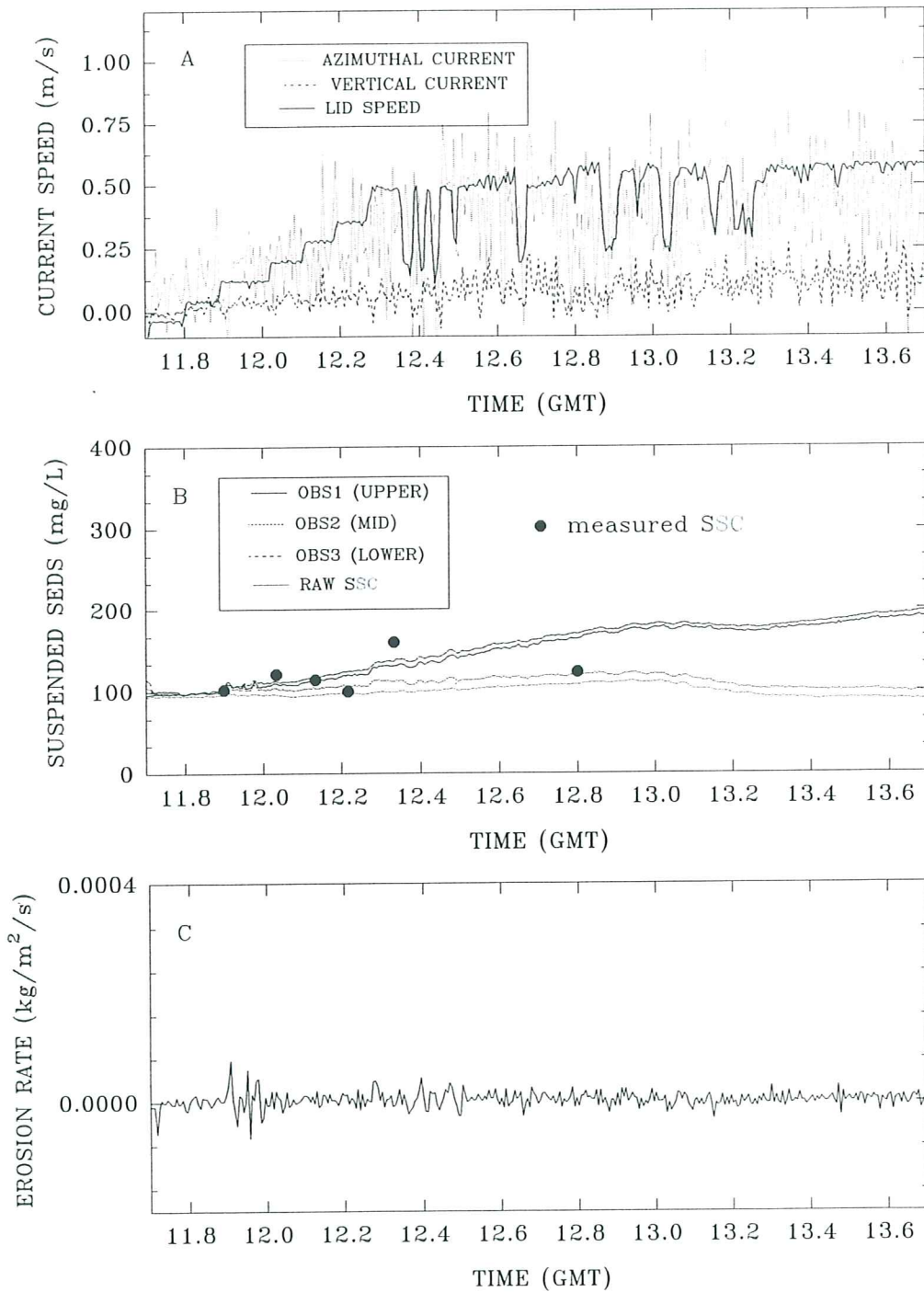


Figure 6.6.1.1. A time-series plot of results from Sea Carousel recorded at site D (LISPUK1) on 8 April, 1995. (A) lid speed and azimuthal and vertical currents at the reference height (0.18 m); (B) suspended sediment concentrations from the three OBS sensors (OBS1 and OBS3 are internal, OBS2 is external), and from pumped samples; and (C) erosion rate. This station was on the side of a creek at a high angle, hence the scatter in the results.

SEA CAROUSEL – LISPUK02 (Humber estuary)

SITE D – 8 APRIL, 1995

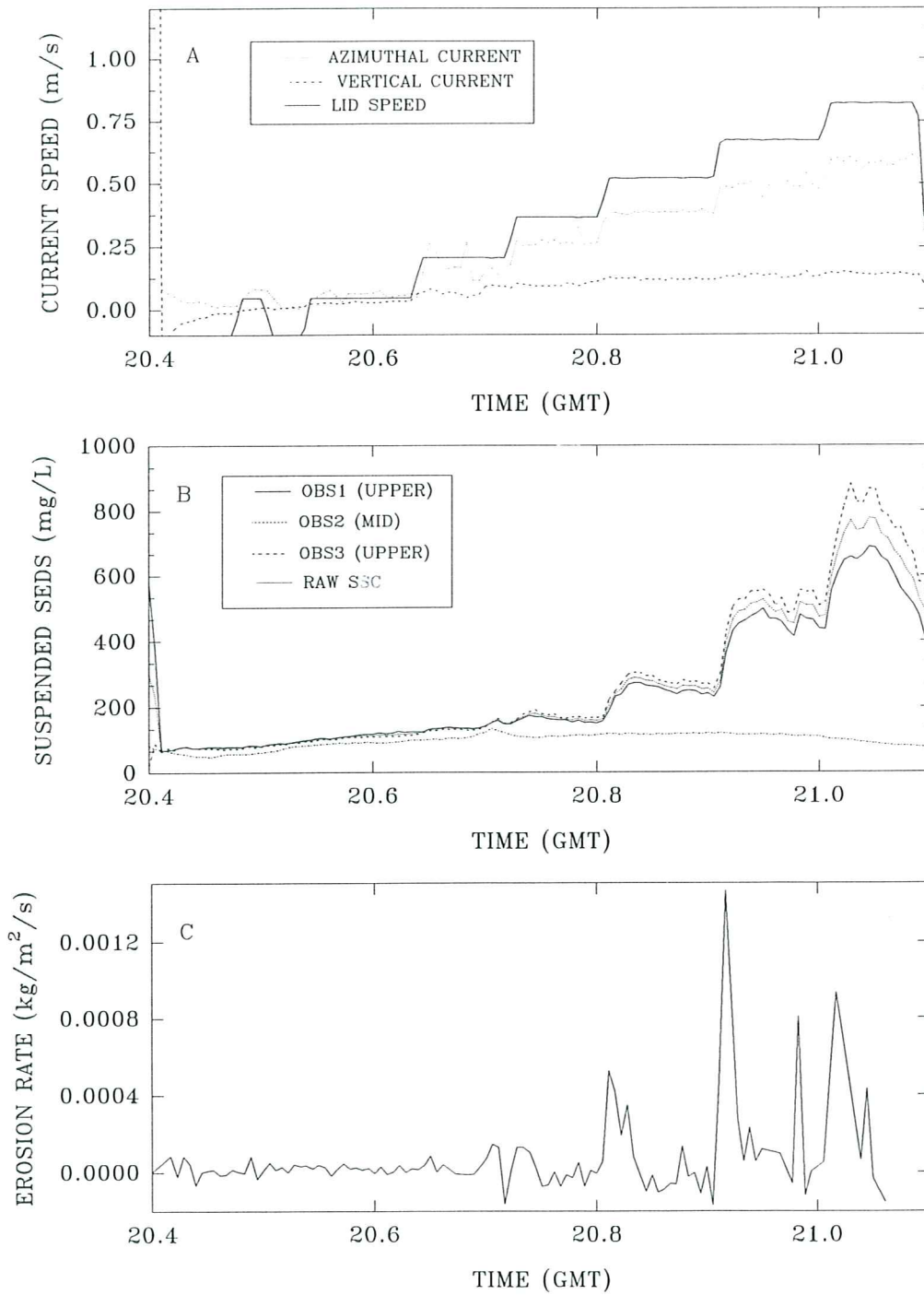


Figure 6.6.1.2. A time-series plot of results from Sea Carousel recorded at site D (LISPUK2) on 8 April, 1995. (A) lid speed and azimuthal and vertical currents at the reference height (0.18 m); (B) suspended sediment concentrations from the three OBS sensors (OBS1 and OBS3 are internal, OBS2 is external); and (C) erosion rate. Notice the Type I erosion rates.

SEA CAROUSEL – LISPUK03 (Humber estuary)

SITE D – 10 APRIL, 1995

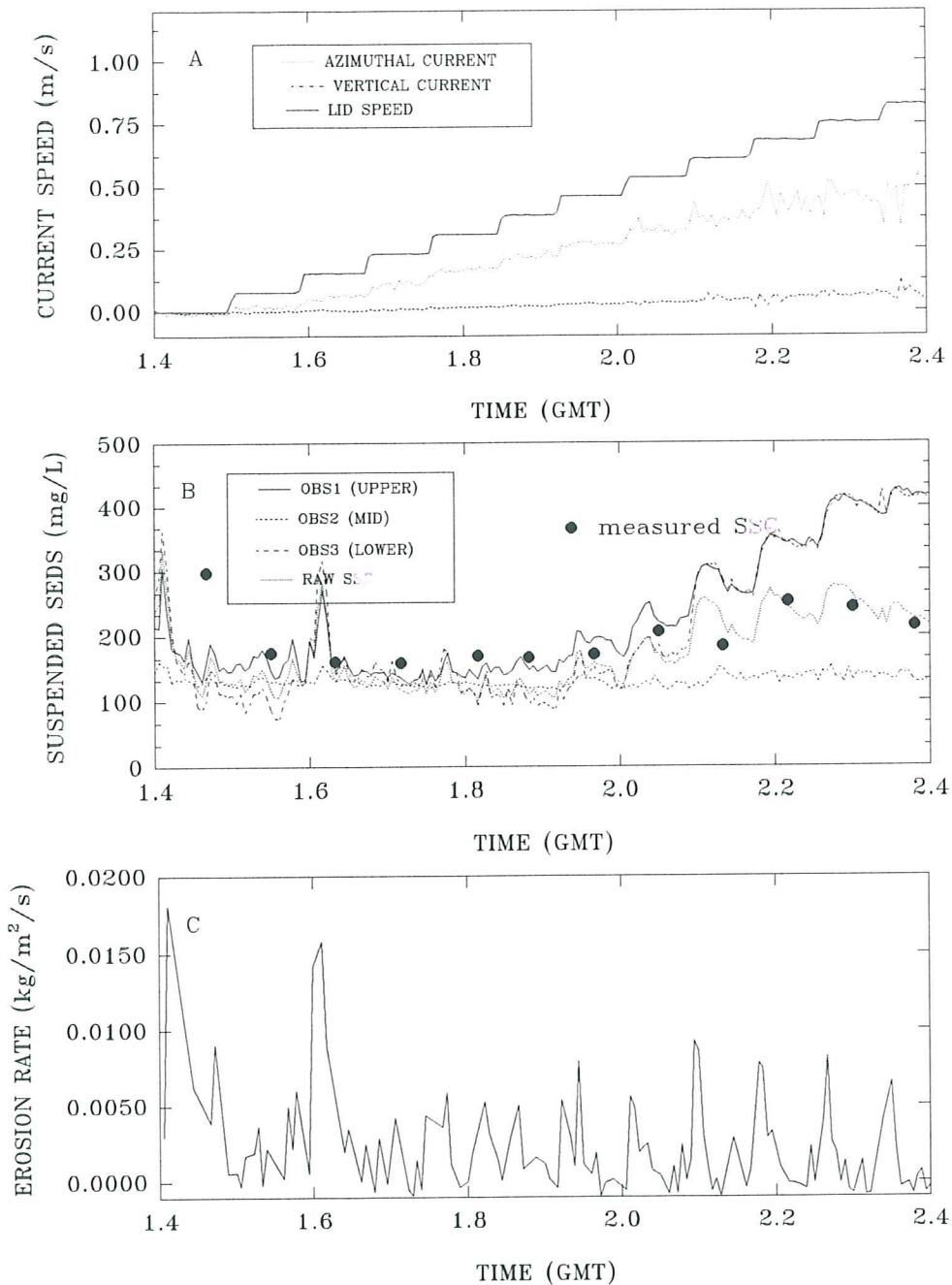


Figure 6.6.1.3. A time-series plot of results from Sea Carousel recorded at site D (LISPUK3) on 10 April, 1995. (A) lid speed and azimuthal and vertical currents at the reference height (0.18 m); (B) suspended sediment concentrations from the three OBS sensors (OBS1 and OBS3 are internal, OBS2 is external), and from pumped samples; and (C) erosion rate. Type I erosion is prevalent throughout the erosion phase.

SEA CAROUSEL – LISPUK04 (Humber estuary)

SITE D – 10 APRIL, 1995

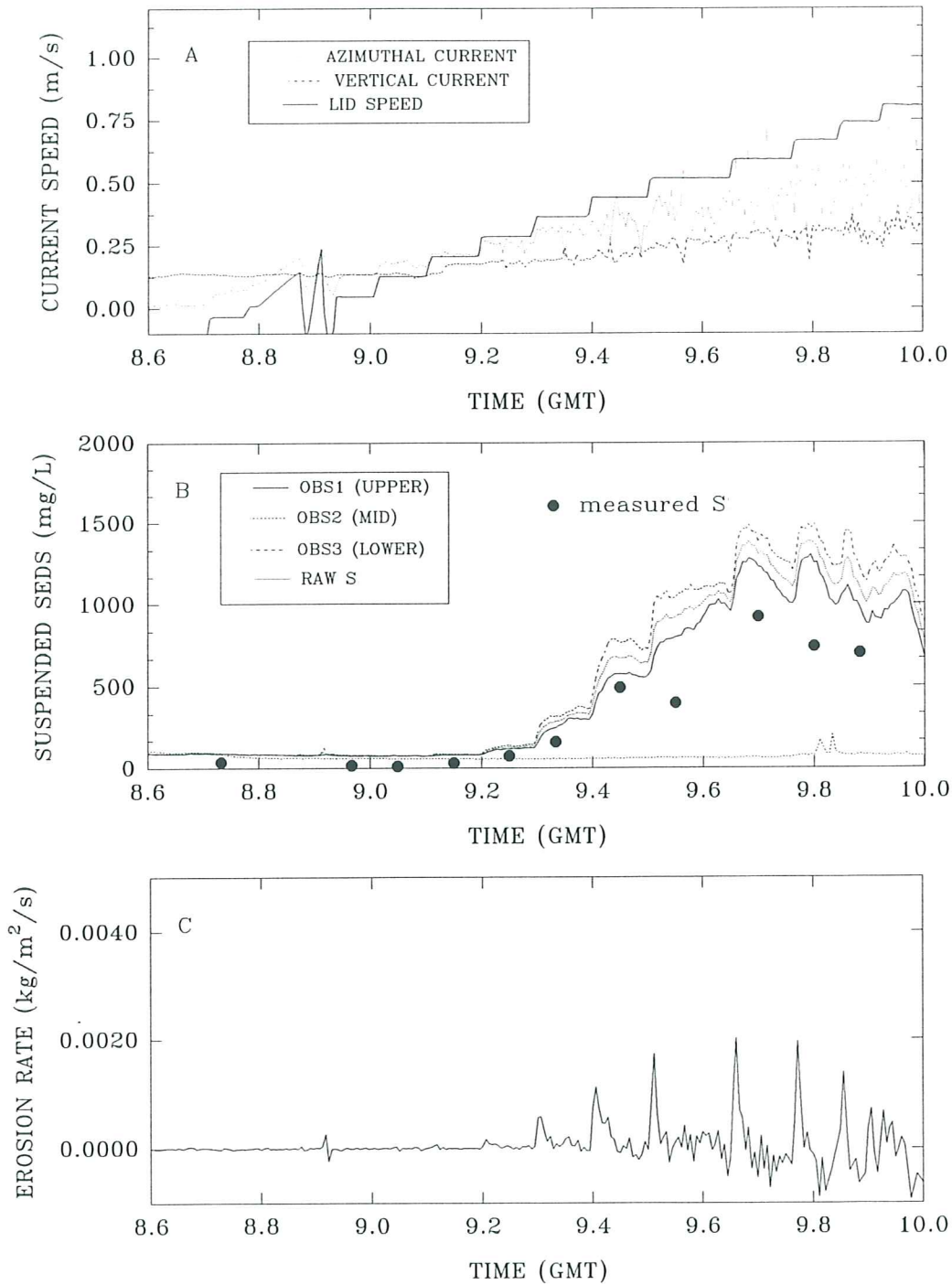


Figure 6.6.1.4. A time-series plot of results from Sea Carousel recorded at site D (LISPUK3) on 10 April, 1995. (A) lid speed and azimuthal and vertical currents at the reference height (0.18 m); (B) suspended sediment concentrations from the three OBS sensors (OBS1 and OBS3 are internal, OBS2 is external), and from pumped samples; and (C) erosion rate. Type I erosion is prevalent throughout the erosion phase.

STATION LISPUK2, SITE D - 8 APRIL, 1995

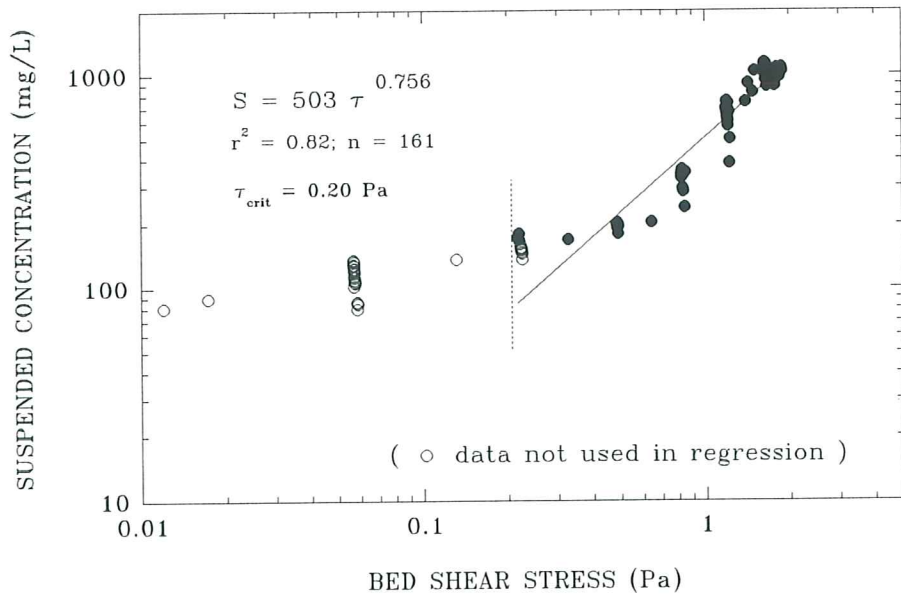
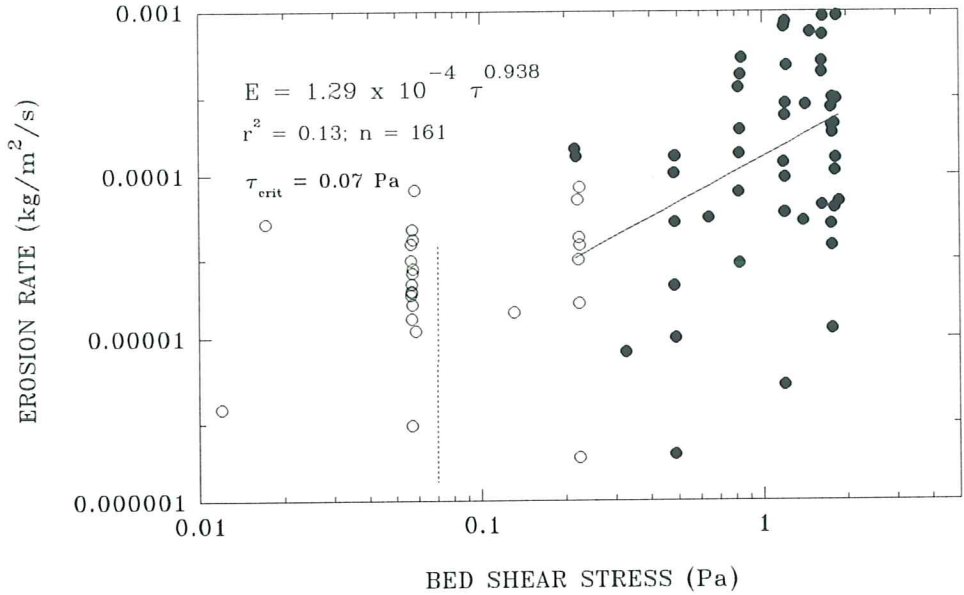


Figure 6.6.1.5. Estimates of the erosion threshold for deployment LISPUK2, site D. The upper panel shows that erosion rate is a power function of applied bed stress; the estimated erosion threshold is 0.07 Pa. The lower panel shows that suspended sediment concentration increases as a power function of applied bed shear stress; the threshold is equated with the stress at ambient concentration and yields a value of 0.20 Pa.

STATION LISPUK3, SITE D - 10 APRIL, 1995

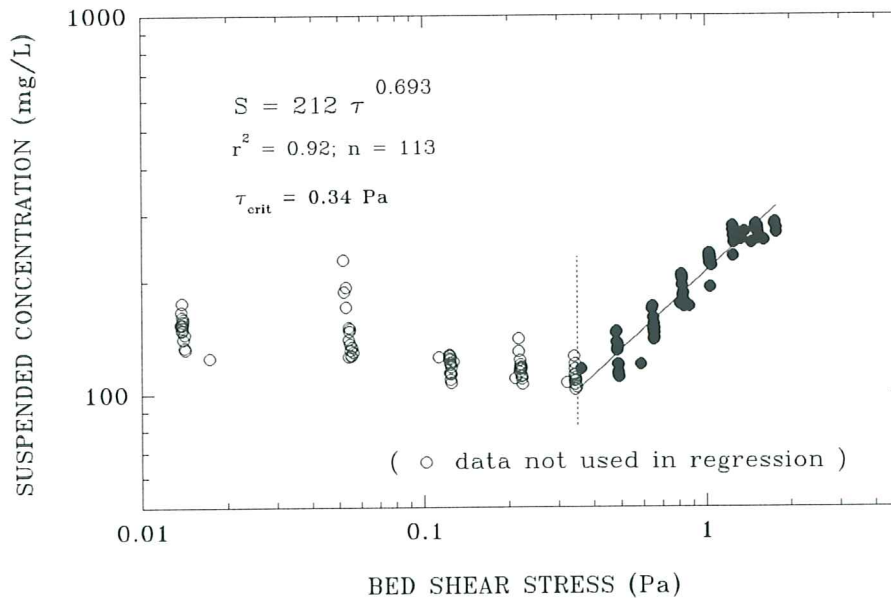
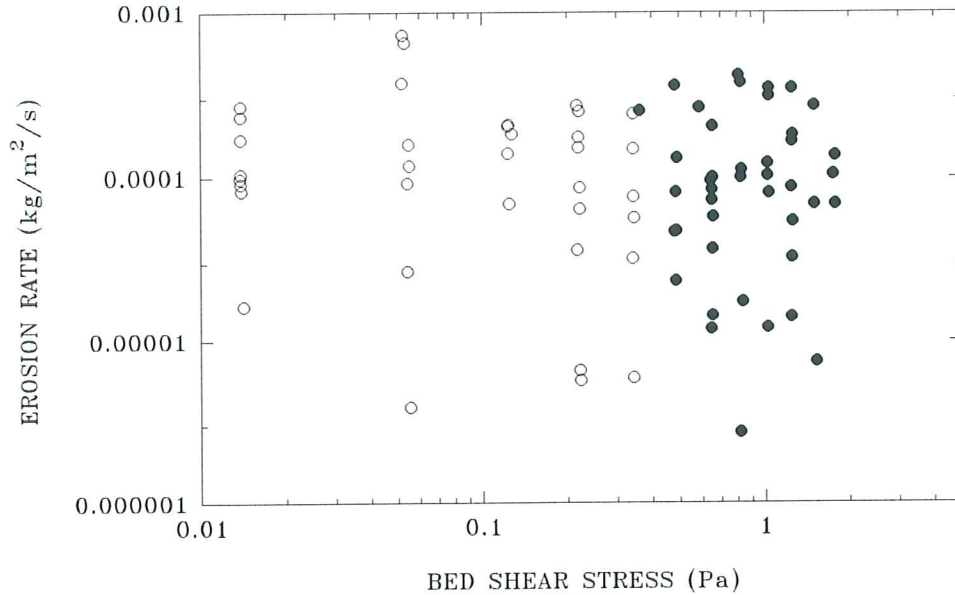


Figure 6.6.1.6. Estimates of the erosion threshold for deployment LISPUK2, site D. The upper panel shows that erosion rate is a power function of applied bed stress; it is not possible to estimate erosion threshold from this plot. The lower panel shows that suspended sediment concentration increases as a power function of applied bed shear stress; the threshold is equated with the stress at ambient concentration and yields a value of 0.34 Pa.

STATION LISPUK4, SITE D - 10 APRIL, 1995

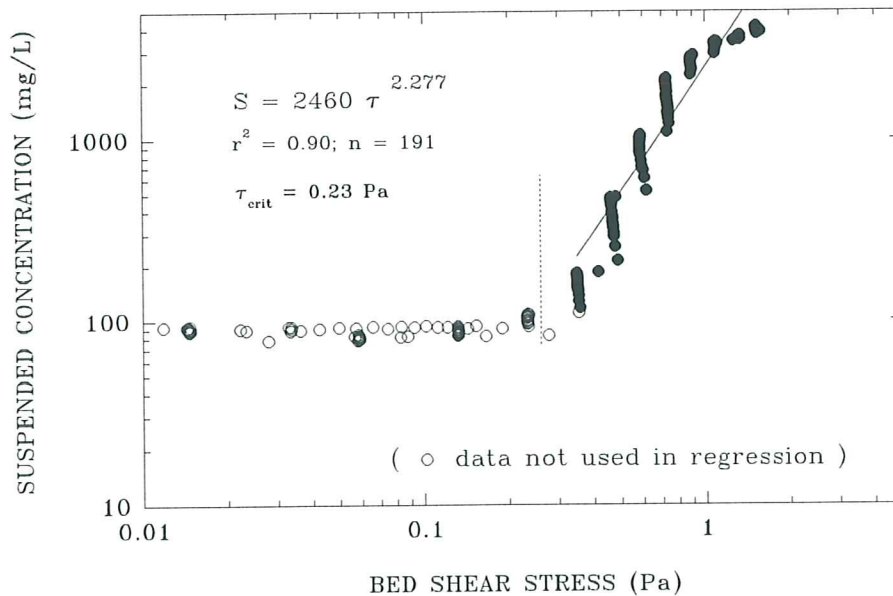
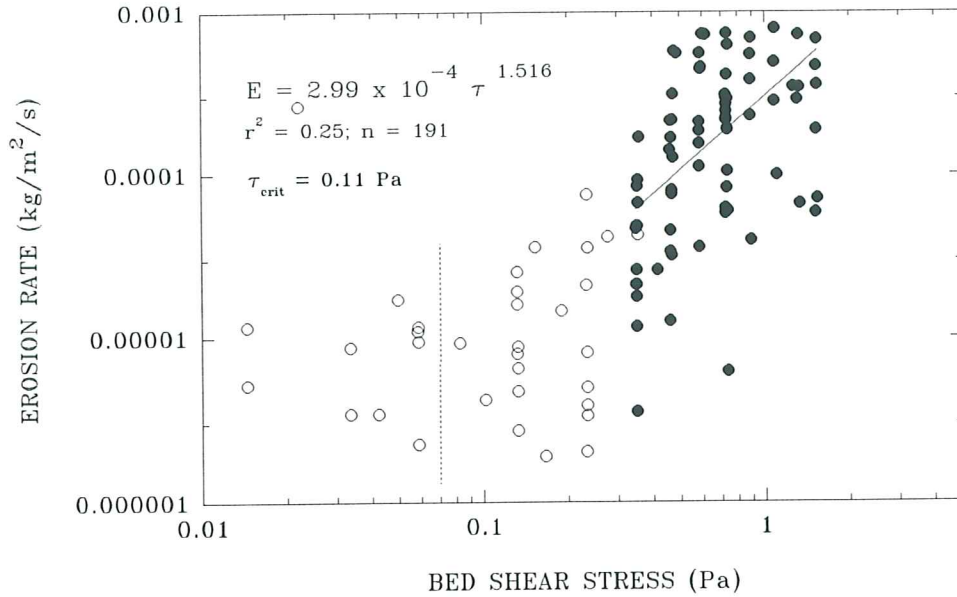


Figure 6.6.1.7. Estimates of the erosion threshold for deployment LISPUK4, site D. The upper panel shows that erosion rate is a power function of applied bed stress; the estimated erosion threshold is 0.11 Pa. The lower panel shows that suspended sediment concentration increases as a power function of applied bed shear stress; the threshold is equated with the stress at ambient concentration and yields a value of 0.23 Pa.

LAB CAROUSEL – LISPUK (Humber estuary)

SITE D (LABEXP6) – 13 APRIL, 1995

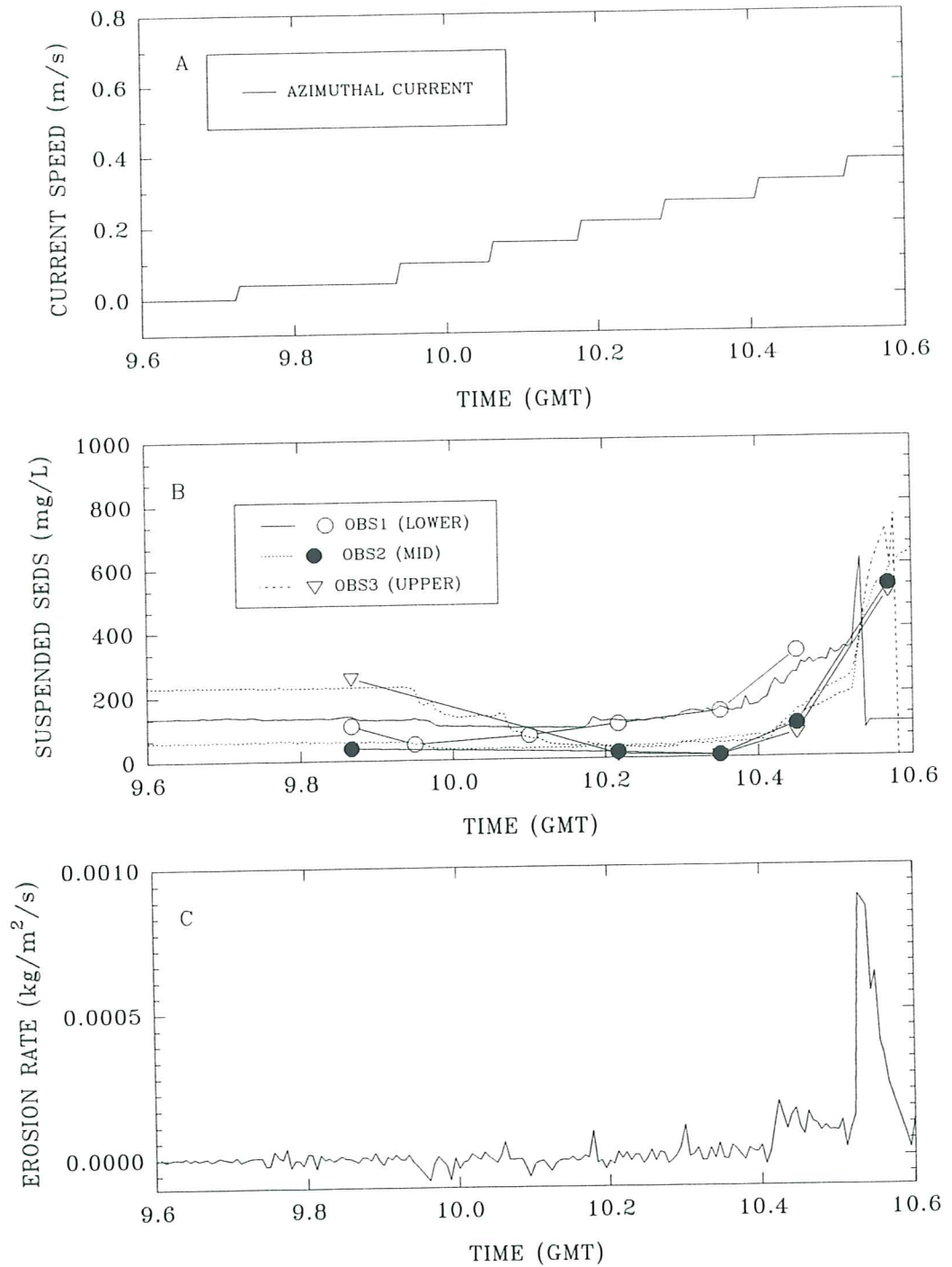


Figure 6.6.2.1. A time-series of Laboratory Carousel experiment (Labexp6) on a site D bulk sample. (A) the azimuthal reference current for a height of 0.18 m above the bed (based on lid rotation); (B) suspended sediment concentration from three OBS's and pumped samples at heights of 0.03, 0.10, and 0.20 m above the base; and (C) erosion rate.

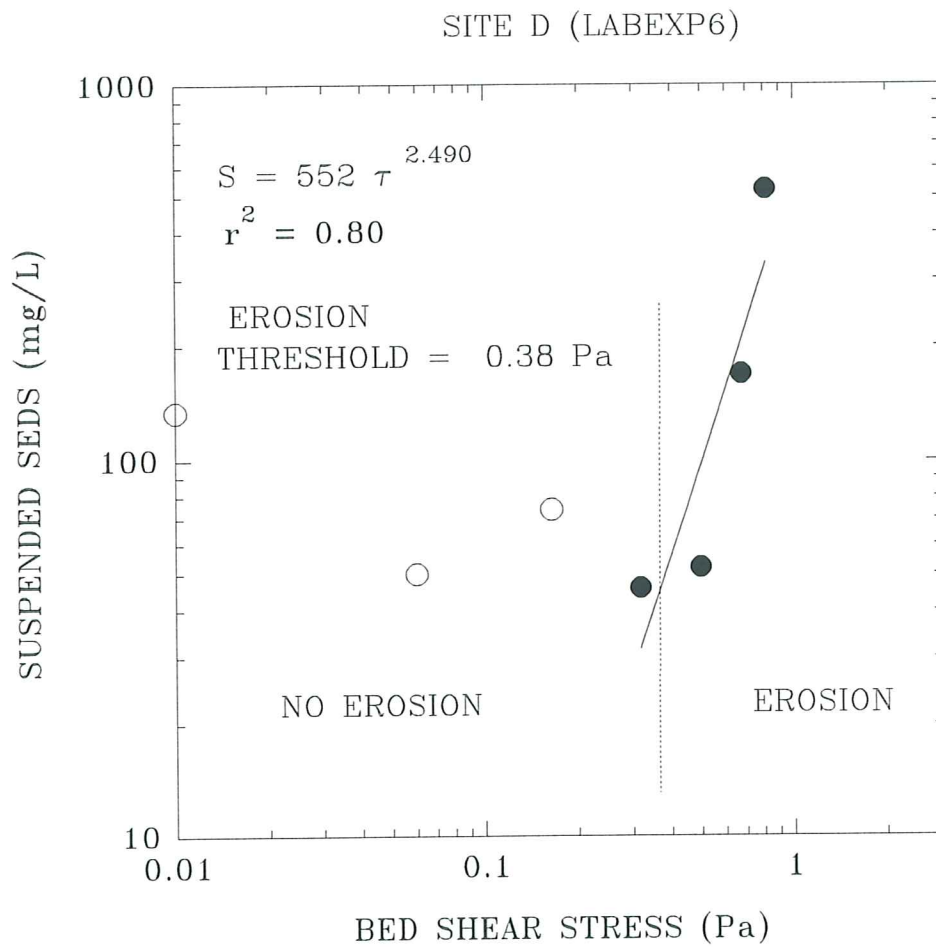


Figure 6.6.2.2. A plot of measured suspended sediment concentration (from pumped samples) versus applied bed shear stress in Lab Carousel for experiment Labexp6 (site D) . Notice the onset of erosion at 0.38 Pa which is based on the extrapolation of concentration to ambient levels.

LISPUK - SITE D, Humber estuary

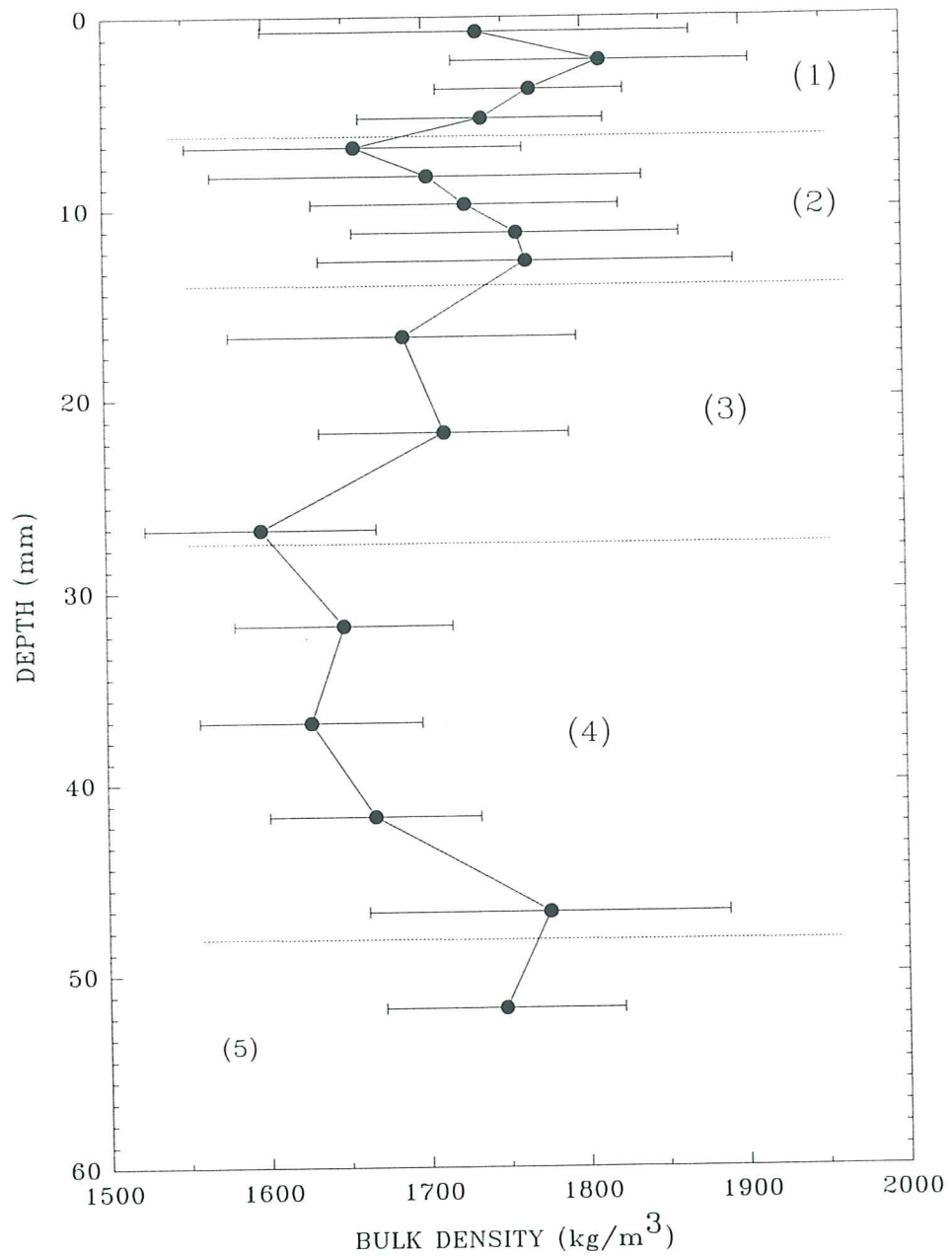


Figure 6.6.3.1. A log of the wet-weight bulk density derived from a Catscan analysis of a syringe core collected at site C/D. Five layers are evident reflecting layering of the substrate. Notice the general reduction in density with depth.

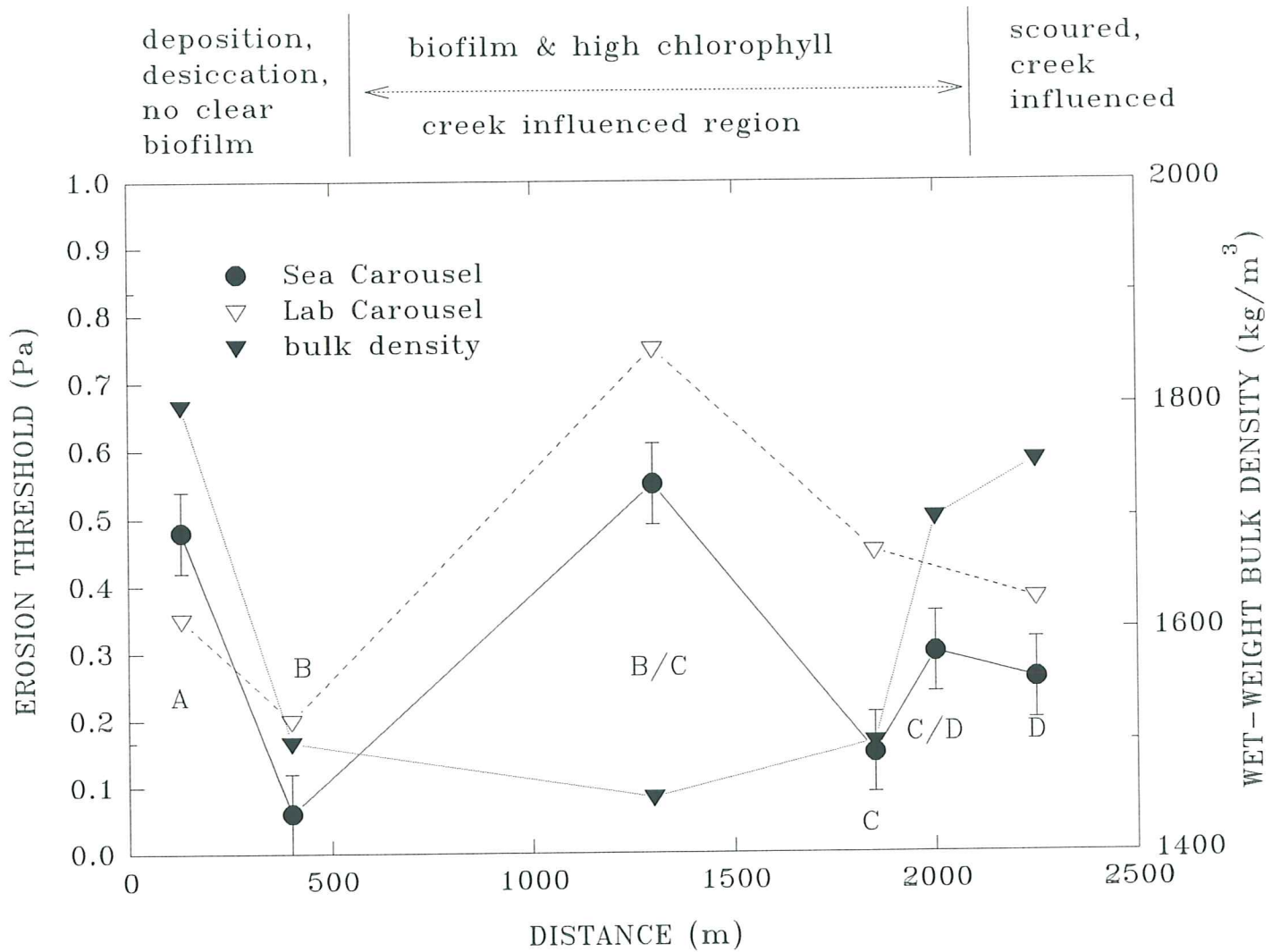


Figure 7.1.1. A summary plot showing erosion threshold from Sea Carousel and surface wet-weight bulk density against distance across the mudflat transect. Notice the three maxima: the largest on the central mudflat (site B/C); the second on the inner mudflat (site A); and the third on the outer mudflat (site D).

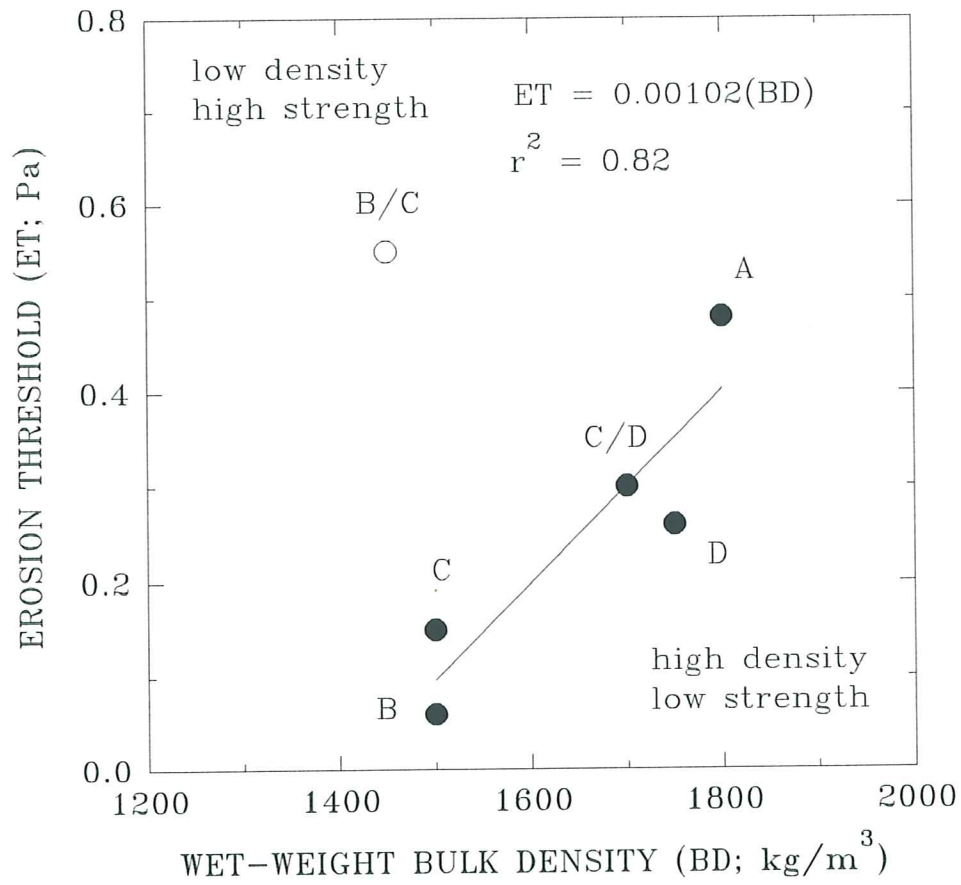


Figure 7.1.2. A scattergram of wet-weight bulk density and erosion threshold from Sea Carousel for the six sites of this study. Notice that site B/C is anomalously stable, presumably due to biostabilization.

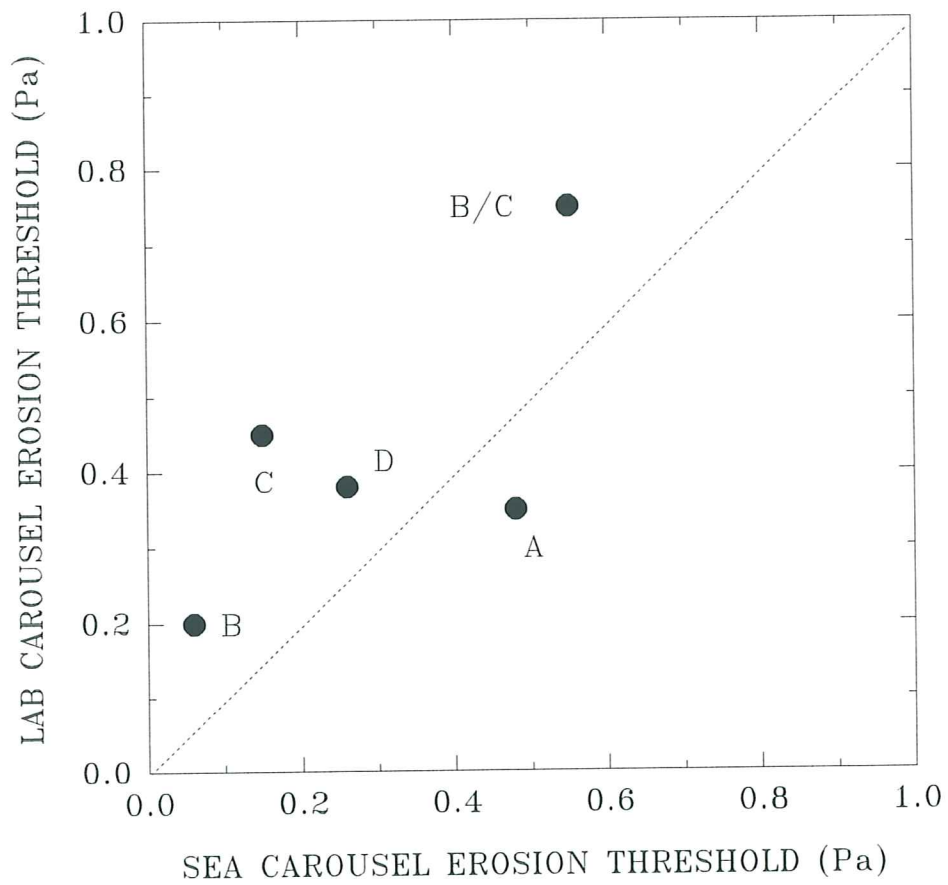


Figure 7.2.1. A comparison between erosion thresholds derived from the Sea Carousel and Lab Carousel for the six sites examined in this study. In general Lab Carousel yielded higher values than Sea Carousel. The exception is site B/C where biostabilization dominated the field signal.

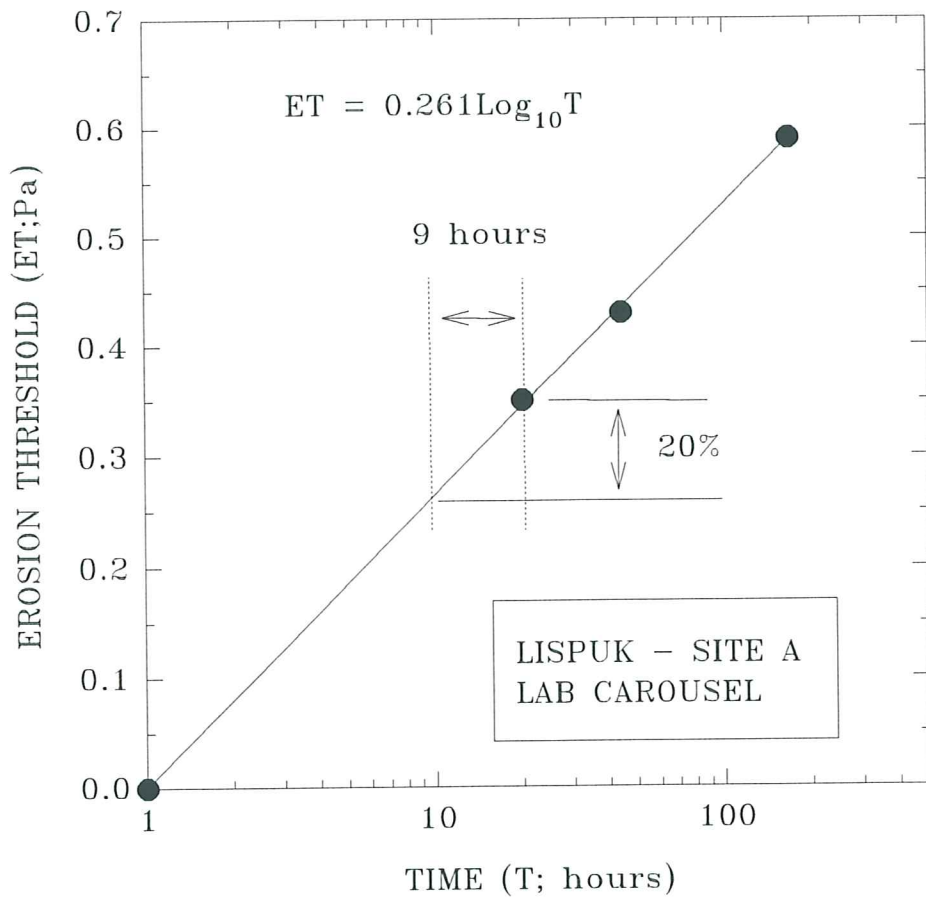


Figure 7.2.2. The effect of consolidation time on erosion threshold of site A sediment deposited in Lab Carousel. The figures shows that a 20% reduction in threshold would result if the time of consolidation was reduced from 24 to 11 hours.

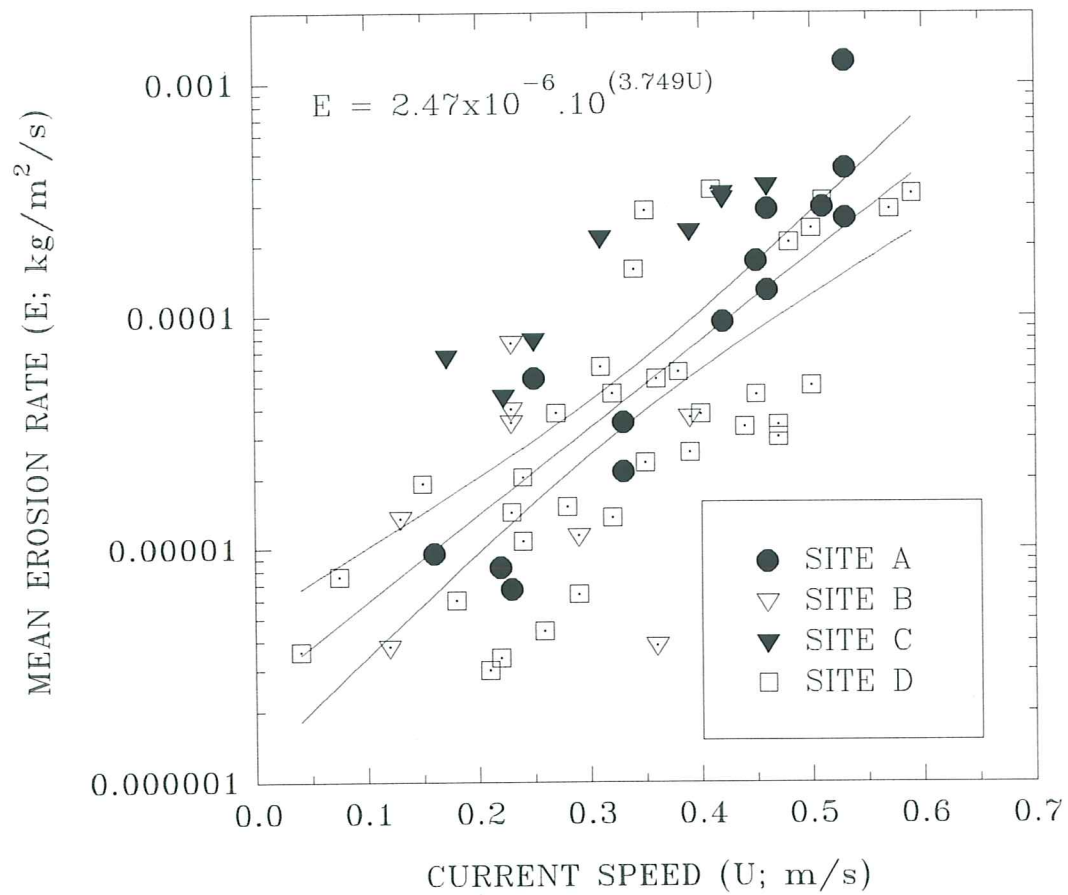


Figure 7.3.1. A regression analysis of mean erosion rate on current speed from data obtained from Sea Carousel. Results show that a single exponential function suffices for all sites.

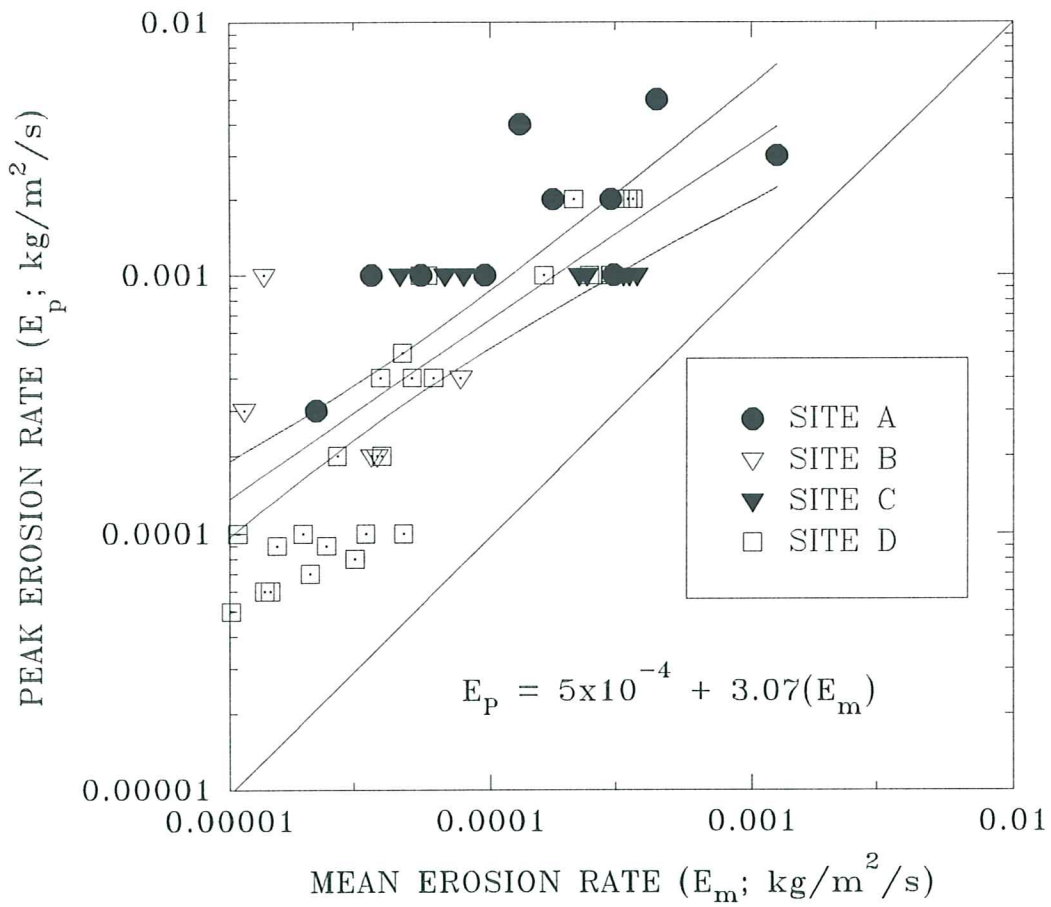


Figure 7.3.2. A correlation between mean erosion rate and peak erosion rate derived from Sea Carousel. Results show that all sites show a similar relationship which can be expressed by a simple linear equation.

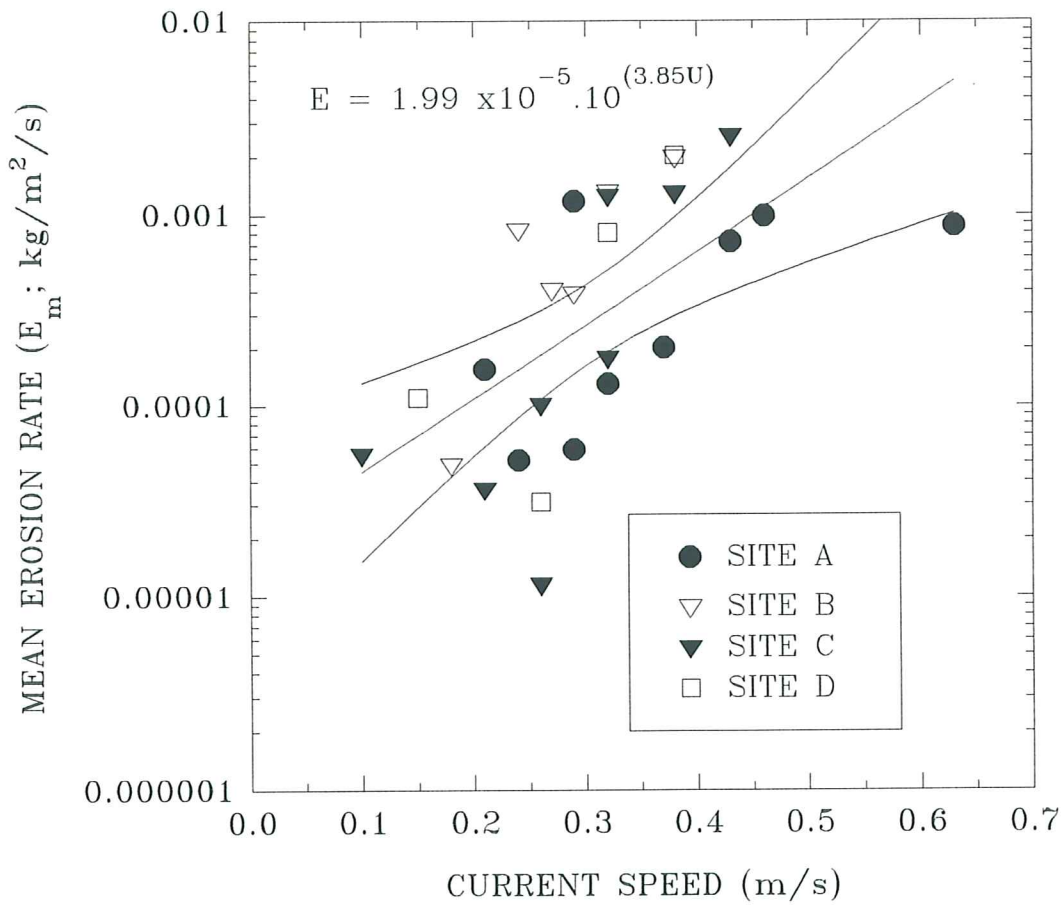


Figure 7.4.1. A regression analysis of mean erosion rate on current speed from data obtained from Lab Carousel. Results show that a single exponential function suffices for all sites. The equation is similar to that derived for Sea Carousel (see Figure 7.3.1) though more scatter prevails.

Table 6.3. Biological sediment characteristics at each Sea Carousel deployment site.

Sea Carousel Station	Site	Water Content (%)	Organic Content (%)	Chlorophyll <i>a</i> ($\mu\text{gm}/\text{gm}$ dry sed.)	Dissolved Carbohydrates (mg/gm dry sed.)	Bacteria Numbers ($10^3/\text{gm}$ dry sed.)	Nematode Numbers ($/\text{gm}$ dry sed.)
1	D	-	-	1.9	0.042	358,394	298
3	D	32.4	4.3	4.7	0.034	166,182	280
4	D	34.0	6.2	4.1	0.042	339,247	162
5	C	34.9	8.4	10.4	0.066	310,280	197
6	C	45.2	9.4	6.6	0.068	608,240	573
7	CD	32.8	5.4	25.2	0.107	623,544	933
8	CD	27.6	4.6	8.0	0.069	705,537	106
9	BC	27.9	4.3	26.4	0.188	-	580
13	A	28.7	6.0	12.0	0.087	244,319	69
14	A	35.3	5.9	12.3	0.094	584,067	92
17	B	41.1	10.2	12.9	0.045	511,057	60
19	B	31.1	8.3	19.4	0.051	670,538	104

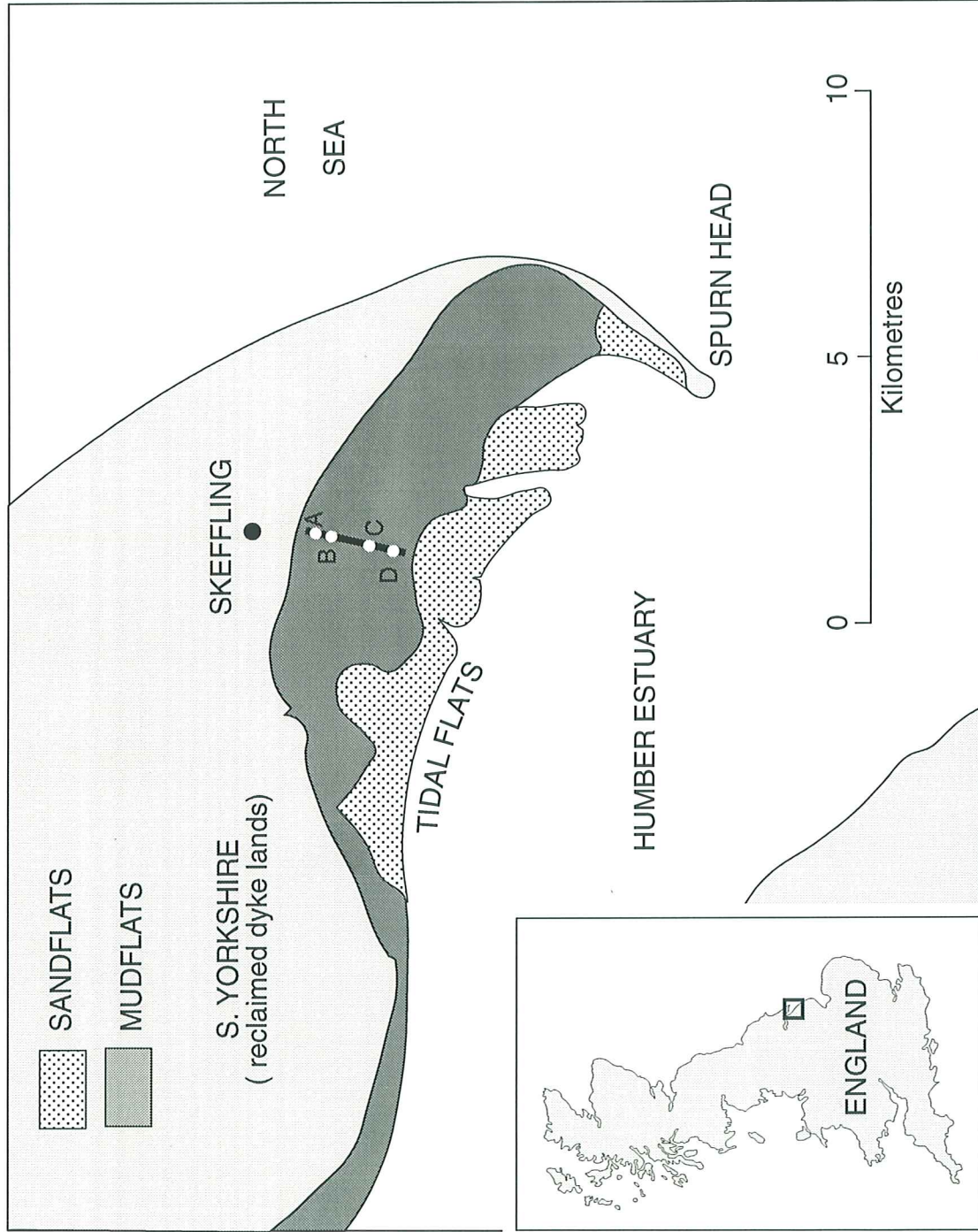


Figure 1.1. A location diagram of the study region, Humber estuary, S. Yorkshire, England. The intertidal transect was located across the mudflats off Skeffling on the northern flank of the estuary.

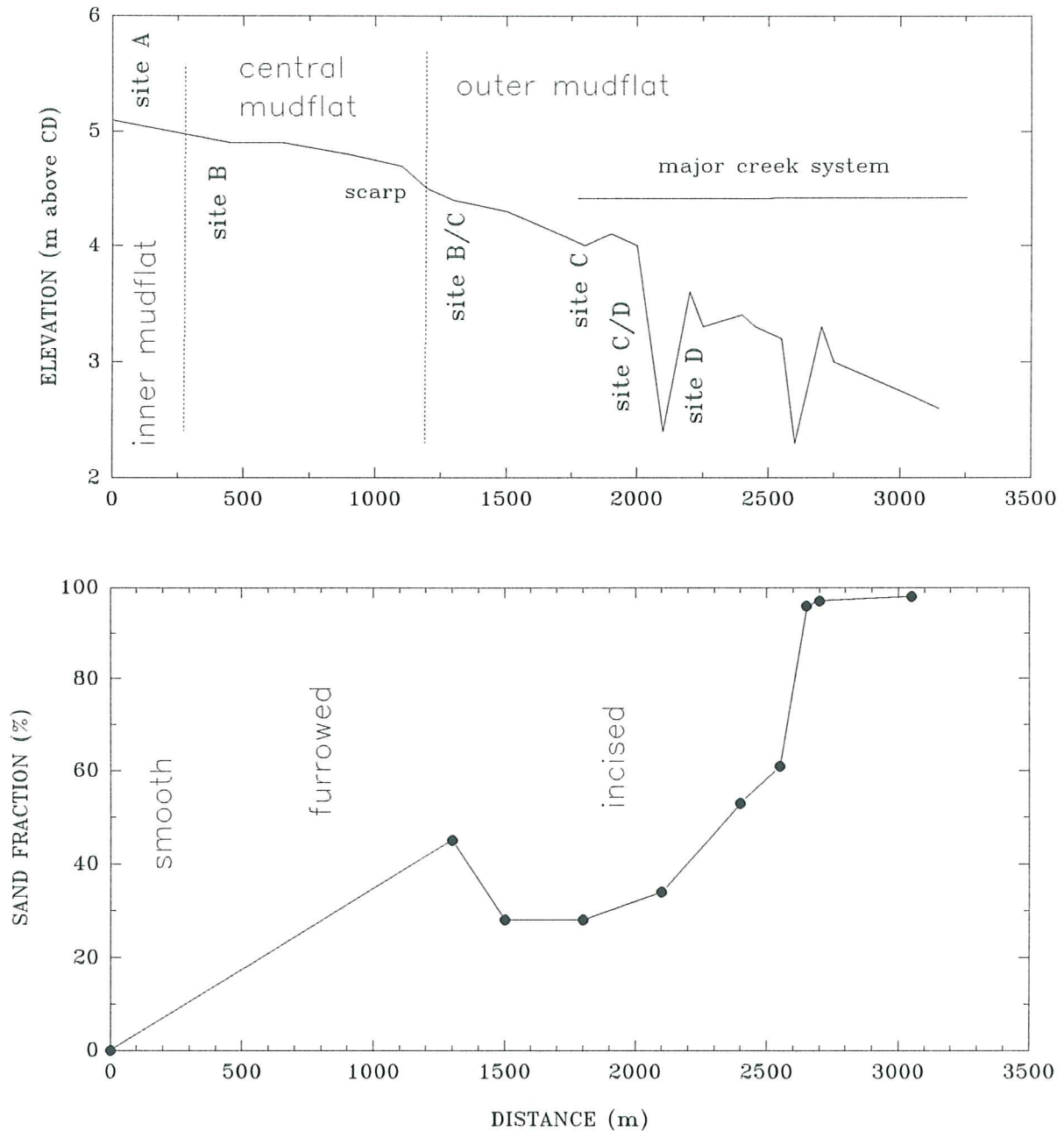


Figure 1.2. A transect of the Skeffling mudflat profile. The stations occupied in this study are marked to show distance from the shoreline and elevation relative to Chart Datum (CD). The sand content of seabed samples taken along the transect is also shown (after K. Black, unpublished data).

GRAIN SIZE

SediGraph 5100 V2.02

PAGE 1

SAMPLE DIRECTORY/NUMBER: SVLHUM /3

UNIT NUMBER: 1

SAMPLE ID: SITE D SURFACE

START 13:12:17 09/19/95

SUBMITTER: UWCC EARTH SCIENCES

REPT 13:22:59 09/19/95

OPERATOR: J.HERNIMAN

TOT RUN TIME 0:03:56

SAMPLE TYPE: CLAY

SAM DENS: 2.7500 g/cc

LIQUID TYPE: Water

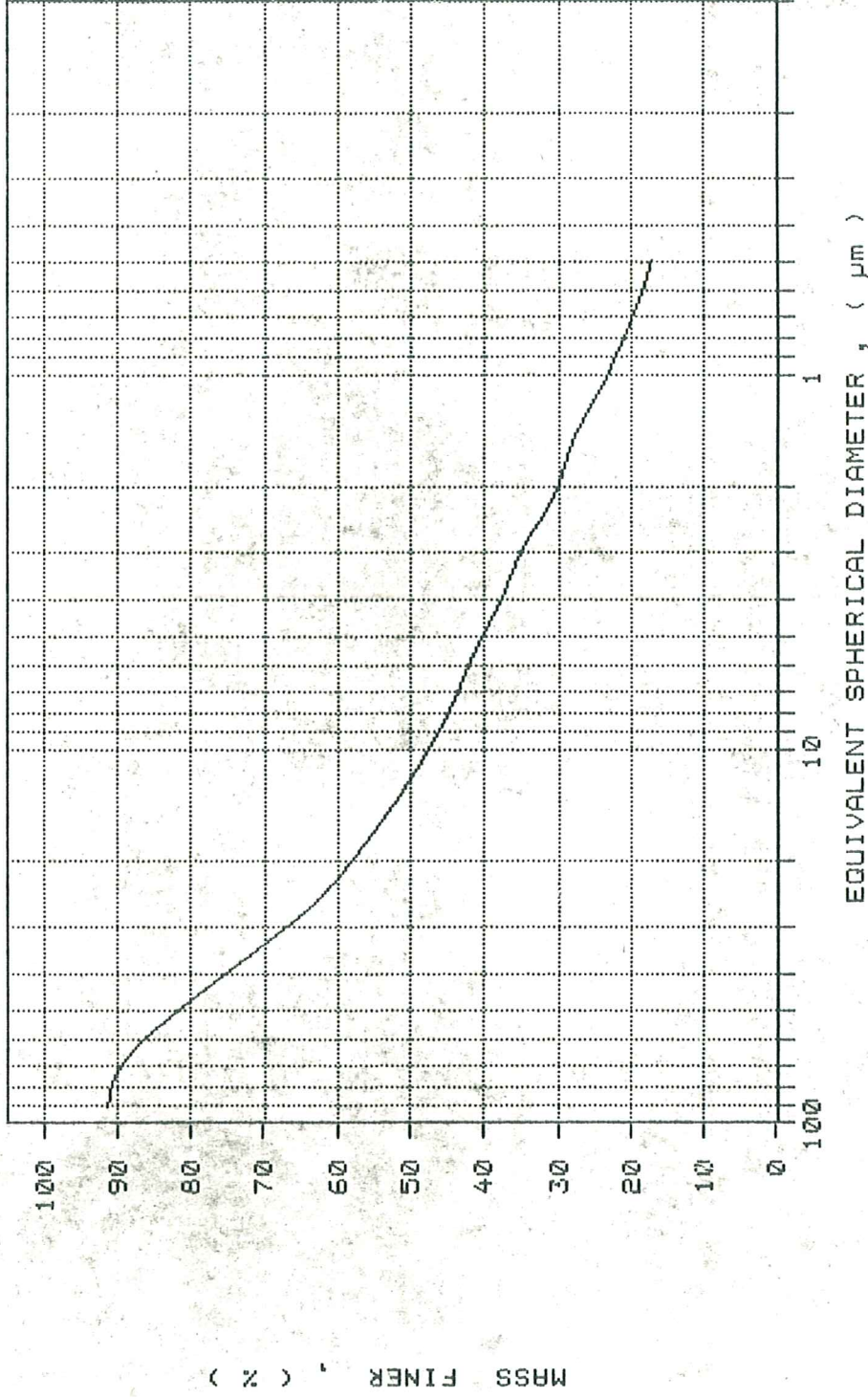
LIQ DENS: 0.9942 g/cc

ANALYSIS TEMP: 34.7 deg C

RUN TYPE: High Speed

LIQ VISC: 0.7268 cp

CUMULATIVE MASS PERCENT FINER VS. DIAMETER



GRAIN SIZE

SediGraph 5100 V2.02

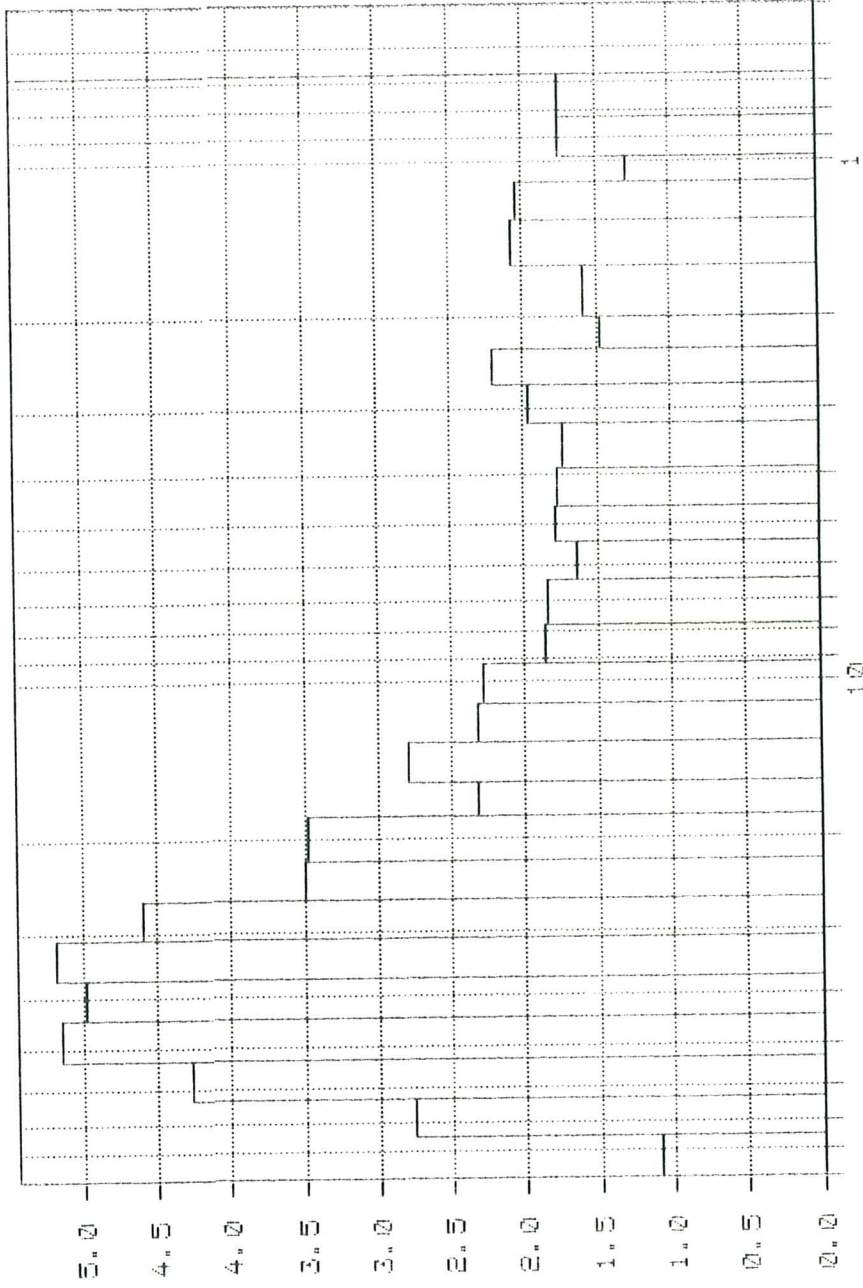
PAGE 2

SAMPLE DIRECTORY/NUMBER: SVLHUM /3
 SAMPLE ID: SITE D SURFACE
 SUBMITTER: UWCC EARTH SCIENCES
 OPERATOR: J.HERNIMAN
 SAMPLE TYPE: CLAY
 LIQUID TYPE: water
 ANALYSIS TEMP: 34.7 deg C

UNIT NUMBER: 1
 START 13:12:17 09/19/95
 REPT 13:16:30 09/19/95
 TOT RUN TIME 0:03:56
 SAM DENS: 2.7500 g/cc
 LIQ DENS: 0.9942 g/cc
 LIQ VISC: 0.7268 cP

RUN TYPE: High Speed

MASS POPULATION VS. DIAMETER



MASS (x 10^4 in total vol)

EQUIVALENT SPHERICAL DIAMETER, (μm)

SAMPLE DIRECTORY/NUMBER: SVLHUM /3
 SAMPLE ID: SITE D SURFACE
 SUBMITTER: UWCC EARTH SCIENCES
 OPERATOR: J.HERNIMAN
 SAMPLE TYPE: CLAY
 LIQUID TYPE: Water
 ANALYSIS TEMP: 34.7 deg C RUN TYPE: High Speed

UNIT NUMBER: 1
 START 13:12:17 09/19/95
 REPT 13:16:30 09/19/95
 TOT RUN TIME 0:03:56
 SAM DENS: 2.7500 g/cc
 LIQ DENS: 0.9942 g/cc
 LIQ VISC: 0.7260 cp

STARTING DIAMETER: 90.00 μ m
 ENDING DIAMETER: 0.50 μ m

REYNOLDS NUMBER: 1.31
 FULL SCALE MASS %: 93

MEDIAN DIAMETER: 12.03 μ m MASS DISTRIBUTION MODAL DIAMETER: 35.29 μ m

DIAMETER (μ m)	CUMULATIVE MASS FINER (%)	MASS IN INTERVAL (%)
90.00	91.3	1.7
75.00	90.2	1.1
63.00	87.4	2.8
53.00	83.1	4.3
44.00	78.0	5.2
37.00	73.0	5.0
31.00	67.8	5.2
26.00	63.2	4.6
22.00	59.7	3.5
18.00	56.2	3.5
15.50	53.9	2.3
13.00	51.1	2.8
11.00	48.8	2.3
9.20	46.5	2.3
7.80	44.6	1.9
6.40	42.8	1.9
5.40	41.1	1.6
4.60	39.3	1.8
3.90	37.5	1.8
3.20	35.8	1.8
2.70	33.9	2.0
2.30	31.6	2.3
2.00	30.1	1.5
1.60	28.5	1.6
1.30	26.4	2.1
1.10	24.3	2.1
0.98	23.0	1.3
0.82	21.3	1.6
0.63	19.5	1.8

GRAIN SIZE

PAGE 1

SediGraph 5100 V2.02

SAMPLE DIRECTORY/NUMBER: SVLHUM /6

UNIT NUMBER: 1

SAMPLE ID: SITE A SURFACE

START 16:14:11 10/20/95

SUBMITTER: UMCC EARTH SCIENCES

REPT 16:18:45 10/20/95

OPERATOR: J.HERNIMAN

TOT RUN TIME 0:04:14

SAMPLE TYPE: CLAY

SAM DENS: 5.7500 g/cc

LIQUID TYPE: Water

LIO DENS: 0.9958 g/cc

ANALYSIS TEMP: 31.5 deg C

RUN TYPE: High Speed

LIO VISC: 0.7766 cP

STARTING DIAMETER: 90.00 μ m

REYNOLDS NUMBER: 1.15

ENDING DIAMETER: 0.50 μ m

FULL SCALE MASS %: 87

MASS DISTRIBUTION

MEDIAN DIAMETER: 27.40 μ m MODAL DIAMETER: 43.00 μ m

DIAMETER (μ m)	CUMULATIVE MASS FINER (%)	MASS IN INTERVAL (%)
90.00	83.6	3.4
75.00	81.5	2.1
63.00	77.7	3.8
53.00	72.4	5.3
44.00	65.8	6.6
37.00	59.6	6.2
31.00	53.7	5.9
26.00	48.6	5.1
22.00	44.3	4.3
18.00	39.5	4.8
15.50	36.4	3.1
13.00	33.6	2.8
11.00	31.9	1.7
9.20	30.2	1.7
7.80	28.6	1.6
6.40	27.0	1.7
5.40	25.6	1.4
4.60	24.1	1.5
3.90	22.5	1.6
3.20	21.9	1.1
2.70	20.7	0.7
2.30	19.7	1.0
2.00	18.5	1.1
1.60	17.2	1.5
1.30	16.5	0.7
1.10	15.8	0.7
0.98	15.2	0.6
0.82	14.2	1.0
0.68	13.2	1.0

SAMPLE DIRECTORY/NUMBER: SVLHUM /6
 SAMPLE ID: SITE A SURFACE
 SUBMITTER: UMCC EARTH SCIENCES
 OPERATOR: J.HERNIMAN
 SAMPLE TYPE: CLAY
 LIQUID TYPE: Water
 ANALYSIS TEMP: 31.5 deg C RUN TYPE: High Speed

UNIT NUMBER: 1
 START 16:14:11 10/20/95
 REPT 16:18:45 10/20/95
 TOT RUN TIME 0:04:14
 SAM DENS: 2.7500 g/cc
 LIQ DENS: 0.9958 g/cc
 LIQ VISC: 0.7766 cp

CUMULATIVE MASS PERCENT FINER VS. DIAMETER



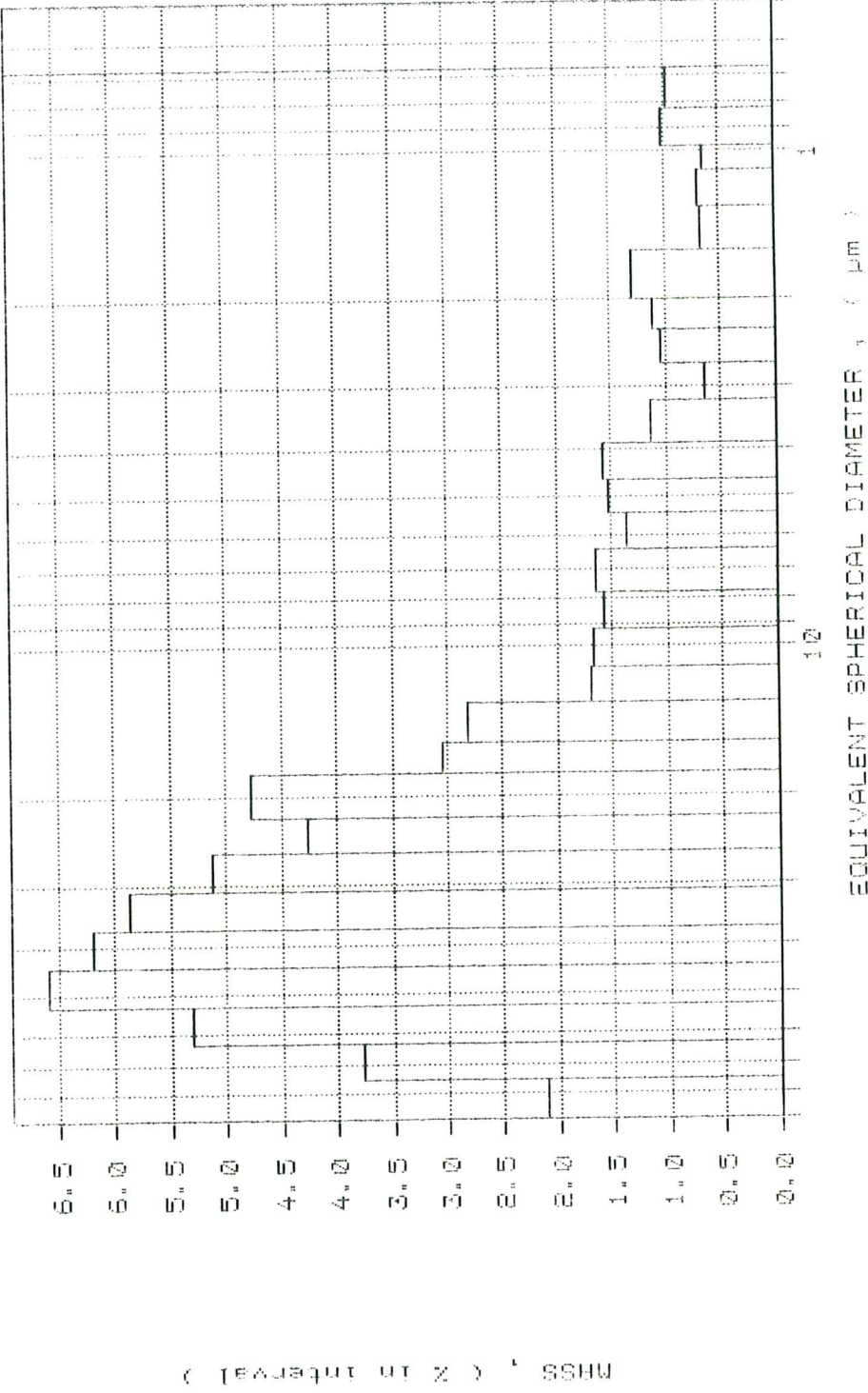
MASS FINER (%)

EQUIVALENT SPHERICAL DIAMETER, (μm)

SAMPLE DIRECTORY/NUMBER: SVLHUM /6
 SAMPLE ID: SITE A SURFACE
 SUBMITTER: UWCC EARTH SCIENCES
 OPERATOR: J.HERNIMAN
 SAMPLE TYPE: CLAY
 LIQUID TYPE: Water
 ANALYSIS TEMP: 31.5 deg C RUN TYPE: High Speed

UNIT NUMBER: 1
 START 16:14:11 10/20/95
 REPT 16:18:45 10/20/95
 TOT RUN TIME 0:04:14
 SAM DENS: 2.7500 g/cc
 LIQ DENS: 0.9958 g/cc
 LIQ VISC: 0.7766 cp

MASS POPULATION VS. DIAMETER



SAMPLE DIRECTORY/NUMBER: SVLHUM /1
 SAMPLE ID: SITE B SURFACE
 SUBMITTER: UWCC EARTH SCIENCES
 OPERATOR: J.HERNIMAN
 SAMPLE TYPE: CLAY
 LIQUID TYPE: Water
 ANALYSIS TEMP: 34.7 deg C RUN TYPE: High Speed

UNIT NUMBER: 1
 START 11:54:10 09/19/95
 REPT 11:58:41 09/19/95
 TOT RUN TIME 0:04:13
 SAM DENS: 2.7500 g/cc
 LIQ DENS: 0.9942 g/cc
 LIQ VISC: 0.7270 cp

STARTING DIAMETER: 90.00 μ m
 ENDING DIAMETER: 0.50 μ m

REYNOLDS NUMBER: 1.81
 FULL SCALE MASS %: 100

MEDIAN DIAMETER: 6.72 μ m MASS DISTRIBUTION MODAL DIAMETER: 35.31 μ m

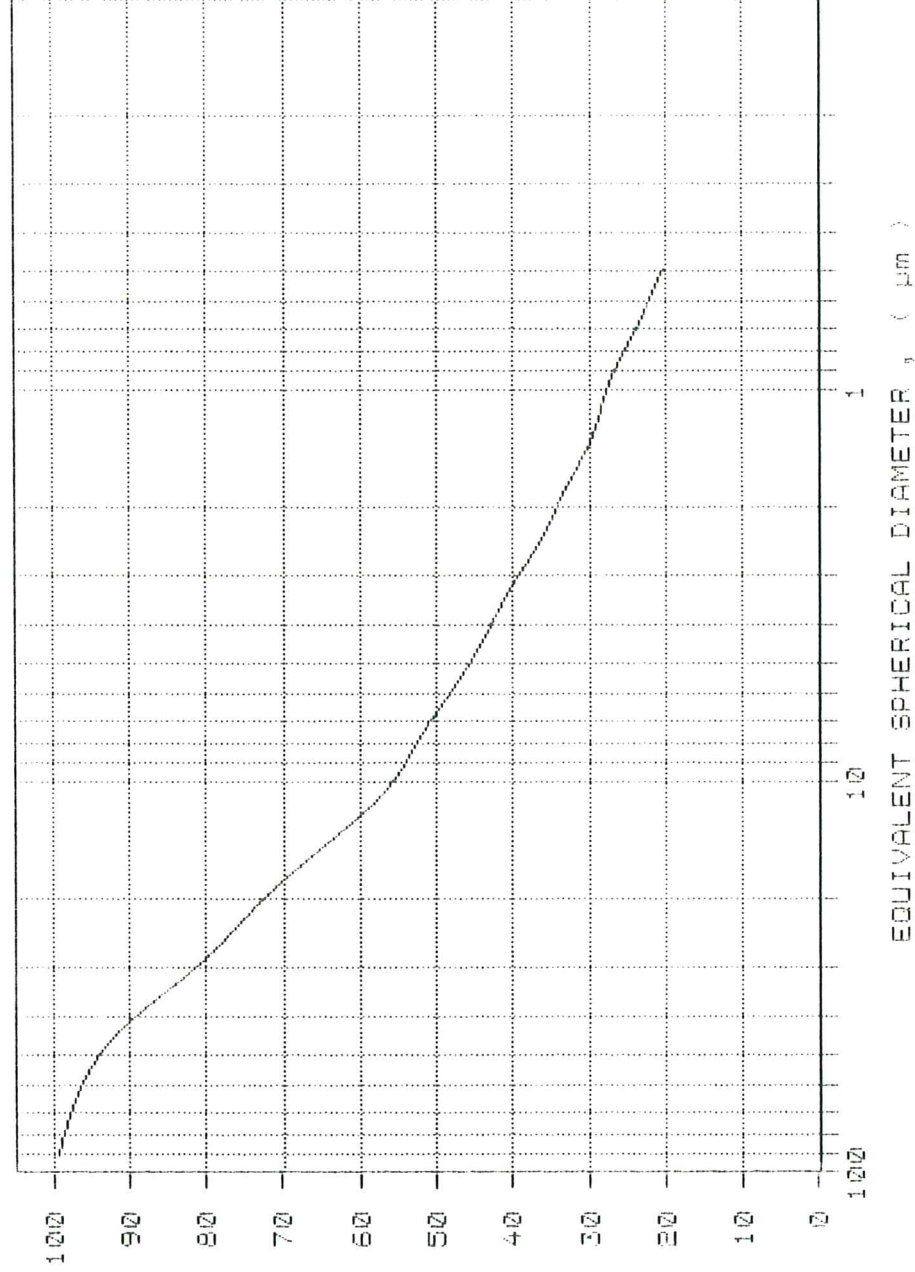
DIAMETER (μ m)	CUMULATIVE MASS FINER (%)	MASS IN INTERVAL (%)
90.00	99.2	0.8
75.00	98.0	1.1
63.00	96.6	1.4
53.00	94.7	2.0
44.00	91.4	3.3
37.00	87.0	4.4
31.00	82.2	4.8
26.00	76.0	4.1
22.00	74.6	3.5
18.00	69.9	4.6
15.50	66.2	3.7
13.00	61.3	4.9
11.00	57.3	4.0
9.20	54.3	3.0
7.90	52.2	2.1
6.40	49.2	3.0
5.40	46.6	2.6
4.50	44.5	2.1
3.90	42.6	2.0
3.20	40.1	2.4
2.70	37.7	3.4
2.30	35.6	2.1
2.00	34.3	1.4
1.60	31.7	2.5
1.30	29.4	2.3
1.10	28.3	1.1
0.98	27.5	0.8
0.82	25.6	1.3
0.68	23.5	2.2

SAMPLE DIRECTORY/NUMBER: SVLHUM /1
 SAMPLE ID: SITE B SURFACE
 SUBMITTER: UWCC EARTH SCIENCES
 OPERATOR: J.HERNIMAN
 SAMPLE TYPE: CLAY
 LIQUID TYPE: Water
 ANALYSIS TEMP: 34.7 deg C

UNIT NUMBER: 1
 START 11:54:10 09/19/95
 REPT 11:58:41 09/19/95
 TOT RUN TIME 0:04:18
 SAM DENS: 2.7500 g/cc
 LIQ DENS: 0.9942 g/cc
 LIQ VISC: 0.7270 cp

RUN TYPE: High Speed

CUMULATIVE MASS PERCENT FINER VS. DIAMETER



EQUIVALENT SPHERICAL DIAMETER, (µm)

GRAIN SIZE

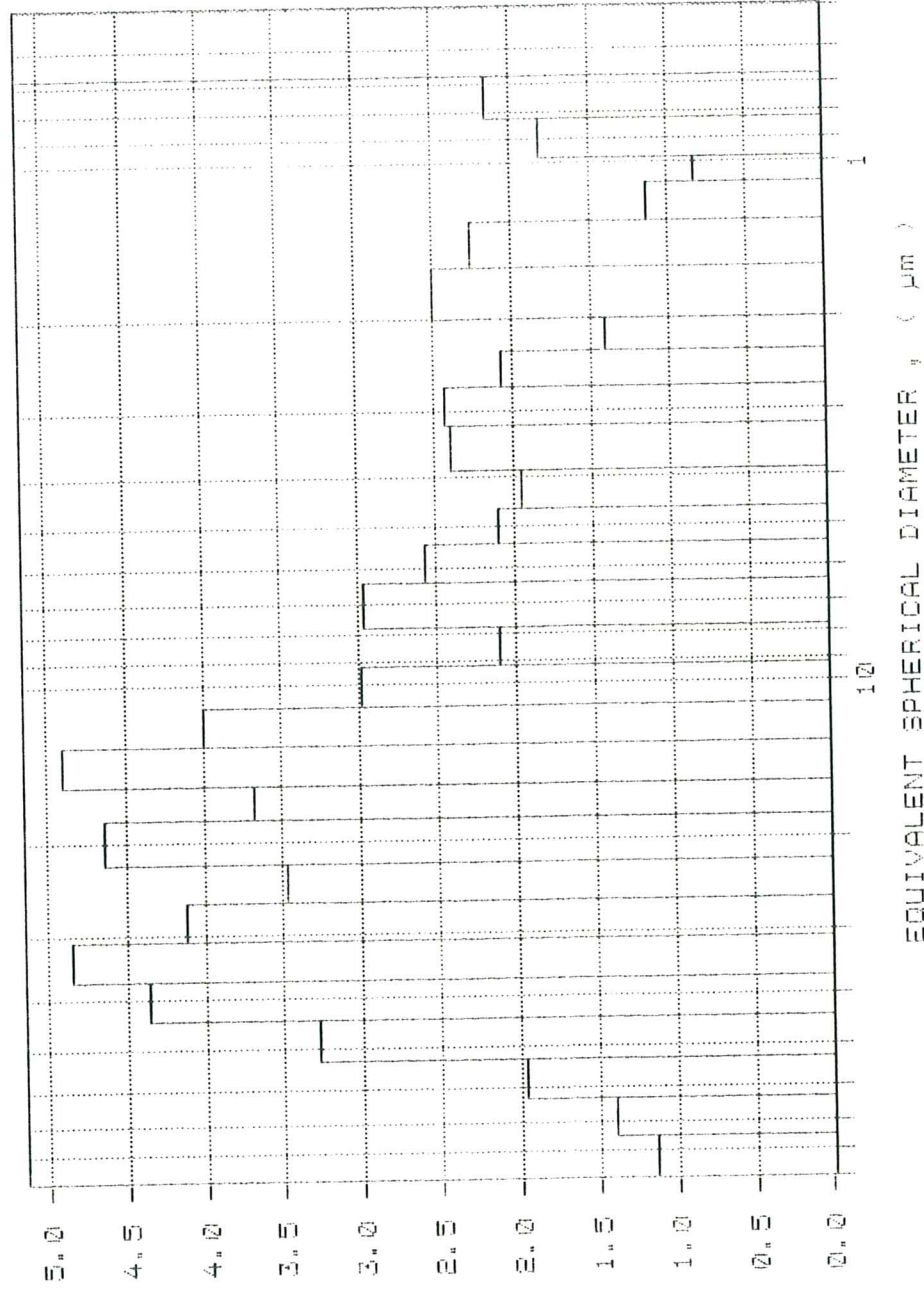
PAGE 8

SediGraph 5100 V2.02

SAMPLE DIRECTORY/NUMBER: SVLHUM /1
 SAMPLE ID: SITE B SURFACE
 SUBMITTER: UWCC EARTH SCIENCES
 OPERATOR: J.HERNIMAN
 SAMPLE TYPE: CLAY
 LIQUID TYPE: water
 ANALYSIS TEMP: 34.7 deg C RUN TYPE: High Speed

UNIT NUMBER: 1
 START 11:54:10 09/19/95
 REPT 11:58:41 09/19/95
 TOT RUN TIME 0:04:13
 SAM DENS: 2.7500 g/cc
 LIQ DENS: 0.9942 g/cc
 LIQ VISC: 0.7270 cp

MASS POPULATION VS. DIAMETER



EQUIVALENT SPHERICAL DIAMETER, (µm)

GRAIN SIZE

PAGE 1

Sediograph 5100 V2.02

SAMPLE DIRECTORY/NUMBER: SVLHUM /4

UNIT NUMBER: 1

SAMPLE ID: SITE B/C SURFACE

START 15:38:26 10/20/95

SUBMITTER: UMCC EARTH SCIENCES

REPT 15:43:08 10/20/95

OPERATOR: J.HERNIMAN

TOT RUN TIME 0:04:26

SAMPLE TYPE: CLAY

SAM DENS: 2.7500 g/cc

LIQUID TYPE: Water

LID DENS: 0.9959 g/cc

ANALYSIS TEMP: 31.4 deg C

LID VISC: 0.7777 cp

RUN TYPE: High Speed

REYNOLDS NUMBER: 1.15

STARTING DIAMETER: 90.00 μ mENDING DIAMETER: 0.50 μ m

FULL SCALE MASS %: 99

MASS DISTRIBUTION

MEDIAN DIAMETER: 14.12 μ m MODAL DIAMETER: 33.07 μ m

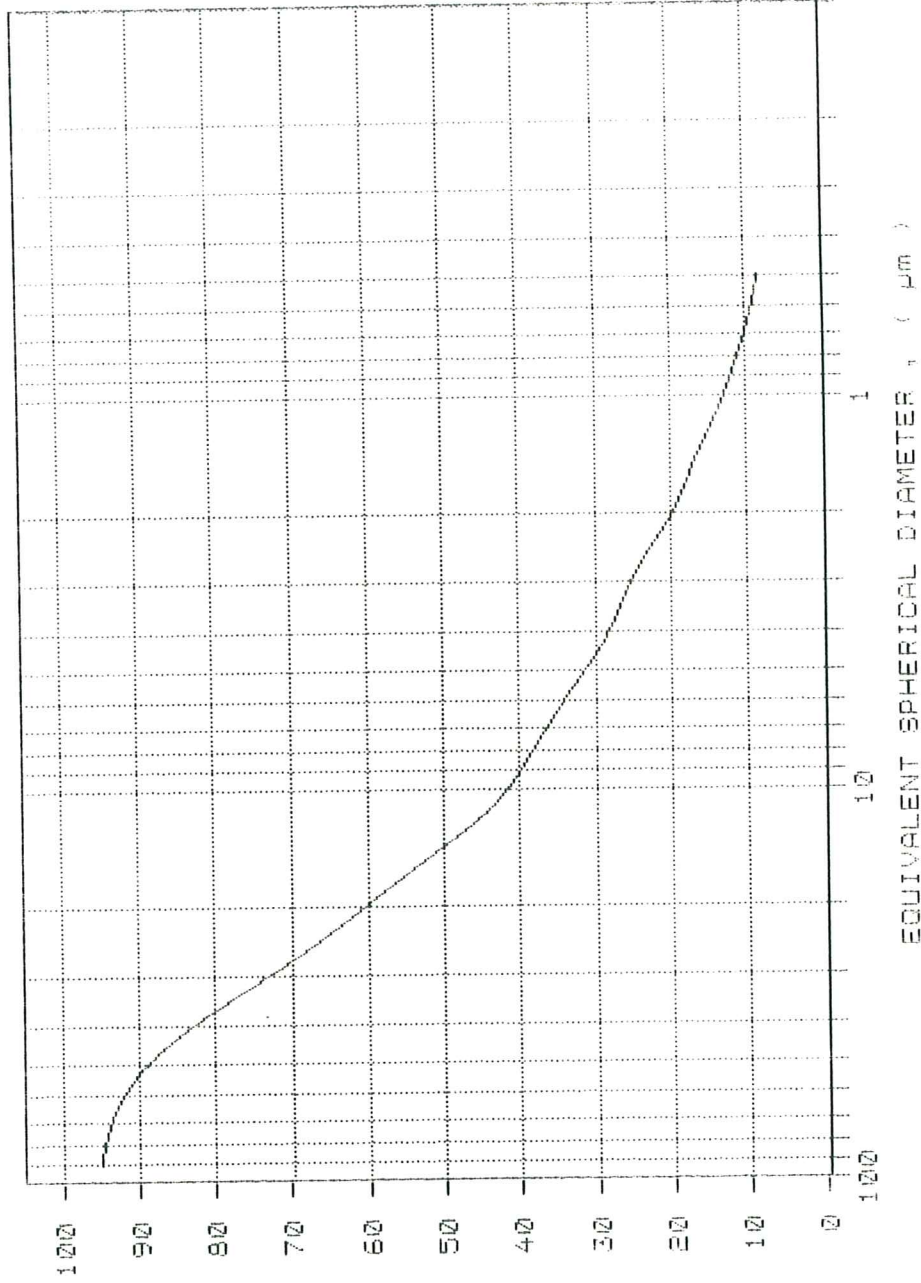
DIAMETER (μ m)	CUMULATIVE MASS FINER (%)	MASS IN INTERVAL (%)
90.00	95.0	4.0
75.00	94.1	0.9
63.00	92.5	1.6
53.00	89.9	2.6
44.00	85.5	4.4
37.00	80.2	5.4
31.00	74.0	6.1
26.00	68.1	5.9
22.00	63.0	5.1
18.00	57.2	5.8
15.60	53.0	4.2
13.00	47.5	5.5
11.00	43.3	4.3
9.20	40.1	3.2
7.80	37.3	2.3
6.40	35.0	2.3
5.40	32.4	2.6
4.60	29.9	2.5
3.90	27.8	2.1
3.20	25.9	1.9
2.70	24.0	1.9
2.30	21.7	2.3
2.00	19.7	1.9
1.60	17.6	2.2
1.30	15.5	2.0
1.10	13.8	1.8
0.98	12.7	1.1
0.82	11.3	1.4
0.68	9.9	1.4

SAMPLE DIRECTORY/NUMBER: SVLHUM /4
 SAMPLE ID: SITE B/C SURFACE
 SUBMITTER: UWCC EARTH SCIENCES
 OPERATOR: J.HERNIMAN
 SAMPLE TYPE: CLAY
 LIQUID TYPE: Water
 ANALYSIS TEMP: 31.4 deg C

UNIT NUMBER: 1
 START 15:38:26 10/20/95
 REPT 15:48:08 10/20/95
 TOT RUN TIME 0:04:26
 SAM DENS: 2.7500 g/cc
 LIQ DENS: 0.9955 g/cc
 LIQ VISC: 0.7777 cp

RUN TYPE: High Speed

CUMULATIVE MASS PERCENT FINER VS. DIAMETER



MASS FINER (%)

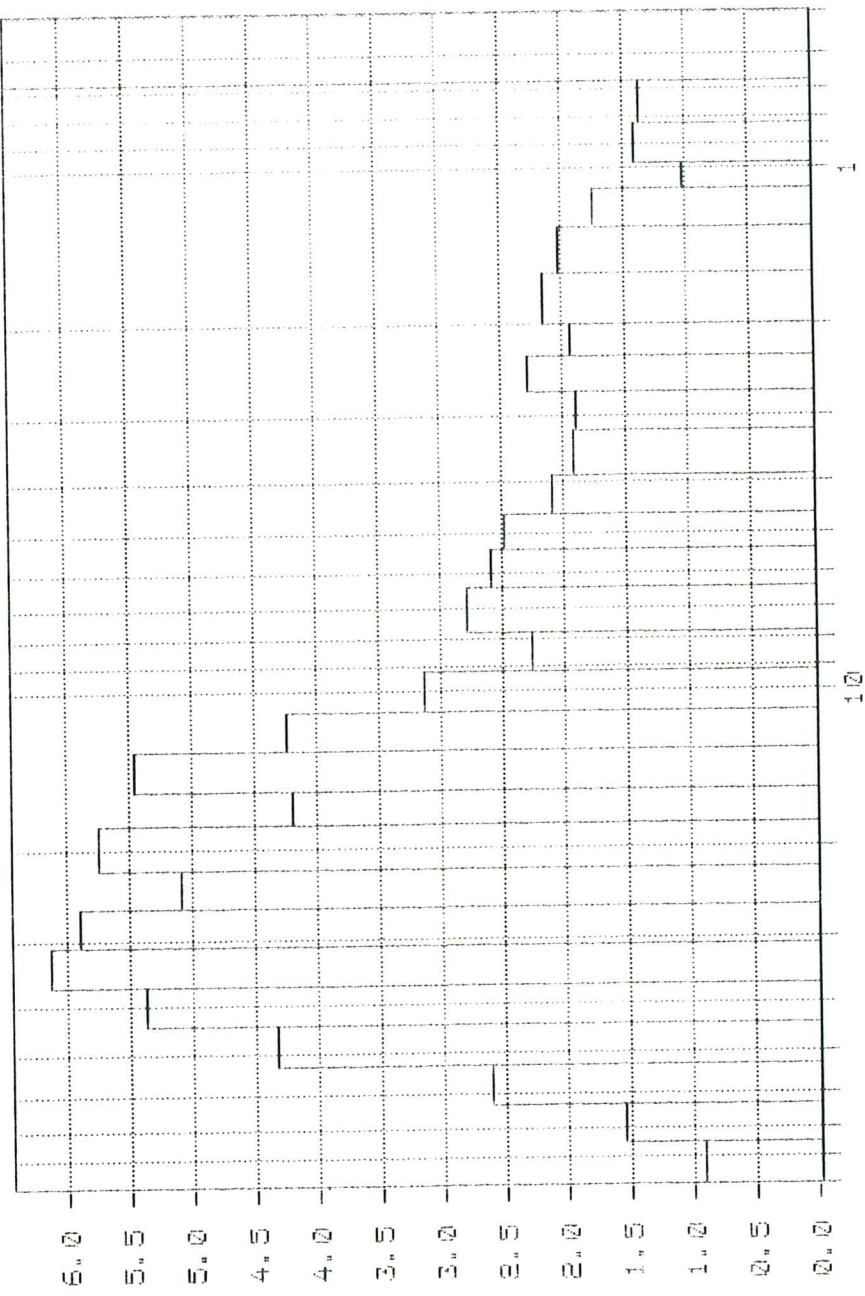
EQUIVALENT SPHERICAL DIAMETER (µm)

SAMPLE DIRECTORY/NUMBER: SVLHUM /4
 SAMPLE ID: SITE B/C SURFACE
 SUBMITTER: UMCC EARTH SCIENCES
 OPERATOR: J.HERNIMAN
 SAMPLE TYPE: CLAY
 LIQUID TYPE: Water
 ANALYSIS TEMP: 31.4 deg C

UNIT NUMBER: 1
 START 15:38:26 10/20/95
 REPT 15:48:08 10/20/95
 TOT RUN TIME 0:04:26
 SAM DENS: 2.7500 g/cc
 LIQ DENS: 0.9959 g/cc
 LIQ VISC: 0.7777 cp

RUN TYPE: High Speed

MASS POPULATION VS. DIAMETER



EQUIVALENT SPHERICAL DIAMETER, (µm)

MASS POPULATION (%)

GRAIN SIZE

SediGraph 5100 V2.02

PAGE 1

SAMPLE DIRECTORY/NUMBER: SVLHUM /2

UNIT NUMBER: 1
START 12:08:49 09/19/95
REPT 12:59:22 09/19/95
TOT RUN TIME 0:08:58
SAM DENS: 2.7500 g/cc
LIQ DENS: 0.9942 g/cc
LIQ VISC: 0.7268 cp

SAMPLE ID: SITE C SURFACE

SUBMITTER: UMCC EARTH SCIENCES

OPERATOR: J.HERNIMAN

SAMPLE TYPE: CLAY

LIQUID TYPE: Water

ANALYSIS TEMP: 34.7 deg C RUN TYPE: High Speed

STARTING DIAMETER: 90.00 μ m
ENDING DIAMETER: 0.50 μ mREYNOLDS NUMBER: 1.81
FULL SCALE MASS %: 91

MASS DISTRIBUTION

MEDIAN DIAMETER: 28.05 μ m MODAL DIAMETER: 50.02 μ m

DIAMETER (μ m)	CUMULATIVE MASS FINER (%)	MASS IN INTERVAL (%)
90.00	87.8	3.2
75.00	85.6	2.1
63.00	80.8	4.9
53.00	73.6	7.2
44.00	65.2	8.3
37.00	58.3	7.0
31.00	52.5	5.7
26.00	48.4	4.1
22.00	45.8	2.7
18.00	43.5	2.3
15.60	41.8	1.7
13.00	39.4	2.4
11.00	37.6	1.7
9.20	36.2	1.4
7.80	34.9	1.3
6.40	33.2	1.7
5.40	31.4	1.8
4.60	30.0	1.4
3.90	29.2	0.8
3.20	28.0	1.1
2.70	26.5	1.5
2.30	24.9	1.6
2.00	23.6	1.3
1.60	21.7	1.9
1.30	19.7	2.0
1.10	18.3	1.4
0.98	17.5	0.8
0.82	16.1	1.4
0.68	14.8	1.2

GRAIN SIZE

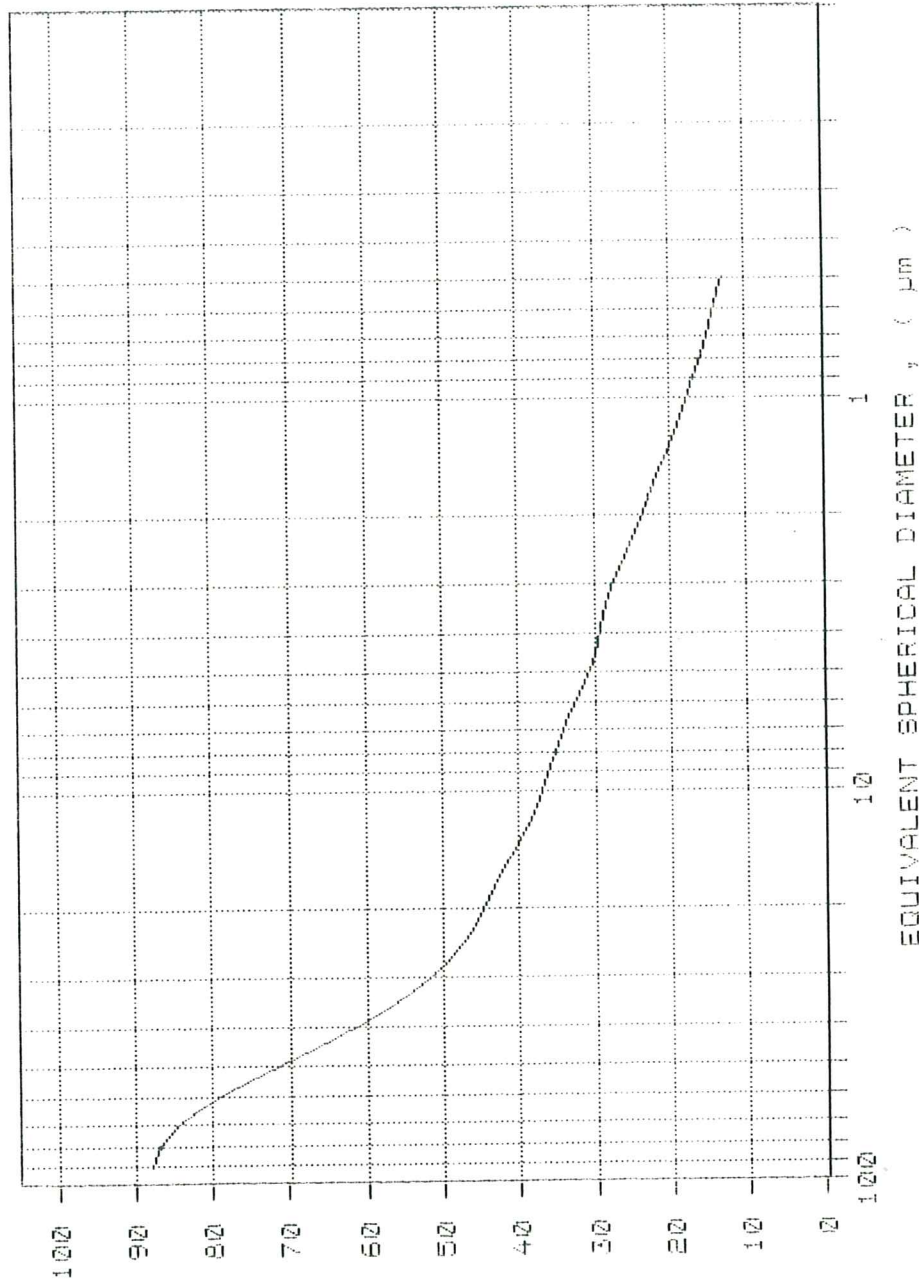
PAGE 2

SediGraph 5100 V2.02

SAMPLE DIRECTORY/NUMBER: SVLHUM /2
 SAMPLE ID: SITE C SURFACE
 SUBMITTER: UWCC EARTH SCIENCES
 OPERATOR: J.HERNIMAN
 SAMPLE TYPE: CLAY
 LIQUID TYPE: Water
 ANALYSIS TEMP: 34.7 deg C RUN TYPE: High Speed

UNIT NUMBER: 1
 START 12:08:49 09/19/95
 REPT 12:59:22 09/19/95
 TOT RUN TIME 0:03:58
 SAM DENS: 2.7500 g/cc
 LIQ DENS: 0.9942 g/cc
 LIQ VISC: 0.7256 cp

CUMULATIVE MASS PERCENT FINER VS. DIAMETER



EQUIVALENT SPHERICAL DIAMETER, (µm)

SediGraph 5100 V2.0E

GRAIN SIZE

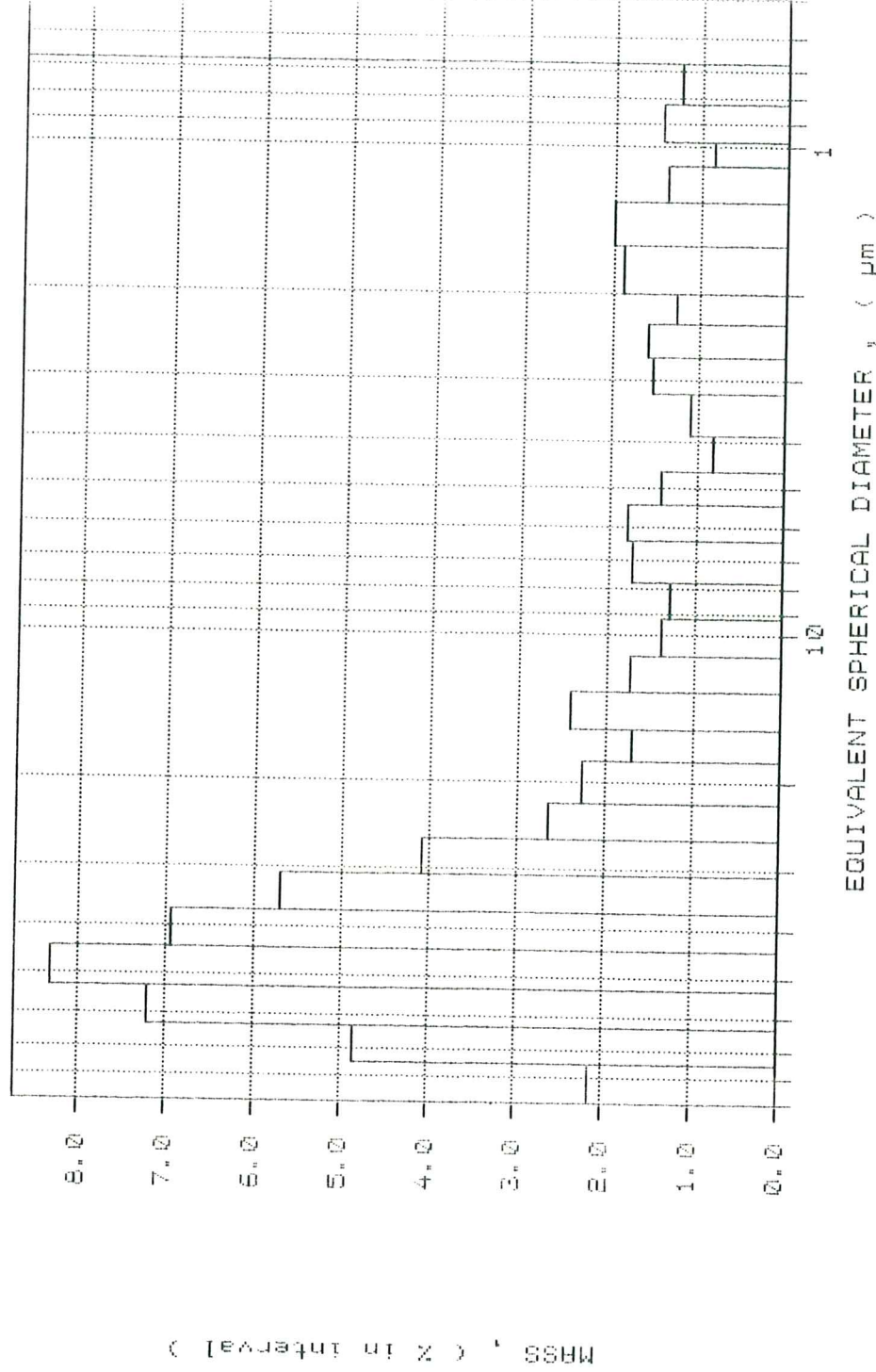
PAGE 1

SAMPLE DIRECTORY/NUMBER: SVLHUM /2
SAMPLE ID: SITE C SURFACE
SUBMITTER: UMCC EARTH SCIENCES
OPERATOR: J.HERNIMAN
SAMPLE TYPE: CLAY
LIQUID TYPE: Water
ANALYSIS TEMP: 24.7 deg C

UNIT NUMBER: 1
START 12:08:49 09/19/77
REPT 12:59:22 09/19/77
TOT RUN TIME 0:08:17
SAM DENS: 2.7500 g/cc
LIQ DENS: 0.9942 g/cc
LIQ VISC: 0.7268 cp

RUN TYPE: High Speed

MASS POPULATION VS. DIAMETER



GRAIN SIZE

PAGE 1

SediGraph 5100 V2.02

SAMPLE DIRECTORY/NUMBER: SVLHUM /5

SAMPLE ID: SITE C/D SURFACE

SUBMITTER: UWCC EARTH SCIENCES

OPERATOR: J.HERNIMAN

SAMPLE TYPE: CLAY

LIQUID TYPE: Water

ANALYSIS TEMP: 31.4 deg C RUN TYPE: High Speed

UNIT NUMBER: 1

START 15:00:18 10/20/95

REPT 15:04:45 10/20/95

TOT RUN TIME 0:04:09

SAM DENS: 2.7500 g/cc

LID DENS: 0.9958 g/cc

LID VISC: 0.7769 cp

REYNOLDS NUMBER: 1.15

FULL SCALE MASS %: 92

STARTING DIAMETER: 90.00 μ mENDING DIAMETER: 0.50 μ m

MASS DISTRIBUTION

MODAL DIAMETER: 47.62 μ mMEDIAN DIAMETER: 17.81 μ m

DIAMETER (μ m)	CUMULATIVE MASS FINER (%)	MASS IN INTERVAL (%)
90.00	99.4	-1.4
75.00	91.4	8.1
60.00	87.2	4.2
50.00	81.0	6.2
44.00	79.5	7.5
37.00	67.0	6.5
31.00	61.5	5.5
26.00	57.1	4.4
22.00	59.7	3.4
18.00	50.2	3.5
15.60	47.7	2.4
13.00	45.0	2.7
11.00	42.9	2.1
9.20	40.4	2.5
7.80	38.0	2.4
6.40	35.4	2.6
5.40	33.5	1.9
4.60	31.9	1.6
3.90	30.4	1.5
3.20	28.4	2.0
2.70	26.7	1.7
2.30	25.2	1.5
2.00	24.0	1.3
1.50	22.0	1.9
1.20	20.4	1.6
1.10	19.1	1.3
0.98	18.3	0.8
0.82	17.2	1.1
0.50	16.1	1.1

GRAIN SIZE

SediGraph 5100 V2.02

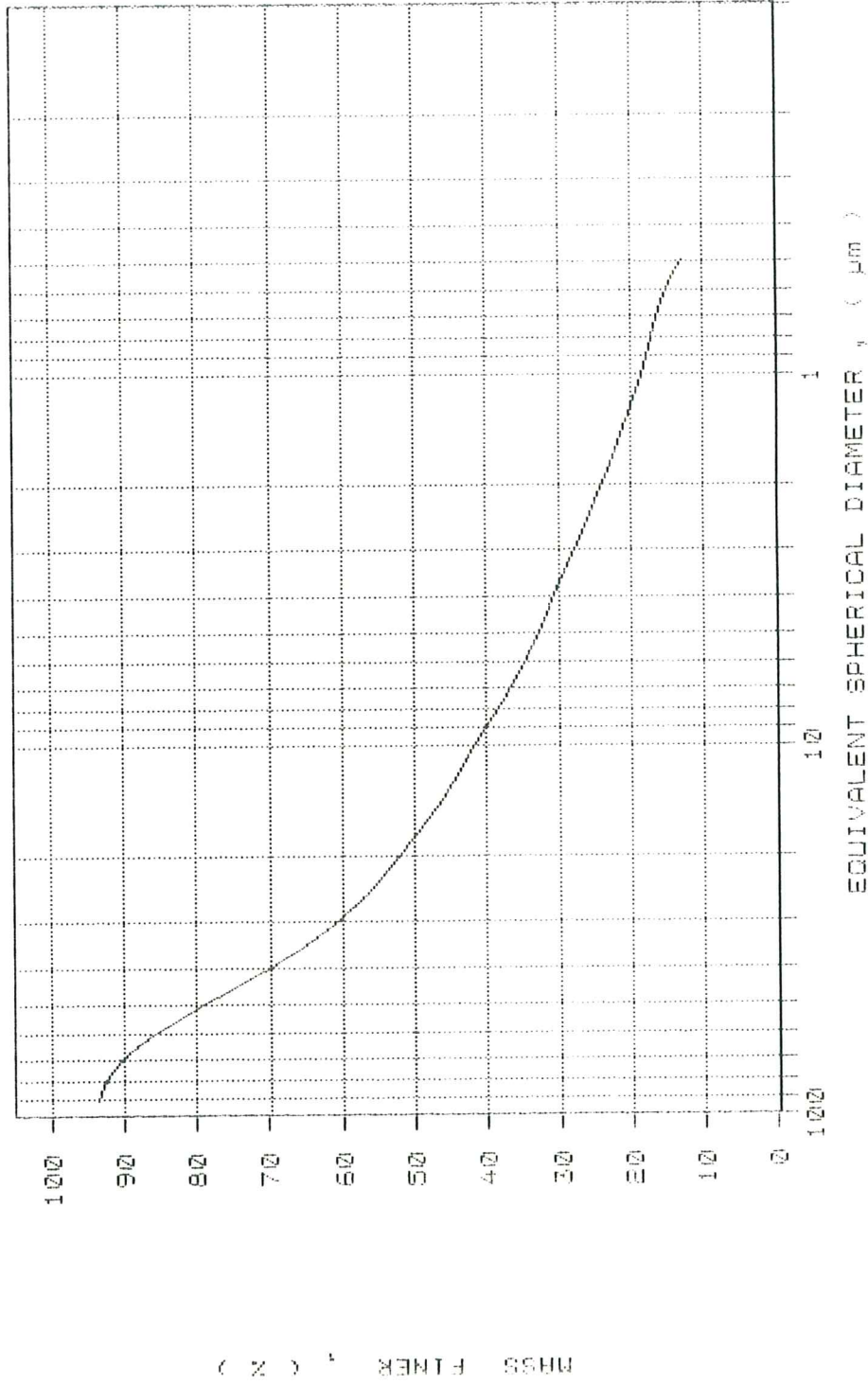
PAGE 2

SAMPLE DIRECTORY/NUMBER: SVLHUM /5
SAMPLE ID: SITE C/D SURFACE
SUBMITTER: UWCC EARTH SCIENCES
OPERATOR: J.HERNIMAN
SAMPLE TYPE: CLAY
LIQUID TYPE: Water
ANALYSIS TEMP: 31.4 deg C

UNIT NUMBER: 1
START 16:00:18 10/20/95
REPT 16:04:45 10/20/95
TOT RUN TIME 0:04:09
SAM DENS: 2.7500 g/cc
LIQ DENS: 0.9958 g/cc
LIQ VISC: 0.7769 cp

RUN TYPE: High Speed

CUMULATIVE MASS PERCENT FINER VS. DIAMETER



MASS FINER (%)

EQUIVALENT SPHERICAL DIAMETER (μm)

GRAIN SIZE

PAGE 3

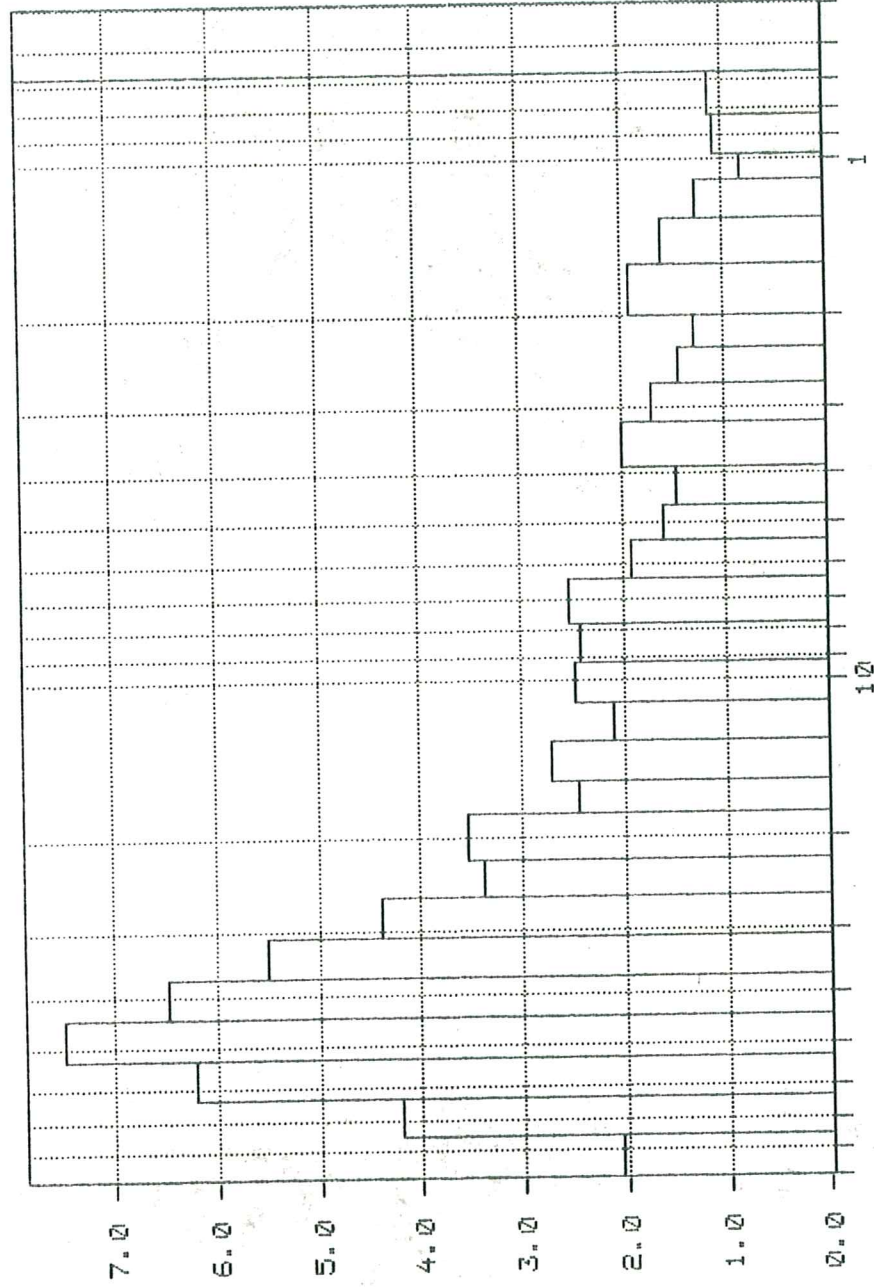
SediGraph 5100 V2.02

SAMPLE DIRECTORY/NUMBER: SVLHUM /5
 SAMPLE ID: SITE C/D SURFACE
 SUBMITTER: UWCC EARTH SCIENCES
 OPERATOR: J.HERNIMAN
 SAMPLE TYPE: CLAY
 LIQUID TYPE: Water
 ANALYSIS TEMP: 31.4 deg C

UNIT NUMBER: 1
 START 16:00:18 10/20/95
 REPT 16:04:45 10/20/95
 TOT RUN TIME 0:04:09
 SAM DENS: 2.7500 g/cc
 LIQ DENS: 0.9953 g/cc
 LIQ VISC: 0.7769 cp

RUN TYPE: High Speed

MASS POPULATION VS. DIAMETER



MASS , (% In Interval)

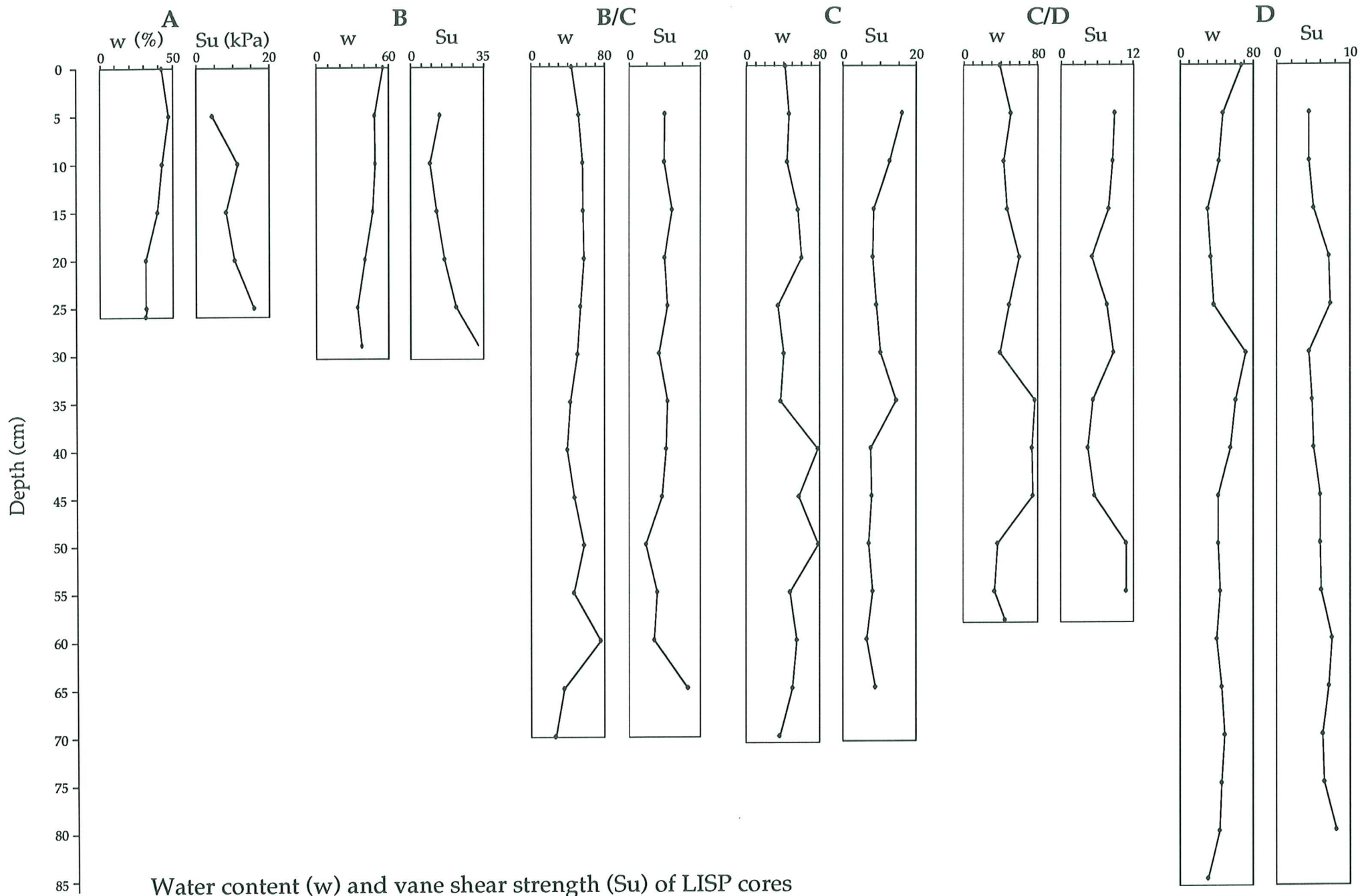
EQUIVALENT SPHERICAL DIAMETER , (µm)

APPENDIX 5

GRAIN SIZE ANALYSES OF SURFACE SEDIMENTS

Grain size procedure

A sample approximately 2 g in size was taken from the surface of the core. This was then immersed in Calgon (10%) and left for 24 hours. The sample was then wet sieved through a 90 micron sieve. Any sediment retained in the sieve was placed to dry in the oven. Once dry, this was weighed in order to calculate the percentage greater than 90 microns in diameter and thus the percentage finer than 90 microns. When this was known, the finer fraction was placed in an sonic bath for 2 minutes and then run through a Micromeritics Sedigraph™ to produce the grain size distribution for the finer fraction.



Water content (w) and vane shear strength (Su) of LISP cores

Site A		
Depth (m)	Water content (%)	Su (kPa)
0	42.026	
0.05	46.741	6.442
0.1	42.279	13.301
0.15	39.348	10.183
0.2	31.121	12.469
0.25	31.665	17.873
0.26	30.410	

Site B		
Depth (m)	Water content (%)	Su (kPa)
0	56.240	
0.05	46.097	13.924
0.1	47.135	9.352
0.15	44.313	12.469
0.2	34.875	16.210
0.25	26.381	21.971
0.29	31.427	32.701

Site B/C		
Depth (m)	Water content (%)	Su (kPa)
0	44.107	
0.05	52.027	10.079
0.1	56.296	9.872
0.15	56.667	12.054
0.2	57.899	9.975
0.25	54.241	10.807
0.3	50.727	8.521
0.35	42.804	10.807
0.4	39.703	10.391
0.45	47.532	9.352
0.5	57.609	4.780
0.55	46.680	7.897
0.6	76.017	7.066
0.65	36.132	16.522
0.7	26.896	

Site C		
Depth (m)	Water content (%)	Su (kPa)
0	43.435	
0.05	47.980	16.095
0.1	45.773	12.774
0.15	58.067	8.431
0.2	62.276	8.175
0.25	35.754	9.197
0.3	42.174	10.219
0.35	38.407	14.562
0.4	80.222	7.664
0.45	58.944	7.920
0.5	81.249	7.153
0.55	49.290	8.209
0.6	56.838	6.546
0.65	51.843	8.936
0.7	37.097	

Site C/D		
Depth (cm)	Water content (%)	Su (kPa)
0	40.246	
0.05	52.376	8.936
0.1	44.382	8.625
0.15	48.164	7.897
0.2	61.588	5.196
0.25	50.585	7.689
0.3	40.552	8.729
0.35	78.754	5.299
0.4	75.325	4.468
0.45	76.602	5.611
0.5	37.563	10.807
0.55	34.570	10.807
0.58	46.245	

Site D		
Depth (m)	Water content (%)	Su (kPa)
0	66.838	
0.05	47.029	4.364
0.1	42.104	4.364
0.15	30.291	4.988
0.2	33.336	7.066
0.25	36.774	7.274
0.3	71.608	4.364
0.35	60.372	4.780
0.4	55.037	4.988
0.45	41.922	5.923
0.5	41.851	5.923
0.55	44.068	6.027
0.6	40.150	7.482
0.65	45.729	7.066
0.7	49.206	6.235
0.75	45.418	6.442
0.8	43.642	8.105
0.85	30.457	

APPENDIX 2

WATER CONTENT ANALYSES OF GRAVITY CORES

Water content procedure

Samples were taken from the core at 5 cm intervals. A petri dish was then weighed for the first sample and a plastic sampling device used to take the sample from the core. The sample was then weighed with the petri dish and put into an oven at approximately 40°C for 48 hours. This was repeated for each sample. After 48 hours, the sample and petri dish were weighed. The following equation was then used to obtain the water content of the sample:-

$$\frac{(\textit{Weight wet sample} + \textit{dish}) - (\textit{Weight dry sample} + \textit{dish})}{(\textit{Weight dry sample} + \textit{dish}) - (\textit{Weight dish})} \times 100$$

SITE A				
Depth (m)	Weight dish	Weight (dish + wet sample)	Weight (dish + dry sample)	Water Content (%)
0	7.923	14.807	12.770	42.026
0.05	8.191	17.556	14.573	46.741
0.1	7.919	15.299	13.106	42.279
0.15	7.861	16.796	14.273	39.348
0.2	7.385	14.716	12.976	31.121
0.25	8.090	13.799	12.426	31.665
0.26	7.519	12.961	11.692	30.410

SITE B				
Depth (m)	Weight (dish)	Weight (dish+ wet sample)	Weight (dish + dry sample)	Water Content (%)
0	7.515	14.488	11.978	56.240
0.05	8.066	26.369	20.594	46.097
0.1	7.523	19.85	15.901	47.135
0.15	8.019	20.085	16.38	44.313
0.2	7.927	15.886	13.828	34.875
0.25	8.189	18.508	16.354	26.381
0.29	7.689	19.892	16.974	31.427

SITE B/C				
Depth (m)	Weight dish	Weight (dish + wet sample)	Weight (dish + dry sample)	Water Content (%)
0	7.911	16.788	14.071	44.107
0.05	8.188	19.286	15.488	52.027
0.1	7.697	17.031	13.669	56.296
0.15	8.016	18.931	14.983	56.667
0.2	7.935	18.53	14.645	57.899
0.25	7.516	17.554	14.024	54.241
0.3	8.085	17.721	14.478	50.727
0.35	8.069	22.735	18.339	42.804
0.4	7.375	16.981	14.251	39.703
0.45	7.752	19.798	15.917	47.532
0.5	7.499	19.772	15.286	57.609
0.55	7.856	17.069	14.137	46.680
0.6	8.015	17.754	13.548	76.017
0.65	7.706	15.652	13.543	36.132
0.7	8.074	13.929	12.688	26.896

SITEC				
Depth (m)	Weight (dish)	Weight (dish + wet sample)	Weight (dish + dry sample)	Water Content (%)
0	8.018	14.857	12.786	43.435
0.05	8.084	23.869	18.751	47.980
0.1	7.396	22.899	18.031	45.773
0.15	8.066	24.712	18.597	58.067
0.2	7.519	24.188	17.791	62.276
0.25	8.012	26.894	21.921	35.754
0.3	7.922	23.082	18.585	42.174
0.35	8.179	21.837	18.047	38.407
0.4	7.681	21.814	15.523	80.222
0.45	7.756	23.946	17.942	58.944
0.5	7.876	28.852	19.449	81.249
0.55	7.860	24.158	18.777	49.290
0.6	8.075	20.713	16.133	56.838
0.65	8.081	24.225	18.713	51.843
0.7	7.700	13.905	12.226	37.097

SITE C/D				
Depth (m)	Weight (dish)	Weight (dish + wet sample)	Weight (dish + dry sample)	Water Content (%)
0	7.520	16.312	13.789	40.246
0.05	7.925	23.574	18.195	52.376
0.1	7.910	20.978	16.961	44.382
0.15	7.909	23.521	18.446	48.164
0.2	8.073	18.880	14.761	61.588
0.25	7.698	18.501	14.872	50.585
0.3	7.516	20.087	16.460	40.552
0.35	8.081	20.760	15.174	78.754
0.4	7.380	16.013	12.304	75.325
0.45	7.858	20.697	15.128	76.602
0.5	7.507	16.245	13.859	37.563
0.55	7.755	18.090	15.435	34.570
0.58	7.757	12.061	10.700	46.245

APPENDIX 4

VANE SHEAR STRENGTH MEASUREMENTS OF GRAVITY CORES

SITE D					
Depth (m)	Weight (dish)	Weight (dish + wet sample)	Weight (dish + dry sample)	Water Content (%)	
0	8.189	13.391	11.307	66.838	
0.05	7.759	27.430	21.138	47.029	
0.1	7.883	27.013	21.345	42.104	
0.15	7.850	24.664	20.755	30.291	
0.2	7.566	25.397	20.939	33.336	
0.25	8.086	27.021	21.930	36.774	
0.3	7.402	22.881	16.422	71.608	
0.35	8.066	24.108	18.069	60.372	
0.4	7.521	26.065	19.482	55.037	
0.45	8.016	25.603	20.408	41.922	
0.5	7.922	22.500	18.199	41.851	
0.55	8.187	27.338	21.480	44.068	
0.6	7.688	22.080	17.957	40.150	
0.65	7.750	21.485	17.175	45.729	
0.7	7.880	23.660	18.456	49.206	
0.75	7.861	27.222	21.175	45.418	
0.8	7.558	27.280	21.288	43.642	
0.85	7.910	12.536	11.456	30.457	

XRD sample preparation and procedure

The sample was washed in distilled water in order to allow any salts to be dissolved (Sykes, 1992). Without this, in XRD analysis, an untreated sample would show halite (NaCl) as the main mineral as it has a masking effect on the other minerals. The sample was then centrifuged at 3500 r.p.m for 20 minutes. This concentrates the sediment but leaves the salts in solution which can then be removed. The sediment was then resuspended in distilled water and placed in a sonic bath for 10 minutes. In order to obtain the clay particles, the sediment was sieved through a 63 μm sieve. Material finer than 63 μm was then centrifuged at 1000 r.p.m for 5 minutes. The remaining liquid was decanted and the sediment (the silt-size fraction) put aside. This liquid was then centrifuged at 1700 r.p.m for 15 minutes, the liquid decanted and the sediment (the clay-size fraction) pipetted onto a glass slide. This was then left to dry at room temperature. Once dry, the glass slide was placed in the a Phillips PW1729 x-ray generator and scanned from 5-35 $^{\circ}$ 2 θ .

Interpretation of results

Percentages of the individual clay minerals were calculated using the method described by Biscaye (1965).

Biscaye, P.E., 1965. Mineralogy and sedimentation of recent deep-sea clay in the Atlantic Ocean and adjacent seas and oceans. *Geol. Soc. American Bull.*, **76**, pp. 803-832.

Sykes, T.J.S., 1992. *Synthesis of volcanogenic sediment distributions in the Indian Ocean*. Unpub. M.Phil. thesis, University of Wales. 4-4 pp.

	Lat/Lon	% Illite	% Chlorite	% Kaolinite	% Calcite
SITE A	53°37.410'N 00°04.283'E	47.29	22.81	27.81	2.10
SITE B	53°38.193'N 00°04.091'E	57.05	11.97	29.26	1.72
SITE B/C	53°37.99'N 00°03.88'E	66.23	16.71	13.69	3.37
SITE C	53°37.754'N 00°04.026'E	49.43	15.93	32.34	2.30
SITE C/D	53°37.754'N 00°04.026'E	46.30	14.75	36.45	2.50
SITE D	53°37.412'N 00°03.863'E	42.89	17.24	38.40	1.48

Vane shear strength procedure

The vane shear strength of the sediments was carried out using an unmodified Wykeham Farrance Ltd. vane shear apparatus. The shear device consisted of a 4-bladed vane, with each blade 90° from the others. This was driven by a motor at a rotation rate of 89° per minute via pre calibrated springs of differing strengths. When the vane is inserted into the sediment, torque is applied to the vane axis until the sediment shears. When the sample is sheared, the stress pointer moves around the dial, the angle noted and used in the calculation for shear strength. Using Boyce (1977) the shear strength was calculated as follows:-

$$\text{Vane shear strength } (S_u) = \frac{2.t}{[\pi D^2 (H + \frac{D}{3})]} \times (\text{max. degree spring stress})$$

where:

t = spring torque factor (kNm per degree)

D = vane diameter (0.0127 m)

H = vane height (0.0127 m)

Boyce, R.E., 1977. Deep Sea Drilling Project procedures for shear strength measurement of clayey sediment using modified Wykeham Farrance laboratory vane apparatus. In: Barker, P., Dalziel, I.W.D. *et al.*. *Init. Repts. D.S.D.P. 36*. U.S. Government Printing Office: Washington. pp. 1059-1068.

APPENDIX 4

VANE SHEAR STRENGTH MEASUREMENTS OF GRAVITY CORES

APPENDIX 3

X-RAY DIFFRACTION ANALYSES OF GRAVITY CORE SAMPLES